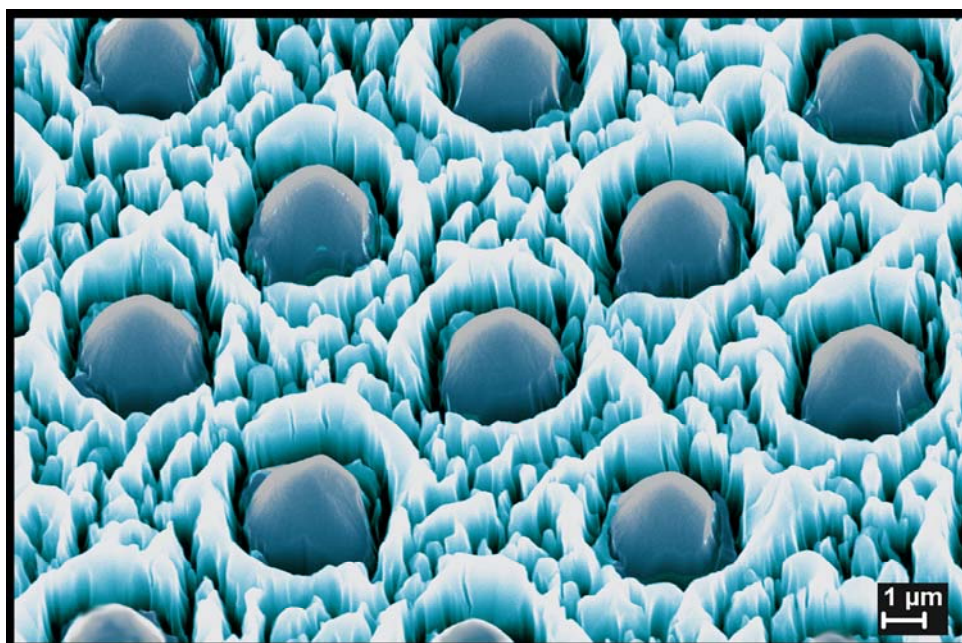RUSSIAN ACADEMY OF SCIENCES

YAROSLAVL DEMIDOV STATE UNIVERSITY

RUSSIAN FOUNDATION FOR BASIC RESEARCH

YAROSLAVL BRANCH OF THE INSTITUTE

OF PHYSICS AND TECHNOLOGY

SCIENTIFIC EDUCATIONAL CENTER

"NANOTECHNOLOGY AND INNOVATIONS"

CENTER FOR COLLECTIVE USE

"DIAGNOSTICS OF MICRO- AND NANOSTRUCTURES"

III INTERNATIONAL CONFERENCE

ON

**MODERN PROBLEMS IN PHYSICS
OF SURFACES AND NANOSTRUCTURES**

BOOK OF ABSTRACTS

YAROSLAVL, RUSSIA

9-11 OCTOBER 2017

* - Institute of Physics and Technology, Russian Academy of Sciences

** - Yaroslavl Branch of the Institute of Physics and Technology, Russian Academy of Sciences

Image on the cover – quartz etched in fluorine-containing plasm

Contents

O1-1: Self organized graphene nanoribbons on cubic-SiC (001): transport and magnetic properties

V. Aristov[1,2], A. Chaika[1] , O. Molodtsova[2] , A. Locatelli[3] , Tevfik O. Mentes[3] ,
A. Sala[3] , Paolo Moras[3] , Polina Sheverdiaeva[3] , and Han-Chun Wu[4]

*1. Institute of Solid State Physics of Russian Academy of Sciences, Chernogolovka, Russia, aristov@issp.ac.ru,
chaika@issp.ac.ru. 2. Deutsches Elektronen-Synchrotron DESY, Hamburg, Germany, victor.aristov@desy.de,
olga.molodtsova@desy.de. 3. Elettra − Sincrotrone Trieste S.C.p.A., Basovizza, Trieste, Italy,
andrea.locatelli@elettra.eu, tevfik.mentes@elettra.eu, alessandro.sala@mensa.it, paolo.moras@trieste.ism.cnr.it,
polina.sheverdyaeva@trieste.ism.cnr.it. 4. School of Physics, Beijing Institute of Technology, Beijing, People's
Republic of China, wuhc@bit.edu.cn.*

Graphene exhibits amazing properties that are of importance both for fundamental investigations and technology. The ability to open gap and to get graphene magnetic are primary challenges in the fields of modern applications. When graphene is prepared as nanostructured layers with a great amount of nano-domain boundaries and ripples it becomes to be the most promising material for graphene-based electronic and spintronic applications because the nano-domain edges can entirely reflect electrons over a great range of energies [1] and hold spin-polarized electronic states [2,3]. In this presentation we report the structure, transport and magnetic properties of continuous and homogeneous nanostructured few-layer graphene with self-aligned nano-domain synthesized on the standard SiC(001)/Si(001) wafers [4-8]. Our low temperature (below 100 K) transport experiments clearly prove that creation of such nano-domain system can induces a charge transport gap greater than 1.3 eV, while the current on-off ratio can reach 10^4 [7, 8]. In addition, we report the magneto-resistance investigation of graphene grown on technologically relevant SiC/Si(001) wafers, where inherent nano-domain boundaries sandwich zig-zag structures between adjacent ripples of large curvature. These measurements disclose an exceptional big positive magneto-resistance in parallel magnetic field with a strong temperature dependence [9]. Theoretical calculations confirm, that observed the transport and magnetic properties of graphene/SiC(001) are interrelated to the localized states at the nano-domain boundaries. Our results show that using purely graphene it is possible to engineer new tunable electronic and magnetic nanostructures.
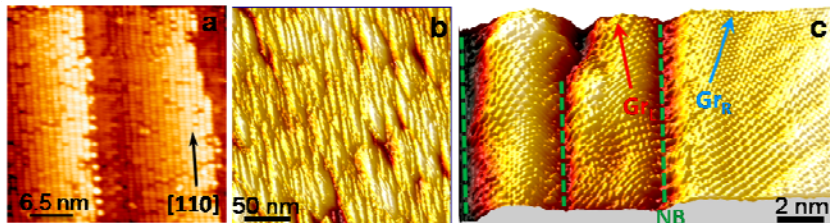
Figure 1. (a) 2D-presentations of atomically resolved STM image of the SiC(001)3×2 reconstruction. The image demonstrates that the step direction is close to the [110] direction of the SiC crystal lattice. (b) Large area STM images of graphene nanoribbons synthesized on the vicinal SiC(001). (c) Atomically resolved STM images of graphene nanoribbons showing the system of domains rotated 17° clockwise (GrR) and 10° anticlockwise (GrL) relative to the NB which is rotated 3.5° anticlockwise from the [110] direction.

1. O.V. Yazev and S.G. Louie, *Nat. Mater.*, 9, p.806, 2010
2. P. Ruffieux et al*., Nature*, 531, p.p.489–492, 2016
3. K. Nakada et al., *Phys. Rev.*, B 54, p.17954, 1996
4. V.Yu. Aristov et al., *Nano Letters*, 10, p.992, 2010
5. A.N. Chaika et al*., Nano Res.*, 6, p.562, 2013
6. A.N. Chaika et al., *Nanotechnology*, 25, p.135605, 2014
7. H.-C. Wu et al., *ACS Nano*, 9, p.8967, 2015
8. A.N. Chaika, V.Yu. Aristov, O.V. Molodtsova, *Prog Mater Sci*., 89, p.1, 2017
9. H.-C. Wu *et al.*, *Nat. Commun.*, 8, p.14453 (2017

O1-2: Modification of graphene at the synthesis in plasma jets

M. Shavelkina[1], R. Amirov[1], A. Naumkin[2]

1. Joint Institute for High Temperatures, Russian Academy of Sciences, Moscow, Russia, E-mail: mshavelkina@gmail.com 2. A.N.Nesmeyanov Institute of Organoelement Compounds of Russian Academy of Sciences Moscow, Russia, E-mail: naumkin@ineos.ac.ru

Graphene as known is formed by a two-dimensional hexagonal lattice consisting of two equivalent sublattices, it has an electronic structure with zero - band gap. The standard method for controlling the width of the band gap of this material is its doping with donor or acceptor impurities. There are two approaches to doping — doping at the stage of synthesis and processing of initially pure material. In this paper, we have been show the possibility of synthesis of graphene doped with oxygen, nitrogen or hydrogen atoms in a plasma jet reactor. The essence of the method consists in the simultaneous injection into the powerful plasma touch (up to 40 kW) of the carbon source together with the plasma-forming gas. In the discharge gap it evaporates to form a carbon vapor, which is then rapidly cooled and in the volume of the metal collector, solid carbon forms. As a source of carbon hydrocarbons (propane-butane mixture, acetylene, methane) has been used. Argon, nitrogen and helium has been used as plasma-forming gases The synthesis parameters (medium pressure, kind and rate of flow of the plasma-forming gas, the ratio of the components in the gas mixture) has been varied within a wide range. The synthesis products are characterized by the methods of electron microscopy, thermogravimetry and X-ray photoelectron spectroscopy. It is established that the obtained samples have morphology in the form of flakes, which are multilayered. The number of layers is from 1 to 9. The lateral size of graphene ranges from 50 to 1500 nm, depending on the type of precursor and the kind of plasma-forming gas. Studies of XPS spectra of samples showed that the graphene structure synthesized in a nitrogen plasma at 710 Torr contains nitrogen atoms predominantly in the pyridine configuration (Figure 1), and when the graphene has been synthesised ofin nitrogen plasma at 350 Torr the graphene structure includes and nitrogen and oxygen-containing functional groups also. Oxygen is also present at the decomposition of hydrocarbons in helium plasma (Figure 2). The spectra of C1s samples synthesized by the decomposition of acetylene in a jet of helium plasma showed the presence of a C-H bond in the structure (Figure 3). In total in graphene synthesized in plasma jets the surface defects predominate over bulk ones. This is ensured their thermal stability.
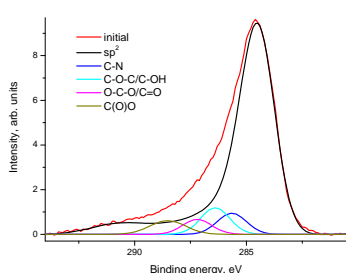
Figure 1. XPS spectra of N (1s) peaks
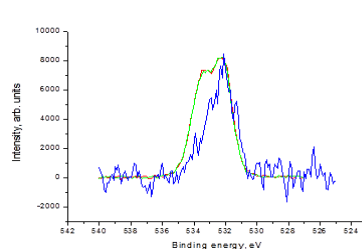
Figure 2. XPS spectra of O (1s) peaks
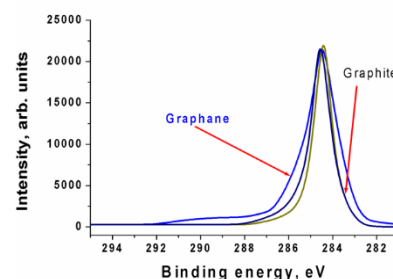
Figure 3. XPS spectra of C (1s) peaks

1.   X. L. Li, H. L. Wang, J. T. Robinson, H. Sanchez, G. Diankov and H. J. Dai, «Simultaneous Nitrogen Doping and Reduction of Graphene Oxide», *J. Am. Chem. Soc.*, 131, pp 15939-15944, 2009
2.   S. C. Ray, N. Soin, T. Makgato, C. H. Chuang, W. F. Pong, S. S. Roy, S.K. Ghosh, A. M. Strydom and J. A. McLaughlin, «Graphene Supported Graphone/Graphane Bilayer Nanostructure Material for Spintronics» DOI: 10.1038/srep03862

O1-3: Photoresponce in graphene under the influence of surface acoustic waves.

O.V. Kononenko, E.V. Emelin, V.N. Matveev, D.V. Roshchupkin

Institute of Microelectronics Technology and High Purity Materials, Russian Academy of Sciences, 6, Academician Osipyan st., Chernogolovka, 142432, Moscow region, Russia. E-mail: oleg@iptm.ru

Theoretical studies predict a range of rich physical phenomena arising from surface acoustic wave (SAW) -graphene interactions. Graphene opens up perspectives for solar power engineering [1, 2]. Graphene can be used as a structure in which the electron-hole pairs are formed due to the radiation effect. Graphene films are a good medium for SAW propagation. The charge transfer by the SAW in graphene [3] and controlling the SAW amplitude by electric potential applied to a graphene film [4] were reported. Here, we have investigated the acoustoelectric current in graphene as a function of UV light illumination.

Graphene films were grown on the nickel catalyst films by the low-pressure chemical vapor deposition (LPCVD) method with a single injection of acetylene [5]. The graphene quality was tested by the SENTERRA Bruker Raman microscope at the laser wavelength 532 nm.

The interdigital transducer (IDT) was fabricated by photolithography on the surface of lithium niobate to excite the SAW. The IDT consisted of 50 pairs of electrodes. The IDTs were fabricated to excite the SAW with the wavelength $\Lambda = 30$ µm at the resonance excitation frequency $f = 115$ MHz.

Transfer of the graphene film was done with the aid of polymethylmethacrylate (PMMA) that was spincoated onto the surface of the graphene film to serve as a support. The PMMA/graphene layer was detached from the substrate by wet-etching of the Ni film with a 1% water solution of hydrochloric acid and then manually laid on the piezoelectric substrate near the IDT. PMMA was then removed from the graphene surface by exposure to acetone in vapor and then liquid form. Two Pt electrodes were formed on the graphene film surface by electron beam lithography and e-beam evaporation. Measurements of the acoustoelectric current were made using a Keithley K2400 source-measurement unit.
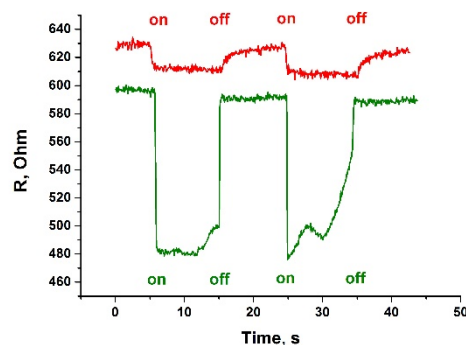
Fig.1. Graphene resistance without the SAW (upper curve) and under the SAW as a function of time periodically illuminated by UV light.

1. K. S. Novoselov, A. K. Geim, S. V. Morozov, D. Jiang, M. I. Katsnelson, I. V. Grigorieva, S. V. Dubonos, and A. A. Firsov, *Nature* 438, 197 (2005).
2. M. I. Katsnelson and K. S. Novoselov, *Solid State Commun*. 143, 3 (2007).
3. V. Miseikis, J. E. Cunningham, K. Saeed, R. O'Rorke, and A. G. Davies, *Appl. Phys. Lett*. 100, 133105 (2012).
4. Z. Insepov, E. Emelin, O. Kononenko, D. V. Roshchupkin, K. B. Tynyshtykbayev, and K. A. Baigarin, *Appl. Phys. Lett*. 106, 023505 (2015).
5. O.V. Kononenko, V.N. Matveev, D.P. Field, D.V. Matveev, S.I. Bozhko, D.V. Roshchupkin, E.E. Vdovin and A.N. Baranov *Nanosystems: Physics, Chemistry, Mathematics*. 5, 117 (2014).

O1-4: Multidimensional data visualization in chirality-dependent carbon nanotubes thermal and electrical properties

V. Kazakov[1], V. Shakhnov[1], A. Glushko[1], V. Makarchuk[1], E. Rezchikova[1], L. Zinchenko[1]

[1]*Bauman Moscow State Technical University, Moscow, Russia, shakhnov@mail.ru*

Many different mathematical models of carbon nanotubes are used for calculation of their properties [1-3]. In chirality-dependent variations analysis, a designer obtains a big numerical data file that has to be analyzed. In our approach, data is visualized [1]. A designer can analyze the obtained numerical and visual information simultaneously. In our presentation, we discuss application of our approach to visual analytics support for research of chirality-dependent carbon nanotube thermal and electrical properties. In [3], we have presented our approach for thermal properties visualization. However, it is difficult to visualize thermal and electrical properties simultaneously. In order to overcome this deficiency we apply two methods: parallel coordinates and heat maps. Both methods have been implemented in our software tool. Fig. 1 shows our main window.
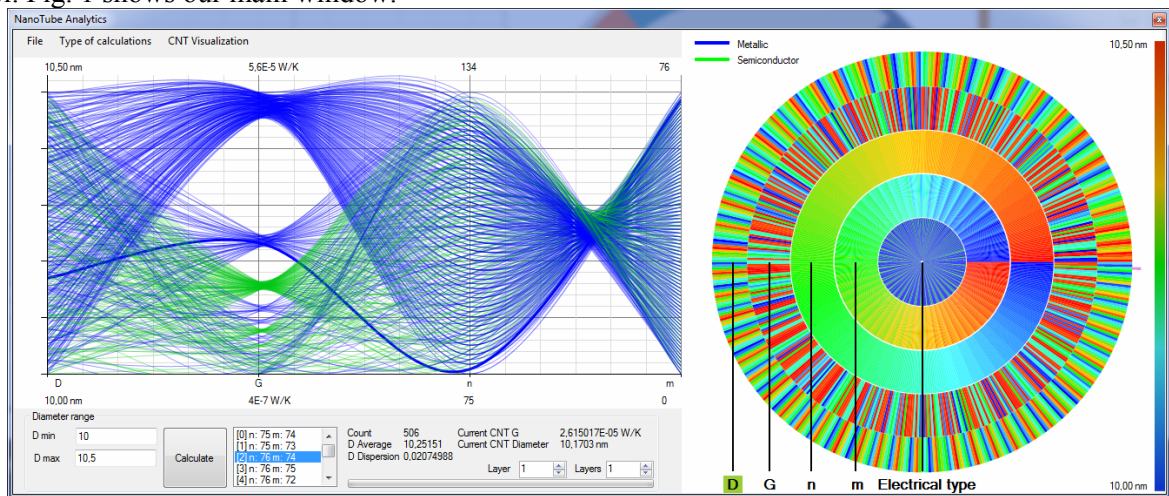
Figure 1. A variation tube analysis mode

The left section shows nanotubes variations by means of parallel coordinates, while the right section shows the presentation by means of circular heat maps. The bottom section is used It should be mentioned that in Fig. 1 we set that carbon nanotubes diameters *D* vary from 10 nm to 10.5 nm and the chirality indices *n* and *m* and the thermal conductivity of nanotubes per unit length *G* are calculated. Nanotubes with semiconductor electrical properties are shown in blue, while green color is used to show metallic nanotubes. In heat maps the outer ring shows the diameters, the next ring shows the thermal conductivity, then the chirality index of n, and then m. The inner circle shows the type of CNT, green - metallic type, blue - semiconductor. Heat maps allow analyzing the distribution of values and their clustering. Finally, we summarized advantages and deficiencies of our approach to visual analytics support for investigation of carbon nanotube variations.

1.   Shakhnov, V.A., Zinchenko, L.A., Rezchikova, E.V.: «Simulation and Visualization in Cognitive Nanoinformatics». *International Journal of Mathematics and Computers in Simulation* 1, 141-147, 2014.
2.   Kazakov, V., Verstov, V., Zinchenko, L., Makarchuk, V. «Visual Analytics Support for Carbon Nanotube Design Automation». In: Samsonovich A., Klimov V., Rybina G. (eds) *Advances in Intelligent Systems and Computing*, vol. 449, 2016.
3.   Shakhnov, V.A., Zinchenko L. A., Makarchuk, V.V., Rezchikova, E. V., Kazakov V.V. «Visual analytics in investigation of chirality-dependent thermal properties of carbon nanotubes». *Journal of Physics: Conference Series*, 1(829), 2017.

O1-5: Engineering of magnetic states in patterned ferromagnetic thin-film nanostructures

V.L. Mironov, E.V. Skorohodov, O.L. Ermolaeva, S.N. Vdovichev, S.A. Gusev and A.A. Fraerman

Institute for Physics of Microstructures, Russian Academy of Sciences, Nizhny Novgorod, Russia,
mironov@ipmras.ru

We discuss the possibilities to control the magnetic states in planar ferromagnetic nanostructures in dependence on varying material parameters, spatial architecture and external influences.

The patterned thin film ferromagnetic nanostructures are produced by e-beam lithography and ion etching. The structure of magnetization is studied by magnetic force microscopy method [1].

We demonstrate the wide set of magnetic states in different nanostructures such as vortex and antivortex states in nanoislands with different shape, helicoidal state in three-layer nanodiscs, domain walls in nanowires, babble and skyrmionic structures in patterned films with perpendicular anisotropy. The special attention is focused on the manipulation of magnetization in nanostructures by nonhomogeneous field of magnetic force microscope probe.

The application of magnetic nanostructures to the design of magnetic logic and data storage system is considered. Additionally the peculiarities of ferromagnetic resonance in ferromagnetic nanostructures are discussed in application to the development of microwave devices.

1. A.A.Fraerman, V.L.Mironov. «Magnetic States and Properties of Patterned Ferromagnetic Nanostructures. In "Frontiers of Nanoscience», Vol. 6, *Nanomagnetism: Fundamentals and Applications (Ed. C. Binns)*, Elsevier, pp. 189 – 216, 2014.

O1-6: Magnetic properties of metal nanowires, obtained by matrix synthesis technique

Zagorskiy D.L.[1], Bedin S.A.[1,2], Frolov K.V.[1], Artemov V.V.[1],Doludenko I.M.[1,3], Lomov A.A.[4], Chuev M.A.[4]

1 Center of Crystallography and Photonics of RAS, Leninsky pr.,59, Moscow   2 Moscow State Pedagogical University, Moscow, Pirogovskaya str,1/1, 3 High School of Economy, Mjasnitskaya,20   4 Physicotechnological Institute of RAS, Nachimovsky pr, 36

Nanowires (NWs) are 1-D nanosize structures, which are of great interest now. Ensembles of metallic NWs could be used as effective emitters of electrons ("cold cathodes"), surfaces for "micro-coolers" and for catalysis, and as the surfaces for non-linear optic units. Another application of NWs is connected with their special magnetic properties, depending on their shape. Among different methods of obtaining of such structures matrix synthesis is most perspective. The popular version of this technique is deposition of desired material inside the pores of specially prepared matrix [1]. In our case the matrix is Polymer track membrane (usually used for fine filtration), the materials are magnetic metals (of iron group) which are deposited inside the pores using galvanic (electrochemical) process [2,3].

Deposition process. Using electrolytes- solutions of salts of corresponding metals – it is possible to obtain replicas of porous structure made by different metals or their combinations. The potentiostatic electrodeposition process was investigated. It was found that it has non-linear character due to diffusion limitation inside the narrow pores. The processes of electrodeposition of monocomponent nanowires - pure magnetic metals (Fe, Ni and Co) were investigated [4,5] as well as deposition of multicomponent NWs. In the last case it is possible to obtain homogeneous structures ("alloys") and heterogeneous ("layers"). Microscopy investigation. Microscopy tests (SEM with elemental analysis) showed that the diameter of NWs is often higher than the diameter of the pores of template (possibly, due to polymer compression). Investigation of ensembles of Fe-Co and Fe-Ni NWs (alloys) demonstrated non-homogeneous distribution of elements (in microscale). It was shown that elemental composition changed along the nanowire` length. The features of electrodeposition were investigated and "anomalous co-deposition" was demonstrated. Mossbauer spectroscopy,The dependence of spectra parameters on pores diameters and grooving voltage was found. For pure Fe it was found that only at the lowest voltage (i.e. at the lowest grove speed) the obtained Fe NWs demonstrate "sextet" typical for pure bulk α-Fe. The dependence of magnetic orientation on pores diameter and grooving condition were also found. Multicomponent spectra were obtained for "alloys" , it was concluded that Fe-Ni wires consists of two phases. Crystal fine fields were estimated by Mossbauer spectroscopy [6,7]. Magnetic properties of obtained NWs were tested with vibrating magnetometer. Fe-Co wires were found to be hard-magnetic, while Fe-Ni are soft-magnetic. At the same time Fe-Ni wires with rather low diameters could demonstrate hard magnetic properties too. All samples demonstrated high magnetic anisotropy. Atomic –force microscopy was also applied for visualization of these nanowires embedded in host matrix.

1.   C. R. Martin, «Nanowires». *Science* 266, pp.1961-1971,1994
2.   N. Lupu (editor). «Electrodeposited NWs and Their Applications», *InTech*, Rijeka, Croatia, 2010
3.   M. Vazquez (editor). «Magnetic Nano- and Microwires»,*Woodhead*, Elsevier, 2015.
4.   V. V. Korotkov et al. «Specific features of electrodeposition of Cobalt into Micro- and Nano-size pores of Track Membranes» *Gal'vanotekh. Obrab. Poverkhn.* 19 (4), 23-27, 2011.
5.   V. V. Korotkov et al. «Electrodeposition of Metals of Iron Groop into the Pores of TM for the Preparation of NWs» *Gal'vanotekh. Obrab. Poverkhn.* 23 (1), 24 (2015).
6.   K. V. Frolov et al. «Synthesis, Phase Composition, and Magnetic Properties of Iron NWs Prepared in the Pores of Polymer Track Membranes» *JETP Lett*. 99, 570-575,2014
7.   K. V. Frolov et al. «Magnetic and Structural Properties of Fe–Co NWs Fabricated by Matrix Synthesis in the Pores of Track Membranes» *JETP Letters*,105, No. 5, pp. 319–326, 2017

O1-7: Obtaining and investigation of multilayer nanowires

Doludenko I.[1,2], Zagorskiy D.[1], Bedin S.[1,3]

[1]*Center of Crystallography and Photonics of RAS, Leninsky pr.,59, Moscow;*
[2]*National Research University Higher School of Economics,* 34 Talinskay, *Moscow;*
[3]*Moscow State Pedagogical University, Moscow, Pirogovskaya str,1/1;*
Email: doludenko.i@yandex.ru

Obtaining and investigation of various types of nanomaterials is an urgent task. It is of great interest to obtain the arrays (ensembles) of parallel oriented nanowires from a large number of alternating layers of magnetic and nonmagnetic metals. This work is devoted to the development of methods for obtaining arrays of nanowires consisting of alternating layers of NiFeCu and Cu. The idea of the work consists in the electrodeposition of metals from a solution containing ions of 3 metals. The method used in this work is based on the difference of the equilibrium potentials of metal deposition. This means that a metal with a lower equilibrium potential (Cu) will precipitate at a lower potential, in contrast to metals with a large equilibrium deposition potential (Ni, Fe). [1] To obtain arrays of multilayer nanowires (NWs0, the deposition was carried out in a polymer matrix of track membranes (thickness – 10 mkm; pore diameter – 0,1 mkm and pores density- 10^8 pores per sq.cm.). At the first stage, in order to create a conductive layer on the matrix, a layer of copper with a thickness of 5-10 mkm was deposited. The composition of the electrolyte for deposition of NWs : $NiSO_4 * 7H_2O$ – 16 g/l; $NiCl_2 * 6H_2O$ – 40g/l; $FeSO_4 * 7H_2O$ – 16 g/l; $CuSO_4 * 5H_2O$ - 5; $C_6H_8O_6$ – 1,5 g/l. Based on article [2], the optimal potentials for deposition of the Cu layer were chosen to be 0.8 V, and for deposition of the NiFeCu layer - 1.8 V. After electrodeposition, the matrix was removed, and we obtained an array of nanowires on a copper substrate.

Three types of nanowires were obtained. In samples 1 and 2, the precipitation was carried out at a constant potential, 0,8 V and 1,8 V respectively. This was done for elemental analysis and detection of the chemical composition of the layers. The results of elemental analysis are presented in Table 1. After that, deposition was carried out with a change in the potential for obtaining of multilayer nanowires (sample №3). Photos of an array of multilayer nanowires are shown in Figure 1.

Table 1

Chemical element	Atomic concentration of Cu layer elements	Atomic concentration of NiFeCu layer elements
Cu	99,57	72.84
Ni	0,16	18.77
Fe	0.27	8.39
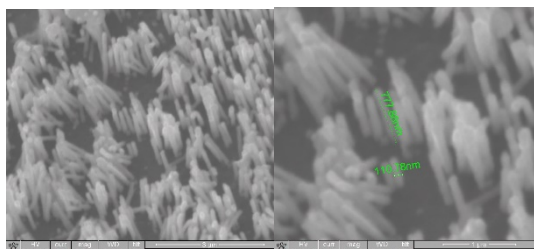
Figure 1. SEM photos of an array of nanowires

Based on the results of elemental analysis, one can see: in layers of Cu, we still have, although in a small fraction, the atoms of Ni and Fe; in layers of NiFeCu, the nickel concentration is 2 times higher than that of iron. A large amount of Cu in in layers of NiFeCu determined by the Cu substrate.

Conclusion

In the course of the work, Elemental analysis results were obtained, confirming the difference in the chemical composition of the layers as a function of the potential. A sample of an array of multilayer nanowires was obtained and its photographs were investigated.

1. Fedosyk V.M. «Nanostructured films and nanowires». *M. : Publishing center BSU*, 2006. – 311.
2. E.V. Armensky «Interuniversity scientific and technical conference of students, graduate students and young specialists». Conference materials. - *M. : MIEM NRU HSE*, 2017. – 502.

O1-8: Phase locking of the spin torque nanooscillators

A. Safin, M. Kapranov, N.Udalov

National Research University "MPEI", Moscow, Russia, E-mail addres: arsafin@gmail.com.

A promising direction in the development of spintronics is related to spin-polarized current transfer in nanodimensional magnetic multilayer structures. Possible applications include magnetic random-access memory, super-responsive magnetic sensors, and oscillators for microwave and THz frequency ranges. The main disadvantages of spin-transfer (or spin-torque) nano-oscillators (STNOs) are low output power of generated oscillations (from several picowatts to several nanowatts) and large width of spectral lines (up to several hundred megahertz in the GHz range), which significantly restrict the application of existing STNOs in telecommunication systems. At present, several methods are known for increasing the power of STNOs, in particular, by using magnetic tunnel junctions with intermediate multiferroic layers, which provide a significant increase in the sample resistance and, hence, in the output power in external magnetic and electric fields. Another possibility is provided by using mutual [1] and/or external synchronization of many STNOs so that their output powers would add on the common load [2]. There are several studies of STNOs phase locking achieved by various physical mechanisms: through electrical connection in series of oscillators, by spin-wave propagation, by antivortices, and by dipolar coupling. Nevertheless, the theoretical description of the synchronization dynamics of STNO is more complicated than traditional limit-cycles oscillators (van der Pole oscillators, Josephson junctions, rotating pendula) which have constant orbit radius, and can be described in single oscillator case by the Adler equation. Due to technologically fabricated nonidentity of STNOs in the network [1] they can be expressed by generalized Adler-like equations. In this work, we investigate analytically and numerically the mutual synchronization dynamics in the complex networks of vortex-based [3,4] spin transfer nano-oscillators (STNOs). We consider the STNO whose free layer configuration is a magnetic vortex. The vortex state can be characterized by in-plane magnetization, and a nanometer-size region of the vortex core with out-of-plane magnetization. We describe the dynamics of many vortices, which gyrotropic motion is driven by the injection of a DC spin-polarized current. They can be described by gyration radiuses $R_l(t)$ and phases $\varphi_l(t)$, or vectors $\mathbf{R}_l = R_l \cdot (\mathbf{e}_x \cos\varphi_l + \mathbf{e}_y \sin\varphi_l)$, where $l = 1..N$. The vortex motion given by $\mathbf{R}_l$ we propose using coupled Thiele equations [3] with additional spin transfer torque terms:

$$G\left(\mathbf{e}_z \times \frac{d\mathbf{X}_l}{dt}\right) + k_l\mathbf{X}_l + D_l\frac{d\mathbf{X}_l}{dt} - \mathbf{F}_{STT,l} - \mathbf{F}_{\text{int}}\left(\mathbf{X}_1, \mathbf{X}_2, ..., \mathbf{X}_N\right) = 0, \qquad (1)$$

where G is the gyroconstant, $k_l\mathbf{X}_l$ k_l is the confining force, D_l is the damping constant, $\mathbf{F}_{STT,l}$ is the spin-transfer torque force, and $\mathbf{F}_{\text{int}}\left(\mathbf{X}_1, \mathbf{X}_2, ..., \mathbf{X}_N\right)$ is the interaction force between STNOs. Using (1) we identify that the introduction of a leader in a network of mutually coupled STNOs, an oscillator having large energy level, in the network induces a profound change in the critical interpillar distances on which mutual synchronization occurs as a function of their radius mismatch for different type of network topologies. The emergence of a leader leads to the reduction of synchronization time between coupled STNOs. We obtain numerically phase portraits showing the transition between synchronized and unsynchronized states for two mutually coupled STNOs with strongly nonidentical energetic parameters, which is equivalent to the impact of a leader.

1.   A.R. Safin, N.N. Udalov, M.V. Kapranov. «Mutual phase locking of very nonidentical spin torque nanooscillators via spin wave interaction», *Eur. Phys. J. Appl. Phys*, 67, 20601, 2014.
2.   A.R. Safin, N.N. Udalov, M.I. Bichurin, R.V. Petrov, A.S. Tatarenko. «Loading characteristics of a spin-transfer nano-oscillator», *Tech. Phys. Lett.*, 43, 3, pp.305-308, 2017.
3.   A.D. Belanovsky, N. Locatelli, P.N. Skirdkov, F. Abreu Araujo, J. Grollier, K.A. Zvezdin, V. Cros, and A.K. Zvezdin. «Phase locking dynamics of dipolarly coupled vortex-based spin transfer oscillators», *Phys. Rev*. B 85, 100409(R), 2012.
4.   V. Flovik, F. Macia, E. Wahlstrom. «Describing synchronization and topological excitations in arrays of magnetic spin torque oscillators through the Kuramoto model», *Sci. Rep.*, 6, 32528, 2016.

O1-9: Charge–coupling effects in SOI thin film magnetosensitive nanotransistor

A. Leonov[2], M. Il'nitsky[1], V. Mordkovich[2] , V. Popov[1]

1. Institute of Semiconductors Physics, Russian Academy of Sciences, Novosibirsk, Russia, E-mail: popov@isp.nsc.ru. 2. Institute of microelectronics technology and Hich Purity Materials, Russian Academy of Sciences, Chernogolovka, Russia
E-mail: alex25.08@mail.ru

SOI thin film Hall type double gates transistor with built – in accumulation channel and metal- insulator- Si- insulator - matal (MISIM) field control system is a very attractive transducer for the nano – and microelectronics providing the increasing of magnetosensitivity, radiation immunity, temperature range of operation and circuit opportunities in compare with conventional Si Hall elements [1]. In this report presented the theoretical and experimental results about the influence of so-called change –coupling effect (CCE) due to variations of gates potentials of the MISIM system on such magnetotransistor properties. It was demonstrated that CCE influence on the transistors channel current and magnetosensitivity.

The detected increase in magnetic induced signal (Hall emf) is not only due to the growth of the channel current for certan values of supply voltage and potentials of the gates, but also to increase the mobility of electrons due to their redistribution in the transverse electric field between the gates, leading to reduce the influence of electrons surface scattering. It was also investigated the dependence of CCE of the channel thickness variations (4 – 200 nm), temperature (2 – 400K), concentration of surface states on SiO_2 -Si interfaces and surface states nature.

1.   M. Baranochnikov, A. Leonov, V. Mordkovich, D. Pazhin and M. Filatov «Some Features of Magnetomettic and Sensor Devices Based on the Field Effect Hall Sensor» *Proc. Advanced Electromagnetics Symposium AES* – 2012 Paris – France, p. 455 – 459

O1-10: Dynamic-XPS measurements by means of new Fast-XPS end-station based on Argus spectrometer at PETRA III (DESY/Hamburg)

Olga Molodtsova[1,2], Sergey Babenkov[3], Victor Aristov[1,4], Frank Scholz[1], Joern Seltmann[1], Ivan Shevchuk[1], Leif Glaser[1], and Jens Viefhaus[1]

1.Deutsches Elektronen-Synchrotron DESY, Hamburg, Germany, olga.molodtsova@desy.de.
2. National Research University of Information Technologies, Mechanics and Optics, Saint Petersburg, Russia. 3. Institut für Physik, Johannes Gutenberg-Universität, Mainz, Germany, sergey.babenkov@desy.de.
4. Institute of Solid State Physics of Russian Academy of Sciences, Chernogolovka, Russia, victor.aristov@desy.de

Using dynamic-XPS method is a big step toward understanding of fast processes on the solid surfaces and sub-surfaces of advanced materials, which are taking place during changing of different conditions. The experimental setup for such experiments, based on a hemispherical electron spectrometer Argus (Omicron NanoTechnology GmbH), have been built up, commissioned and currently is available for regular users of beamline P04 (PETRA III, DESY) [1]. Such combination allows acquiring both traditional scanning and extremely fast snapshot (down to 0.1 sec/spectrum) XPS spectra of several core levels (CL). It opens new possibilities to real time characterization of the fast processes both from quantitative and qualitative point of view by dynamical measuring of XPS. The concept was verified by real time XPS characterization of thermally induced process of graphene formation on model cubic-SiC(001)/Si(001) wafer [2-6]. We were able to control time/temperature/rare-gas pressure parameters and follow the changes in C 1s CL spectra (see Figure). Moreover, we present the dynamic-XPS study of controllable metal-organic interface formation (Indium/CuPcF4) at room temperature conditions, also the investigations of hybrid systems consisting of metal nanoparticles (gold, silver and aluminum) embedded in the organic semiconductor matrix with molecular single crystal properties CuPcFx through study of their fundamental characteristics [7-8].
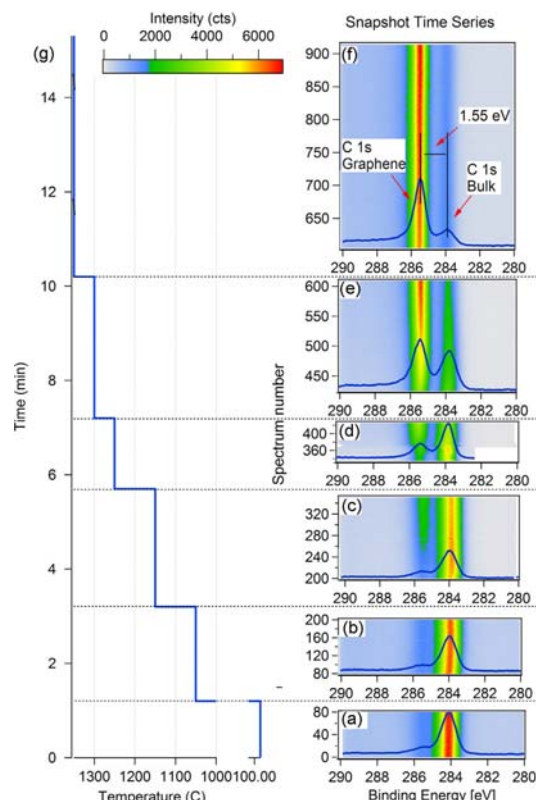
1. S.V. Babenkov, V.Y. Aristov, O.V. Molodtsova et al., «A new fast-XPS end-station for beamline P04 at PETRA III/DESY», *Nuclear Instruments and Methods in Physics Research A*, 777, pp.189-193, 2015

2. A.N. Chaika, O.V. Molodtsova, V.Yu. Aristov et al., «Continuous wafer-scale graphene on cubic-SiC(001)», *Nano Research*, 6, pp.562-570, 2013

3. A.N. Chaika, O.V. Molodtsova, S.V. Babenkov, V.Yu. Aristov et al., «Rotated domain network in graphene on cubic-SiC(001)», *Nanotechnology*, 25, pp.135605 (1-8), 2014

4. H.-C. Wu, A.N. Chaika et al., «Transport Gap Opening and High On-Off Current Ratio in Trilayer Graphene with Self-Aligned Nanodomain Boundaries», *ACS Nano*, 9, pp.8967-75, 2015

5. H.-C. Wu, A.N. Chaika et al., «Large Positive In-Plane Magnetoresistance Induced by Localized States at Nanodomain Boundaries in Graphene», *Nature Communications 8*, pp.14453 (1-9), 2017

6. A.N. Chaika, V.Yu. Aristov, O.V. Molodtsova, «Graphene on cubic-SiC», *Review Paper, Progress in Materials Science*, 89, pp.1-30, 2017

7. O.V. Molodtsova, I. M. Aristova, S.V. Babenkov, V.Yu. Aristov et al., «Morphology and properties of a hybrid organic-inorganic system: Al nanoparticles embedded into CuPc thin film», *J. Appl. Phys.*, 115, pp.164310 (1-7), 2014

8. S.V. Babenkov, O.V. Molodtsova, I.M. Aristova, V.Y. Aristov et al., «Hybrid organic-inorganic systems formed by self-assembled gold nanoparticles in CuPcF4 molecular crystal», *Organic electronics*, 32, pp.228-236, 2016

O1-11: Far-field Optical Superresolution in Scanning Differential Heterodyne Microscope

I. M. Akhmedzhanov, D. V. Baranov, E. M. Zolotov

Prokhorov General Physics Institute, Russian Academy of Sciences, Moscow, Russia
e-mail: eldar@kapella.gpi.ru

Optical heterodyne microscopy is promising method for measurements and characterization of submicron structures. Due to coherent detection system the response of scanning differential heterodyne microscope (SDHM) contains both phase and amplitude information of diffracted optical field at an intermediate radio frequency. Use of common path scheme in SDHM makes it practically insensitive to microphonics, that is especially important in various applications.

Formerly it was shown [1] that application of special mathematical algorithm based on analytical extrapolation of limited optical spectrum makes possible to achieve optical superresolution, the superresolution coefficient being $M \sim 2$. The coefficient M is defined as the ratio of extrapolated spectrum width and original aperture spectrum width.

Here we present the alternate approach to optical resolution enhancement based on the difference of phase and amplitude response of SDHM. In this case the resolution is defined as the width of point spread function and the superresolution coefficient SR is defined as the ratio of amplitude response width and phase response width [2]. The investigation is carried out theoretically and experimentally with metalized phase and dielectric amplitude-phase objects on silicon substrate. Measured superresolution coefficient is $SR = 2.0 \pm 0.5$.
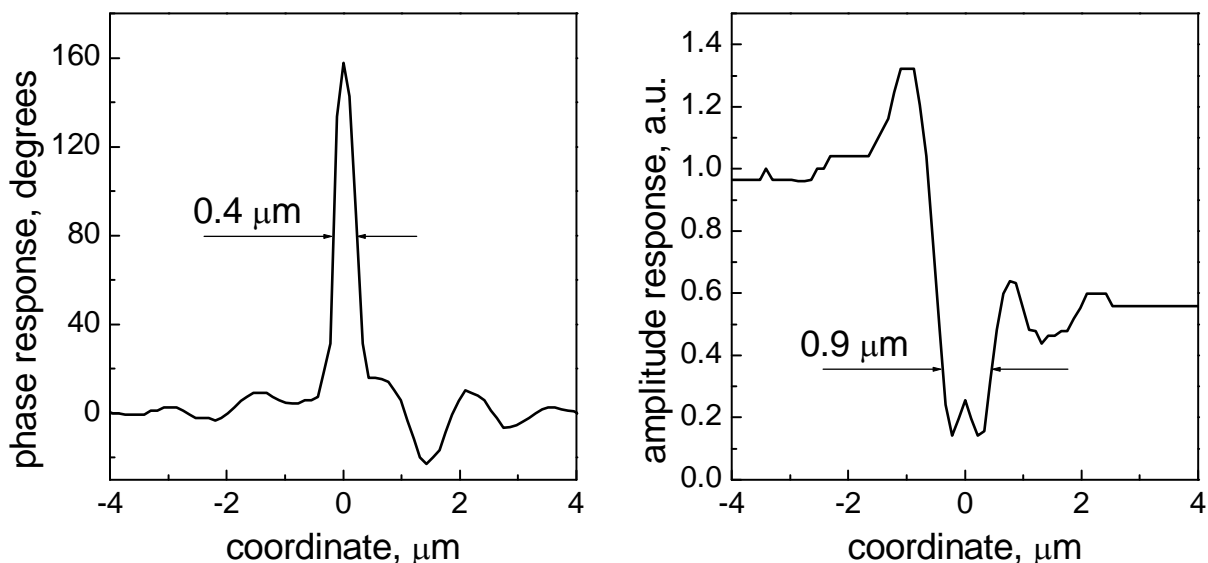
Fig. 1. Experimental complex response of SDHM to test submicron amplitude-phase step-like object.

1.   D. V. Baranov, E. M. Zolotov, "Superresolution processing of the response in scanning differential heterodyne microscopy", in *Advances in Information Optics and Photonics*, ed. A. Friberg and R. Dandliker, SPIE, Bellingham, WA, pp. 229–250, 2008

2.   E. L. Kosarev, *Experimental data processing methods*, Ch. 9, Fizmatlit, Moscow, 2008 (in Russian)

O1-12: Application of spectroscopic ellipsometry to characterization of deposition processes of with monolayer precision

I. Clemente[1,2], A. Miakonkikh[1,2]

1. Institute of Physics and Technology, Russian Academy of Sciences, Moscow, Russia,
clemente.iosif@gmail.com.
2. Moscow Institute of Physics and Technology, Dolgoprudny, Russia.

Modern nanoelectronic applications need precise deposition and treatment of nanometer-thick films. Developing methods such as area selective atomic layer deposition require sub-nanometer measurements of seed and interfacial layers. At the same time, methods of studying such films and also surface processes, i.e. adsorption, desorption, and surface chemical reactions, which occur during their treatment, are necessary. Spectroscopic ellipsometry (SE) [1] is suitable method for this task. SE is an optical technique, so it is non-destructive and contactless. In addition the sample does not require additional preparation, which makes SE a convenient method for *in situ* diagnostics of technological processes. Ellipsometry is able to measure the thickness of films with high precision (~0.1 Å), which are used in studying the initial stages of growth of thin films [2]. Also, ellipsometry is sensitive to a change in the optical properties of monolayer films, which was shown in the study of the deposition of ALD films on graphene [3]. Fig. 1a shows every half cycle measurements of apparent thickness of alumina, where could be seen adsorption of precursor and surface oxidation by plasma (apparent thickness decrease). Fig. 1b depicts graphene apparent thickness during this process.
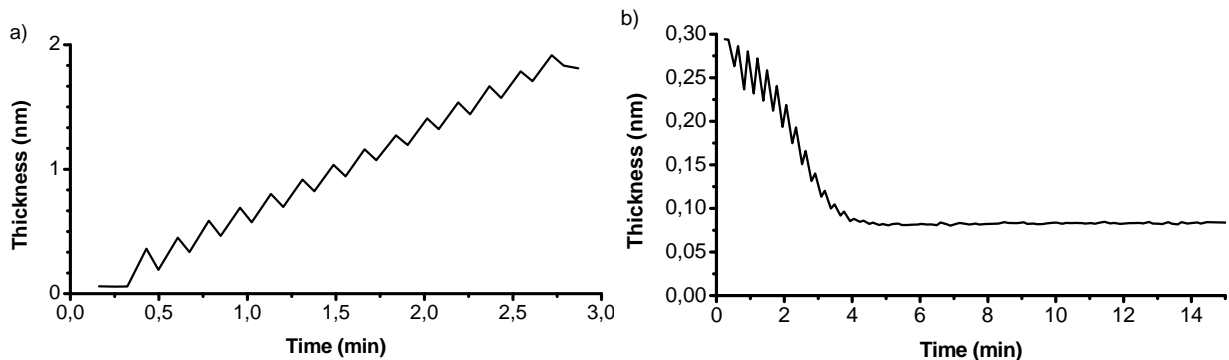
Figure 1. Apparent thickness of deposited alumina (a) and underlying graphene (b) during ALD process by *in situ* ellipsometry.

Results of *in situ* measurements of ALD layers of high-k dielectrics (Al_2O_3, HfO_2) on transparent substrates and graphene will be presented. In the later case the level of damage of graphene during the ALD process could be estimated by *in situ* SE.

Also, SE allows estimating sticking probability coefficient, and desorption rate of different precursor molecules. Results for TMA ($Al(CH_3)_3$) and TEMAH ($Hf(NC_2H_5CH_3)_4$) will be presented. These data are important for development of simulation models of ALD for high aspect structures.

Although ellipsometry also has several disadvantages, such as low spatial resolution (spot diameter up to 1 mm), complexity in developing an optical model that correctly describes the whole series of phenomena, and as a consequence, a simplification of the model, all of the above advantages make spectroscopic ellipsometry a powerful technique for diagnosing the sub-nanometer scale technological processes of nanoelectronics.

1. H. Fujiwara, «Spectroscopic Ellipsometry: Principles and Applications». *John Wiley & Sons, Chichester*, England; Hoboken, NJ, 2007.
2. Clemente I.E., Miakonkikh A.V., «Application of spectral ellipsometry to in situ diagnostics of atomic layer deposition of dielectrics on Silicon and AlGaN», *Proc. of SPIE*, 10224, pp. 1022425-1-7 , 2016
3. I Clemente, A Miakonkikh, O Kononenko, V Matveev, K Rudenko. «Comparative study of thermal and plasma enhanced atomic layer deposition of aluminum oxide on graphene». *IOP Journal of Physics: Conference Series*. In print.

O1-13: Analysis of hydrogen distribution in materials by nuclear backscattering of protons

N. Tkachenko, V. Vostrikov

Skobeltsyn Institute of Nuclear Physics, Moscow State University. email: info@sinp.msu.ru

Перспективными материалами для долговременного хранения водорода являются алюминий, магний, титан. Возможно как применение порошков гидридов, так и твердых расплавов AlxHy, MgxHy и TixHy с нанесенными на поверхность защитными плёнками для предотвращения выхода водорода из аккумуляторов. В реакторостроении гидрид титана используется в качестве замедлителя в компактных реакторах и реакторах на быстрых нейтронах, а также материала защиты. В то же время относительного другого конструкционного материала реакторов – циркония и его сплавов, применяющегося для изготовления оболочек ТВЭЛов, гидрирование приводит к ухудшению механических свойств и сокращает срок службы изделий. Следовательно, для анализа содержания водорода в материалах требуется метод, позволяющий с большой точностью определять относительно большие количества водорода и профиль его диффузии а также деградации содержания с течением времени.

Для определения содержания водорода в материалах широко используются химические методы анализа, позволяющие определить усредненное по объему содержание водорода и разрушающие образец. Это не позволяет применять их в ситуации, когда над образцом планируется провести дополнительные испытания (на теплостойкость или на стойкость к коррозии). Как следствие, для анализа водородосодержащих материалов и контроля его диффузии требуется метод, обладающий неразрушающим характером для последующих испытаний материалов и высоким разрешением по глубине анализа, что позволило бы изучать изделия с нанесенными защитными покрытиями.

На данный момент разработано множество ядерно-физических методов анализа, обладающих неразрущающим характером и позволяющих регистрировать наличие водорода в материалах, однако применение каждого ограничено из-за сути использующихся процессов. Так, анализ с помощью ядерных реакций позволяет осуществлять прямое детектирование водорода и профилирование распространения водорода в материале, но не дает никакого представления о содержании иных элементов в образце и требует привлечения других методов анализа [1]. Широко распространенный метод ядер отдачи имеет сильные ограничения по глубине анализа, что позволяет проводить анализ только изделий без защитных покрытий [2]. Метод определения водорода с помощью резерфордовского обратного рассеяния (РОР) электронов, предложенный в работе [3], обладает неоспоримыми достоинствами в виде прямого детектирования водорода и высокой чувствительности, но применим только к тонким (до 40 нм) пленкам гидридов.

В настоящей работе для анализа водородосодержащих материалов предложен метод, основанный на спектрометрии ядерного обратного рассеяния, позволяющий косвенно обнаруживать водород при одновременном элементном анализе состава изделий на глубину до 100 мкм, что позволяет анализировать пригодность различных защитных покрытий для предотвращения гидрирования конструкционных материалов или выхода водорода из аккумуляторов.

1. L.S. Wielunski, D. Grambole, U. Kreissig b, R.Grotzschel, G. Harding, E. Szilagyi «Hydrogen depth resolution in multilayer metal structures, comparison of elastic recoil detection and resonant nuclear reaction method» *Nuclear Instruments and Methods in Physics Research* B 190 (2002) *p. 693–698.*

2. Joonkon Kim, Han Woo Choi, Hyung Joo Woo, Gi Dong Kim «Hydrogen analysis in diamond like carbon by elastic recoil detection» *Current Applied Physics* 10 (2010) p. 498–502.

3. Maarten Vos «Detection of hydrogen by electron Rutherford backscattering» *Ultramicroscopy* 92 (2002) p. 143–149.

4. Borisov A.M., Vostrikov V.G., Ivanova S.V., Kulikauskas V.S., Lesnevsky L.N., Lyakhovetsky M.A., Romanovsky E.A., Tkachenko N.V., Tyurin V.N. «The Study of Zirconium Alloy Coatings Produced by Microarc Oxidation Using Rutherford and Nuclear Backscattering Spectrometry» *Surface Investigation X-Ray, Synchrotron and Neutron Techniques* 7, 2013, p. 437-441

O1-14: Determination of the ionization distance from emitter surface and ionization zone near surface during field evaporation of molybdenum at high temperatures

O. Golubev and N. Blashenkov

Ioffe Physical-Technical Institute, Russian Academy of Sciences, St. Petersburg, 194021 Russia, e-mail:
O.Golubev@mail.ioffe.ru

The phenomenon of field evaporation, according to which surface atoms are evaporated in the form of positive ions under the action of a strong electric field alone at field strength $F_{ev} \sim 10 - 60$ V/nm has been known for a rather long time [1]. The field ion point sources using both field evaporation and field ionization can be interest for various aims of a nanotechnology. The problem of determining a distance from the emitter surface, at which the formation of ions from field-desorbed atoms take place was originally set in investigation of field ionization of gases and the typical ionization distance x_{cr} for the most gases 0,45-0.60 nm. During the field evaporation of metals at cryogenic T, ions can be multiply charged, $F_{ev} \sim 50\text{-}60$ V/nm and x_{cr} can be smaller than the atomic radius [1] For this reason, it was commonly accepted that x_{cr} in the case of field evaporation has no real physical meaning and atoms are evaporated in the ionized form directly from the emitter surface. But if field evaporation takes place at high emitter T, the situation becomes different. Specific features of field evaporation at high T are (i) sharp drop in the ion charge with increasing of T because of a significant decrease in F_{ev} and (ii) noticeable evaporation activation energy Q_n as compared to nearly zero value for the evaporation at cryogenic T [2]. Once Q_n is nonzero the x_{cr} can also be more significant. The main task of this work was to determine a distance from the emitter surface at which Mo atoms transform into ions under evaporation at high T and F_{ev}. Steady-state field evaporation of Mo at high emitter temperatures T $\sim$ 2000 K has been studied using a magnetic mass- spectrometer equipped a field ion sources and possessing a mass resolution of $\delta m/m \sim 1/200$. The resolution was enough to observe the ions of all 7 isotopes of Mo with masses from Mo^{92} to Mo^{100}. The rise of emitter T leads to sufficient decrease evaporation field strength F_{ev} and at the T = 1400 – 2000 K the value was $F_{ev} \sim 30$ V/nm is noticeable smaller then the value $F_{ev} \sim 46$ V/nm obtained for field evaporation at cryogenic emitter T. While the mass spectra measured during field evaporation at room T showed the presence of predominantly Mo^{+3} ions, an increase of emitter T led to the appearance of Mo^{+2} and Mo^{+} ions, while the main peak observed at T $\geq$ 1400 K was due to Mo^{+} ions. The measured ion energies and F_{ev} values were used to determine the critical ionization distance x_{cr} and ionization zone Δ for single and double charged ions. If for ions Mo^{+} the values are $x_{cr} = 0.51$ nm and $\Delta = 0.27$ nm then for ions Mo^{+2} these values are $x_{cr} = 0.57$ nm and $\Delta = 0.20$ nm. For the process of high temperature field evaporation at not too high F_{ev} these results indicate, first, that Mo atoms are not evaporated in the form of ions directly from the emitter surface, but are ionized near the surface at a distance of about two atomic diameters (Mo atom diameter, 0.278 nm) within the narrow zone of width $\Delta \sim 0.20 – 0.27$ nm. Second, the fact that the values $x^1_{cr} < x^2_{cr}$ and $\Delta^2 < \Delta^1$ apparently confirm the existing notion concerning the formation of multiple charged ions during field evaporation, according to which single charged ions appear first and then exhibit sequential ionization to become multiply charged [3].

1.   E.W. Muller and T.T. Tsong «Field Ion Microscopy, Field Ionization and Field Evaporation»,*Pergamon Press*, Oxforg, 1979
2.   O.L. Golubev at al. *Tech. Phys.*, 52, 10, pp. 1258-1265, 2007
3.   G.L. Kellog, *Surface Science*, 120, pp. 319-326, 1982

O2-1: Self-organization and phase transition in the macroscopically flat lipid multilayers at the surface of colloidal silica

Y.O. Volkov[1], B.S. Roshchin[1], V.E. Asadchikov[1], A.M. Tikhonov[2], V. Honkimäki[3], M. Blanco[3]

1. FSRC «Crystallography and Photonics» RAS, Moscow, Russia
2. Kapitza Institute for Physical Problems RAS, Moscow, Russia
3. European Synchrotron Research Facility, Grenoble, France
E-mail: neko.crys@gmail.com

A phospholipid bilayer on liquid substrate can be used as the simplest model of a cell membrane [1]. Previously, the method of preparation of macroscopically flat lipid films with the use of colloidal silica hydrosols as substrates has been proposed [2]. Due to the specific boundary conditions at air/sol interface, polar lipid molecules exhibit a spontaneous ordering effect, leading to formation of a regular multilayer.

In this report we present the investigations on the dynamics of self-organization and temperature crystal-gel phase transition for lipid multilayers with the simultaneous use of specular x-ray reflectivity, diffuse x-ray scattering and grazing incidence x-ray diffraction techniques. Model phosphocholine (DSPC, DPPC) and phosphoserine (DMPS) lipid films have been studied; silica sol Ludox FM (particle diameter 5 nm, vol. concentration 16% SiO_2, 0.2% NaOH) has been used as substrate. All experiments have been carried at ID31 beamline of European Synchrotron Radiation Facility (radiation energy E = 71 keV, monochromaticity $\Delta E/E \approx 10^{-3}$). Depth-graded distributions of electron density have been extracted from the specular reflectivity curves by the model-independent reconstruction algorithm [3], then further refined with the 1-D scattering curves in the frames of distorted-wave Born approximation with interbilayer interactions' model according to the smectic liquid crystal theory [4].

According to the obtained reflectivity and scattering data, the lipid film spontaneously forms a regular multilayer structure in 1-3 hours after the deposition on a sol substrate. Electron density distribution corresponds to a periodic stack of 4-6 sub-layers with period d close to the thickness of crystallic lipid bilayer (68 Å for DSPC and 65 Å for DPPC), while overall thickness of self-ordering region corresponds to the Debye screening length in silica sol ($\Lambda_D \approx 500$ Å). However, electron density distribution in bilayer stack exceeds known theoretical values [5] by 10-12%. We assume the latter might be explained with absorption of Na^+ ions from substrate within the lipid layer following the electroporation effect [6].

Grazing diffraction scan reveals a single characteristic peak at $q_{xy} \approx 1.48$ Å^{-1} for DSPC and DPPC lipids, which corresponds to hexagonal crystallic lattice with cell parameter $a \approx 4.91$ Å. Estimated surface area per one hydrocarbon chain S equals 20.8 Å^2, being in a good agreement with its theoretical value for hexagonal crystallic phase of DSPC and DMPS lipids [1].

Additionally, a temperature phase transition in the DMPS lipid layer have been observed. Under ambient temperature (23°C) DMPS prepared at the surface of silica sol forms an ordered multilayer structure similar to the described above. Analysis of X-ray reflectivity data shows a regular stack with period $d \approx 152$ Å. Grazing diffraction finds a single peak at $q_{xy} \approx 1.54$ Å^{-1}, which corresponds to the hexagonal crystallic lattice with cell parameter $a \approx 5.03$ Å. However, after heating the sample up to 40°C the diffraction peak vanishes while depth-graded lipid stack dissipates, which indicates melting of lipid film. It should be noted that within a comparable time after cooling the sample (around 3 hours) no evidence of re-ordering have been found; the latter points that the crystal-liquid phase transition is irreversible for the DMPS lipid multilayer.

1. D. M. Small, «The Physical Chemistry of Lipids», *Plenum Press*, NY, 1986.
2. A. M. Tikhonov, *JETP Letters* 92, pp. 394-397, 2010.
3. I. V. Kozhevnikov, *Nucl. Instr. Meth. Phys. Res*. A 508, pp. 519-541, 2003.
4. H. Petrache, N. Gouliaev, S. Tristram-Nagle et al., *Phys. Rev*. E 57, pp. 7014-7024, 1998.
5. N. Kucerka, M.-P. Nieh, J. Katsaras, *Biochim. Biophys. Acta* 1808, pp. 2761-2771, 2011.
6. A. Tikhonov, V. Asadchikov, Y. Volkov et al., *JETP Letters* 104, pp. 880-887, 2016.

O2-2: Diffusion effect on nucleation in supersaturated surface solutions

M. Sorokin[1], V. Dubinko[2], V. Borodin[1]

1. Russian Research Centre 'Kurchatov Institute', Moscow, Russia, m40@lab2.ru
2. National Science Center 'Kharkov Institute of Physics and Technology', Kharkov, Ukraine

The nucleation of islands in a supersaturated solution of surface adatoms is considered taking into account the possibility of diffusion profile formation in the island vicinity [1,2]. In this case the conventional analytical approach, based on the Fokker-Planck equation (FPE) or similar treatments might fail, because one has to consider the deviation of the adatom concentration in the nucleus vicinity from the average one. Indeed, the diffusion profiles of adatoms in the islands vicinity include adatoms previously emitted by the clusters (Fig. 1), so that the island growth has the memory effect and might lose the Markovian property, which is prerequisite for the FPE.
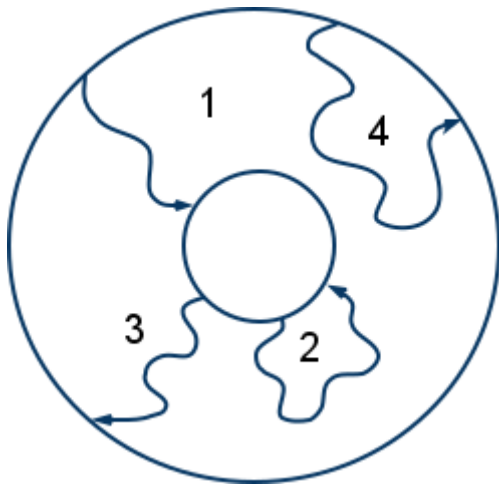
g. 1. Processes contributing to the adatom transport in the zone of influence of a selected island [1].
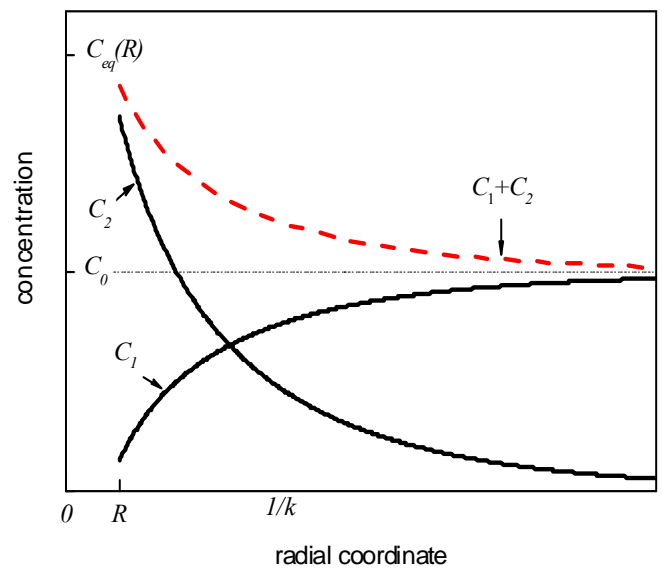
Fig. 2. The concentration profiles of adatoms, participating in the separated absorption (C_1) and desorption (C_2) processes. Their sum C_1+C_2 (dashed curve) provides diffusional profile in the vicinity of a selected island, where both processes are taken into account.

Even for sufficiently large nuclei, where diffusion profiles of adatoms adjust themselves to the actual island sizes, the probabilities of absorption and desorption of adatoms at the island interfaces should be redefined in order to get rid of the current **2** and to use the only the 'net' absorption current **1** and desorption **3** for the evaluation of kinetic coefficients (Fig. 2). When applied to the problem of surface island nucleation, our treatment predicts the steady-state nucleation barrier, which coincides with the conventional thermodynamic expression, even though no thermodynamic equilibrium is assumed and the adatom diffusion is treated explicitly. The effect of adatom diffusional profiles on the nucleation rate pre-exponential factor is also discussed. Monte-Carlo simulation is employed to analyze the applicability domain of the Fokker-Planck equation and diffusion effect beyond it. It is demonstrated that diffusional cloud is tending to slowdown the nucleation process.

1.   M.V. Sorokin, A.E. Volkov, «Effect of diffusion on nucleation of two-dimensional nanoislands», *Phys. Rev*. E, 72, pp. 051603/1-8, 2005
2.   M.V. Sorokin, V.I. Dubinko, V.A. Borodin, «Applicability of the Fokker-Planck equation to the description of diffusion effect on nucleation», *Phys. Rev*. E, 95, pp.012801/1-8, 2017

O2-3: Metallic nanoparticles self-assembled in organic matrix: morphology and the electronic properties

I.M. Aristova[1] , O.V. Molodtsova[2,3] , V.Yu. Aristov[1,2] , and S.V. Babenkov[4]

1. Institute of Solid State Physics of Russian Academy of Sciences, Chernogolovka, Russia, aristova@issp.ac.ru, aristov@issp.ac.ru.
2. Deutsches Elektronen-Synchrotron DESY, Hamburg, Germany, olga.molodtsova@desy.de, victor.aristov@desy.de. 3. National Research University of Information Technologies, Mechanics and Optics, Saint Petersburg, Russia.
4. Institut für Physik, Johannes Gutenberg-Universität, Mainz, Germany, sergey.babenkov@desy.de

Today, the information technologies have impetuous spreading in all spheres of our life due to simultaneous super miniaturization, increase of performance and, consequently, expansion of the scope of functions provided by next generation of mobile gadgets. In this regard, more capacious, robust, compact and faster memory storages have an enormous demand. Resistive random-access memory (RRAM) would revolutionize the information technology industry [1]. Materials with a high on-off resistance ratio, e.g. hybrid organic–inorganic systems, mainly consisting of inorganic nanoparticles blended into an organic matrix could become the basis for RRAM. Properties of the hybrid organic-inorganic systems composed of metallic nanoparticles distributed in an organic matrix as a function of nominal metal content was studied by transmission electron microscopy and by surface- and bulk sensitive photoelectron spectroscopy [2-4]. The properties of the nano-composite thin-film are supposed to be significantly dependent on their microstructure, i.e. the size, concentration, bulk- and size-distribution of nanoparticles.
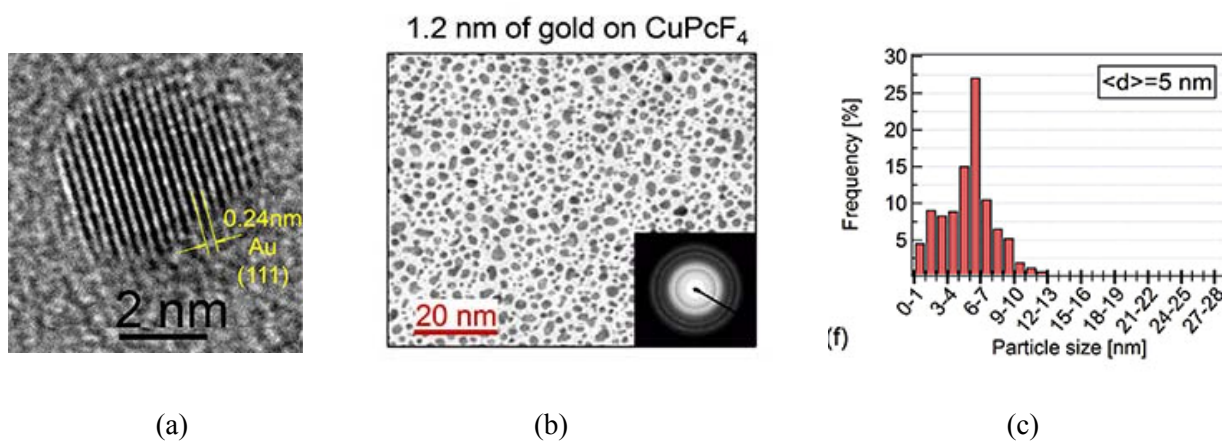
Figure 1. (a) High resolution TEM image of defect-free gold nanoparticle, taken at 0.4 nm of deposited gold (JEM 2100, 200 keV). (b) TEM image of $CuPcF_4$ organic films with embedded gold nanoparticles for nominal gold coverage of 1.2 nm; Inset: Electron diffraction pattern for corresponding deposition, which prove that diffraction originates from gold NPs with ordinary fcc structure. (c) Histogram with size distributions of gold NPs, taken from electron micrographs of (b).

1.   J.C. Scott and L.D. Bozano, *Adv. Mater.*, 19, p.1452, 2007
2.   V.Yu. Aristov, O.V. Molodtsova et al., *Appl. Phys. Lett.*, 97, p.113103, 2010
3.   O.V. Molodtsova, I.M. Aristova et al., J. *Appl. Phys.*, 115, p.164310, 2014
4.   S.V. Babenkov, O.V. Molodtsova et al., *Org. Electr.*, 32, p.226, 2016

O2-4: Microspherical FeFe$_2$O$_4$ particles massive forming by rotating magnetic field

I. Shorstkii[1] , N. Yakovlev[2]

1.   *Kuban State University of Technology, Krasnodar, Russia, i-shorstky@mail.ru*
2.   *Institute of Materials Research and Engineering, A*STAR, Singapore, niko-y@imre.a-star.edu.sg*

In current paper, a novel method, based on a dipole interaction of magnetic spherical particles FeFe$_2$O$_4$ in an external rotating magnetic field (ERMF) of highly ordered three-dimensional arrays formation is proposed. According to obtained photo and video materials of application, the transfer of an array of particles from a fibrous dispersed to a cubic face-centered dense packaging described.

The structure of dense packing particles array obtained from the effect of an ERMF interaction with internal magnetic field of the particles presented at Fig.1. The formation of such arrays in ERMF can be described in several stages:

- nucleation and formation of two centers with the maximum intensity of the magnetic field in the volume of the array, with oppositely rotating particles;
- increasing number of particles involved in rotation in these centers;
- merging of two centers until the formation of a homogeneous density of a bulk array of particles.

The ferromagnetic properties of this material are manifested equally in all directions of the main axes of the FeFe$_2$O$_4$ crystal lattice from the action of the ERMF and allow one to react quickly to changes in the angle of rotation of the external magnetic field. This behavior of particles is fully explained by the presence of magnetic properties in the ferromagnetic particles used, with a narrow hysteresis loop and the cubic lattice structure.

Possibility of forming the structure of magnetic particles with a given geometry opens new perspectives in various science fields, from microelectronic engineering fields to controlled filtration creation with external rotating magnetic field application.
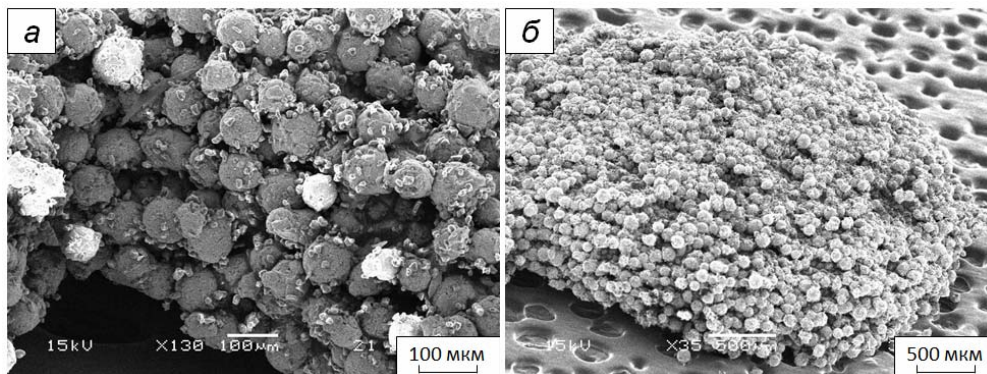
Fig 1. SEM-images of magnetic particles layer at x130 (a) and x35 (b) magnification.

1. Li Y. H., Chen C.Y., Sheu S.T., Pai J.M. «Dynamics of a microchain of superparamagnetic beads in an oscillating field». *Microfluidics and nanofluidics*. T-13, № 4, C 579-588, 2012.

2. J.H.E. Promislow, A.P. Gast, and M. Fermigier. *J Chem. Phys*., vol. 102(13), pp. 5492-5498, 1995.

3. Шорсткий И.А. «Динамическое фильтрующее устройство» Патент Р.Ф. № 2544695 от 22.11.2013г.

O2-5: Self-organization processes in silicon substrates with a buried glass layer exposed to an annealing in non-isothermal reactor

Yu. Denisenko

Yaroslavl Branch of the Institute of Physics and Technology, Institution of Russian Academy of Sciences, Yaroslavl, Russia, E-mail: den-yur55@mail.ru

The artifacts of a modifying the defective subsystem of (001)-oriented silicon substrates subjected to co-implantation with high concentrations P and O ions and two-stage annealing were studied [1]. In the first stage of annealing, the substrates were exposed to the 5-minutes lamp heat treatment in the non-isothermal reactor. Here, the temperature difference between "cold" and "hot" sides of the substrate varied from 1.5 to 3.5 ˚C dependent on its average temperature T (Fig.1). The second stage of annealing was represented by usual isothermal procedures in the usual furnace (1150 ˚C, 1 - 4 h), after the cleaved specimens were studied using scanning electron microscopy. The panoramic SEM images reveal information indicative of both nanostructuring of void defects in a near-surface layer and two kinds of self-organization processes in it. The first type of defect structure is set of octahedron pores surrounded by {111} planes (non-isothermal "prehistory" conditions: average T=1100 ˚C, grad $T > 0$). The pores arise from self-organization process and governed by the coalescence of several stable pores to form a single one. The second type of the defect structures is a set hollow nanotubes oriented along axes of screw components of misfit dislocations (non-isothermal "prehistory" conditions: average T= 900 °C, grad $T > 0$). The formation of this type defect structures reflects adequately dislocation self-organization process in the dissipative system. For example, due to lack of ability of energy dissipation by a controlled motion of dislocations, a spontaneous rearrangement of dislocation subsystem can occur. A blocking of the motion by impurities (oxygen, phosphorus) can cause to an evolution of the subsystem, and plastically dissipated energy spends on formation of new defects. One of the basic elements of such rearrangement may be a pinning process that restricts the passage of a dislocation by a glass layer. In that case, a creation of the helical turn on the screw dislocation can occur. The formation of nanotubes is accompanied by pipe diffusion of vacancies and their coagulation in the core of the dislocation to form a continuous, hollow channel along its axis.

For all substrates, which had been faced to the lamp irradiation in non-isothermal reactor (average T varied from 1100 to 900 °C, grad $T < 0$), a plastic flow of surface material by dislocations movement along the slip systems <110> / (111) took place. With increase isothermal annealing time up to 4 hours, the stresses led to the formation of regular array of microcracks. In the control specimens without any non-isothermal "prehistory" no formation of a void defect structure occurred.
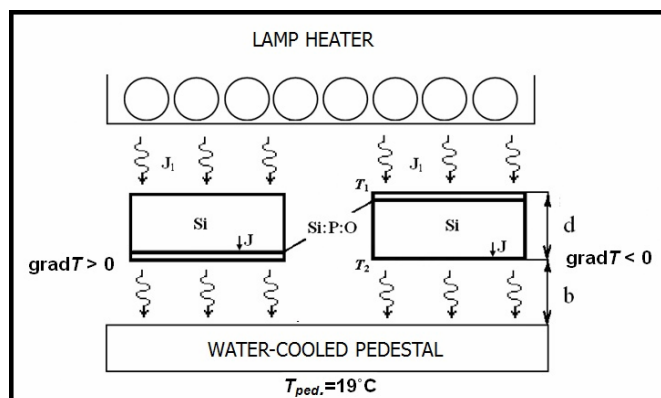
Figure 1. The arrangement of a temperature gradient across the depth of silicon substrates in the non-isothermal reactor.

1. Yuri. I. Denisenko and Valery. I. Rudakov, «Formation of nanoporous structure in silicon substrate using two-stage annealing process», *International Conference on Micro-and Nano-Electronics (ICMNE-2016), Moscow-Zvenigorod, Russia*. Issued by International Society for Optics and Photonics, 2016, 10224-70

O2-6: Vanadium surface oxidation under oxygen ion bombardment

N. Alov

Lomonosov Moscow State University, Faculty of Chemistry, Moscow, Russia, n_alov@mail.ru

The growth of oxide layer on vanadium surface induced by oxygen ion bombardment was studied by angle-resolved X-ray Photoelectron Spectroscopy (ARXPS). On the basis of fine structure analysis of V 2p spectra it was concluded that under the oxygen ion bombardment at room temperature the ion-beam induced surface oxidation of vanadium occurs and the oxides V_2O_3, VO_2 and V_2O_5 are formed in the surface layers. After long time of ion irradiation VO_2 is predominating in the oxide film. Different population of individual vanadium oxidation states is obtained with thin oxide films produced by thermal oxidation. The differences observed are caused by different radiation stability of vanadium oxides formed under the oxygen ion-beam irradiation. The distribution of individual vanadium oxidation states within the oxide film was determined. The ARXPS spectra measured at different detection angles show that the distribution of individual oxide states within the oxide layer formed by oxygen ion bombardment is not homogeneous. The outer part of the oxide film being enriched by V_2O_5 and the lower oxides present predominantly in the inner region of the oxide film.

O2-7: Dynamics and the mechanisms of the formation of nanostructures during plasma treatment of epitaxial $Pb_{1-x}Sn_x$Te films

E.S. Gorlachev[2], S.P. Zimin[1], I.I. Amirov[2], V.V. Naumov[2], E. Abramof[3], P.H.O. Rappl[3]

1. Yaroslavl State University,Yaroslavl, Russia, zimin@uniyar.ac.ru. 2. Yaroslavl Branch of the Institute of Physics and Technology, Russian Academy of Sciences, Yaroslavl, Russia, em51@mail.ru. 3. Laboratório Associado de Sensores e Materiais, Instituto Nacional de Pesquisas Espaciais, São José dos Campos, Brazil, rappl@las.inpe.br.

$Pb_{1-x}Sn_x$Te solid solution, which is widely used in optoelectronics, is currently receiving great new interest due to it demonstrating topological insulator properties at room temperature for $x \geq 0.6$. One of the most prospective approaches to the enhancement of its properties is the nanostructuring of the topological insulator surface. The aim of this work was to study the dynamics and the mechanisms of the formation of nanostructures, which take place during the plasma treatment of the $Pb_{1-x}Sn_x$Te surface. Initial epitaxial $Pb_{1-x}Sn_x$Te films with 2 μm thickness were grown on BaF_2(111) substrates using molecular beam epitaxy [1]. The plasma treatment of the films was carried out in radio-frequency inductively coupled argon plasma [1]. The RF bias power was 300 W, the treatment duration was varied in the range of 10-60 s with additional 10-15 s second stage treatment. The study of the surface morphology of the films was performed with scanning electron microscopy (SEM) using the Supra 40 microscope. The films discussed in this report had $x = 0.4$. The initial film surface was flat with triangular dislocation exit pits. The density of the pits was $7 \cdot 10^8$ cm^{-2}. After the 20 s plasma treatment, the pits were partially etched and obtained a hexagonal shape according to crystallographic properties of the film, with the simultaneous formation of a ripple relief with ~10 nm height. After the 40 s treatment there took place a full removal of the pits and a formation of array of inclined vertical nanostructures with spherical "caps" on their tops with 30-50 nm diameter (fig. 1). Their height was up to 150 nm and the density was $4 \cdot 10^9$ cm^{-2}. Finally, after the 60 s treatment the height of the resulting nanostructures increased up to 370 nm, while the density decreased to $2 \cdot 10^9$ cm^{-2}. The nanostructures also now had a more conical vertical shape. Additional second treatment resulted in a removal of the "caps" and the increase of the uniformity of the nanostructures with them obtaining a cubical shape in [111] orientation. The "caps" indicate that the nanostructure formation includes the vapor-liquid-solid mechanism, while a transition to a conical and cubical shape is due to a micromasking mechanism and anisotropic physical sputtering, respectively. Therefore, the results of this report show a capability of the variation of the shape and size of nanostructures on the $Pb_{1-x}Sn_x$Te surface during plasma treatment.
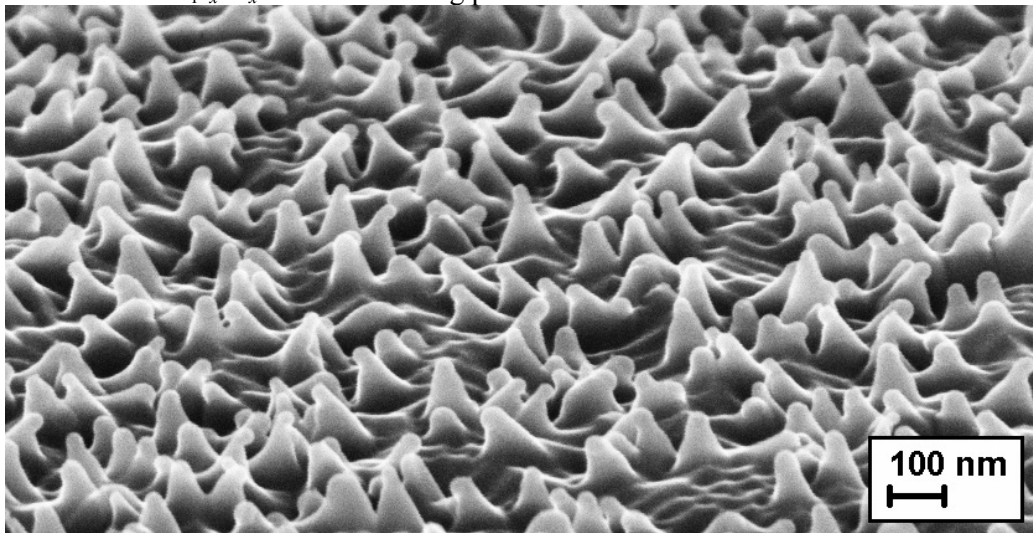
Fig. 1. SEM image of the nanostructures on the surface of the $Pb_{0.6}Sn_{0.4}$Te film after the 40 s plasma treatment.

1. S.P. Zimin, I.I. Amirov, E.S. Gorlachev, V.V. Naumov, E. Abramof and P.H.O. Rappl, «Plasma sputtering of $Pb_{1-x}Eu_x$Te films with varied composition and structure», *J. Surf. Investig. X-ray, Synchr. Neutron Techn.*, 10, pp. 623-626, 2016

O2-8: Implantation-induced nanovoids in strained layers and dots

P. Gaiduk

Department of Physical Electronics and Nanotechnology, Belarusian State University, Minsk, Belarus,

gaiduk@bsu.by

The formation of new Si-based materials with enhanced light absorption is of great importance for the development of high efficient photodetectors. A possible approach for enhanced light absorption is connected to excitation of localized surface plasmons after interaction of photons with nano-cavities, metallic nano-shells and nano-particles. The plasmonic excitations are then transferred to the semiconductor to generate additional electron-hole pairs.

The concept of this study is based on self-organized formation of voids in strained Si/SiGe(Sn) hetero-structures. The effects of strain-driven self-assembly of nano-voids in ion-implanted Si/SiGeSn/Si layers, gettering and segregation of impurities and formation of buried nano-shells and nano-dots of Ge, Sn and Au in Si layers located nearby of a p-n-junction are the main features of our approach.

Strained structures of Si/SiGe(Sn)/Si are grown in a solid-source MBE instrument. To suppress strain relaxation during growth, the thickness of the SiGe layers is chosen below the critical level for their relaxation. The samples are then implanted with 60-keV He^+ ions followed by high temperature annealing to create 2D layer of self-assembled nano-voids.

It is registered by transmission electron microscopy (TEM) that the Si/SiGe/Si layered system is strained after both MBE growth and following high temperature annealing. Ion implantation of He^+ results in formation of a 2D array of near-spherically shaped voids at a depth of 500 nm. The voids are of 10-25 nm in size, and they are exclusively adjusted with the original SiGe strained layer. Most of the voids are of facetted tetrakaidecahedron shape which is close to the equilibrium for Si.

Thermal annealing of ion implanted Si/SiGe/Si structure with deposited Au results in the accumulation of Au in the voided SiGe layer. Depending on annealing temperature, segregated Au atoms cover the walls of the voids or create metallic nanodots. High temperature (850°C) annealing results in bulk Au-Si eutectic phase formation.

Optical measurements of the Si/SiGe/Si samples show a successive increase of the reflectivity in the spectral range of 800 – 1800 nm after Au deposition, He^+ implantation and high temperature annealing. A comparison with the plan-view TEM pictures of the Au-coated surface evidences that the major reflectivity changes are due to plasmonic-related light scattering on the Au nanoparticles. Impact of structural transformation in the Si/SiGe layers on spectral dependence of the photocurrent in the Si/SiGe structures will be reported as well.

It will be discussed in the talk that metallic nano-shells possess unique, geometrically tuneable optical resonances. In contrast to solid metallic nanostructures, which exhibit only a weak tunability with size or aspect ratio, the optical resonance of the nano-shells is very sensitive to geometry of the metallic shells. By varying the relative core and shell thicknesses, the absorption and scattering properties of metallic nano-shells can be varied in a broad range of the optical spectrum. Another favorable difference of metallic nano-shells as compared to nanoparticles is their potentially higher resistivity that might be useful to overcome the problem of the Ohmic dissipation channel for plasmonic excitations. Metallic nano-shells can be made to either preferentially absorb or scatter light by varying the size of the particle relative to the wavelength of the light at their optical resonance with a possibility to tune the plasmon resonance of nano-shells into the near-infrared region of the spectrum. Finally, special attention will be devoted to possible plasmonic structures for the enhancement of the efficiency of Si-based photodetectors.

O2-9: Morphological changes in the surface of polyacrylonitrile carbon fiber under nanosize ion-beam modification

A M. Borisov[1], V.A. Anikin[1], V.A. Kazakov[1,2], A.V. Makunin[3],
E.S. Mashkova[3], M.A. Ovchinnikov[1,3], S.V. Savushkina[2]

*1. Moscow Aviation Institute (National Research University), Moscow, Russia, anatoly_borisov@mail.ru.
2. Keldysh Research Center, Moscow, Russia, cossac@mail.ru. 3. Skobel'tsyn Institute of Nuclear Physics,
Moscow State University, Moscow, Russia, es_mashkova@mail.ru*

It has been known, that high-fluence noble gas and nitrogen ion irradiation of polyacrylonitrile carbon fiber with energies 10-30 keV can lead to ion-induce surface corrugation, when fiber modification into depth for an order of magnitude of ions projective range 10-50 nm leads to quasiperiodic micro-relief formation on a fiber surface with height and period of corrugated elements $0.3 - 1.0$ μm [1]. In present article regularities of corrugation in one-dimensional carbon composite KUP-VM reinforced by VMN-4 carbon fibers have been observed under 30 keV Ar^+ ion irradiation at variable temperature range from 250 to 600 °C. SEM microscopy and laser goniophotometry were used to determine the temperature dependences of period, face slopes and height of ion-induced corrugations, see Figure 1. It has been found that   the   most
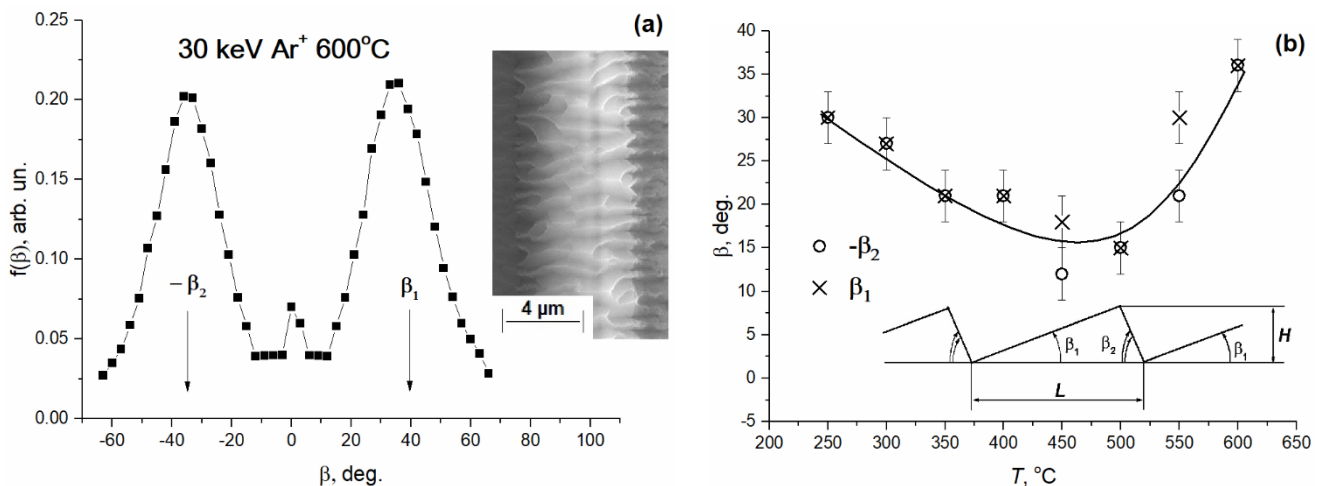
Figure 1. SEM image of corrugated VMN-4 fiber morphology after high-fluence ($6\cdot10^{18}cm^2$) Ar^+ ion irradiation of KUP-VM composite at temperature 600 °C and distribution f(β) of the slope angles of the corrugations (a) and temperature dependencies of the slope angles β_1, β_2 (b)

significant corrugation occurs at temperatures 250 and 600 °C, in contrast to irradiation at 400-500 °C, where the temperature dependence of the corrugation slope face angles shows a minimum. This feature can be associated with general regularities of the radiation dimensional changes in graphite materials [2]. In particular, it was shown in [3] that under neutron irradiation the temperature of about 400°C separates the shrinkage of carbon-based materials at low temperatures and their swelling under elevated temperatures. A special experiment with the masking of ion irradiation shows carbon fibers shrinkage after irradiation at temperatures 300 ° C and their swelling after irradiation at 600 °C.

1.   N.N. Andrianova, A.M. Borisov, E.S. Mashkova, E.S. Parilis, Yu.S. Virgiliev, «Ion-Induced Modification and Crimping of Carbon Composite Fibers», *Horizons in World Physics*, 280, pp. 171-190, 2013.

2.   T.D. Burchell, «Radiation Effects in Graphite and Carbon-Based Materials», *MRS Bulletin*, 22, pp. 29-50, 1997

3.   Yu.S. Virgil'ev, I.P. Kalyagina, «O mehanizmah radiacionnogo formoizmeneniya grafita», *Atomic Energy*, 31, pp. 497-503, 1971 (in Russian)

O2-10: Radiation-heterogeneous processes in the system

B_2O_3 / SiO_2 + H_2O

S.Z.Melikova

Institute of Radiation Problems, Azerbaijan National Academy of Sciences, Baku, Azerbaijan
e-mail: sevinc.m@rambler.ru

Boron-containing materials are widely used as materials of nuclear reactors. Under normal and emergency conditions of nuclear reactors, these materials are exposed to ionizing radiation and temperature in contact with the coolant-water [1-3]. Therefore, in order to reveal the patterns of defect formation in boron-containing materials and the accumulation of explosive gas mixtures (H_2 + O_2), it is necessary to study the regularities of radiation-heterogeneous processes in contact with coolants in a reactor environment.

In order to refine the mechanism of radiation-heterogeneous processes in the B_2O_3 / SiO_2 + H_2O system, the kinetics of accumulation of molecular hydrogen in the radiolysis of water in the presence of borosilicate at room temperature T = 300 K was studied. The kinetics of the accumulation of molecular hydrogen under heterogeneous radiolysis of water in systems [B_2O_3 / SiO_2 + H_2O] and [B_2O_3 / SiO_2 + H_2O_l] has been studied.

On the basis of the initial linear sections of the kinetic curves, the values of the velocities and the radiation-chemical yields of hydrogen in the systems studied are determined. The values of the velocities and radiation-chemical yields of molecular hydrogen in radiation-heterogeneous radiolysis of water in two states at T = 300 K are given in table 1.

Table 1.

The values of the velocities and radiation-chemical yields of molecular hydrogen under radiation-heterogeneous radiolysis of water in two states at T = 300 K

№	Irradiated systems T=300 K	$W(H_2)$, $molecul \cdot g^{-1} \cdot s^{-1}$	$G(H_2)$, molecul/100eV
1	B_2O_3/SiO_2+H_2O	$8{,}33 \cdot 10^{12}$	0,51
2	$B_2O_3/SiO_2+H_2O_l$	$5{,}56 \cdot 10^{13}$	3,4

In addition, as seen from the table, when heterogeneous radiolysis of water in the state of complete coating of the layer of borosilicate (borosilicate + H_2O_l), the observed values of the radiation-chemical yields of hydrogen are about 6.6 times greater than in heterogeneous radiolysis of water in the adsorbed state on the surface borosilicate. This indicates that in the case of borosilicate in the water volume there is an effective transfer of energy from the solid phase to the water molecules.

1. Gasanov A.M., Samedov E.A., Melikova S.Z. «Structural peculiarities of borosilicates and its correlation with radiation-catalytic activity», *Radiation Safety Problems in the Caspian Region. NATO Science Series. IV Earth and Environmental Sciences*, v.41, pp.23-27, 2005

2. Melikova S.Z., Garibov A.A., Gadzhieva N.N., Nadzhafov A.I. «Peculiarities of radiothermoluminescence of gamma-irradiated borosilicates», *Surface Engineering and Applied Electrochemistry*,v.49, №4, pp.326-330, 2013

3. Garibov A.A., Melikova S.Z., Ismailov Sh.S. «Defect formation in borosilicates by a resistance method γ-quantum irradiation», *Journal of Radiation Researches*, v.1, №1, pp.62-65, 2014

O2-11: Design principles for nanosystems of advanced superionic conductors

A.V. Andreeva, A. L. Despotuli,

Institute of Microelectronics Technology and High Purity Materials, Russian Academy of Science, Chernogolovka, Moscow Region, Russia, Email: andreeva@ipmt-hpm.ac.ru

Super ionic conductors (SIC) are defined as solid compounds with unusually high ionic conductivity σ_i (e.g. mobile ions H^+, Li^+, Cu^+, Ag^+, F^-, O^-) far below melting point and even at 300 K. Their conductivity may be purely ionic σ_i required for solid electrolytes (SE), which used for supercapacitors and batteries. Other compounds show mixed conductivity with both high σ_i and electronic σ_e. Such solids have applications mainly as electrodes in fuel cells and batteries. Among all solid ionic conductors, we distinguished a new class of advanced superionic conductors (AdSICs) whose crystal structure is close to the optimum for fast ion-transport (FIT) and determines a record-high level of ion-transport characteristics ($\sigma_i \approx 0.3$ Cm/cm at 300 K, activation energy $E_a \approx 4\ k_B T_{300} \approx 0.1$ eV) [1-2]. The central challenge in ionics of AdSICs is the influence of atomic structure on the ion-transport and polarization processes in the space charge region of a AdSIC/ electronic conductor heterojunction, which is the key functional element of nanoionic devices. In this work, the descriptors based on a group of symmetry of a rigid sublattice and local symmetry of interconnected interstitial sites among which ions move are formulated for AdSICs. We reveal a fundamental relationship between anion packing and ion transport in AdSICs and expose the desirable structural attributes of fast solid ion conductors. It is shown that it is characteristic 3D – percolation network of FIT tunnels in the AdSIC structure. We find that definite cubic space groups such as Im3m and P4$_1$32 for anion frameworks, which allow direct hops between adjacent tetrahedral sites, are most desirable for achieving of highest σ_i. The AdSIC is formed during phase transitions when one sublattice of initial structure «fuses» and transforms into «liquid-like» state. Thus, there is a co-operative excitation of ions and their transition from normal lattice sites of initial lattice into interstitial sites of "rigid" sublattice, which is reconstructed, forming more close-packed structure. Diffusion mechanisms for SE with various concentrations of mobile defects are discussed.

A creation of 3D - percolation networks of low-energy pathways for mobile ions plays the central role for design of materials with high σ_i. It is proposed 3-D design of ionic conductors at different levels of scale: atomic level is on the scale of elementary cell (it is characteristic structural feature of AdSIC); mezo level - domain structure, micro- level polycrystalline structure (Fig.1).
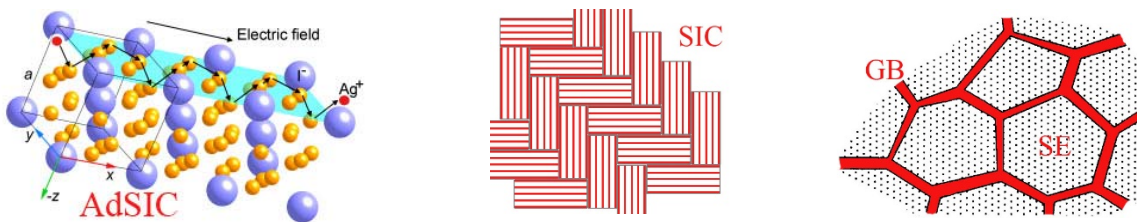
Fig.1 Various levels of organization of 3D -network of ion transport pathways

The important role of the coherence of heterojunctions and grain boundaries (GB) in AdSIC is underlined. Structural models of some special GB are presented. It is shown a new distinctive property of AdSIC among other solid ionic conductors: it is absence of the universal dynamic response. In the frame of new nanoionic fundamentals, ways of creating coherent and semi-coherent interfaces in supercapacitors with carbon based composite electrodes and high quantum capacitance are discussed. The atomic structure models of interfaces between AdSIC and composite electrode, including advanced carbon nanostructures such as graphene and/or ropes of single wall carbon nanotubes are presented. We think these findings provide important insight into ion-transport in AdSICs and serve as design principles of new nanoionic devices.

1. A.V. Andreeva, A.L Despotuli, «Interface design in nasystems of advanced superions conductors», *Ionics*, 11, pp.152-160, 2005.
2. A.L Despotuli., A.V. Andreeva, B.Rambabu, «Nanoionics od advanced superionic conductors», *Ionics*, v.11, pp.306-314, 2005.

O2-12: Dynamic properties of nanosystems with hopping ionic conductivity

A.L. Despotuli, A.V. Andreeva

Institute of Microelectronics Technology and High Purity Materials, Russian Academy of Science,
Chernogolovka, Moscow Region, Russia
Email: despot@ipmt-hpm.ac.ru

This work initiated the research program in the field of "dynamic non-linear ionics". The canonical physical-mathematical formalism for the description of ion transport in solids is based on the concept of a regular crystalline potential landscape, i.e., the heights η of potential barriers are *const*. However, the variation of η with space coordinate can be considerable in objects of solid-state ionics. For example, local regions with η variation ≈ 0.5 eV/nm exist in disordered solid electrolytes (SE) and in crystals of superionic conductors. Various degrees of ordering occur near surfaces and in the region of interphase and intercrystalline boundaries where specific ion dynamics can arise on the nanoscale due to a non-uniform potential landscape. Besides, despite the importance of nanoionic impulse devices with fast ionic transport (FIT), their development at modern level (i.e., by using numerical simulation methods) is currently not possible. The reason is absence of basic (conventional) theory of ionic hopping transport on nanoscale. In order to solve this problem a theoretical system -"structure-dynamic approach (SDA) of nanoionics" [1-3] was created. It allowed carrying out the computer experiments and describing the relationship between the ionic transport, space charge distribution, dielectric polarization and energy dissipation in model SE-nanostructures (heterojunctions etc.). SDA gives a description of dynamic behavior of nano-systems with FIT in a non-uniform potential landscape. It introduces some new physical quantities such as Maxwell displacement current on a potential barrier, effective field, size factor etc.

In SDA, the sequence of cause-consequence relations is the following: impulse or harmonic external action $G(t) \rightarrow$ appearance of t-dependent distribution of excess charges on the system of the crystallographic planes $\{X^j\}$ (minima of potential landscape) in the nanostructure $\rightarrow$ appearance of non-uniform electric field $F(r, t)$ which is induced by excess charges $\rightarrow$ changes in the $\eta(r)$ barrier heights on the value of field additives $\Omega(r, t) \rightarrow$ the change of ionic transport kinetics determined at $G(t) \ll p$ (where the parameter p is defined by conditions of the problem) by the sum of $\Omega(r, t)$ field additives $\rightarrow$ t-dependent non-linear response of nanostructure.

Computer experiments have shown the prognostic efficiency of SDA. For the first time the physical basis of the emergence of "universal" dynamic response (Jonsher's law) $\text{Re}\sigma^* \propto \omega^n$ ($n \approx <1$) was revealed in SE-nanostructures, i.e., the real part of the complex conductivity $\text{Re}\sigma^*$ is a power function of the frequency ω of external action. It is shown that with increasing ω of the external influence the areas with comparable values of ionic conductivity and Maxwell displacement currents are not disappear in the samples with non-uniform potential landscape. This leads to about constant angle of phase shift between current and voltage on the sample electrodes. The obtained result explains the methodology of impedance spectroscopy, which uses the term "element with a constant phase shift". These "elements" (with unknown physical content) include formally in equivalent electrical circuits for the fitting of their dynamic response to experimental data.

In computer experiments for realistic (by geometry) models of SE-nanostructures we discovered the dimensional factor .The knowledge of this factor is important because it allows using on nanoscale the concept of «effective uniform field» and approach of the electrostatic Gauss field. It is shown that the dimensional factor is determined by the smallness of an average distance r_i between ions of mobile type in materials with hopping conductivity. The obtained result is formulated as a reciprocity theorem between excess charges and field additives to η. It is found that objects of nanoionics should be considered as dynamical non-linear systems, which key parameters depend on external influence. The nonlinearity of SDA-equations is shown to manifest itself in non-commutativity of operators of a current generator.

1. A. L. Despotuli., A. V. Andreeva. «Maxwell displacement current and nature of Jonsher's "universal" dynamic response in nanoionics», *Ionics*, 21, pp. 459–469, 2015.
2. A. L. Despotuli., A. V. Andreeva. «Method of uniform effective field in structure-dynamic approach of nanoionics», *Ionics*, 22, pp. 1291–1298, 2016.
3. A. L. Despotuli., A. V. Andreeva. «Dimensional factor and theorem of reciprocity in structure dynamic approach of nanoionics» (in press), 2017.

O2-13: Hierarchical macroporous silicon structures for anodes of lithium-ion batteries

G. Li, E. Astrova, N. Preobrazhenskiy, A. Rumyantsev, V. Zhdanov, A. Likhachev

Ioffe Physical–Technical Institute, Russian Academy of Sciences, St. Petersburg, 194021 Russia
E-mail: GalyaFedulova@ mail.ioffe.ru

The method of electrochemical etching is based on the anodization of silicon wafers in a solution of hydrofluoric acid. Porous silicon anodes obtained by this method demonstrate long cycle life and are promising for practical use. For example, the anodes we obtained earlier on the basis of regular macroporous structures with sufficiently thin walls provide the work of the anode for 1400 cycles at a capacity of 1000 mAh/g, maintaining a high Coulomb efficiency 99% [1]. However, the bottleneck for practical application of such anodes is the high cost of monocrystalline silicon wafers of microelectronic quality. The anode price can be significantly reduced when we use solar-grade silicon wafers.

In the present work we study formation of macropores in the breakdown regime controlled with light. For photo-electrochemical etching we used textured samples of n-Si (100) with the resistivity of $\rho = 3$ Ohm * cm, the hole lifetime $\tau_p = 1$ ms and the thickness of 180 μm. The experiments were carried out in three different electrolytes: the 4% hydrofluoric acid solution on the aqueous basis, on the basis of 30% hydrogen peroxide and on the basis of organic solvent: dimethylformamide (DMF). The samples were illuminated from the backside. We studied the effect of illumination intensity and voltage applied to the silicon-electrolyte interface on the morphology of the pores, porosity, valence and etching rate. The conditions for the transition from the regime of cylindrical macropores with smooth walls to a breakdown regime with secondary pores of different crystallographic orientation were determined. It was found that the layers obtained in DMF have the highest porosity (up to 60%). On their basis, we prepared membranes and fabricated anodes with copper contact. The anodes were tested in coin-like cells CR2032 with respect to the lithium counter electrode at room temperature. The electrolyte was 1M $LiPF_6$ in a mixture of EC/PC/DEC/EMC/MA (TC-E810 Tinci). Cycling of anodes was carried out in the galvanostatic mode in the voltage range from 10 mV to 2 V. The charge capacity was restricted by Q = 1000 mAh/g. Charge / discharge time is 5 hours.
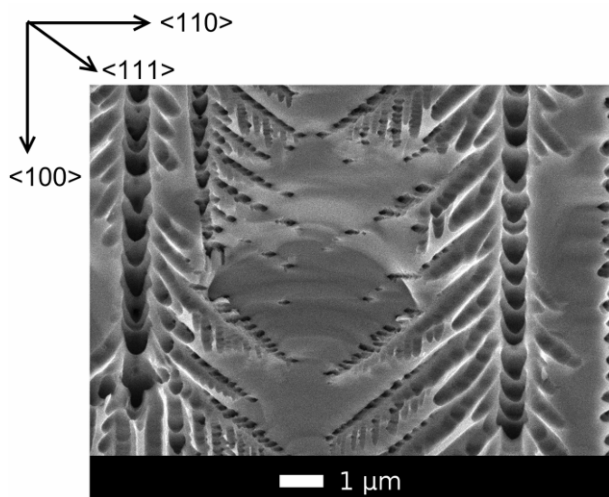
Fig. 1 Breakdown pores with different crystallographic orientation, obtained in DMF at the voltage of 10 V
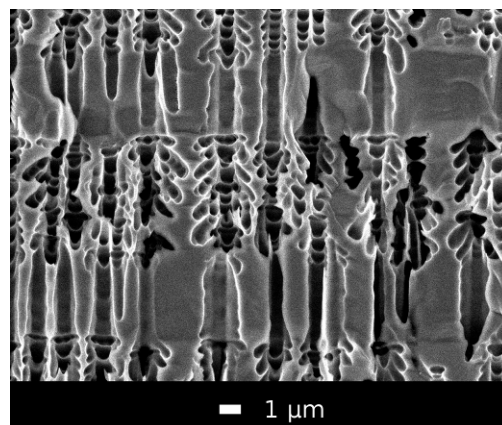
Fig. 2 Morphology of the pores formed under the periodic change of voltage during the etching in DMF: transition from the cylindrical macropores to the breakdown pores and vice-versa.

1.   G.V. Li, A.M. Rumyantsev, V.S. Levitsky, E.V. Beregulin, V.V. Zhdanov, E.I. Terukov, E.V. Astrova. «Application of Silicon Zig-zag Wall Arrays for Anodes of Li-ion Batteries» *Semiconductor Science and Technology*. v.31, 1, № 014008 (8pp), 2016

O2-14: Investigation of influence of the curvature of nanoscale channels on the permeability of methane-helium mixtures

A. Ukolov, M. Bubenchikov

National Research Tomsk State University, Tomsk, Russia
E-mail: Ukolov33@gmail.com

In this paper we study the degree of separation of methane-helium mixtures using classical molecular dynamics in meandering channels. Curved channels are used for the object of investigation, the walls of which are composed of diamond nanoparticles of radius 4 nm. The calculations show that the tortuosity of the channel itself is a selectivity factor in the problems of passing molecules through nanoporous layers. The obtained results also make it clear that it is possible to isolate a certain frequency of velocity oscillations associated with the initial velocity of molecules and the width of the curvilinear channel.

Mathematical modeling proved to be simple and effective in the case of using ideal spheres of carbon material as nanoparticles. In this case, a centrally symmetric interaction potential can be used for calculations, and fragments of a nanoporous structure can be made from balls[1]. Having thus constructed a curved channel, we obtain an unobvious result, that the tortuosity of the channel appreciably inhibits methane molecules, thereby increasing the selectivity of the separation of the methane-helium mixtures separated by layers of compacted carbon nanomaterials.
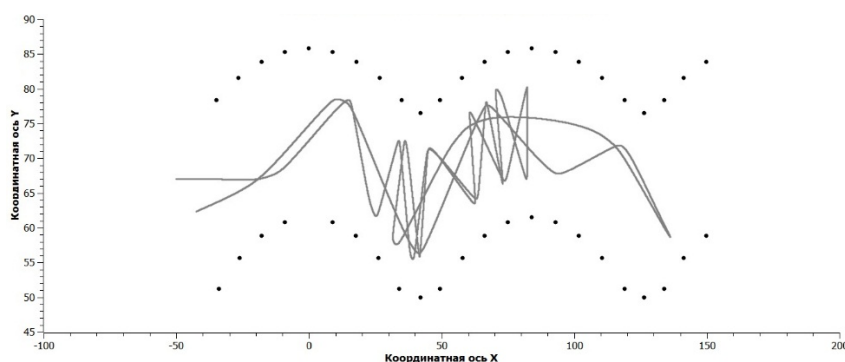
Fig. 1. Path of methane molecule launched with an initial velocity of 450 m / s
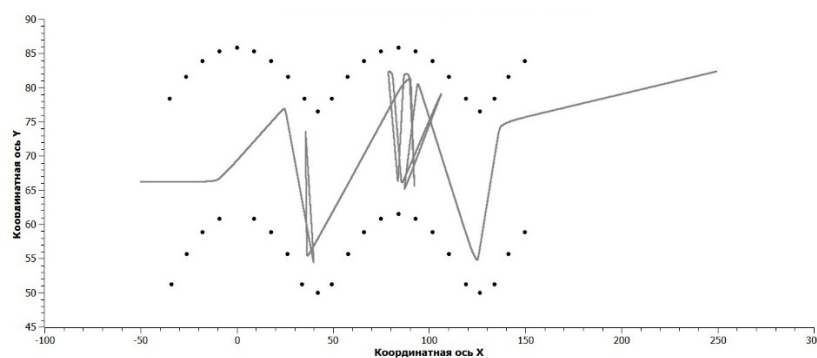
Fig. 2. Path of the helium atom launched with an initial velocity of 900 m / s

1. Rudyak V.Y. «The calculation and measurements of nanoparticles diffusion coefficient in rarefied gases» *J. Aerosol Science*. – 2003. – Vol. 34, suppl. 1. – P. 579–580. 97

O2-15: Radiation and catalytic properties of the n-ZrO$_2$+n-Al$_2$O$_3$ systems in the process of hydrogen production from water

Imanova G.T., Agayev T. N.

Institute of Radiation Problems of Azerbaijan NAS B. Vagabzadeh St., 9
e-mail: gunnel_ismayilova55@mail.ru

Influence of interaction between n-ZrO$_2$ and n–Al$_2$O$_3$ on their radiation and catalytic activities in the process of hydrogen production from water is investigated. It is established that as a result of interaction between n-ZrO$_2$ and n-Al$_2$O$_3$ the new phase n-ZrO$_2$-n-AI$_2$O$_3$ is formed that leads to reduction of radiation and catalytic activity in comparison with separate components and the additive sum of their activities.

Regularities of dependences of radiation and catalytic activity from the maintenance of components of the n-ZrO$_2$ - n–Al$_2$O$_3$ system are received in the process of hydrogen production. Mechanisms of processes of energy transfer and transmission in the studied nano dimensional systems are offered.

Taking into account these factors, values of length of a free run of electrons in the volume forms of Al$_2$O$_3$ are determined in next cases: $L_{ev}=10^2$nm at electrons energy $E_g =10$eV, and $L_{ev}=10$nm at $E_g=10^3$eV [26]. Therefore for radiation and catalytic processes in case of classical volume forms of catalysts samples, usually the sizes of pores R are more than $10 \div 10^2$мкм. Therefore the main part of carriers of charges are localized and recombined in the volume centers and don't reach a surface. When matching the size of a particle of nano-oxide systems for radiation and catalytic decomposition of water we were guided by the principle $R \leq L$. In these oxide systems the nonequilibrium carriers of charges formed under the influence of gamma radiations can come to a surface and near-surface amount of nano-oxides. The surfaces of nano-oxides are characterized by big concentration of defective conditions and especially anion vacancies. Coordination and nonsaturated cations on a surface create the acceptant centers with various force as concentration of the acceptant centers in nano-ZrO$_2$ is more, than in nano-AI$_2$O$_3$.

Thus in case of radiation and catalytic processes of decomposition of water thanks to effective transformation, energy transfer, availability of the strong acceptant centers of a surface and nanodimensional spaces between particles, and also to participation of secondary electronic radiations from nano-catalysts, high yields of molecular hydrogen can be reached.

O3-1: Modification of the GaP(100) surface electronic structure by sulfur passivation

M. V. Lebedev, T. V. Lvova, V. L. Berkovits

Ioffe Institute, St. Petersburg, Russia, mleb@triat.ioffe.ru

Gallium phosphide (GaP) is a III–V semiconductor with a wide indirect band gap of 2.26 eV used in light-emitting devices and detectors of ultraviolet radiation. Nowadays an exploding interest in this semiconductor is related to applications as photocathode material for solar-driven water splitting [1].

Performance of semiconductor devices is determined in a great extent by electronic structure of the semiconductor surface. Therefore, modification of the surface electronic structure is one of the most urgent problems in the semiconductor physics and technology. Passivation with sulfide solutions is known to remove the native oxide layer and to form a thin sulfide surface layer which can result in the reduction of the density of the surface gap states. As it was shown on the example of GaAs(100) surface, the solvent of the sulfide solution can modify essentially chemical and charge transfer processes at the semiconductor/solution interface, as well as surface passivation efficiency [2].

The objective of the present study is to elucidate the role played by solvent of the sulfide solution in the electronic structure modification of the GaP(100) surface. The surface electronic structure is investigated by synchrotron photoemission spectroscopy (SXPS) and reflectance anisotropy spectroscopy (RAS).

SXPS data showed that the n-GaP(100) surfaces treated with aqueous or alcoholic solutions of ammonium sulfide [$(NH_4)_2S$] exhibit complex solvent-depended electronic structure. In particular, the valence band maximum determined with respect to Fermi level, as well as the core level binding energies of the sulfide layer measured with the most surface sensitive mode are found at 0.75–1.0 eV higher binding energies once the n-GaP(100) surface was treated with the solution of $(NH_4)_2S$ in 2-propanol, instead of aqueous $(NH_4)_2S$ solution. That is in the top near-surface layer (~15 Å thick, when the valence band edge is measured with the excitation energy of 90 eV) of the n-GaP(100) treated with the solution of $(NH_4)_2S$ in 2-propanol the flat bands conditions are achieved, whereas the same near-surface layer of n-GaP(100) treated with the aqueous $(NH_4)_2S$ solution is characterized by an upward band bending of about 0.75–1.0 eV. On the other hand, when the valence band edge spectra are measured with the excitation energy of 650 eV (information depth is ~50 Å) the band bending of the n-GaP(100) surface treated with both solutions is nearly the same.

RAS allows investigating of the surface electric field of the band bending region. For (100) surface of cubic semiconductors, the value of derivative-like anisotropy signal $\Delta R/R$ in spectral region of balk optical transition E_1 at near 3.7 eV is proportional to surface electric field. As it seen, after the sulfide treatment in 2-propanol sulfide solution (Fig. 1) the derivative like structure near 3.7 eV almost disappears indicating that the surface electric field deceases at least by a factor of 10. For the surface treated with aqueous sulfide solution such an effect is smaller (Fig. 1). In contrast, for p-GaP(100) the sulfide treatments cause an increase of surface electric field by a factor of 3.

Figure 1. RAS of n-GaP(100): native-oxide-covered surface (1); surface treated with the solution of $(NH_4)_2S$ in 2-propanol (2); surface treated with aqueous $(NH_4)_2S$ solution (3).

1.   M. Malizia, B. Seger, I. Chorkendorff, and P. C. K. Vesborg, «Formation of a p–n heterojunction on GaP photocathodes for H_2 production providing an open-circuit voltage of 710 mV», *J. Mater. Chem. A* 2, pp.6847–6853, 2014

2.   M. V. Lebedev, «Passivation at semiconductor/electrolyte interface: Role of adsorbate solvation and reactivity in surface atomic and electronic structure modification of III–V semiconductor», *Appl. Surf. Sci.* 254, pp.8016–8022, 2008.

O3-2: Poly-Si and α-Si films on Si_3N_4/SiO_2/c-Si artificial substrates

K. Chizh[1], L. Arapkina[1], O. Uvarov[1], V. Kalinushkin[1], V. Yuryev[1],
A. Novikau[2], S. Prakopyeu[2], O. Nalivaiko[3], P. Gaiduk[2]

1.   *A. M. Prokhorov General Physics Institute of RAS, Moscow, Russia, E-mail: chizh@kapella.gpi.ru.*
2. *Belorussian State University, Minsk, Belarus, E-mail: novikaua@bsu.by. 3. JSC "Integral", Minsk,*
Belarus

Low temperature formation process of columnar poly-Si on Si_3N_4 dielectric substrates is required for many practical applications including diode bolometer IR detectors, which are presently of interest due to possible mass production using CMOS manufacturing cycle [1]. We deposited Si on Si_3N_4/SiO_2/Si(001) substrates at several temperatures: 300, 420, 450, 500 and 650°C. The samples grown at different temperatures after their cooling have been studied by RHEED. Results demonstrate transformations of the silicon structure with the increase of the deposition temperature. A uniform halo observed in RHEED patterns of the samples grown at 300°C corresponds to the uniform amorphous Si phase. Some signs of ordering looking as wide rings are present in diffraction patterns of Si deposited at 420°C. For Si grown at 450°C, a pattern corresponding to the polycrystalline phase with some degree of grain ordering to the columnar structure is observed (some diffraction rings are seen as segments). Samples produced at 500°C demonstrate a more pronounced segmental diffraction pattern, which is interpreted as a fingerprint of a more regular columnar structure. RHEED patterns mostly composed of rings with some segmental reflexes, resembling the pattern of the samples obtained at 450°C, are registered for Si grown at 650°C.
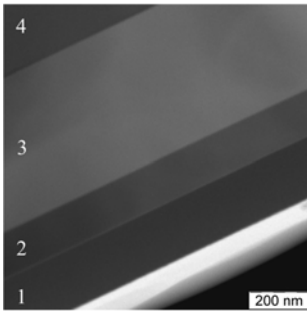
Figure 1. TEM images of the sample with a Si film deposited at T = 300°C; 1 - Si film, 2 - Si_3N_4, 3 - SiO_2, 4 c-Si.
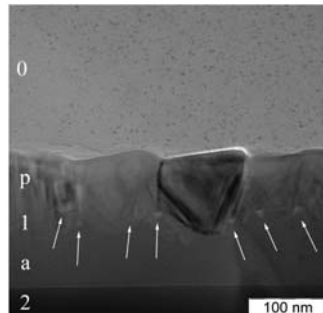
Figure 2. TEM images of the sample with a Si film deposited at T = 450°C; 0 is epoxy, 'a' is a-Si and 'p' is p-Si
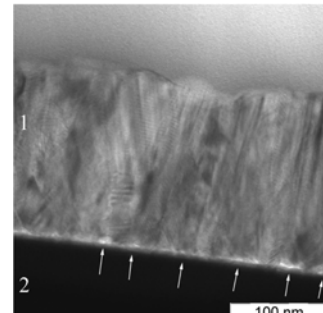
Figure 3. TEM images of the sample with a Si film deposited at T = 500°C; designations are the same as in Fig. 1;

Details of these structural transformations have been revealed using high resolution transmission electron microscopy. As it is seen from Fig. 1, a homogeneous layer of amorphous Si is formed at 300°C. The HR TEM images completely correspond to the RHEED pattern of this sample. Images of the samples grown at 450°C (Fig. 2) are in a drastic contrast to those of Si deposited at 300°C. Crystallization of Si starts at the distance of about 100 nm from Si_3N_4 at this temperature. Only columnar grains grow at grater distances from the dielectric substrate. This also agrees with the corresponding RHEED pattern. Some unrecognized details are also observed in the images in Fig. 2 close to the interface of α-Si and poly-Si which correspond to some 3D formations of unresolved morphology and oval shape ('bubbles'). They are less dense than the surrounding substance. We assume that their appearance is a characteristic feature of Si growth on Si_3N_4. Si deposition at 500°C results in formation of a film of columnar poly-Si starting directly from the Si_3N_4 surface (Fig. 3). This corresponds with the diffraction pattern. However, "bubbles" are also observed at the interface between Si and Si_3N_4. This enhances our assumption about the connection of "bubbles" emergence and poly-Si growth on Si_3N_4. It should be emphasized that the demonstrated process of the bilayer Si film formation paves a way to some practical applications. The thickness of the poly-Si layer can be easily controlled, an additional amorphous Si layer can be deposited atop the poly-Si to ensure, e.g., precise formation of platinum silicide thin films on polysilicon for diode bolometer detectors. The research is funded through the RFBR grant # 16-52-00186.

1.   V.A. Yuryev, K.V. Chizh, V.A. Chapnin and V.P. Kalinushkin, «Metal silicide/Si thin-film Schottky-diode bolometers», *Proc. SPIE*, 9519, 95190K, 2015

O3-3: Characterization of thin-film silicon structures

E. Zaytseva, O. Naumova, B. Fomin

Rzhanov Institute of Semiconductor Physics, Siberian Branch of Russian Academy of Sciences, Novosibirsk, Russia,
E-mail ifp@isp.nsc.ru

Currently, thin silicon-on-insulator (SOI) films are a basic material for silicon micro- and nanoelectronic devices. A fundamental property of any fully depleted films is so called coupling-effect – the interrelation between the potentials on the interfaces of Si film with adjacent insulator films [1]. The potential coupling causes a redistribution of carriers in the films. As a result, all parameters of the heterosystems Si/SiO_2 including the carrier-mobility depend on the potentials at the interfaces [2].

Under conditions of the coupling effect, each interface must be characterized independently of each other. Because of the proximity of the two interfaces in thin films, the kinetics of the defects accumulation/annealing at heterointerfaces changes, when there is any decrease in the thickness of the film and during manufacture of devices based on them. This is especially important for internal interface Si/buried oxide (BOX), since it can be created by a non-standard method. For different SOI technologies, the methods for obtaining this interface are fundamentally different: thermal oxidation, "internal" oxidation (due to oxygen implanted in silicon), bonding, etc.

A fundamental parameter of semiconductor materials is the charge carriers mobility. It allows one to judge the nature of the interaction of free carriers with the crystal lattice. In thin-film devices due to the coupling effect, the field dependence of the mobility method is not applicable for the characterization of the Si / SiO_2 system, which is widely used for bulk MOSFETs [3].

The aim of this work was to develop an approach that allows to independently characterize the inner Si/SiO_2 (BOX) interface of thin-film transistors under the coupling-effect conditions. For this purpose, double-gate SOI MOS transistors with different Si/SiO_2(BOX) interface were used. The thickness of the Si films was 30 nm. Temperature dependences of electron mobility in the temperature range of (78 – 300) K for different distributions of charge carriers over the film were measured.

It was shown that by controlling the charge carrier distribution by the potentials of the two gates, it is possible to localize the charge carriers near a specific interface. Due to this, the influence of the second interface and volume component is excluded even at room temperature. From the temperature dependences of the mobility measured under such conditions, mobility components related to surface roughness scattering and scattering on surface phonons were determined. By changing the distribution of charge carriers over the film, the profile of these components over the thickness of the film was obtained. It allowed us to evaluate the quality of the film not only near the interface, but also in volume.

Thus, a non-destructive method was proposed that allows one to independently study the quality of the internal interface Si/SiO_2 (BOX) of thin-film structures under coupling-effect conditions. This method can be used not only for silicon devices, but for any thin-film devices.

1.	Rudenko T., Nazarov A., Kilchytska V., Flandre D., «A review of special gate coupling effects in long-channel SOI MOSFETs with lightly doped ultra-thin bodies and their compact analytical modeling», *Solid-State Electronics*, 117, pp. 66-76, 2016
2.	Naumova O. V., Zaytseva E. G., Fomin B. I., Ilnitsky M.A.,Popov V. P., «Density dependence of electron mobility in the accumulation mode for fully depleted SOI films» *Semiconductors*, 49, pp.1316-1322 (2015)
3.	S. Cristoloveanu, N. Rodriguez, F. Gamiz, «Why the universal mobility is not», *IEEE Transaction on Electron Devices*, 57, pp.1327-1333, 2010.

O3-4: Surface structuring as a method of modifying the properties of materials

Zvezdin N.Yu.[1], Paporkov V.A.[1], Rud N.A.[1], Savinsky N.G.[2], Prokaznikov A.V.[2]

[1]*Yaroslavl Demidov State University, Sovyetskaya, 14, Yaroslavl, 150000 Russia*
[2]*Yaroslavl Branch of the Institute of Physics and Technology, Russian Academy of Sciences, Universitetskaya, 21, Yaroslavl, 150007 Russia*

Structuring and modification of the surface leads to the appearance of new properties in traditional materials and systems. These properties cover a wide range of physical and chemical characteristics, such as the electrophysical and adsorption parameters of the system, magnetic and magneto-optical properties, as well as the interaction of structured systems with external electromagnetic radiation. The reaction of the system to external influences of any type proceeds primarily through interaction with the surface, therefore the modification of the surface can have a decisive influence on the resulting response of the system.

One of the wide spreading methods used for surface modification is the creation of a porous space in a number of materials, and, first of all, in the basic material of modern electronics – silicon. The porous space is a kind of surface embedded in the volume, therefore, the properties of such modified materials is quite unusual (Fig.1-a). It concerns the processes involved in pore formation, which are expressed in characteristic of self-organizing manifestations of certain regularities, both in time and in space (Fig.1-b).
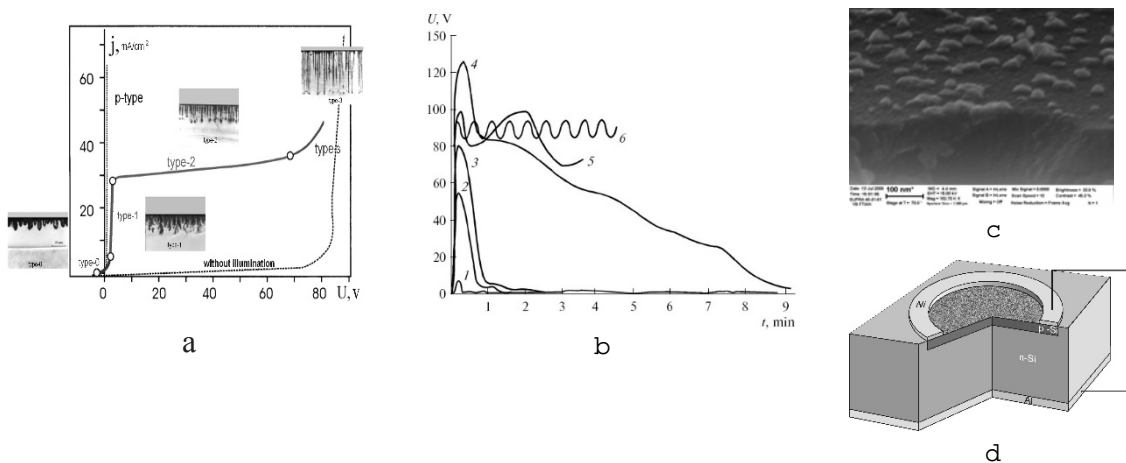
Figure 1. a – Current-voltage characteristics of silicon of p-and n-type with and without illumination. Corresponding morphological types of *n-Si* are formed when the working point of the anodizing process is on the corresponding part of the CVC. b – Dependence of the voltage *U* against time *t* in the n- type silicon taken during anodization under different conditions, for an electrolyte solution consisting of HF and isopropanol in different ratios. c – Structure made from porous silicon and nickel nanodots and (d) schematic diagram of a photovoltaic cell consisting of a porous silicon layer (thickness 120 nm) on the basis of the *p+_Si*, *p+_Si* layer (thickness 1 μm), upper nickel (Ni) contact, and lower aluminum (Al) contact.

Theoretical ideas proposed in the work, explain the phenomenon of bifurcation of Andronov-Hopf type by regularities of charge transfer near the interface semiconductor/electrolyte by consideration of surface charge levels. The presence of chaotic and oscillatory behavior of the electrophysical characteristics of the system during anodization is associated with the synchronization of the individual local regions of porous space formation. Analogous phenomena are observed in sensory systems based on porous silicon, which have a similar

nature. Synchronization of the local areas described in the framework of probabilistic cellular automata. The developed model gives a wide range of behavior of the system being studied: from the leading centers (pacemaker) and simultaneous changes of system parameters with different characteristics to chaotic regimes. There are regimes characterized by the formation of fractal porous borders. For these regimes it is typical the dominance of chaotic motion in the system of charge carriers that participate in the processes of anodic oxidation comparing with the usual drift in an external field. In the field of high potentials there is a noticeable filamentation of the current similarly to processes occurring in the plasma.

Deposition of metals from solutions into pores in silicon leads to the formation of metallic clusters inside the pores in the form of polyhedron and a continuous film on the surface of the sample. The dependence of the magnetic properties with respect to the direction of the magnetic field taken by means of a vibration magnetometer testifies to their difference for magnetic clusters and a continuous surface film. The shape of polyhedron is formed as a realization of the minimum of the ratio of volume to area with allowance for the symmetry of the crystals. Thus, the crystalline structure as well as the magnetic structure of the deposited metals directly depend on the conditions of metallic objects formation.

Metal clusters formed on the surface of systems of the type of photovoltaic elements serve as sufficiently powerful concentrators of the incident electromagnetic radiation (Fig.1-c,d). Dispersion curves describing the splitting of the edge modes with the splitting off the soft plasmon mode are calculated. The contribution of edge modes to the formation of color staining of nanostructures depending on their shape and dimensions is associated with the curvature of the structures formed.

The optical properties of finely dispersed compounds of various substances obtained by chemical synthesis have been studied, which exhibit sharp, narrow peaks in the optical density spectra associated with the excitation of plasmon modes localized in small regions. The number, height and positions of the peaks change during the course of the chemical synthesis process, and also depending on the monitored parameters of the system. The areas of application of this effect in microelectronic devices, in particular, in photovoltaic cells, are analyzed.

A technology based on the use of metal clusters as energy concentrators for electromagnetic radiation has been developed and implemented in creating of photovoltaic devices. It is demonstrated that the use of the developed technology leads to a significant increase in the efficiency of photovoltaic cells.

A technology for the formation of nanoperforated systems based on porous aluminum deposited by a cobalt film is proposed. In such devices, the magneto-optical response increases by more than an order as a result of the formation of a surface plasmon-polariton.

Structuring of semiconductor crystals and deposition them with a thin magnetic film leads to the formation of a complex magneto-optical response from a three-dimensional system in which the diffraction and interference processes play an important role for a complex volume structure far from plasmon resonance.

The superposition of effects of different levels and orders is considered when forming the resulting magneto-optical response from structures such as magneto-photonic crystals in regions far from plasmon resonances. The contributions to the magneto-optical response of interference and diffraction phenomena at maxima of various orders in three-dimensional systems such as magneto-photonic crystals are studied. It is shown that the use of an integral response for the analysis of magneto-optical effects leads to the disappearance of interference phenomena. The zero-order diffraction maximum adequately reflects the magnetic component of the magneto-optical response.

O3-5: A new approach to surface research problems

M. Makoviychuk

Yaroslavl Branch of the Institute of Physics and Technology, Institution of Russian Academy of Sciences
E-Mail: makoviychuk@rambler.ru

Any attempt to look at nature with "deterministic eyes" is a naive intuitive belief in the triviality of the influence of fluctuations in the environment. The systematic theoretical and experimental studies carried out in recent years have shown that, in a wide class of natural phenomena, the random nature of the medium, despite its seemingly disorganizing effect, can induce a much richer variety of regimes than those that are possible under the corresponding deterministic conditions.

Unlike internal fluctuations, which are negligibly small for macroscopically large systems, the fluctuations due to the randomness of the medium are very important. The main difference between internal fluctuations and external noise is that the fluctuations of the medium behave not as inverse powers of the characteristic size of the system. In addition, unlike internal fluctuations, the stochastic of the medium is not of microscopic origin. External noise often manifests itself in a turbulent, or chaotic, state of the environment and reflects the dependence of external parameters on a large number of interrelated environmental factors. Because of this, the fluctuations of the medium change not in proportion to the inverse of the characteristic size of the system. That is why they do not disappear at the macroscopic level of the description of the system.

The intensity of external noise within certain limits can be controlled - if the experiment is carefully set up, the noise level can be lowered. On the other hand, the intensity of the fluctuations of the medium can be controlled in a controlled manner to investigate its effect on the behavior of the system. This is another difference between external noise and internal fluctuations, making it much more malleable "material" in the hands of the experimenter.

Thus, taking into account the foregoing, a special place among the new electrophysical methods of information analysis that meet the requirements of defect-impurity engineering is the method of joint measurement of the sheet resistance and its spectral density of flicker fluctuations in the structures - the defect-impurity flicker-noise spectroscopy.

O3-6: Distant light guiding by liner chain of Au and Si nanoparticles

M. Yu. Barabanenkov[1], Yu. M. Barabanenkov[2]

3. *Institute of Microelectronics Technology, Russian Academy of Sciences, 142432 Chernogolovka, Moscow Region, IMT RAS, barab@iptm.ru*
4. *V.A Kotelnikov Institute of Radioengineering and Electronics, Russian Academy of Sciences, Mokhovaya 11, 125009 Moscow,GSP-3 Russia*

Assembles of nanoparticles are useful in a variety of optical applications because of their resonant interaction with electromagnetic (EM) radiation. Among the most remarkable effects in optoelectronics is EM energy guide below the diffraction limit along chains of nanoparticles since such an idea had been proposed in [1]. Recently [2] we developed a quantitative approach to solution of problem on radiation losses in optical discrete nanowaveguides consisting of dielectric or metallic coupled nanoparticles. The approach is based on new form for collective extinction cross-section of particle ensemble written in terms of incident electric field work on self-consistent currents excited inside particles. In the electric dipole single scattering and neighbour coupling approximations, we revealed a few megahertz transparency band in the terahertz frequency range (orange color) in the spectra of straight chain of closely spaced Au nanospheres with radius of 76 nm with the length of a few centimeters. In the both cases of Au and Si spheres the EM excitation frequencies lie in the spectral vicinity of the corresponding Mie resonance conditions. However, there is no long-range EM energy transfer along linear chain of Si particles. The explanation of this dissimilarity is given in the currently presented report in terms of the resonant condition for the particle coupling parameter.

System for self-consistent scalar amplitudes $I^{(j)}$ of currents excited in N coupled small spherical particles has the form ($j = 2,3,\cdots,N$) [2]

$$I^{(j)} = (-1)^{j-1} 2\cos\vartheta \frac{\sin(N+1-j)\vartheta}{\sin(N+1)\vartheta} \; ,$$

$$\cos\vartheta = -1/2a_{12}$$

(1)

Fig. 1. Illustration to the dispersion Eq.(1): the dependence of the real (curve 1, ○,●) and imaginary (dashed curve 2, △,▲) parts of ϑ on the real part of the coupling parameter. Curves 1 and 2 represent the exact resonant condition $a''_{12} = 0$. Open and solid symbols represent theoretically possible implementation of the resonant condition in the case of two closely spaced Au or Si spheres, respectively.

A complex auxiliary variable $\vartheta = \vartheta' + i\vartheta''$ satisfies the second Eq.(1) which has sense of a dispersion equation. The dispersion relation requires for distant excitation transfer that $\vartheta'' = 0$, $\vartheta' \to 0$ and $\vartheta' = 0$, $\vartheta'' \to 0$ in the case of big ($2|a'_{12}| \geq 1$) and small ($2|a'_{12}| < 1$) values of a'_{12}, respectively. The most important equality $\vartheta'' = 0$ holds only in the case of Au particles. Open and solid symbols in Fig.1 immediately show that the condition of distant excitation transfer is satisfied only in the case of Au particles. Really, in the limit $a'_{12} \to -0.5 - 0$ both quantities ϑ' and ϑ'' tend to zero (open symbols in Fig.1). From the other hand, in the case of Si particles calculated values $a'_{12} \to -0.45$ is relatively far from the limit $a'_{12} \to -0.5 + 0$. Such values of the real part of the coupling parameter have relatively big magnitudes of ϑ'' (solid triangles in Fig.1) that cause exponential currents decreasing according to $I^{(j)} \to (-1)^{j-1} \exp[-(j-1)\vartheta'']$.

1. M. Quinten, A. Leitner, J. R. Krenn, and F. R. Aussenegg, "Electromagnetic energy transport via linear chains of silver nanoparticles," *Opt. Lett.* 23, pp.1331-1333,1998

2. Yu.N. Barabanenkov, M.Yu. Barabanenkov, "Radiation losses and dark mode at light guiding by a liner chain of nanoparticles", *JOSA A*, 34, pp.321 – 330, 2017

O3-7: Anisotropy of plasmons in metal nanoclusters on semiconductor surfaces

V.L. Berkovits, V.A. Kosobukin, V.P. Ulin, A.V. Korotchenkov, F.Y. Soldatenkov,
P.A. Alekseev, V.S. Levitskii

Ioffe Institute, 194021 Saint Petersburg, Russia, E-mail address: vladimir.berkovits@mail.ioffe.ru

Plasmonic anisotropy of metal-semiconductor structures has been established, for the first time, for In nanoclusters formed electrochemically on InAs(001) surface [1]. Reflectance anisotropy (RA) spectroscopy revealed a characteristic spectral feature red-shifted in increasing either the permittivity of surrounding medium or the sizes of nanoclusters [2], the behavior being typical of plasmons. In this work, we have observed plasmonic anisotropy for gold nanoclusters formed on GaAs(001) surfaces, which structures are of interest for designing highly efficient solar cells. Experimentally, the plasmonic anisotropy of Au nanocluster arrays is studied by reflectance anisotropy spectroscopy. This technique measures the spectral dependence of anisotropy signal $\Delta R/R=2(R_\alpha-R_\beta)/(R_\alpha+R_\beta)$, where R_α and R_β are the reflectances of normally incident light waves linearly polarized along [110] and [$1\bar{1}0$] semiconductor axes, respectively. For cubic bulk semiconductors $\Delta R/R=0$, therefore appearance of the non-zero anisotropy signal $\Delta R/R$ unambiguously evidences the presence of surface-region anisotropy. We prepare Au nanoclusters from an ultrathin (~14 nm) Au film deposited on oxide-free, chemically nitridized GaAs surface. After vacuum annealing of such Au/GaAs structure at ~300ºC, AFM reveals a surface layer of Au nanoclusters whose sizes are ~20-30 nm. Formation of the nanoclusters results in the following. First, a broad deep appears at 2.5 eV in the reflectance spectrum of Au/GaAs structure (curves 1 and 2 in Fig. 1). Second, a resonant feature appears in RA spectrum $\Delta R/R$ at about 2 eV (curve 3 in Fig. 1). The reflectance deep is related with plasmon absorption in Au nanoclusters and the feature in RA spectrum evidences for the plasmonic anisotropy. Unlike In/InAs structures, spectral position of the plasmonic RA feature for Au/GaAs structures is insensitive to permittivity of surrounding dielectric. We conclude that Au clusters (~5 nm in size) responsible for the $\Delta R/R$ spectral feature are buried in near-surface region of GaAs crystal due to diffusion of Au atoms in annealing.

Fig. 1. Reflectance spectra of Au-GaAs structure before (1), and after (2) annealing, and $\Delta R/R$ spectrum (3).

For In/InAs structures measured plasmonic RA signal on the level of $|\Delta R/R|\sim0.4$ [1,2] is found to agree well with the related theory [3]. To explain the RA spectra, the nanocluster sizes or/and intercluster distances along axes [110] and [$1\bar{1}0$] of InAs crystal are estimated to differ by a few percents. Following the ideas of [1-3], we ascribe the effects of optical absorption and anisotropy (Fig. 1) of Au/GaAs structures to collective modes of dipole plasmons excited at normal light incidence in a layer of Au nanoclusters located near GaAs surface. For Au nanoclusters plasmons exist only below 2.5 eV, and smaller scale of observed spectrum $|\Delta R/R|\sim0.06$ (Fig. 1) and its larger width as compared with a single Au nanoparticle could be due to inhomogeneous broadening of the spectrum.

1. V.L. Berkovits, V.A. Kosobukin, V.P. Ulin, etc., «Reflectance anisotropy spectroscopy of metal nanoclusters formed on semiconductor surface», *JETP Lett*. 98, 614 (2013).
2. V.L. Berkovits, V.A. Kosobukin, V.P. Ulin, etc., «Plasmonic anisotropy of In nanocluster arrays on InAs(001) surface observed by differential reflectance spectroscopy», *Surf. Sci*. 632, L19 (2015).
3. V.A. Kosobukin, A.V. Korotchenkov, «Plasmonic anisotropy spectroscopy of metal nanoparticles on semiconductor surface», *Phys. Solid State* 58, 2536 (2016).

O3-8: The propagation of light-induced excitation of Si along the solid/(water solution of NaCl) interface

D.I. Tetelbaum[1], A.V. Stepanov[2], Yu. A. Mavricheva[1]

5. *Lobachevsky University, Nizhniy Novgorod, Russia, tetlbaum@phy.unn.ru*
6. *Chuvash State Agriculture Academy, Cheboksary, Russia,for.antonstep@gmail.com*

The new kind of long-range effect at irradiation of silicon by the light is revealed for the system including the fluoroplastic vessel filled by the H_2O:NaCl solution and two silicon samples on cap of the vessel. When one of the samples is irradiated by light, the properties of other sample are changed. This effect only takes place when both samples are covered by native oxide. The effect is interpreted using the model which was previously proposed for long-range effect in light-irradiated solid samples and is based on influence of hypersound waves (which are generated in the layer of native oxide) on the defect system of solid. In this work, we carry out the simulation of the hypersound waves propagation along the $(H_2O$:NaCl)/solid interface taking into account the $(Na^+-H_2O)_n$ clusters which assumed to be the sources of secondary oscillations and provide the long-distance penetration of the hypersound waves.

Molecular dynamic simulation of hypersound propagation through solid-water interface was provided via LAMMPS code [1]. ReaxFF force field potential [2] with charge equilibration method [3] was used. The periodic boundary condition for simulation box was used. The effect of average distance between clusters and the orientation were investigated. The instantaneous density change at the middle of the simulation box in water was indicated at start moment of simulation. We track the water density wave propagation during simulation time and calculate wave amplitude dynamics. The aim of the calculation is to established if the oriented clusters can provide enhanced propagation distance of hypersound along the solid/water interface.

1. Plimpton S. «Fast Parallel Algorithms for Short-Range Molecular Dynamics», *J. of Comp. Phys.*, 117, 1-19, 1995
2. Monti, S., et al. «Exploring the conformational and reactive dynamics of biomolecules in solution using an extended version of the glycine reactive force field», *Phys. Chem. Chem. Phys.*, 15, 15062-1507, 2013.
3. Rappe A. K., Goddard W. A. «Charge equilibration for molecular dynamics simulations», *J. of Phys. Chem.*, 95, 3358-3363, 1993.

O3-9: Influence of ambient and temperature of annealing on dislocation-related luminescence in silicon

A.A. Nikolskaya, D.S. Korolev, A.N. Mikhaylov, A.I. Belov, D.I. Tetelbaum

Lobachevsky Nizhny Novgorod State University, Nizhny Novgorod, Russia, alena.nikolskaya.1994@mail.ru.

The modern development of electronic technology requires the transition to smaller sizes of electronic components to increase the data transfer speed. At the same time, the size reduction physically limited by dimensional effects. Approaches of optoelectronics and integrated optics can be used as alternative methods of signal transmission. At the same time, compatibility of the developed approaches with microelectronic technology is important. Traditional material of microelectronics – silicon is an indirect band gap semiconductor; this fact makes difficult to use silicon as light emitter. One of the promising approaches to enhance its luminescent properties is using of the defect engineering approach, in particular, the creation of structures with dislocation-related luminescence (DL), one of bands (D1) of which is at ~ 1.5 μm and corresponds to the transparency window of quartz fibers. In addition, the creation of DL centers by ion implantation, which is considered in this paper, is very relevant since this method is compatible with traditional microelectronics technology. In this paper, the dependence of the parameters of DL (intensity, peak position) on the conditions of heat treatment with variation of temperature and atmosphere of post-implantation annealing has been studied.

Experimental samples were prepared on n-Si (resistivity of 4.5 $\Omega \cdot$cm) with (100) orientation and p-Si (resistivity of 1 $\Omega \cdot$cm) with (111) orientation wafers. Implantation with silicon ions was carried out with an energy of 100 keV and a dose of $1 \cdot 10^{15}$ cm^{-2}. To determine the most favorable conditions for the appearance of DL, investigations were carried out to establish the effect of ambient (depending on the proportions of the N_2 and O_2 components in the gas mixture) and annealing temperature (from 900 to 1100 °C) on the luminescence intensity.

It was found that the behavior of the D1 band intensity as a function of the oxygen content in the annealing atmosphere is significantly different for silicon initially doped with boron and silicon doped with phosphorus. For p-Si samples (boron concentration 10^{16} cm^{-3}) DL is observed under all annealing conditions and its intensity is practically independent of the oxygen content in the annealing atmosphere. In the case of n-Si samples, DL is observed only for annealing in an oxygen-containing atmosphere, and its intensity increases with increasing O_2 content. The observed regularities are apparently related to different environments of dislocation centers during annealing in different atmospheres.

The dependence on the annealing temperature is also different for the studied samples, which is explained by the difference in the character of the evolution of point defects. In case of n-Si the generation rate of intrinsic interstitial atoms increases with enhancing oxidation rate at high temperatures. At the same time, in p-Si, in which the intensity of PL is determined by the evolution of interstitial atoms accumulated during implantation, the dependence on the annealing temperature is related to the competition between their expenditure on the formation of D1 centers and their loss due to the diffusion to the surface. For annealing in a mixed atmosphere, optimum annealing conditions were found. Annealing in an optimum atmosphere at different temperatures has shown that the maximum of luminescence intensity is reached at 900 ° C for p-Si and 1100 ° C for n-Si.

O3-10: Получение методом ВЧ магнетронного распыления многослойных структур ZnS/SiO$_2$, ZnSe/SiO$_2$

Р. Закирова, В. Кобзиев, Н. Костенков, П. Крылов, И. Федотова

Удмуртский государственный университет, Ижевск, Россия, E-mail: ftt@udsu.ru

Исследования управляемых процессов роста наночастиц полупроводниковых материалов представляют большой интерес в связи с возможностью их применения в инжиниринге волновых функций материалов [1]. Исследование процессов создания полупроводниковых наночастиц по тонкопленочной технологии, широко применяемой в производстве интегральных схем, является актуальным направлением в материаловедении.

Синтезировали многослойные структуры методом ВЧ магнетронного напыления на установке Катод-1М. Для возможности позиционирования подложкодержателей относительно магнетронов и нагревателя и их сканирования по заранее заданной программе был разработан программно-аппаратный комплекс, использующий микросистему управления оборудованием [2]. Процесс формирования многослойных пленок включал в себя чередующиеся процессы напыления по заданной программе слоев сульфида или селенида цинка и диэлектриков. Толщина слоев диэлектриков в структурах не менялась. Менялось общее число пар ZnS (ZnSe)/диэлектрик и толщина слоев ZnS (dZnS) или ZnSe (dZnSe). Число пар слоев выбиралось таким образом, чтобы обеспечить суммарную толщину пленок порядка 0.4 μm. Температура подложек при напылении поддерживалась 150°С. Распыление мишени ZnS, ZnSe производилось при ВЧ мощности разряда 200W, а распыление мишени SiO$_2$ при мощности 300W. После напыления образцы достигали комнатной температуры без разгерметизации вакуумной системы. Толщина слоев для SiO$_2$ составляла 11.25 Å. В пленках ZnS/SiO$_2$ толщины ZnS составляли 7.8, 15.6, 23.4, 31.2 и 39 Å, а число пар слоев — 215, 152, 118, 96, 81. В пленках ZnSe/SiO$_2$ толщины ZnSe составляли 12, 20, 28, 36, 44 и 52, а число пар слоев — 200, 150, 114, 94, 80, 69.

Толщину слоистых пленок и скорость роста отдельных слоев определяли с помощью МИИ-4 и по спектрам пропускания, которые имели осциллирующий характер, обусловленный интерференционными явлениями. Показатель преломления определяли по спектрам пропускания с использованием конвертного метода [3] и по спектрам отражения. Спектры оптического пропускания и отражения (диапазон 300−1100 nm) регистрировали на спектрофотометре СФ-56. Структуру нанокомпозитных пленок исследовали методами рентгенодифракционного анализа на автоматизированном дифрактометре ДРОН-3.0 [4] в монохроматическом излучении Fe–$K\alpha$ и просвечивающей электронной микроскопией на электронном микроскопе ЭМ-125. После проведения цикла исследований дополнительно проводили отжиг в вакууме при 400°С.

Многослойные структуры ZnS/SiO$_2$, являются рентгеноаморфными, а структуры ZnSe/SiO$_2$ содержат аморфную матрицу SiO$_2$ и ZnSe кубической фазы. Пропускание структур в области длин волн 400-1100 нм структур составляет 80-95%. С увеличением толщины слоев полупроводников показатель преломления и ширина запрещенной зоны меняются.

Нагрев мультислойных структур ZnS/SiO$_2$ и ZnSe/SiO$_2$ приводит к перераспределению элементов по глубине, показатель преломления уменьшается, ширина запрещенной зоны увеличивается. На примере мультислойных структур ZnSe/SiO$_2$ показано, что образцы с малой концентрацией полупроводников являются более стойкими при нагреве.

1.   М. Б. Мурадов, Г. М. Эйвазова, Я. М. Елчиев, «Влияние термического отжига на структуру и оптические свойства наночастиц сульфида меди, сформированных в объеме полимерной матрицы», *Прикладная физика*, №5, сс. 94-97, 2010.

2.   С.С. Алалыкин, П.Н. Крылов «Микросистема управления оборудованием», *ПТЭ*, № 5, сс. 160–161, 2009.

3.   В.В. Брус, М.Н. Солован, Э.В. Майструк, И.П. Козярский, П.Д. Марьянчук, К.С. Ульяницкий, J. Rappich «Особенности оптических и электрических свойств поликристаллических пленок CdTe, изготовленных методом термического испарения», *ФТТ*, т. 56, вып. 10, сс. 1886–1890, 2014.

4.   С.С. Алалыкин, П.Н. Крылов «Автоматизация серийной установки рентгеноструктурного анализа Дрон-3», *ПТЭ*, № 2, сс. 149–150, 2005.

О3-11: Спектрофотометрический анализ в пленках a-Si:H a-nk-C:H

Б.А. Наджафов

Институт Радиационных Проблем НАН Азербайджана
e-mail: bnajafov@inbox.ru

В работе исследованы спектры ИК поглощения в пленках a-Si:H a-nk-C:H (a-аморфные, nk-нано кристаллические) в диапазоне энергии 0,03 ÷ 3,0 эВ. Определены оптические коэффициенты поглощения (α) пленок для слабо и сильно поглощающих областей спектра, а также коэффициенты преломления (n) и коэффициенты ослабления ($к_0$) для различных прозрачных и не прозрачных подложек.

В мировой науке проводилось достаточное исследование в направлении измерения и изучения тонких пленок. Однако в направлении измерения интерференции и расчета оптического поглощения не получены конкретные формулы, которые могли бы упростить результаты экспериментальных работ. В этой работе проводился краткий анализ опубликованных многочисленных статей и получены расчеты, улучшающие работы исследователей. Пленки Si и их сплава характеризуется различными структурными фазами. Наиболее интересными из них являются кристаллическими зерна, находящиеся в аморфной матрице. Нано размерные эффекты тонких пленок сопровождаются образованием нано трубок, нано проволок, нано частиц, фуллеренов, эндо фуллеренов, графитов, графинов, квантовая точка, квантовая яма, кластеров и др. Образование этих нано материалов обычно связано структурными дефектами, наличием и ролью водорода в их составе. В литературе оптические свойства нано материалов изучены недостаточно. Поэтому измерение оптических параметров – коэффициентов поглощения (α), отражения (R), пропускания (T), преломления (n), коэффициент ослабления ($к_0$), толщины (d) тонких пленок и определение на их основе ширины запрещенной зоны ($Е_0$) представляют интересным. Используя условие сохранения энергии можно найти коэффициент поглощения α [1].

$$\alpha = f(R, T, k_0, n)$$

Отметим, что $к_0$ - показывает ослабление света в системе пленке-подложке.

Это уравнение хорошо согласуется с уравнением для прозрачной подложки в сильно и слабо поглощающих областях спектра. Здесь $R = R_1 = R_2 = R_3$ соответственно отражение света пленка-воздух, пленка-подложка, подложка-воздух. α - коэффициент поглощения данной пленки, Т- пропускание пленки, n- коэффициент преломления пленки.

Данные параметры можно также определить с помощью спектрометров ИКС-21, ИКС-14А, ИКС-22, ИКС-29, Фурье-ИК, Varian 640 JR, в области энергий 0,03 ÷ 3,0 эВ и более.

1. *Физика гидрогенизированного аморфного кремния.* Под редакцией Дж. Джоунопулоса и Дж. Льюковски . Пер . с англ. Л. И . Косарева и А. А Андреева. Москва «Мир» .вып. 2 .1988 , 447 с.

O3-12: Effect of optical nonhomogeneities on travelling thermo-optics switching waves along silicon wafer surface on lamp-based heating

V.Ovcharov, V.Prigara, A.Kurenya,V.Rudakov

Yaroslavl Branch of the Institute of Physics and Technology, Institution of Russian Academy of Science, Yaroslavl, Russia, ovcharov.vlad@gmail.com

Technological processes for the fabrication of semiconductor micro- and nano-devices include a thermal treatment stage. Silicon continues to be used as the basic material in semiconductor technology and the most prevalent setups for thermal processes are rapid thermal processing ones (RTP), the major element of which is a lamp-based chamber. A silicon wafer in such a chamber is a part of the multicomponent thermodynamic system, and its behavior depends on controlling parameters giving a heat input to the wafer and a heat output from it.

The silicon wafer demonstrates a complex behavior at high energy fluxes incident on the wafer and leaving it. It reveals the following effects: bistability, temperature and optical self-induced oscillations, temperature switching waves. The effects are dependent both on the doped level of the whole silicon wafer and the doped level of the surface layer where semiconductor devices are fabricated. In specific thermal modes, the optical property variations along the wafer surface are responsible for causing thermo-optics switching waves [1]. A plausible coincidence between experimental and theoretical parameters of the heat transfer process of the wafer with thermal chamber elements is needed to be gained. It requires, in its turn, more complex models of the chamber, a deeper sense of interacting incoherent radiation with silicon wafer and refining experimental techniques for the observation of the effects.

In the paper the theoretical and experimental studies of thermo-optics switching waves are carried out. These waves travel along the silicon wafer surface on heat treatment into a lamp-based chamber in dependence on the parameters of the optical nonhomogeneities on the wafer surface and heat transfer conditions between the wafer and the elements of the chamber. The intervals of the parameters controlling by the thermal system modeling the chamber and characteristics of the optical nonhomogeneities including the mode of travelling the switching waves are obtained.

1.   V.V. Ovcharov, A.L. Kurenya, V.I. Rudakov, V.P. Prigara, "Temperature switching waves in a silicon wafer on lamp-based heating", In *International Conference on Micro-and Nano-Electronics 2016*, pp. 1022422-1022422. International Society for Optics and Photonics, December 2016.

O3-13: Additive technology for high-temperature ceramic MEMS sensors

A.Vasiliev[1,2] , A.Nisan[2], G.Potapov[2], A.Pisliakov[1], I.Shakhnovich[2], N.Samotaev[3]

[1]*National research center" Kurchatov institute",Moscow, Russia, A-A-Vasiliev@yandex.ru.*
[2]*RIIT LLC, OSTEK enterprise, Moscow, Russia*
[3]*National research nuclear university MEPhI, Moscow, Russia*

One of most usable type of gas sensors applied for the monitoring of composition of gas admixtures in the atmosphere and technological gases is semiconductor gas sensor. Operation principle of these sensors is based on the change in carrier (electrons of holes) concentration at the chemisorption of donor or acceptor gases. To accelerate sorption process, the nanoparticle consisting sensing layer of wide band metal oxide semiconductor should be heated to a temperature of $200 - 500^0C$. On the other hand, heating power of the sensor must be minimized to assure the possibility to use the sensors in wireless and autonomous instruments. The solution of this contradictory requirement is the application of MEMS technology.

Recently developed technology of silicon MEMS for the fabrication of low power consuming semiconductor gas sensor (Fondazione Bruno Kessler (FBK, Italy), AMS (Austria), Figaro (Japan)) or polyimide substrate [1] have evident disadvantages due to restricted annealing and working temperature (about $300 - 350^0C$ for both microhotplate, and 450^0C for FBK's unit). Another problem is the application of expensive and sophisticated equipment in silicon technology and the use of sputtering processes in the fabrication of noble metal (Pt, Au) layers. The third problem is low flexibility of traditional microelectronic process leading to difficulties in the fabrication of different modifications of sensors using the same process. These problems make the silicon technology hardly usable in sensor manufacturing. We present an overview of our results obtained with the application of additive aerosol and ink jet technologies for the fabrication of high temperature (up to $400 - 500^0C$) gas, flow, and temperature sensors. The application of jet printing in combination with ceramic MEMS structures enables flexible fabrication of cost efficient devices with thermal characteristics compatible with those of silicon based MEMS.

We developed the technology of thin ceramic membranes usable in high-temperature ceramic MEMS devices operating at temperature up to $450 - 500^0C$. The material of membrane is Al_2O_3, LTCC, or yttria stabilized zirconia – YSZ (10 – 20 μm thick). Membrane is stretched on rigid frame made of the same material as membrane to assure its robustness.

The metallic inks with Pt, Au, and Ag nanoparticles can be printed over these ceramic membranes giving stable (Pt) microheater working up to 500^0C. The heater is fabricated using ink or aerosol jet printing with Pt nanoparticle. Typical particle size of these inks is of $3 - 8$ nm. After sintering, this print gives a microheater stable at temperature up to 500^0C. Power consumption of the sensor is ~80 mW at 450^0C, this is comparable with Si-based MEMS. Cantilever shaped microhotpalate made by laser cutting of the membrane improves the stability of the microheater at temperature cycling and decreases power consumption. The nanoparticle sensing layers of chemoresistive of thermochemical gas sensors based on metal oxide semiconductors or catalysts are printed using the same technique giving efficient semiconductor and thermocatalytic gas sensors. The temperature cycling of the sensing layer enables an improvement of sensor selectivity, in particular, for CO and H_2 gases and a decrease in power consumption down to < 1 mW. The sensors demonstrate usual response to gases, it is equal, for example, to factor of $7 - 10$ at methane concentration of 1 vol. %. Detection limit of selective measurement of CO and H_2 is of about 1 ppm. Smart modules fabricated for controlling MEMS sensors assure plug-and-play operation mode of sensor units. This module realizes the algorithms of signal linearization and provides information about sensor calibration, type of gas sensor, target gas and other data necessary to recognize the sensor via digital bus. Important advantage of these smart sensor units is the possibility to replace them easily by precalibrated ones for periodical recalibration in laboratory conditions.

The main field of application of such sensors, in addition to normal condition devices, is high temperature use in car industry, heavy accident and combustion process monitoring.

1. Mathilde Rieu, Malick Camara, Guy Tournier, et al. Fully inkjet printed SnO_2 gas sensor on plastic substrate. Sensors and Actuators, B, 236 (2016), 1091-1097.
2. A.A. Vasiliev, A.V. Pisliakov, A.V. Sokolov, et al. Non-silicon MEMS platforms for gas sensors. Sensors and Actuators, B, 224 (2016), 700-713.

O3-14: Micro- and nanochannel formation by dry e-beam etching of resist

A. Rogozhin[1], M. Bruk[1,2], E. Zhikharev[1], F. Sidorov[1,3], D. Streltsov[4]

[1]*Institute of Physics and Technology of RAS, Moscow, Russia, rogozhin@ftian.ru*
[2]*L.Ya. Karpov Institute of Physical Chemistry, Moscow, Russia, marbruk@yandex.ru*
[3]*Moscow Institute of Physics and Technology, Dolgoprudny, Russia, fedor.sidorov.92@gmail.com*
[4]*Enikolopov Institute of Synthetic Polymer Materials of RAS, Moscow, Russia, dmitry.streltsov@gmail.com*

Nanofluidics can provide numerous novel technology possibilities [1]. Lots of physical mechanisms operate efficiently in the nanoscale range, for example, Van der Waals forces, electrokinetic effects, and rarefied dynamics [2]. On the other hand, many of the biological processes involving fluids operate within pores of nanoscopic dimensions. Exploring the fluid transport across nanoscale objects could lead to new solutions to big challenges [1]. The transition from microfluidics to nanofluidics requires new technologies. The fabrication method for micro- and nanofluidic channels and systems is required.

Dry e-beam etching of resist (DEBER) in combination with standard e-beam lithography could be the solution. DEBER is a method of relief formation in some positive resists during electron-beam exposure in vacuum [3-5]. The method is based on the chain depolymerization reaction, which takes place in the polymer resists during e-beam exposure at the glass-transition or higher temperatures. The volatile reaction products (monomers) are pumped out during exposure. The method could be realized in a number of e-beam lithography systems, scanning electron microscopes (SEM) or focused e-beam induced processes (FEBIP) systems. The method provides high vertical resolution but the lateral resolution is low.

In this study, micro- and nanochannels obtained by the DEBER method are presented (Fig. 1). The sensitivity of the resist in the DEBER method is 100-1000 times higher than in the standard e-beam lithography. As a result, the throughput of the method is comparably high. Although the lateral resolution is only about 100-200 nm the method could be used in combination with the standard lithography. As a result, large parts of the nanofluidic system could be quickly formed by the DEBER method. For small elements, high-resolution e-beam lithography can be used in the same fabrication system.
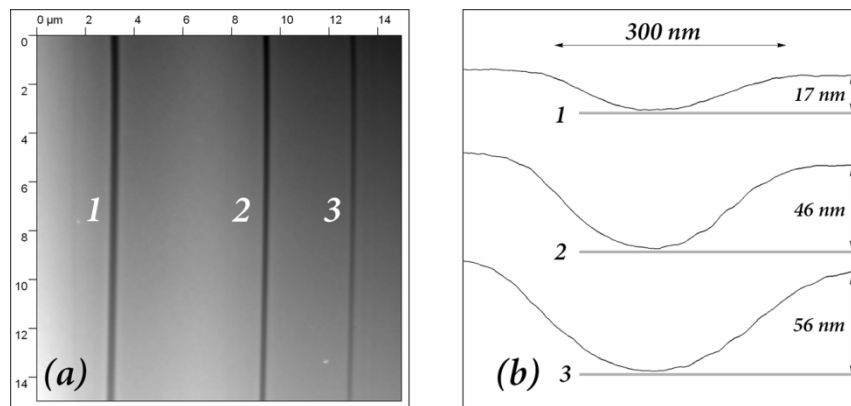
Fig. 1 (a, b). AFM image of channels, obtained by DEBER method, and their profiles. The channels were obtained in the Ultra-55 SEM system with exposure time 1 s (curve 1), 4 s (curve 2) and 16 s (curve 3).

1. L. Bocquet and P. Tabeling, "Physics and technological aspects of nanofluidics", Lab Chip, **14**, pp.3143-3158, 2014
2. P. Tabeling, *Introduction to microfluidics*, Oxford Univ. Press, UK, 2005
3. M.A. Bruk, E.N. Zhikharev, V.A. Kalnov, A.V. Spirin, D.R. Streltsov, Russian Federation patent 2478226, Russian Bulletin of Inventions, **9**, 2013
4. M.A. Bruk, E.N. Zhikharev, D.R. Streltsov, V.A. Kalnov, A.V. Spirin, "The new dry method of mask (relief) formation by direct electron-beam etching of resist", Microelectronic Eng., **112**, pp.1-4, 2013
5. M.A. Bruk, E.N. Zhikharev, A.E. Rogozhin, D.R. Streltsov, V.A. Kalnov, S.N. Averkin, A.V. Spirin, "Formation of micro- and nanostructures with well-rounded profile by new e-beam lithography principle", Microelectronic Eng. 2016, **155**, pp.92-96, 2016

O3-15: Investigation surface transition regions of microelectromechanical SOI sensor interfaces

L. V. Sokolov

Institute of Aircraft Equipment, Zhukovsky, Moscow region, 140180 Russia, sokol@niiao.com

The results of analysis of the single silicon–glassy dielectric–single silicon surface morphology used in the microelectromechanical system monolithic chip of a MEMS sensor [1, 2] are presented. Possible reasons for the formation of mechanical stresses local centers from used the production technology are discussed. Investigation of the transition surface regions at the interfaces of the silicon hetero-structure offers a qualitative analysis of a possible formation stress centers reasons in order to optimize the production technology. The interfaces are studied with scanning electron microscopy and atomic force microscopy (AFM).The formation of nanoscale clusters, presumably, clusters of silicon atoms, is found in the transition layer in the local area under the frame of a MEMS sensor and local formations of glass nanoclusters are detected in the surface layer of the silicon membrane. Such formations probably appear because of interfacial interactions of the glassy dielectric components in the vapor phase with the surface layer of single silicon in the solid phase, accompanied by mutual diffusion of the components. The defects resulting in these processes may cause local mechanical stresses.

A lot of formations in the form of nanoscale bubbles are found on the surface of the glassy dielectric layer, the cause of the origin of which may be humidity during the high temperature process of the direct thermocompression bonding of silicon wafers into the SOI structure.

There are crack nucleation centers in the glassy dielectric layer on the chip surface close to the marks of the anode contact elements. Micro-cracks of nanometer depth diverge radially from these centers. A probable cause of micro-cracks may be the hard modes of anodic bonding of Pyrex glass support and the chip sensor.

1.   Leonid V. Sokolov. «Conceptual basis for creating new-generation high-stable high-temperature microelectromechanical sensors based on a silicon-on-isolator hetero-structure with a monolithic integral tensoframe for intelligent transducers» *Proceedings of ISMTII-2009, 9th International Symposium on Measurement Technology and Intelligent Instruments*, volume 3. S-Petersburg, 29 June – 2 July 2009, pp. 248-251.
2.   Leonid V. Sokolov. «Research of SOI Microelectromechanical Sensors with a Monolithic Tensoframe for High-Temperature Pressure Transducers» *219th ECS Meeting Transactions. Advanced Semiconductor-on-Insulator Technology and Related Physics 15. Edited by Y. Omura et al.*, Volume 35, Issue 5, pp. 135-141. 1-6 May, 2011, Montreal, QC, Canada.

P1-1: Magnetic fluctuations sorted by magnetic field in MnSb clusters embedded in GaMnSb thin films

A. Dmitriev

Institute of Problems of Chemical Physics, Russian Academy of Sciences, Chernogolovka, Russia,
E-mail address aid@icp.ac.ru

Dynamics of magnetization reversal of the MnSb clusters embedded in GaMnSb thin films has been studied [1]. The lognormal distribution of ferromagnetic MnSb cluster sizes $f(D)$ has been extracted from the field and temperature dependences of magnetic viscosity $S(T,H)$ in GaMnSb thin films. An average cluster diameter D=55 nm is in agreement with the magnetic force microscopy data. Magnetic anisotropy constant $3.2 \cdot 10^4$ erg/cm^3 has been determined. The fluctuation field H_F=7 Oe and the activation volume V_A=$1.7 \cdot 10^{16}$ cm^3 have been calculated from the magnetic viscosity data. Stepped sweeping of the magnetic field expands the windows of experimentally detectable fluctuations. The change in the reversal magnetic field provides the scanning of the MnSb clusters sorting them by fluctuation time (or frequency).

The generality of the processes of spontaneous and induced magnetization reversal of MnSb clusters embedded in GaMnSb thin films was found. Kinship of thermally activated and field-induced processes of magnetization reversal reflected in the fact that the maximum magnetic field dependence of the viscosity of $S(H)$ coincides with the coercive field H_C of sample. The analysis of this experimental fact has allowed to obtain a formula that establishes a connection of the H_C with parameters of model describing the $S(H)$ dependence. This formula is identical to the well-known Kneller law determined the temperature dependence $H_C(T)$ of non-interacting superparamagnetic nanoparticles [2].

1.   A.I. Dmitriev, A.D. Talantsev, O.V. Koplak and R.B. Morgunov, «Magnetic fluctuations sorted by magnetic field in MnSb clusters embedded in GaMnSb thin films», *J. Appl. Phys*., 119, pp.073905-1-6, 2016
2.   E.F. Kneller and F.E. Luborsky, «Particle Size Dependence of Coercivity and Remanence of Single Domain Particles», *J. Appl. Phys*., 34, pp.656-658, 1963

P1-2: Epitaxial growth of bi-layered Fe-FeMn films and study of their magnetoresistive properties

V. Berezin, <u>A. Chernykh</u>, D. Irzhak, G. Mikhailov

Institute of microelectronics technology and high purity materials RAS, 6, Academician Ossipyan str, Chernogolovka, Moscow Region, 142432, Russia, E-mail address: mikhailo@iptm.ru

Investigation was made how epitaxial quality of the grown bi-layered Fe-FeMn films with different order of the layers influences on their magnetoresistive properties. The work is motivated by potential application of investigated structures in spintronics.

High-vacuum pulse laser deposition technique was applied for film growing on the R-faced sapphire substrate. It was demonstrated by application of X-Ray diffraction that FeMn/Fe/Mo/R-sapph films with Fe-layer beneath FeMn-layer are epitaxially grown; their epitaxial relations are following FeMn(200)||Fe(200)||Mo(200)||R-pl, FeMn[022]||Fe[022]||Mo(022)|| $Al_2O_3[11\overline{2}0]$ with 4° inclination of the normal (fig. 1). X-Ray analysis also showed that besides of high epitaxial quality Fe(100) layer growth the epitaxy of FeMn(100) layer is observed despite of large interlayer lattice parameters mismatch. For the bi-layered film growth with FeMn layer beneath Fe-layer the epitaxial growth was not realized. Fabricated for magnetoresistive experiments bridge-type structures were temperature treated above FeMn Neel temperature followed by slow cool-down procedure in external in-plane magnetic field.
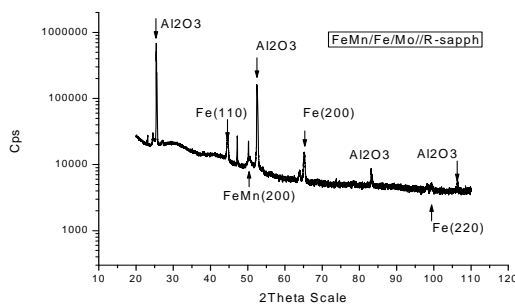
Fig.1. X-Ray θ-2θ scan for FeMn(200)/Fe(200)/Mo(200)/R-pl. film.
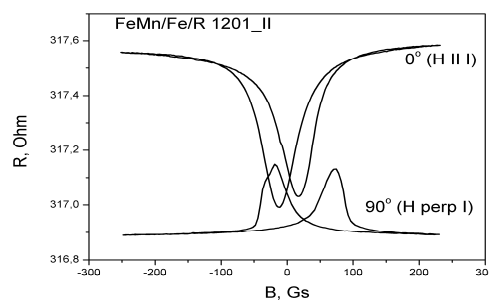
Fig.2. Magnetoresistance of FeMn(200)/Fe(200)/Mo(200)/R-pl. bridge-type structure annealed in magnetic field perpendicular to the bridge axis.

Appearance of an exchange bias in magnetoresistive epitaxial bridge-type structure dependences appoints the non-compensated (polar) interface between antiferromagnetic FeMn and ferromagnetic Fe layers (fig. 2).
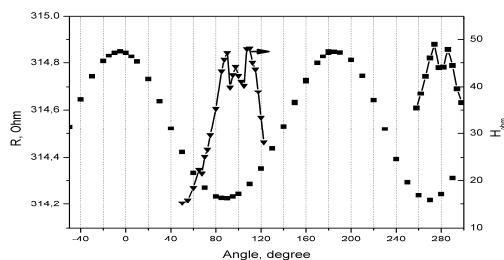
Fig. 3. Dependence of FeMn/Fe/Mo/R bridge resistance and exchange bias versus direction of in-plane magnetic field. The bridge was preliminary annealed in magnetic field perpendicular to the bridge axis.
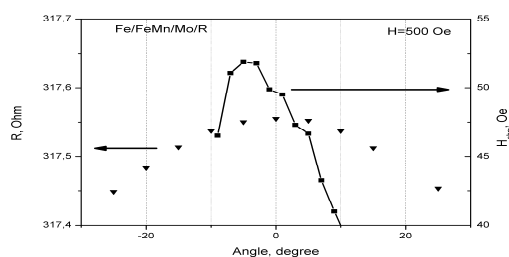
Fig. 4. Dependence of FeMn/Fe/Mo/R bridge resistance and exchange bias versus direction of in-plane magnetic field. The bridge was preliminary annealed in magnetic field along to the bridge axis.

Mutual displacements of exchange bias and anisotropic magnetoresistance versus the direction of in-plane magnetic field (fig's. 3 and 4) is originated from non-coincidence in about 8° angle of FeMn antiferromagnetic vector with [100] axis in Fe layer that is beneath FeMn layer.

P1-3: Deposition of C, CH, CH$_2$ and CH$_3$ onto graphene

V. Stelmakh[1] , A. Dzhurakhalov[2] , I. Yadgarov[3]

1.   *State Technical University, Tashkent, Uzbekistan, vasiliycat17@rambler.ru. 2. University of Antwerp, Antwerpen, Belgium, dzhurakhalov@mail.ru. 3 Tashkent institute of textile and light industry, Tashkent, Uzbekistan, iyadgarov@mail.ru.*

Using energy minimization method the more stable structures of CH, CH2 and CH3 molecules and of defect-free graphene were found. For description of the interatomic potential we used Brenner interatomic potential [1], which is specifically parameterized for the carbon and hydrogencarbon systems. Then by the molecular dynamics method and using the same Brenner potential, computer modeling of deposition of C, CH, CH$_2$ and CH$_3$ particles onto defect-free graphene was carried out.

The results of computer simulations, the structures and the various structural changes of graphene caused by the deposition of carbon atoms and CH, CH$_2$ and CH$_3$ molecules are presented and discussed. Some results of deposition are shown in the figure below.
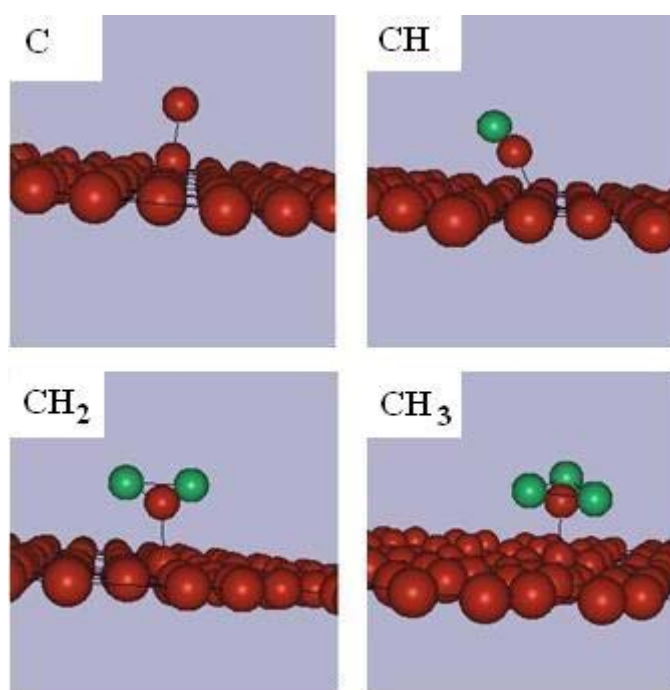
Figure. The C, CH, CH$_2$ and CH$_3$ deposited on graphene. Red circles are carbon atoms, green circles are hydrogen atoms.

1.   D.W. Brenner, O.A. Shenderova, J.A. Harrison, S.J. Stuart, B. Ni and S.B. Sinnot, «A second-generation reactive empirical bond order (REBO) potential energy expression for hydrocarbons», *J. Phys: Condens. Matter*, 14, pp783-802, 2002

P1-4: Sputtering of graphene by low-energy carbon atoms at different angles of incidence

V. Stelmakh[1]

1.   *State Technical University, Tashkent, Uzbekistan, vasiliycat17@rambler.ru*

For theoretical analysis of sputtering of graphene the carbon atoms as the causing sputtering with an energy of 100 electron-volts (eV) were selected. For a description of the interatomic interaction the Brenner interatomic potential [1], which is a good description of the interatomic interaction of carbon, was used. Computer rectangular model of a defect-free graphene, consisting of 112 carbon atoms with the distance between the nearest atoms is 1.42 angstrom, with the imposition of periodic boundary conditions along the graphene plane was built. The angle of incidence of carbon atoms, measured from the normal to the graphene along armchair- and zigzag-directions, from 0° to 85° in steps of 5° was varied. As demonstrated by computer simulations, at angles greater than 75° sputtering of graphene is not observed. For each angle and each direction of incidence place of falling in the defect-free graphene 100 times random was set. According to the results of computer simulation the sputtering and deposition rates for each angle of incidence and each directions were determined. These rates were obtained under the assumption that the flow of falling carbon atoms is so weak that the sputtered graphene does not become much amorphous structure due to impact this flow. Graphs of these rates on the angle of incidence were obtained and discussed.

1.   D.W. Brenner, O.A. Shenderova, J.A. Harrison, S.J. Stuart, B. Ni, S.B. Sinnot, J. *Phys: Condens. Matter* 14, 783 (2002).

P1-5: Ion bombardment as a way to change the current-voltage characteristics of the p-i-n-diode

V. Stelmakh[1] , A. Leiderman[2]

7. *State Technical University, Tashkent, Uzbekistan, vasiliycat17@rambler.ru.*
8. *2. Physicotechnical institute, Tashkent, Uzbekistan, ley@uzscinet.uz.*

One of the important indicators of semiconductor devices is their current-voltage characteristic (CVC) and, accordingly, one of the important issues of how to change the current-voltage characteristics in the production of the device. Here, the possibility of changing the CVC p-i-n-diode by creating uneven distribution of concentration of the recombination impurity by ion bombardment of the starting material was examined. As bombarding ions the carbon ions and boron ions were chosen, and as a starting material the crystal of silicon carbide, which is a typical material for the production of p-i-n-diodes, was selected. To simulate the processes of implantation of bombarding ions and of the formation of defects in silicon carbide SRIM program [1] was used. It was found it is possible to choose such modes of ion bombardment, that the distributions of vacancies $N_R(x)$ in silicon carbide are linear $N_R(x)=B \cdot (x+x_0)$ or are with a minimum of type $N_R(x)=C/[(x-a)^2 \cdot (x-b)^2]$, where B, C, x_0, a, b are some parameters.

If one assumes that these vacancies are determining recombination centers, then according to our calculations the CVC of p-i-n-diode could be of the form $J \sim U^{4+\beta}$, where $-0.8<\beta<0.8$. For conventional linear distribution of recombination impurities CVC of type $J \sim U^4$ (see [2]) would be observed.

Thus, the creation of the uneven distribution of recombination impurities by ion irradiation changes the CVC of p-i-n-diode.

1. http://www.srim.org
2. E.I. Adirovich, P.M. Karageorgiy-Alkalaev, A.Yu. Leiderman, «Double injection currents in semiconductors». *Soviet Radio*, Moscow, 1978.

P1-6: The role of the scavenger in electrochemical exfoliation of graphite

N. Savinski[1], D. Puhov[1], M.Lebedev[1], L.Mazaletskiy[1], S.Vasilev[1], M. Izumov[1], E.Parshin[1],
M. Soloviev[2], A. Surovtsev[3],

1 Yaroslavl Branch of the Institute of Physics and Technology, Institution of Russian Academy of Sciences
2 Yaroslavl State Technical University
3 Joint Stock Company Research Institute "Yarsintez"

The exceptional electronic, thermal, optical, and mechanical properties of graphene render it a remarkable candidate for the next generation of electronic and optoelectronic devices [1]. Consequently, techniques for the scalable production of high-quality, solution - processable graphene are needed. Among the numerous protocols employed to date, the exfoliation of bulk graphite is most common for harvesting graphene sheets on a large scale because of its low process complexity and costs. Direct exfoliation in the solid state (e.g., scotch-tape cleavage, ball milling or in a liquid phase (e.g., liquid phase sonification, shear force exfoliation, also known as physical exfoliation, provides feasible means for producing graphene with a low number of defects. In comparison, chemical exfoliation, which generally relies on Hummers' method, offers a wide range of flexibility for the production of graphene oxide (GO) and related materials because of the potential scalability, impressive conversion efficiency (~100%), and superior processability [2]. Unfortunately, the unique physical properties of graphene are seriously compromised and cannot be sufficiently recovered, even upon reduction, because of the appreciable fraction of oxygen groups and defects that are left behind. These oxygen groups restrict its usage in fine applications [3]. Electrochemical exfoliation has recently emerged as a promising strategy for producing graphene on an industrial scale with high efficiency, at low cost, and in an environ-mentally friendly manner. Anionic intercalation (primarily in aqueous electrolytes) is less time demanding and can take less than 1 h. However, the graphene produced is generally decorated with functional oxygen groups that occur due to the positive potentials used, especially with acidic electrolytes. Nevertheless, the radicals (e.g., HO•) generated from water electrolysis will unavoidably disrupt the graphitic structure during the exfoliation process [4]. Therefore, it is highly desirable to eliminate these radicals to ultimately improve the quality of the graphene. In this study, the electrochemical exfoliation of graphene is carried out in the presence of a series of antioxidants (such as ascorbic acid, hydrazine, sodium borohydride, dimethylsulfoxide (DMSO), (2,2,6,6-tetramethylpiperidin-1-yl)oxyl (TEMPO)), 2,2,6,6-tetramethyl-4-one-piperidin-1-yl)oxyl (IPON), Dimer (2,2,6,6-tetramethylpiperidin-1-yl)oxyl-fulvalene (YARSIM-0215) in a neutral aqueous electrolyte (ammonium sulfate) to suppress the formation of radicals from water electrolysis. Remarkably, using TEMPO, the electrochemically exfoliated graphene (EG) produced is of exceptionally high-quality, and the process gives high exfoliation efficiencies.

1. Novoselov, K. S.; Geim, A. K.; Morozov, S. V.; Jiang, D.; Zhang, Y.; Dubonos, S. V.; Grigorieva, I. V.; Firsov, A. A. «Electric Field Effect in Atomically Thin Carbon Films.» *Science*, v. 306,pp.666, 2004.
2. Savinski N. ,Vasiliev S., Naumov V., Soloviev M., Shvircova N. «The oxidation of exfoliated graphite» *Bulletin Of The Yaroslavl State University. A series of Natural and technical Sciences* . v 4. pp.73-79, 2013.
3. Savinski N. ,Vasiliev S., Naumov V., Soloviev M., Shvircova N. «Microwave heating of intercalated graphite» *Bulletin Of The Yaroslavl State University. A series of Natural and technical Sciences*. v 4. pp. 80-86, 2013.
4. S.Yang,S. Brüller,Z.Shuai Wu,Z. Liu,K. Parvez,R. Dong,F. Richard,P. Samorì, X. Feng,K. Müllen «Organic radical-assisted electrochemical exfoliation for the scalable production of high-quality grapheme». J. Am. Chem. Soc., v.137,pp 13927−13932, 2015

Р1-7: Методика количественного фазового анализа определения содержания фуллеренов в фуллереновой саже

С.П. Кузькина, Р.М. Закирова, П.Н. Крылов

ФГБОУ ВО «Удмуртский государственный университет», Ижевск, Россия, ftt@udsu.ru

Наиболее распространенный способ получения фуллеренов – дуговая технология, при которой образуется фуллереносодержащая сажа. Одним из методов контроля содержания фуллеренов в саже может быть рентгеновский фазовый анализ: качественный и количественный.

Рентгеновский количественный фазовый анализ основан на определении интенсивностей линий исследуемых фаз и сравнении интенсивностей линий определяемых фаз между собой или с интенсивностью линии эталонного образца, полученной на дифрактограмме [1]. Все методы количественного фазового анализа основаны на том, что каждое вещество даёт определённый набор интерференционных линий, который не зависит от других веществ, присутствующих в образце. Соотношение интенсивностей линий данной фазы не меняется, хотя интенсивность каждой линии пропорциональна содержанию фазы в веществе [2]. При одном и том же содержании определяемой фазы интенсивность её линий изменяется в зависимости от среднего коэффициента поглощения рентгеновских лучей в образце. Поэтому необходимо найти эту зависимость и определить коэффициент поглощения образца либо устранить влияние фактора поглощения. Исследование структуры фуллеренов и фуллереновой сажи проводили на автоматизированном рентгеновском дифрактометре ДРОН-3.0 [3]. Съемку исследуемых образцов вели на монохроматизированном Fe-K_α излучении в пошаговом режиме методом постоянного времени в интервале брэгговских углов 2θ от 10 до 100°. Шаг сканирования составлял 0.1°. Время съемки в каждой точке 2θ составляло 30 сек. В качестве монохроматора использовали кристалл пирографита. На дифрактограмме фуллереновой сажи четко определяются три фазы: кристаллические графит и фуллерен (С60) и аморфная фаза. Аморфная фаза состоит из собственно сажи, т.е. неструктурированного углерода. Для определения содержания фуллерена в саже использовали метод измерения отношений интенсивностей аналитических линий [2], который заключается в следующем. Измеряют интенсивность аналитических линий (в нашем случае $I_\text{ф}$ и $I_\text{г}$) по одной для каждой фазы. Поскольку анализируются две фазы, то составляют систему двух уравнений:

$$\frac{I_\text{ф}}{I_\text{г}} = k\left(\frac{C_\text{ф}}{C_\text{г}}\right), C_\text{ф} + C_\text{г} = 1, \tag{1}$$

где C_i – массовая доля фазы i.

Коэффициент *k* можно определить съемкой смесей с известным содержанием фаз. Решая систему уравнений (1), находят содержание фаз. Относительная погрешность данного метода составляет 1-3%. Для построения градуировочного графика были приготовлены смеси из чистого фуллерена С60 и графита с известным содержанием фаз. В качестве аналитических линий были выбраны отражения (002) графита и (311) фуллерена С60, как наиболее интенсивные и близкие по углу отражения. Интегральные интенсивности рефлексов считали как площади под профилем кривых отражений графита и фуллерена с четко проведенной линией фона. По отношению интегральных интенсивностей аналитических линий графита и фуллерена был построен градуировочный график в координатах $I_\text{ф}/I_\text{г} = f(C_\text{ф}/C_\text{г})$. По уравнению полученной градуировочной прямой определили коэффициент пропорциональности *k*, что позволило находить содержание фуллерена в саже по формуле: $I_\text{ф}/(I_\text{ф} + kI_\text{г}) = f(C_\text{ф})$. Предложена и отработана методика определения количества фуллерена в фуллереновой саже методом количественного рентгенофазового анализа.

1. С.С. Горелик, Ю.А. Скаков, Л.Н. Расторгуев. *Рентгенографический и электронно-оптический анализ*. М.: МИСИС, 2002
2. А.А. Русаков. *Рентгенография металлов*. М.: Атомиздат, 1977
3. С.С. Алалыкин, П.Н. Крылов. «Автоматизация серийной установки рентгеноструктурного анализа ДРОН-3» ПТЭ, 2, с. 149–150, 2005

P1-8: Computer simulation of the interaction of fullerenes with carbynes

V. Stelmakh[1]

9.   *State Technical University, Tashkent, Uzbekistan, vasiliycat17@rambler.ru.*

Using energy minimization method the stable structures of both freestanding fullerene and freestanding carbynes (C_n, n=5,6) were found. For description of the interatomic potential Brenner interatomic potential [1], which is specifically parameterized for the carbon systems, was used. Then by the same energy minimization method and using the same Brenner potential, computer modeling of the interaction of the fullerene with the carbines was carried out.

The results of computer simulations, the various structural changes of both the fullerene and the carbynes caused by their interaction as well as binding energies of these formed structures are presented and discussed. Some results are shown in the figure below.
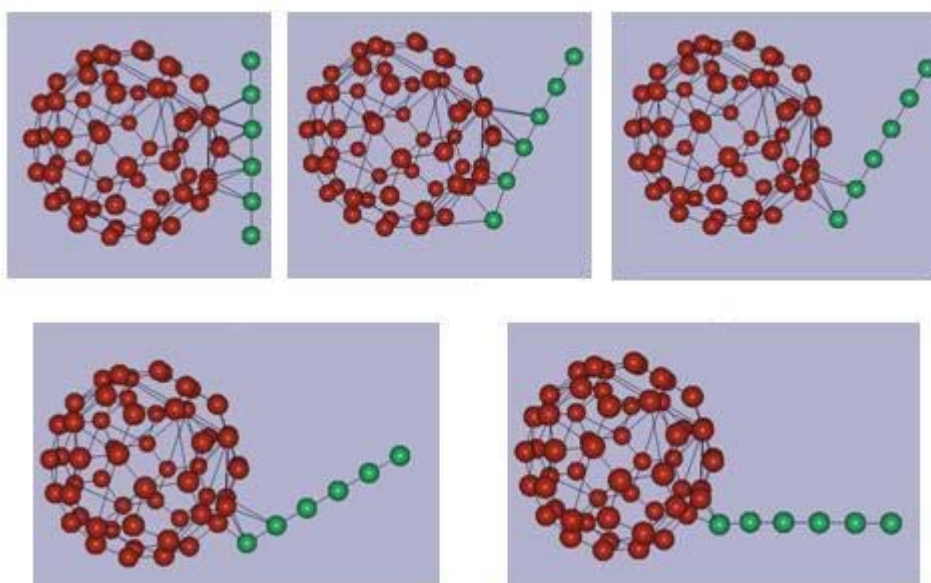
Figure. Some cases of interaction fullerene with carbynes. Red circles are carbon atoms of fullerene, green circles are carbon atoms of the carbyne C_6.

1.   D.W. Brenner, O.A. Shenderova, J.A. Harrison, S.J. Stuart, B. Ni, S.B. Sinnot, *J. Phys: Condens. Matter* 14, 783 (2002).

P1-9: Circularly polarized light detector based on MDP structure of CoPt / (Al$_2$O$_3$/SiO$_2$/Al$_2$O$_3$) / InGaAs / GaAs

A.V. Zdoroveyshchev[1], A.V. Kudrin[1], M.V. Dorokhin[1], P.B. Demina[1], O.V. Vikhrova[1], I.L. Kalentyeva[1], M.V. Ved'[1]

[1]NIFTI UNN, 603950, Nizhny Novgorod, Gagarin Ave., 23/3.

Circular-polarized light detectors showing the connection between electrical properties (current or voltage) and sign or/and degree of light polarization can be used in optical information transmission systems. In this paper, we proposed a version of detector for circular-polarized light based on the effect of magneto-circular dichroism (MCD).

Structures studied were a layer of In$_{0.15}$Ga$_{0.85}$As (thickness ≈200 nm) grown on *i*-GaAs substrate by the MOS hydride epitaxy method. On surface of semiconductor structure, a layer of combined Al$_2$O$_3$ / SiO$_2$ / Al$_2$O$_3$ dielectric with a total thickness of 170 nm was formed by electron-beam evaporation and then a Co$_{0.45}$Pt$_{0.55}$ layer 8 nm thick was also formed on dielectric by the electron-beam evaporation method. The function of the dielectric was to electrically isolate photosensitive layer of InGaAs from metallic ferromagnetic CoPt layer when investigating the planar photoconductivity of structure. In addition, To InGaAs layer, In-ohmic contacts were created. Thus, structure of the photoresist element was formed, which demonstrated a p-type conductivity and had a dark layer resistivity of 89 kΩ / kv. The photoconductivity was investigated by lighting the structure with circularly polarized light through a CoPt layer falling on photoresistor perpendicular to surface. Structure was placed in a magnetic field oriented perpendicular to plane. The efficiency of circularly polarized light detecting (D_{eff}) was determined as follows:

$$D_{\text{eff}} = R_{\text{left}} - R_{\text{right}} / R_{\text{left}} + R_{\text{right}}, \tag{1}$$

where R_{left} and R_{right} is the resistance of structure when illuminated by light of corresponding polarization.

Because the CoPt layers [1] have a pronounced perpendicular magnetic anisotropy (Fig. 1 continuous line), the detection efficiency of circularly polarized light has shown a dependence on wavelength of falling light. The highest value of registration efficiency (Fig. 1 symbol) was ≈ 0.75% for wavelengths close to the optical absorption edge of InGaAs layer (920 nm). The form of magnetic field dependence of efficiency detection and the magnetic field dependence of structure magnetization almost coincided. Apparently, the presence of the MCD effect in CoPt layer leads to a dependence of transmission coefficient on the direction of circular polarization of light and the magnetization of layer. The result is a difference in the number of photoexcited carriers in InGaAs layer, which leads to a difference in recorded resistance of InGaAs layer and the possibility of detecting the direction of circular polarization.
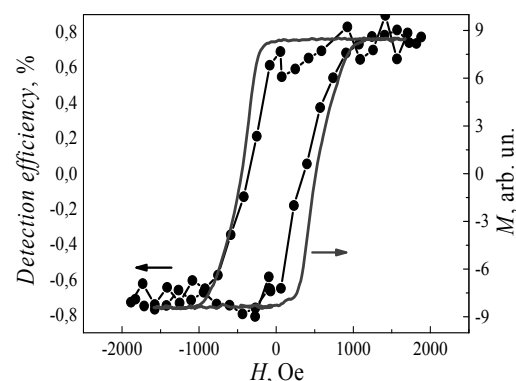
Fig.1. – The magnetic field dependence of the structure magnetization (continuous line) and the efficiency of circularly polarized light detection (symbols).

1. A.V. Zdoroveyshchev, M.V. Dorokhin, O.V. Vikhrova et al., «Properties of CoPt ferromagnetic layers for application in spin light-emitting diodes», *Physics of the Solid State*, 58, No. 11, pp. 2267-2270, 2016.

P1-10: Formation of the ferromagnetic semiconductor (Ga,Mn)As by ion implantation and pulse laser annealing

Yu.A. Danilov[1] , I.L. Kalentyueva[1] , A.V. Kudrin[1] , S.A. Pavlov[2] , A.E. Parafin[2] , E.A Pitirimova[1] , D.S. Tolkachev[1] , O.V. Vikhrova[1] , A.V. Zdoroveishchev[1] , R.R. Yakubov[1]

1. N.I. Lobachevsky State University, Nizhny Novgorod, Russia, E-mail addres: danilov@nifti.unn.ru.
2. Institute for Physics of Microstructures, Russian Academy of Sciences, Nizhny Novgorod, Russia

Ferromagnetic semiconductor is a material having simultaneously semiconductor and ferromagnetic properties. Such a combination of properties is achieved by heavy doping of ordinary semiconductors with transition element impurities. A typical example of the ferromagnetic semiconductor is $Ga_{1-x}Mn_xAs$ ($x \approx 0.05$) grown by the molecular beam epitaxy method at ~250°C and having a Curie temperature, T_C, approximately equal to 110 K. In the case of Mn ion high-dose implantation into GaAs, there is a serious problem of annealing radiation defects. The use of rapid thermal annealing at the temperatures above 700°C has a secondary effect related with formation of ferromagnetic clusters such as MnAs and GaMn. This effect is conditioned by exit of a fraction of Mn atoms from solid solution through low equilibrium Mn solubility in GaAs.

We used the technique of pulsed laser annealing (PLA) for recovering the crystal structure and impurity activation in Mn ion-implantation doped GaAs. The structural, electrical and magnetic properties of GaAs irradiated with Mn^+ ions and annealed by a nanosecond pulse of the excimer laser were studied. The irradiation with Mn^+ ions was performed at room temperature into i-GaAs(100) wafers. The ion energy was 50 or 200 keV, implantation doses were up to 5×10^{16} cm^{-2}. The excimer (KrF) laser LPX-200 has a wavelength of 248 nm, pulse duration of $\approx$30 ns and a pulse energy density up to 500 mJ/cm^2.

The layers, irradiated by Mn^+ ions even at a dose of 5×10^{13} cm^{-2}, were amorphous. The GaAs:Mn annealed by the laser pulse with an energy density of 125 mJ/cm^2 and above showed that PLA caused the ion-irradiated layer recrystallization. It was found that there is a threshold ion dose $\approx 1\times10^{15}$ cm^{-2} for the *p*-type conductivity formation upon PLA with 200-300 mJ/cm^2.
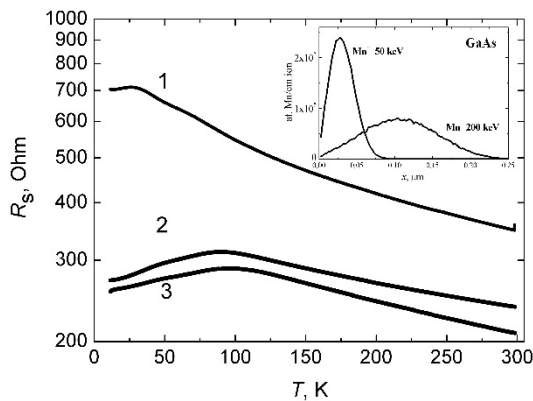
Fig.1. Measurement temperature dependences of the sheet resistance of GaAs:Mn layers after PLA for Mn^+ ion doses: (1) 1×10^{16}, (2) 3×10^{16}, (3) 5×10^{16} cm^{-2}. The ion energy was 200 keV. The inset shows the distributions of Mn ion ranges in GaAs, calculated for energies of 50 and 200 keV by TRIM code.

The dependencies of the sheet resistance, R_S, on the measurement temperature for three implantation doses are shown in Fig.1. These curves contain a characteristic peak, which associated with an increase in carrier scattering near T_C. We can see that the T_C value increases up to $\approx$ 110 K with Mn^+ ion dose. Galvanomagnetic measurements detect anomalous Hall effect with a hysteresis loop up to T_C. Also, the negative magnetoresistance was observed up to 120 K. We believe that during non-equilibrium recrystallization by short laser pulse the implanted Mn atoms are incorporated with a rather high efficiency (from 15 to 40 %) into Ga sites. The resulting high concentration of holes (much higher than 10^{20} cm^{-3}) and Mn atom magnetic moments cause ferromagnetic ordering in implanted laser-annealed GaAs layers.

P1-11: High-temperature intrinsic ferromagnetism in the InFeSb semiconductor

A.V. Kudrin, Yu.A. Danilov, V.P. Lesnikov, O.V. Vikhrova, D.A. Pavlov, Yu.V. Usov,
E.A. Pitirimova, I.N. Antonov, R.N. Kryukov

N.I. Lobachevsky State University, Nizhny Novgorod, Russia, E-mail addres: kudrin@nifti.unn.ru.

A search for new ferromagnetic semiconductors is aimed at creating effective spin injectors for spintronic devices, operated at room temperature. In this work we present the results of fabrication and the investigation of InFeSb/GaAs structures with the room temperature ferromagnetism. The $\approx$ 40 nm-thick InFeSb layers were fabricated on *i*-GaAs substrates by pulsed laser deposition. In the vacuum chamber the solid targets (InSb and Fe) were periodically sputtered by Nd:YAG laser. The ratio of the sputtering times t_{Fe}/t_{InSb} was varied in the range 0.08 – 0.17. The substrate temperature was 30, 150, 200 and 250°C. The Fig. 1 shows the high resolution transmission electron microscopy (HRTEM) image of the cross-section of the InFeSb/GaAs structure with t_{Fe}/t_{InSb} = 0.17 and a growth temperature (T_g) of 250°C. Due to the large lattice mismatch (14.6 %) between InSb layer and GaAs matrix the large number of stacking faults arise on {111} planes. The stacking faults appear as the net of straight lines at an angle of ~ 70° with respect to etch other. The HRTEM images do not reveal the presence of any visible second phase inclusions with a lattice differ from zinc-blende InFeSb matrix. The transmission electron diffraction (TED) pattern obtained from InFeSb/GaSb interface also supports the zinc-blende type lattices (InFeSb and GaAs) only.
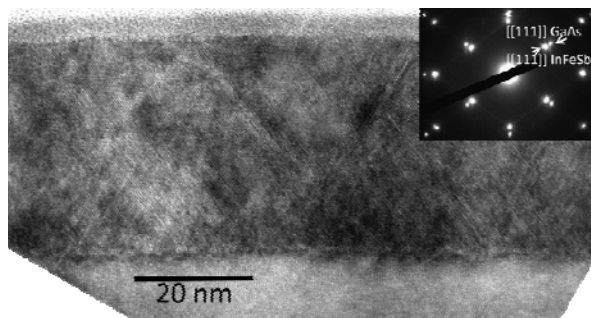
Fig. 1. The HRTEM images of the InFeSb/GaAs structure. The inset shows the TED pattern of the InFeSb/GaSb interface.
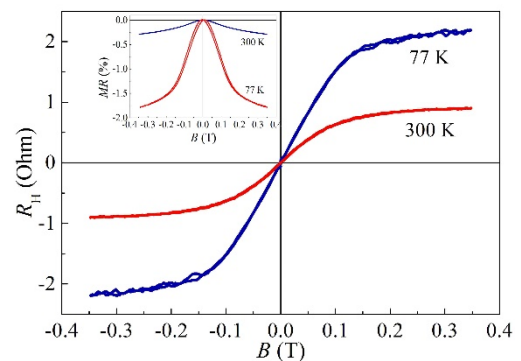
Fig. 2. The $R_H(B)$ dependences of the InFeSb/GaAs structure at 300 and 77 K. The inset shows magnetoresistance dependences on *B* oriented perpendicularly to the plane.

The Fig. 2 shows the Hall resistance dependences on external magnetic field ($R_H(B)$) at 300 an 77 K for the InFeSb/GaAs structure (t_{Fe}/t_{InSb}=0.17, T_g = 250°C). The $R_H(B)$ dependences reveal the anomalous Hall effect up to a room temperature: the dependences are nonlinear with a saturation at the magnetic fields $\geq$ 1500 Oe. The negative magnetoresistance with a bend at ~ 1500 Oe also confirms spin-depended character of the carriers transport in the InFeSb layer. Thus, the obtained InFeSb layers are a single-phase zinc-blende crystal with the room-temperature ferromagnetic properties.

P1-12: Investigation of the electrophysical properties of $Ge_2Sb_2Te_5$ thin films for phase change memory application deposited by magnetron sputtering

A. Yakubov[1], P. Lazarenko[1], A. Scherchenkov[1], S. Kozyukhin[2], A. Babich[1], D. Terekhov[1]

10.   National Research University of Electronic Technology, Moscow, Russia, *alexsey007@mail.ru*

11.   Kurnakov Institute of General and Inorganic Chemistry, Russian Academy of Sciences, Moscow, Russia

Currently electric phase change memory (or PCM) is one of the candidates for the replacement of the flash memory. The advantages of PCM in comparison with flash memory are following: low power consumption, high reading and writing rates, a large number of write cycles, high radiation resistance. Principle of the PCM operation is based on the rapid reversible phase transformations between amorphous and crystalline states, which takes place in PCM materials under low-energy external influences. The material of $Ge_2Sb_2Te_5$ (GST225) is considered to be the most promising for use in PCM devices. But many questions related to the electrophysical properties, in particular the peculiarities of phase transitions in PCM materials are still open. Therefore, the aim of the work is investigation of the electrophysical characteristics and peculiarities of the phase transitions.

Investigated $Ge_2Sb_2Te_5$ thin films were deposited by magnetron sputtering (MS). The pressure of Ar during the process was $2 \cdot 10^{-2}$ Torr. The substrate temperature did not exceed 50 °C. Depositing rate was 2.2 nm/s. Atomic force microscope (NT-MDT Solver Pro) were used to investigate the thicknesses and morphologies of thin films. The thicknesses of the films were in the range from 40 to 390 nm. X-ray diffractometer (Rigaku Smart Lab) was used for the investigation of thin film structure. According to the X-ray diffraction (XRD) as-deposited films had amorphous structure. Scanning electron microscope (Philips XL 40) with EDXR spectrometer was used for the microanalysis of MS thin films. EDXR results showed that composition of as-deposited thin films was Ge = 24.8 at.%, Sb = 21.3 at. %, Te = 53.9 at.%.

The resistivity temperature dependences for thin films were investigated on a special stand, containing heating stage HFS600E-PB4 Linkam and picoammeter Keithley 6485. Planar structures containing TiN+W electrodes with fixed interelectrode distances (1.5 mm), and deposited upon them GST225 thin film were fabricated on oxidized c-Si substrates. The resistivity temperature dependences for the GST225 thin films were studied from room temperature to 400 °C with a heating rate of 5 °C/min in an argon atmosphere.

Differential scanning calorimetry (DSC) was carried out with using of DSC–50 (Shimadzu) analyzer. Thin films were scraped off from the monocrystalline Si substrates, and pressed and sealed in Al pans, which limited measurements to 635°C. Measurements were carried out at heating rate of 10 °C/min in an inert atmosphere of nitrogen.

The results of the investigations of the resistivity temperature dependences showed that sharp drop in resistivity for GST225 were observed in the ranges from 180 to 195 °C. According to X-ray diffraction such drop is caused by the crystallization of as-deposited films. Analysis of XRD data indicated that annealed thin films at given temperature have cubic structures. This transition is accompanied by the appearance of an exothermic peak on DSC curves. Cooling after the phase transition showed that the resistivity has a non-metallic dependence. Second phase transition from metastable rock salt to stable hexagonal structures was observed in the temperature range from 360 to 400 °C. The resistivity at cooling after the second phase transition has a metallic dependence. This transition was confirmed by the data of DSC and XRD.

Thus, it was shown that sharp drops in resistivities for $Ge_2Sb_2Te_5$ thin films were observed in the temperature ranges from 180 to 195 °C and from 360 to 400 °C, which correlates with the changes of the thermal properties detected by DSC.

According to the XRD analysis, such changes of the electrical and thermal properties are caused by the phase transitions to the cubic and hexagonal structures, respectively.

P1-13: Growth of high quality Ge epitaxial layer on Si(001) substrate using hot-wire chemical vapor deposition

V. Shengurov[1], S. Denisov[1], V. Chalkov[1], A. Nezhdanov[2], V. Trushin[1], D. Filatov[1], D. Prokhorov[1], Y. Buzynin[3], A. Buzynin[4], N. Baidus[1]

1. *Physical Technical Research Institute, Lobachevskii State University of Nizhny Novgorod, Nizhny Novgorod, Russia, shengurov@phys.unn.ru*
2. *Lobachevskii State University of Nizhny Novgorod, Nizhny Novgorod, Russia*
3. *Institute for Physics of Microstructures, Russian Academy of Sciences, Nizhny Novgorod, Russia*
4. *Prokhorov General Physics Institute, Russian Academy of Sciences, Moscow, Russia*

Because of recent progress in the Si-based optoelectronics, the heteroepitaxy of Ge on Si has attracted an increased attention. It is necessary to grow the Ge layers with low density of dislocations and smooth surface. At present, various methods are applied in these purpoeses problem, such as growing the graded-composition SiGe buffer layers, high-temperature annealing, or chemical-mechanical polishing. However, the application of the methods listed above complicates the hererostructure fabrication process.

In the present work, we report on the growth of the Ge epitaxial layers with high crustal quality, low dislocation density ($\sim 1 \cdot 10^5$ cm^{-2}), and smooth surface (RMS roughness ≈ 0.37 nm) on the Si (001) substrates at low temperature by hot wire chemical vapor deposition (HW CVD).

The Ge epitaxial layers were grow on Si (001) in a home-made HW CVD system. Monogermane (GeH$_4$) was used as the gaseous Ge precursor. The grwoth was performed at constant substrate temperature ($\sim 350°C$), as well as in a two-stage mode: ith initial Ge layers were grown at 350°C whereas the main thick layers were grown at 500°C. The temperature of the hot Ta wire was 1300 - 1500°C. Also, the Ge layers doped by phosphorus by the evaporaion of GaP compound fromn an effusion cell have been grown. The grownt Ge layers were examined by various methods, including doule-crystal X-ray diffraction (DXRD), transmision electron microscopy (TEM), atomic force microscopy (AFM), Raman spectroscopy, etc.According to the DXRD data, in the Ge layers of ≈ 1 mkm in thickness, the values of the full width at half maximum (FWHM) of the (004) reflection were 0.08 to 0.1° for the layers grown in the constant temperature regime and $\sim 0.05°$ for the layers grown in the two-stage mode.

We demonstrated a *p-i-n* diode based on a Ge/Si anisotype heterojunction, which can be applied as a photodetector. The Ge epitaxial layers on Si are suitable also for the use as the virtual substrates for the fabrication of the solar cells based on the III-V compound semiconductors.

P1-14: Investigation of the direct piezoelectric effect in vertically aligned carbon nanotubes

A. A. Konshin, M.V. Ilina, O.I. Ilin, O.A. Ageev
Southern Federal University, REC "Nanotechnologies", Taganrog, Russia

One of the main directions in development of modern electronics is a nanopiezotronic - a field of science that explores the flexo- and piezoelectric properties of nanomaterials. Particular attention in this area is paid to carbon nanostructures characterized by high scalability, speed and energy efficiency and exhibiting anomalous piezoelectric properties [1].

The purpose of this work is research of the direct piezoelectric effect in vertically aligned carbon nanotubes (CNTs) by using atomic force microscopy (AFM).

As a sample was used an array of vertically oriented carbon nanotubes with a diameter of 43 ± 7 nm, a length of 1.4 ± 0.2 μm and a density of 128 μm^{-2}, grown by the method of plasma-chemical deposition from the gas phase (PECVD). The study of the arrays was carried out by AFM method using Ntegra (NT-MDT). In the process of preliminary scanning of the CNT's array surface in a semi-contact mode, individual nanotubes were swung under the mechanical action of the AFM probe and combined into bundles under the action of Van der Waals forces. During the second scanning pass by the Kelvin probe, the surface potential of the CNT was measured at a distance of 15 nm from the array's surface. During the second part of the research, a piezoelectric current was measured in the AFM power spectroscopy mode with a change in the force of the mechanical interaction of the probe with a bundle of nanotubes.

The analyse of obtained AFM images showed that at the peak of the CNT bundles with a diameter from 50 to 160 nm (Fig. 1, a), a negative surface potential was observed from -60 to -110 mV, but near the base of the bundles there was a positive potential of 90 to 130 MV (Fig. 1, b). The appearance of a negative potential on the nanotube bundle is due to their flexural deformation caused by unification.

a)   *b)*
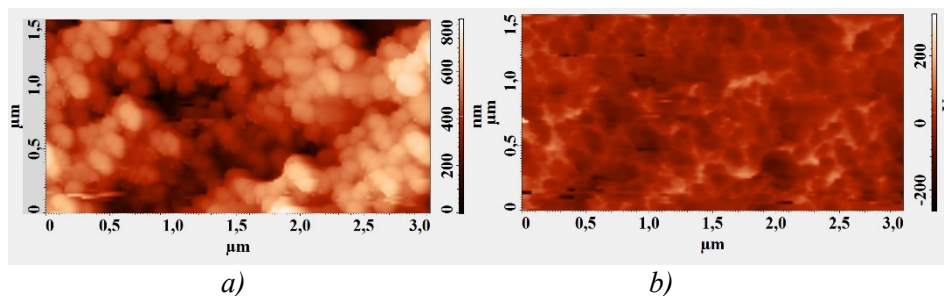
Fig.1. - AFM images of an array of oriented CNTs: a) - surface relief obtained in a semi-contact mode; b) is the distribution of the surface potential

The results of experimental researches showed that when a probe of an AFM was applied to a CNT bundle in the "lower electrode / CNT / AFM probe" system, a current up to -15 nA was detected, which is due to the presence of a surface potential at the top of the bundles. When the position of the probe relative to the surface of the array varied from 300 to -50 nm, the current varied from 0 to -16 nA, which indicates an increase in the potential of nanotubes with increasing compression deformation.

Thus, the piezoelectric effect in oriented carbon nanotubes was experimentally confirmed and the experimental values of the surface potential of the CNT bundles on the magnitude of their deformation were obtained. These data correlate with the theoretical research that we conducted earlier [2]. The obtained results can be used in the development and research of piezotronic devices based on carbon nanotubes.

1. S. Chandratre et al., *Appl. Phys. Lett.*, 100, 023114 (2012).
2. Ageev O.A., Blinov Yu.F., Il'in O.I., Konoplev B.G., Rubashkina M.V., Smirnov V.A., Fedotov A.A., *Phys. Solid State*, Vol. 57, No. 4, p. 825, 2015.

P1-15: SXPS study of InAs/(Cd,Zn)(Se,Te) heterovalent interfaces

<u>M. V. Lebedev</u>[1], I. V. Sedova[1], S. V. Sorokin[1], G. V. Klimko[1], G. Yu. Cherkashinin[2], S. Nappini[3], E. Magnano[3], P. S. Kop'ev[1], S. V. Ivanov[1]

1. Ioffe Institute, St. Petersburg, Russia, mleb@triat.ioffe.ru. 2. TU-Darmstadt, Darmstadt, Germany. 3. IOM CNR Laboratorio TASC, Trieste, Italy

Heterovalent structures are of increasing interest both for fundamental research and device applications. Combining materials of different chemical groups (e.g., III–V and II–VI) in a single-crystal heterostructure provides unique possibilities to tune the electronic structure and the band offset values, which determine the energy barriers for electron and hole transport. Many combinations of III–V and II–VI compounds can be lattice matched to one another providing an avenue to create heterojunctions with large offset potentials that can be used for cladding and window layers. In particular, interfaces in the InAs/(Cd,Zn)(Se,Te) system are very promising for laser diodes [1], while addition of Mn into the II–VI layer makes possible the using of these interfaces in spin-injecting heterostructures [2].

The objective of the present study is the analysis of the band offsets and the chemical bonds at the coherent InAs/CdSe and InAs/ZnTe/CdSe interfaces grown by molecular-beam epitaxy (MBE). The thickness of CdSe layer was 3 nm, while the thickness of the intermediate ZnTe layer was 3 ML (~1 nm). The studies were performed by synchrotron-radiation photoemission spectroscopy (SXPS) on the BACH beamline of the synchrotron Elettra (Trieste, Italy). In order to obtain the depth distribution of different species the core levels of the heterojunction constituents were measured at different excitation energies from 180 to 1300 eV providing the information depth variation from 1.9 nm (less than thickness of the CdSe layer) up to 8.5 nm.

Typical core level spectra obtained from InAs/CdSe and InAs/ZnTe(3ML)/CdSe heterostructures are shown in Fig. 1. For clarity, the spectra of the InAs/ZnTe(3ML)/CdSe heterostructure were shifted by 0.15 eV to higher binding energies to normalize the position of the Cd 4d core level. As the binding energies of the Cd 4d and Zn 3d core levels are very close to each other, the corresponding photoemission in the InAs/ZnTe(3ML)/CdSe heterostructure were fitted in order to separate these core levels (Fig. 1).
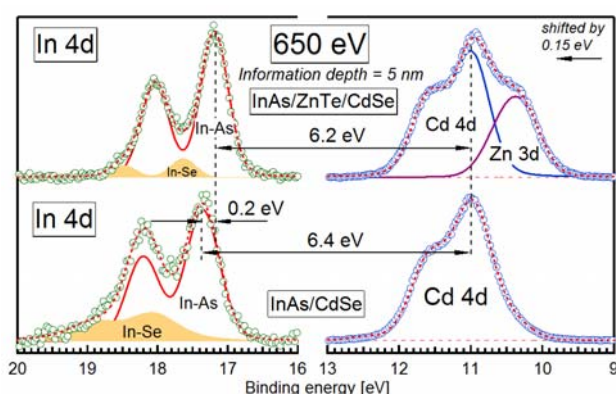
Figure 1. In 4d, Cd 4d and Zn 3d core level spectra for InAs/CdSe and InAs/ZnTe(3ML)/CdSe heterostructures measured with the excitation energy of 650 eV. For clarity, the core level spectra of the InAs/ZnTe(3ML)/CdSe heterostructure were shifted by 0.15 eV towards higher binding energies.

Obviously, the insertion of a thin ZnTe layer into the InAs/CdSe heterostructure results in the increase of the valence band offset (VBO) at the InAs/CdSe interface approximately by 0.2 eV (Fig. 1). The determined InAs/CdSe VBO values are 1.02 ± 0.08 eV and 1.19 ± 0.08 eV for InAs/CdSe and InAs/ZnTe(3ML)/CdSe heterostructures, respectively. Simultaneously, the VBO at the buried InAs/ZnTe interface can be estimated as 0.25 ± 0.06 eV.

As opposed to the GaAs/ZnSe interface [3], the diffusion of the InAs epilayer components to the CdSe epitaxial layer is quite weak, thus confirming the abruptness of the InAs/CdSe interface. Little amount of the In–Se chemical bonds is visible at the interface (Fig. 1), while the As–Se chemical bonds are observable only within the CdSe layer directly grown on InAs and occur presumably around diffused As atoms.

1. S.V. Ivanov et al., «A 2.78 mm laser diode based on hybrid AlGaAsSb/InAs/CdMgSe double heterostructure grown by molecular-beam epitaxy», *Appl. Phys. Lett*. 82, pp. 3782–3284, 2003
2. T. Gleim et al, "Energy level alignment at zinc blende Cd(Mn)Se/ZnTe/InAs(100) interfaces", Appl. Phys. Lett. 99, 072111, 2011
3. T. A. Komissarova et al, «Electronic, structural and chemical properties of GaAs/ZnSe heterovalent interfaces as dependent on MBE growth conditions and ex situ annealing», *Semicond. Sci. Technol*. 32, 045012, 2017

P1-16: Electrophoretic formation of CNT/NiO$_x$ porous nanocomposite electrode material

A. Alekseyev[1], E. Lebedev[1], A. Sysa[1, 2], A. Dudin[3], E. Kitsyuk[2], D. Gromov[1]

1.National Research University of Electronic Technology, Zelenograd, Russia, salvionn@gmail.com

2.Scientific Manufacturing Complex "Technological Centre", Zelenograd, Russia, kitsyuk.e@gmail.com

3.Institute of Nanotechnologies of Microelectronics, Russian Academy of Science, Moscow, Russia, alexanderdudin@msn.com

Electric power supply grows constantly, and it is essential to develop energy storage systems for electronic equipment, mobile devices, micro- and nanoelectromechanical systems (MEMS and NEMS) with higher power density, efficiency and stability. In this work, one of possible ways of nanocomposite CNT/NiO$_x$ electrode material creation for applying in electrochemical capacitors is examined. Features of the combination consist of carbon nanotubes (CNTs) play a skeleton role with providing stability and high power rate, and nickel oxide (NiO$_x$), which is active material, increases the specific capacity due to faradaic processes. The electrophoretic deposition (EPD) represents well-known simple and versatile method of manipulation and deposition of nanoparticles, such as CNTs, in liquid suspensions under the applying of an electric field.

The catalyst of Co/Mo/MgO was used to obtain a carbon material with a high content of multiwall CNTs via chemical vapor deposition with methane pyrolysis at 900°C. After synthesis, in order to remove metal inclusions and amorphous carbon and functionalize CNTs, powder was consequently rinsed in concentrated hydrogen peroxide, hydrochloride and mixtures of nitric and sulfuric acids at elevated temperatures. Final average tube diameter and length were 20 nm and 1.5 μm respectively.

For suspension, as a solvent, the 50 ml ethanol/acetone mixture was used in volume ratio of 1:1. Nickel(II) nitrate hexahydrate (Ni(NO$_3$)$_2$·6H$_2$O) was added in different amounts as a precursor of NiO$_x$ and as a charger of a CNT's surface at the same time. Quantity of added CNTs equalled 2 mg. In order to improve suspension stability, 2 mg of hydroxypropyl cellulose with 0.4 mg of sodium lauryl sulfate, as a dispersing agent and a surfactant respectively, were added. Then solutions were beaten up in an ultrasonic bath with ice for 20 minutes. Finally, they were centrifuged for 10 minutes at 10000 RPM with temperature of 14°C, with a view to make badly dispersed particles settle down, and decanted from sediment.

In deposition process was used DC power supply with 30 V applied. As anode was used a golden plate, and as cathode – pretreated Ti or Ni foil. The deposition area was the 1x2 cm^2 rectangular, and the distance between electrodes was 1 cm. 30 seconds deposition acts were alternated with 5 minutes drying in order to obtain better uniformity and prevent cracking because of mechanical strain, arising during drying.

Examination of obtained samples showed tendency of deposit to aim substantially the edges of the foil work area and follow some determined lines. With more deposition cycles, it is possible to create more uniform coatings. After the deposition in the suspension with 10 mg of charger salt within was obtained a sponge-like porous structure. 9 cycles leaded to 2.27 μm thickness total. 18 cycles gave amount of deposit around 1 mg. Average relative atomic content was 0.8:1:3 = C:Ni:O.

For electrical characteristics studying were assembled asymmetric samples of capacitors with a blank Ti foil as a counter electrode, cellulose separator and 0.5 M KOH solution as electrolyte. They were exposed to cyclic voltammetry with potentiostatic and galvanostatic modes. Stable values of specific capacity at scan rate of 10 mV/s for capacitors with electrodes obtained by 3 and 9 EPD cycles in 10 mg charger salt suspension were 4 and 3.5 mF/cm^2 respectively.

Apart from that, the possibility of local deposition of described material on narrow Ti electrodes, 30-70 μm width with 10-50 μm spacing in between, was confirmed. Thereby, EPD method can be used in producing of the planar electrochemical capacitor with interdigital structure.

P1-17: A new mechanism of twin boundary formation

A.S. Ksenz[1], S.I.Bozhko[1], A.M.Ionov[1]

1. Institute of Solid State Physics Russian Academy of Sciences, Chernogolovka, Russia, E-mail addres: adm@issp.ac.ru (www.issp.ac.ru)

Studies using scanning tunneling microscopy of the Pb film growth on the vicinal surface of Si (5 5 7) showed that the growth occurs in accordance with the Stranski-Krastanov scenario [1]. The elongated along the step edge have a layered structure. Statistical analysis of the STM image reveals predominant thickness of the layers of 2 nm, which corresponds to 7 monolayers of Pb. The observed stratification of the Pb nanoislands is well described in terms of electron growth [2], namely, the island layers are a set of quantum wells separated by a semi transparent walls for the conduction electrons. Island stratification resulted in reduction of conductive electrons energy due to quantum confinement.

DFT modeling demonstrated that quantum wells could be formed by the sequence of the twin boundaries. Subsequent DFT simulations showed that the formation of the twin boundary induced by creation of standing waves in electron subsystem of the Pb layer. Results of DFT modeling are in a good agreement with experiment.

1. D. A. Fokin, S. I. Bozhko, V. Dubost et al., Phys. Status Solidi C, 1–4 (2009)
2. P. Czoschke, Hawoong Hong, L. Basile et al., Phys. Rev. B 72, 075402 (2005)

Р1-18: Изучение процессов наноструктурирования углеродных нанотрубок в растворе с аэросилом в электрическом поле

А.П. Кузьменко, Тет Пьо Наинг, Мьо Мин Тан

[1]ФГБОУ ВПО « Юго-западный государственный университет», Россия, Курск, E-mail addres: apk3527@mail.ru

Процессы самоорганизации и самосборки функционализированных карбоксильными группами многостенных углеродных нанотрубок (МУНТ – СООН) в дионизированной воде (ДВ) в присутствии ультрадисперсного аэросила (α-SiO$_2$) и под влиянием электрического поля изучены методами ИК-Фурье (Nicolet iS50, 0.125 см$^{-1}$), комбинационного рассеяния света (КРС) (Omega Scope™ рамановский микроспектрометр, 532 нм, 0.8 см$^{-1}$), конфокальной (КМ), атомно-силовой (АСМ) SmartSPM и сканирующей электронной микроскопии (СЭМ) (JSM JEOL 6610). Полученный коллоидный раствор (КР) МУНТ – СООН в дионизированной воде (H$_2$O$_{дв}$) с добавлением α-SiO$_2$ в соотношении 1:2 наносился методом из капли в межэлектродный промежуток печатной платы [1]. На электроды подавалось постоянное напряжение (варьируемое от 15 до 25 В). На микрофотографиях (рис. 1 *а*) видны катод и анод с расстоянием между ними 1500 мкм, обозначенные «+» и «–».

а　　　　　　　*б*　　　　　　　*в*
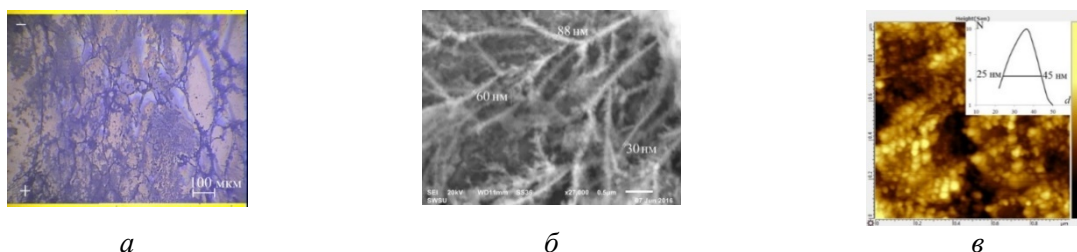
Рис. 1 – КМ и СЭМ изображения в осадке из КР на ситалле с ЛКО, ФС и ДС при *U* = 19 В (*а*), ФС и ЛКО (*б*), АСМ изображения ЛКО и ФС (*в*)

Обнаружено, что в процессе самосборки и/или самоорганизации формируются диффузные, фрактальные структуры или линейно-кусочные образования, размеры которых уменьшаются как 1/*U*, а скорость их роста возрастает как *U*^{2}. Установлено, что МУНТ – СООН + α-SiO$_2$ + H$_2$O$_{дв}$ в электрическом поле управляемо ориентируются. Полученные результаты показали, что интенсивное ультразвуковое диспергирование комплексов в виде МУНТ – СООН + α-SiO$_2$ + H$_2$O$_{дв}$ вызывает появление внутри МУНТ – СООН ОУНТ с центрально-осевым расположением, что подтверждено возбуждениями КРС в коротковолновой области – РДМ (Рис. 2). Многообразие возникающих структур в постоянном электрическом поле обусловлено как существованием смешанных типов *sp*^{2} – гибридизации с π- и σ-углеродными связями, так и металлической и полупроводниковой проводимостями, что, само по себе, указывает на большое практическое значение такого структурирования с учетом перспектив развития наноэлектроники.
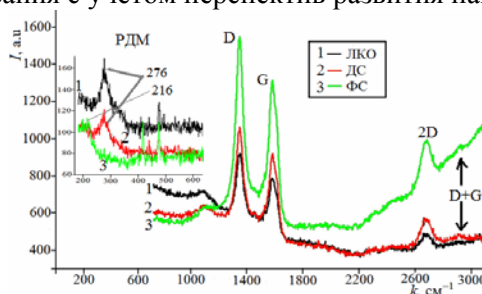
Рис. 2 – Спектры КРС структур ЛКО, ДС и ФС, образованных из МУНТ – СООН + α-SiO$_2$ + H$_2$O$_{дв}$. Вставка 1 в области РДМ.

1. Кузьменко А. П., Тет Пьо Наинг, Мьо Мин Тан, Добромыслов М.Б., Чан Ньен Аунг. *Известия Юго-Западного государственного университета. Серия техника и технологии*, №3(16), С. 39 – 50, 2015.
2. Dresselhaus M. S., Jorio A., Hofmann M., et. al. *Nano Letters*, Vol. 10, P. 751 – 758, 2010.

P1-19: Thermomigration p^+-channels in Si (100) substrates: microstructure and composition

S. Simakin[1], A. Lomov[2], B. Seredin[3], M. Seredina[3]

12. Yaroslavl Branch of the Institute of Physics and Technology of Russian Academy of Sciences, Yarosslavl, Russia, simser@mail.ru. 2. Institute of Physics and Technology of Russian Academy of Sciences,Moscow, Russia, lomov@ftian.ru . 3. Platov South-Russian State Polytechnic University, Novocherkassk, Russian

The method of thermomigration (TM) is a promising basis for power electronics technology due to the unique possibility of creating narrow channels with sharp boundaries perpendicular to the surface of the semiconductor substrate [1]. The process of local recrystallization with the help of TM occurs due to the successive motion under the influence of the temperature gradient of the liquid zone of the solvent. One of the main problems of creating recrystallized channels is the minimization of deformation and the concentration of structural defects at the channel boundary.

The results of a study of the microstructure of the separation p-channel of a silicon power thyristor obtained by the TM method of liquid aluminum-silicon bands are presented. The $p +$ -channels (see Fig.) With a width of 100 μm were created along the (100) and (010) directions on a commercial substrate Si (100)(P) (40 om sm) 500 μm thick in the temperature range 1100-1200 ° C in a specialized installation [2]. Typical speed of migration of the zone was 500-700 microns per hour. The structural characterization of the formed channels was carried out by the method of X-ray diffraction topography and double crystal rocking curves using copper radiation. The impurity profiles both across the channel and along its depth were characterized using secondary ion mass spectrometry.
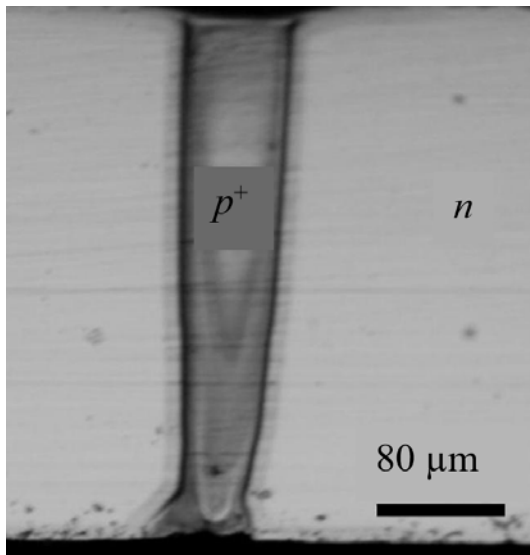
The diffraction 004 rocking curves from the sample surface located near the channel boundary show the presence of two maxima: the main one, corresponding to reflection from the silicon substrate, and an additional reflection at smaller Bragg angles from the crystal lattice of the channel. The angular distance between them allowed us to estimate the change in the lattice parameter in the channel as $\Delta d / d \approx (2 \div 3.5) \ 10^{-4}$. An analysis of X-ray topography 440 reflection images of channel of a sample shows a considerable stress gradient near the channel boundaries. In these regions, the formation of dislocations is possible because of the partial relaxation of stresses at the boundaries and other microdefects. Secondary ion mass spectrometry revealed an increased concentration of oxygen and carbon along the boundaries of the channel compared to its body. The concentration of aluminum in recrystallized silicon is in the range $\sim 2 \cdot 10^{-19}$ cm^{-3} depending on the temperature of the thermo-migration process.

Fig. Optical image of the cleavage of a silicon substrate with a thermomigration channel.

1.   V. N. Lozovskii, L. S. Lunin, and B. M. Seredin, «Peculiarities of obtaining power silicon devices by means of thermomigration», *Elektron.Tekh*., Ser. 2: Poluprov. Prib., No. 2–3 (236), pp.103–115, 2015. (*in Russian*).

2.   V. N. Lozovskii, B. M. Seredin, A. S. Polukhin, and A. I. Solodovnik, «Equipment for production silicon structures by thermomigration», *Elektron. Tekh.,* Ser. 2: Poluprov. Prib., No. 5 (239),pp. 65-76, 2015. (*in Russian*).

P1-20: Determination of the Atomic Density of a Thick Film by the Rutherford Backscattering Spectroscopy (RBS)

E. Parshin[1] , N. Melesov[1]

1.   *Yaroslavl Branch of the Institute of Physics and Technology, Institution of Russian Academy of Sciences, Yaroslavl, Russia, par1959@yandex.ru, dartnik@mail.ru.*

The studies of thick films (using aluminum and vanadium oxide as examples) were carried out by the RBS method to determine the atomic density of chemical elements. In solving similar problems for thin films, a number of assumptions are usually used: the dissipation of the projectile ion energy throughout the path before and after scattering is constant; the scattering cross section over the entire thickness of the film do not varies; the beam is transmitted through the thin target with only very little loss of particles. These assumptions lead to inadequate results already for films that are 0.1 μm in thickness. In reality, the analysis complicates by the principle nonlinearity of the dependence on energy both the dissipation and the scattering cross section and their mutual superposition in the resulting spectrum. Also, there is superimposing of signals on each other from different elements composing both the studied sample and the substrate. An example of spectra obtained by RBS analysis is shown in Fig. 1. The samples were analyzed by ion beam He^+ which has energies in the range 0.7-1.8 MeV, and it obtained with a linear accelerator K2MV HVEE. The total resolution of the measurements is 18 keV.
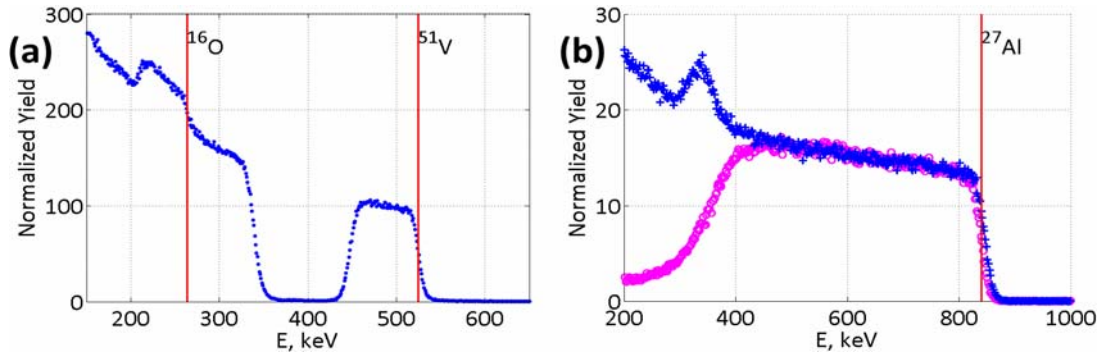
Fig. 1. Examples of spectra obtained from thick films: a – 100 nm VO_x on a Si substrate at $E_0 = 0.7$ MeV and φ = 160 °; b – 1.0 μm Al on a substrate of Si (crosses) and C (circles) at $E_0 = 1.5$ MeV and φ = 160°. The authors showed that in the approximation of a homogeneous film, it is possible to determine the atomic density of a chemical element by a numerical solution of the integral equation for total energy losses of ions scattered at the inner film boundary:

$$E_b = K\left(E_0 - \int_0^a n \cdot \varepsilon(E) dx \right) - \int_0^{a'} n \cdot \varepsilon(E) dx', \tag{1}$$

where K is the kinematic scattering factor (depends on the target atom mass); E_0 is the initial energy of He^+ ions; $\varepsilon(E)$ is the energy loss function; n is the atomic concentration of target element; a and a' are paths which the projectile ion passed through the substance before and after scattering, respectively; the Ox axis is directed along the projectile ion motion before scattering, and the Ox' axis is directed along the projectile ion motion after scattering.

Also, an algorithm was developed that decomposes an integral signal from chemical element to signals from elementary sublayers (the sublayer thickness is mainly determined by the system resolution). In this case, the energy of the projectile ion passing through the elementary sublayer at a depth x is convenient to determine by the expression [1]:

$$E(x) = E_0 - x \cdot n \cdot \varepsilon + \frac{1}{2} \cdot x^2 \cdot n^2 \cdot \varepsilon \cdot \varepsilon' - \frac{1}{6} \cdot x^3 \cdot n^3 \cdot (\varepsilon'' \cdot \varepsilon^2 - \varepsilon'^2 \cdot \varepsilon), \tag{2}$$

where ε' and ε'' are the first and second derivatives of the energy dissipation with respect to energy.

Such an approach allows us to carry out sequential refinements of the function $n(x)$, to a satisfactory convergence of the solution of the integral equation (1) for all sublayers.

1.   Lawrence R. Doolittle, "Algorithms for Rapid Simulation of Rutherford Backscattering Spectra", *Nuclear Instruments and Methods in Physics Research*, B9, pp.344-351, 1985

P1-21: Computer modeling thin film growth on the surface by low energy cluster deposition

Rasulov A.M.

Ferghana Polytehnic Institute, Ferghana str., 86, Ferghana, 150100 Uzbekistan, arasulov59@mail.ru

This report describes the parallelization strategy applied to low energy cluster beam deposition (LECBD) on the surface of crystals. Nanoclusters on surfaces are interesting for a wide range of chemical, magnetic, electronic and optical properties. Bimetallic particles can be produced displaying either core-shell structures or forming alloys with, eventually, a segregated surface. The possibilities of synthesis outside equilibrium conditions widely increase the range of possible cluster composition and structure. Such particles can be modelled at the atomic scale allowing detailed comparison with experiment. Such studies are facilitated either by depositing the clusters on surface or embedding them into a matrix. Deposited and embedded particles can be modelled on their turn, at the atomic scale. By accumulating them, it is possible to synthesised nanostructured layers with specific properties. Cluster assembled films are formed by deposition on a surface and such films could be modelled as well. Specifically, clusters on surfaces can be obtained by atomic deposition followed by thermal diffusion. This method applies for atomic species forming islands rather then wetting the surface. Such a method was used, for instance, to produce cobalt clusters on a silver surface. These clusters precipitate preferentially on pre-existing defects, or the atoms form defects at landing, themselves acting as sinks for cluster growth. Clusters in the gas phase are produced by laser ablation or by condensation and then extracted into a supersonic beam directed toward the substrate surface. By the latter method, clusters at thermodynamic equilibrium are formed while clusters outside equilibrium can be synthesised with the former. These both techniques allow mass selection so that homogeneous populations of deposited clusters can be formed, with identical deposition conditions. It is well known from both experiment and modelling that clusters slowing down at supersonic velocities do not fragment upon impact.

For study of characteristics of LECBD processes one of best methods is the computer simulation using Molecular Dynamics. However, in this case the calculation time is dramatically increased with increasing the number of atoms in the studied system. The parallelization of algorithm for simulation of LECBD characteristics results in considerable decreasing the calculation time. The parallelization strategy adopted is a multidimensional domain decomposition of the simulation box using a link cell method and a Verlet list method for each sub-domain independently. The program paradigm is based on explicit massage passing, and the standard Massage-Passing Interface (MPI) was chosen in order to achieve portability.

P1-22: Calculation of quantization energy levels in submicron MOSFETs using Monte Carlo simulation

O. Zhevnyak[1], Ya. Zhevnyak[1], I. Myachikova[2]

1. Belarussian State University, Minsk, Belarus, Zhevnyakol@tut.by. 2. Belarussian State Academy of Aviation, Minsk, Belarus, Myachikova@tut.by.

As known there is an energy quantization in silicon inversion layers [1]. With co-authors we had showed this phenomenon may be influential for electron properties in MOSFET's current channel at definite conditions [2]. However these conditions are not deeply studied.

The purpose of present work is the investigation of gate and drain bias effect on structure of quantization energy levels in MOSFET's conduction layer (current channel). This effect is determined by changing of potential slope along the transistor's channel. On figure the general potential profiles into the MOSFET substrate are schematically presented.
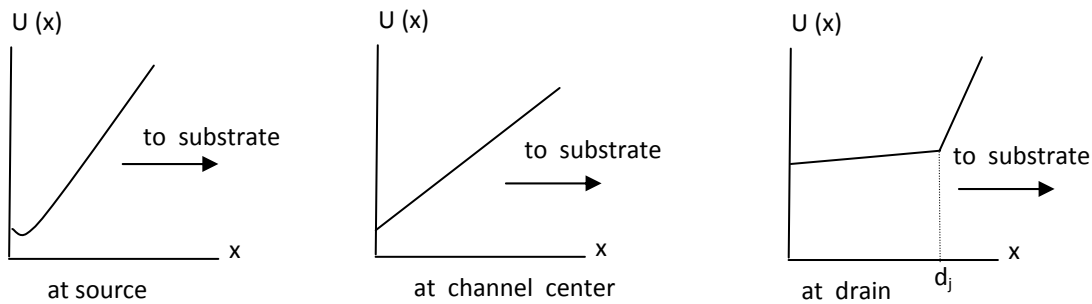
Figure. Potential slope along the transistor's channel. d_j is the drain deepness into MOSFET substrate.

Evidently the structure of quantization energy levels is not uniform along the channel.

In present work we have calculated the quantization energy levels by direct solution of Schrödinger equation

$d^2\psi/dt^2 + 2m/\hbar^2(E-U(x))\psi = 0$ using infinite mathematical series. Used bound conditions were $\psi(0)=\psi(\infty)=0$. The potential profiles $U(x)$ at each channel section are obtained by using Monte Carlo simulation of electron transport in MOSFETs and solution of Poisson equation [3].

The energy levels structures along the transistor's channel are calculated. We have considered MOSFETs at a wide range of gate and drain bias with channel length is less 0.4 μm. Gate oxide is equal 7 nm and drain deepness into MOSFET substrate is equal 0.1 μm. The obtained data show that for studied conditions the quantization energy levels are appeared only at source end of channel. In other regions of channel the energy quantization is not arisen as the distance between nearest energy levels is less than the temperature energy broadening.

1. M. V. Fischetti, S. E. Laux, «Monte Carlo study of electron transport in silicon inversion layers», *Phys. Rev.*, B48, pp.2244-2274, 1993
2. V. Borzdov, O. Zhevnyak, F. Komarov, V. Galenchik. «Monte Carlo simulation of integral electronics device structures». *BSU*, Minsk, 2007 (in Russian)
3. O. Zhevnyak, «Temperature effect on electron transport in conventional short channel MOSFETs: Monte Carlo simulation», *Proc. SPIE*, 7025, pp.1M-1-8, 2008

P1-23: ON ONE PECULIARITY OF THE MODEL DESCRIBING THE INTERACTION OF THE ELECTRON BEAM WITH THE SEMICONDUCTOR SURFACE

M.A. Stepovich[1, 3], A.N. Amrastanov[1], E.V. Seregina[2], M.N. Filippov[4]

1. Tsiolkovsky Kaluga State University, Kaluga, Russia, m.stepovich@rambler.ru, an_amr@mail.ru. 2. Bauman Moscow State Technical University (National Research University), Kaluga Branch, Kaluga, Russia, evfs@yandex.ru. 3. Ivanovo State University, Ivanovo, Russia, m.stepovich@rambler.ru. 4. Kurnakov Institute of General and Inorganic Chemistry RAS, Moscow, Russia, mn@filippov.org.ru

The problem of heat distribution in semiconductor materials irradiated with sharply focused electron beams in the absence of heat exchange between the target and the external medium has been considered by mathematical modeling methods. In the quantitative description of energy losses by probe electrons, a model based on a separate description of the contributions to the energy of absorbed and backscattered electrons is used [1]:

$$\rho(M) = \frac{1,085(1-\eta)P_0}{\pi^{\frac{3}{2}} a_1^2 z_{ms} \left(1-\eta+\eta\frac{z_{ss}}{z_{ms}}\right)} \left\{ \exp\left\{ -\left[\frac{x^2+y^2}{a_1^2} + \left(\frac{z-z_{ms}}{z_{ms}}\right)^2 \right] \right\} + \frac{\eta a_1^2}{(1-\eta)a_2^2} \exp\left\{ -\left[\frac{x^2+y^2}{a_2^2} + \left(\frac{z-z_{ss}}{z_{ss}}\right)^2 \right] \right\} \right\}.$$
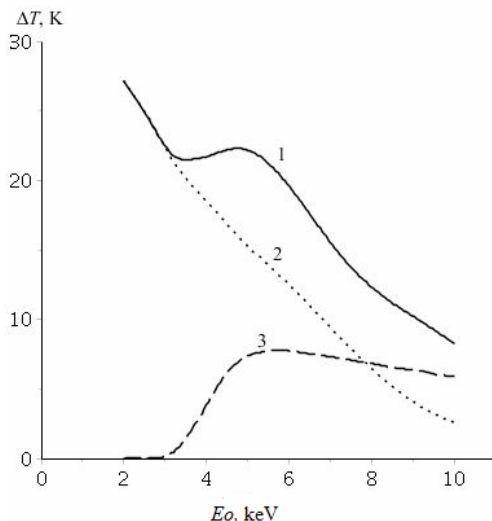
Using the features of this approach, the nonmonotonic dependence of the temperature of the maximum heating of the target ΔT on the energy of the primary electrons E_0 is explained. As an illustration, the figure shows the dependence of the maximum heating of the samples ΔT on the energy of the primary electrons E_0 for GaAs (curve 1). The results of the calculations show that the contribution of electrons absorbed in the target (curve 2) to the total energy losses of the probe electrons in the target (curve 1) is decisive for the probe energy of less than about 2...3 keV, and then the curve 2 decreases monotonically. We note that for heavy semiconductors, the energy loss of the absorbed electrons becomes practically zero at an energy of about 8 keV. For light samples and samples with average ordinal numbers (including GaAs), the energy losses absorbed by the target absorbed and back scattered (reflected) electrons become commensurate with the electron energy of the probe about 8 keV, and at higher energies the contribution of backscattered electrons predominates. This can be explained by the deeper penetration and large scattering in the target of the probe electrons and, as a consequence, the lower probability of the exit from the target of electrons experiencing small-angle scattering in the volume of the semiconductor. As for backscattered electrons, curve 3 is characterized by a maximum of about 4…5 keV, and then curve 3 monotonically decreases. The presence of a rather sharp increase in the contribution of reflected electrons to the total curve leads to the formation of a "step" in the figures of the dependence of the maximum temperature on the energy of the primary electrons (curve 1). We also note that backscattered electrons least influence the value of the maximum heating for light samples and, in part, samples with average ordinal numbers; this effect is observed most in heavy semiconductor targets.

1. N.N. Mikheev and M.A. Stepovich, «Distribution of Energy Losses in Interaction of an Electron Probe with Material», *Industrial Laboratory*, Vol. 62, No. 4, Pp.221-226, 1996.

P1-24: Self-organization of nanoparticles Ni on the surface (0001) Bi_2Te_3

S.V. Chekmazov[1], A.A. Rychkov[2], A.M. Ionov[1], L.V. Yashina[2], A.V. Kuz'min[1], S.S. Khasanov[1], S.I. Bozhko[1]

1. *Institute of Solid States Physics, Russian Academy of Sciences, Chernogolovka, Moscow District, Russia, adm@issp.ac.ru (www.issp.ac.ru). 2.Moscow State University, Moscow, Russia, info@rector.msu.ru (www.msu.ru).*

Self assembling of magnetic Ni nanoparticles on the surface (0001) of the topological insulator Bi_2Te_3 has been observed by means of a scanning tunneling microscope. The Ni particles 10÷20 nm in diameter deposited onto a cleaved Bi_2Te_3(0001) surface formed one-dimensional chains along the $[1\bar{2}\bar{1}0]$. The distance between nanoparticles was in the range of 20÷70 nm. The origin of self-organization is discussed in the terms of the indirect exchange coupling via the surface states of a topological insulator.

The contact author e-mail address: chekmazov@issp.ac.ru.

I would like to participate in The III International Conference «Modern problems in the physics of surfaces and nanostructures» with poster presentation.

P1-25: Thickness dependence of the crystalline structure parameters of Pt films deposited by magnetron sputtering at room temperature

R.V. Selyukov, V.V. Naumov, S.V. Vasilyev

Yaroslavl Branch of the Institute of Physics and Technology, Institution of Russian Academy of Sciences,
rvselyukov@mail.ru

The existence of stress-depth gradients and texture-depth gradients in thin films is well-established fact [1]. It's well known also that the recrystallization temperature of thin films is significantly lower than of corresponding bulk materials [2]. Thus the properties of as-deposited and heat-treated films depend on the film thickness h. The thickness dependence of the crystalline structure parameters of as-deposited and annealed Pt thin films is investigated in this work.

Pt films with h=20-100 nm were deposited on oxidized Si(100) wafers by magnetron sputtering at room temperature. Vacuum annealing at 500°C/60 min was carried out after deposition. X-ray diffraction investigations were performed before and after annealing: θ-2θ diffraction patterns (ARL X'tra diffractometer), pole figures Pt(111) and rocking curves Pt(111) (DRON-3M diffractometer) were recorded. The average size of coherently diffracting domains D and average lattice microstrain ε were calculated using the approximation of Pt(111) and Pt(222) diffraction peaks by Voigt profiles. The texture type, texture axis orientation and relative crystallinity degree δ were determined by pole figure analysis. Full width at half maximum (FWHM) of rocking curve Δα was considered as the parameter of crystalline texture quality. The average lateral size of grains L was measured using SEM micrographs (Zeiss Supra-40). It was found for as-deposited films that Δα decreases and δ increases with increasing h (Fig. 1). We made assumption that the growing layers don't affect the Δα and δ of underlying layers during deposition. Under this assumption we can consider these results as the evidence of the non-uniformity of Δα and δ depth distributions. Δα and δ depth distributions were calculated using experimentally obtained dependencies Δα(h) and δ(h). Annealing leads to the increasing of D and decreasing of ε for all specimens. Δα decreases and δ increases for all h after annealing and Δα(h) and δ(h) are almost independent of h for thicknesses more than 20 nm (Fig. 1). The relative and absolute changes of Δα and δ for 20 nm film is much greater than for films with larger h. This fact indicates that the recrystallization of 20 nm film is more effective in comparison with thicker films. Different annealing effectiveness for the films with various h can be explained by decreasing of recrystallization temperature with decreasing h.
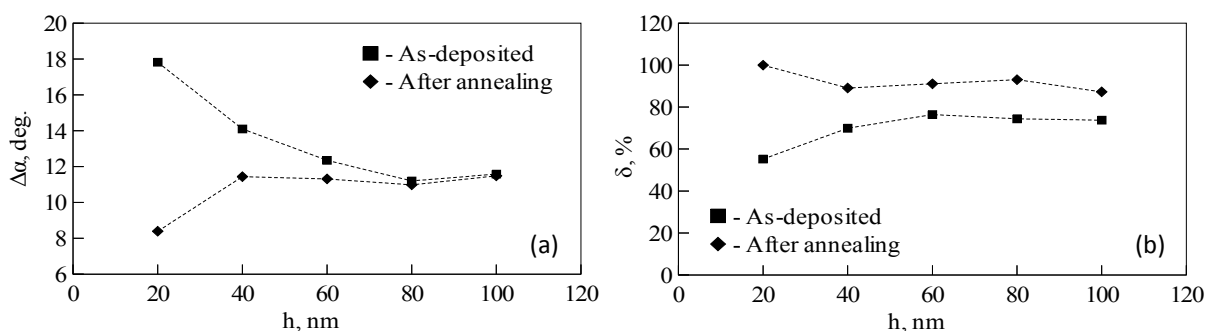
Fig. 1. Δα (a) and δ (b) as the functions of film thickness h for as-deposited and annealed at 500°C/60 min Pt film.

Diffraction peak Pt(111) of 20 nm annealed film has Laue oscillations. For all films the lateral size of grains has unimodal distribution before annealing but recrystallization leads to the growth of secondary grains and bimodal distribution are observed after annealing. The fraction of recrystallized grains in 20 nm film is larger than in thicker films. Thus the diffraction maximum Pt(111) of 20 nm annealed film is the sum of two profiles: Voigt profile and Laue function, the latter is the contribution of secondary grains.

1. Y.Kuru, U.Welzel and E.J.Mittemeijer, «Coexistence of colossal stress and texture gradients in sputter deposited nanocrystalline ultra-thin metal films», *Appl. Phys. Lett.*, 105, 221902, 2014

2. C.C.Wong, H.I.Smith, C.V.Thompson, «Surface-energy-driven secondary grain growth in thin Au films», Appl. Phys. Lett., 48, pp.335-337, 1986

P1-26: Problems of creation of surface laser-induced nano and microstructures and methods of its modelling

P. Trokhimchuck

Lesya Ukrayinka East Eoropean National University, Lutsk, Ukraine, trope1650@gmail.com

Problems of creation surface nano and microstructures have large value for the development of modern optoelectronics and Relaxed Optics (RO) [1, 5]. The structural and geometrical sizes of laser-irradiated semiconductors are depending from regimes of irradiation (wavelength, time and nature of light absorption in matter) [1]. Light scattering centers may be having stable or unstable (metastable) nature. Therefore we have two types of Relaxed Optical phenomena. Processes of first are depended on temporal parameter of irradiation; processes of second type aren't depended on this parameter. Weakly studied are the processes of self-absorption of optical radiation in matter, especially for high irradiation intensities [1]. These processes are connected with phase transformations in irradiated matter.

The problems of modelling the laser-induced phase transformations in irradiated matter are very difficult [1]. The creation of laser-induced surface nano and microstructures may be having various nature [1]. These structures have various geometrical sizes and physical properties and structural symmetry.

For example, laser-induced nanostructures on silicon have sizes from 15-20 nm (irradiation of nanosecond pulses Nd-laser with wavelength 1064 nm [3]) to 20000-30000 nm (irradiation of nanosecond pulse series the eximer KrF-laser with wavelength 248 nm [2]). The hexagonal nanocolumns with height 150-200 nm were created on diamond germanium substrate after irradiation of nanosecond pulses of second harmonic of Nd-laser (wavelength 532 nm) [3].

These results may be modelled and explained on the basis of cascade model of optical excitation of proper chemical bonds in the regime of saturation excitation [1]. This model allows estimating the intensity of irradiation for creation proper solid state structures from crystal symmetry to quasicrystal and amorphous. For case of light absorption on stable centres we must have next chain of transformation of silicon with diamond symmetry: diamond, hexagonal, triclinic, monoclinic, quasicrystals and amorphous. Estimation of distribution energy for case the irradiation silicon of series the nanosecond pulses Nd-laser is confirming this scenario.

For case of light absorption on unstable and metastable centers the temporal characteristics of irradiation haven't notable influence. In this case we can use stationary regimes of irradiation. This fact explains the positive results of Nd-laser annealing of ion-implanted silicon layers [1]. Methods of estimation of energy regimes of irradiation are analogous to previous case [1]. But we don't need to select the appropriate chain of relaxation times.

So for modelling processes of laser-induced surface structures we use models that are based on cascade model of excitation the chemical bonds in the regime of saturation excitation [1].

1. P. P. Trokhimchuck, «Relaxed Optics: Realities and Perspectives». *Lambert Academic Publishing*, Saarbrukken, 2016.
2. A. G. Pedraza, M. D. Foulkes, D. H. Lowndes. «Silicon microcolumn arrays grown by nanosecond eximer-laser irradiation», *Appl. Phys. Let*., 74, pp. 2222-2224, 1999
3. A. Medvids, «Nano-cones Formed on a Surface of Semiconductors by Laser Radiation: Technology Model and Properties», *Nanowires Science and Technology*, ed. Nicoletta Lupu, Inech, Vukovar, pp. 61–82, 2010
4. V. S. Makin, «Regularities of creation of ordering micro- and nanostructures in condensed matter for laser excitation of mode of surface polaritons», *D.Sc. Thesis, State University of Informative Technologies, Mechanics and Optics, Saint-Petersburg*, 2013 (In Russian)
5. P.P. Trokhimchuck, «Problems of Reradiation and Reabsorption in Nonlinear and Relaxed Optics», *International Journal of Advanced Research in Physical Science*, 4, Is.2. pp. 37-50, 2017

P1-27: Electrostatically actuated MEMS switch in a hot operation mode

I. V. Uvarov, V. V. Naumov, A. N. Kupriyanov, O. M. Koroleva, E. I. Vaganova, I. I. Amirov

Yaroslavl Branch of the Institute of Physics and Technology RAS, Yaroslavl, Russia, i.v.uvarov@bk.ru

MEMS switches are widely used in radio frequency and microwave systems [1]. Among several mechanisms driving the switch electrostatic actuation is very attractive because it allows a simple design, low power consumption, and compatibility with microtechnology. The main drawback is a high actuation voltage, which can be overcome by lowering the stiffness of the moveable electrode. However, it increases the probability of stiction. Recently we designed and fabricated the switch with the active contact breaking mechanism, that allows to detach the electrodes in case of stiction. Testing in the cold mode confirmed the significant mechanical reliability of the device [2]. An important parameter of the switch is the ability to work in the hot mode, i.e. to be actuated repeatedly when a voltage differential exists between source and drain. In this regime the additional failure mechanisms take place at the contact area causing the rapid degradation of the contact [3]. Here we present the results of testing the switch in the hot mode.

The switch is shown in Fig. 1. The movable electrode (source) is an aluminum beam attached to the torsion springs. Platinum gate and drain electrodes are located under the each arm of the beam. The beam has platinum contact bumps on its bottom side. Initially the beam is in a horizontal position. When the voltage is applied to one of the gates, the beam tilts under the electrostatic force and touches the drain. When the gate voltage is removed, the beam returns to the initial state. If the elastic force of the springs is insufficient to overcome stiction between the beam and the drain, the active contact breaking mechanism is used: the voltage is applied to another gate and the beam tilts to the opposite direction.
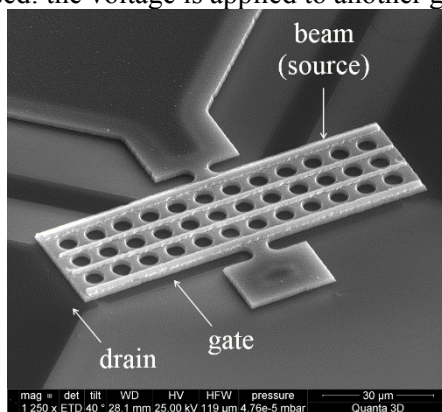
Fig. 1. SEM image of the switch.
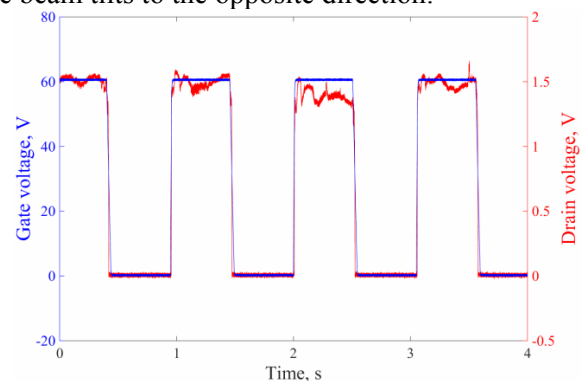
Fig. 2. Gate and drain voltage of the switch during the cyclic operation. Source voltage is 1.5 V.

Testing of the switch is performed in ambient air under normal conditions. The measurements are done in the low-current mode, so that no stiction is observed and the contact brakes passively. Actuation voltage is in the range of 29-46 V depending on the beam width. Experimental values are 25% lower than predicted by FEM simulation probably because of the deformation of the beam. Cyclic operation of the switch is shown in Fig. 2. The unsteady drain signal indicates that the contact is not completely stable. The initial value of the contact resistance is about 1 kΩ, and after several hundred cycles it increases to 100 kΩ limiting the lifecycle. It is clear that the lifecycle has to be improved. We plan to investigate the contact degradation in detail and to choose the materials allowing to reduce the contact resistance and to increase the reliability.

1.   G.M. Rebeiz. «RF MEMS: Theory, Design, and Technology», *John Wiley & Sons, Inc.*, Hoboken, New Jersey, 2003
2.   I.V. Uvarov, V.V. Naumov, O.M. Koroleva, E.I. Vaganova, I.I. Amirov, «A low actuation voltage bistable MEMS switch: design, fabrication and preliminary testing», *Proc. SPIE*, 10224, 102241A, 2016
3.   B.F. Toler, R.A. Coutu, J.W. McBride, «A review of micro-contact physics for microelectromechanical systems (MEMS) metal contact switches», *J. Micromech. Microeng.*, 23, 103001, 2013

P1-28: Critical thickness for dislocation nucleation in $Ge_{1-x}Si_x$/Si (001) heteroepitaxial system

O.S. Trushin[1], E. Glazkov[2], E. Granato[3] and See-Chen Ying[4]

1. Yaroslavl Branch of the Institute of Physics and Technology of RAS, Yaroslavl, Russia, otrushin@gmail.com
2. P.G. Demidov Yaroslavl State University, Yaroslavl, Russia
3. LAS, National Institute for Space Research, São José dos Campos, Brazil
4. Department of Physics, Brown University, P.O. Box 1843, Providence, Rhode Island, 02912, USA

Heteroepitaxial systems play an important role in modern microelectronic technology. Due to the lattice mismatch between the film and the substrate, considerable elastic strain energy is accumulated in epitaxy. For sufficiently thick films, defects will form leading to the relaxation of strain energy and to the loss of coherent epitaxy. Controlling the film-substrate interface quality and preventing defect formation is an important problem of modern technology[1]. In this work we studied atomistic mechanisms of misfit dislocation nucleation in $Ge_{1-x}Si_x$/Si(100) heteroepitaxial systems (with x varying in the range from 0.1 up to 0.5). We explored these systems in three dimensions using molecular statics methods with Stillinger-Weber semi-empirical interatomic potential [2]. We used combination of Repulsive Bias Potential activation procedure and Nudget Elastic Band method for generating Minimum Energy Paths for transitions from the coherent epitaxial (defect free) state to the state containing an isolated defect (misfit dislocation, shown in fig.1). We have already used this method successfully before to study the process of dislocation nucleation in pure Ge film on Si(001) substrate [3]. In this work we extended the research to the random alloy $Ge_{1-x}Si_x$ thin films on Si(001) using similar methodology and model geometry. Start configurations of the $Ge_{1-x}Si_x$ films were prepared by random substitution of Ge atoms in the film according to the required chemical composition. For each composition of the film being studied, configurations containing a 90^0 dislocation have been generated using methodology described above. The energy of the final state containing the defect has been compared with initial coherent epitaxial state and energy gain due to strain relaxation been estimated. In such a way we were able to extract information about the dependence of critical thickness on the film composition (fig.2).
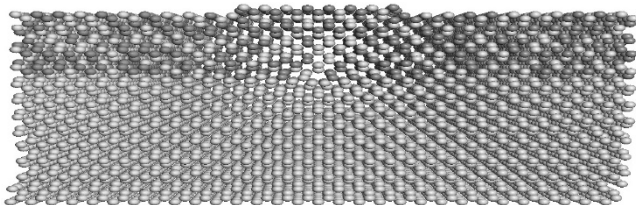
Fig.1 Side view of the model with dislocation in the middle. Dark balls represent Ge atoms, white - Si.
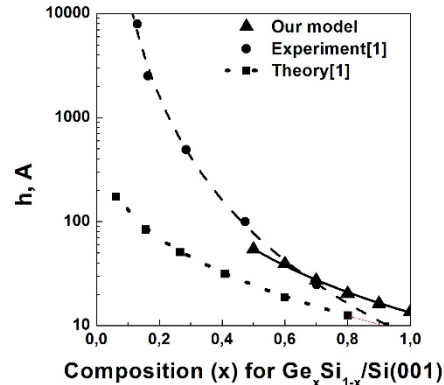
Fig.2 Dependence of critical thickness on film composition

In summary, we have used atomistic modeling to get systematic estimates of the critical thickness of $Ge_{1-x}Si_x$/Si(001) heteroepitaxial system as function of its composition. The results are in better agreement with available experimental data than those from an analytical theory based on a Matthew-Blakeslee continuum model, where the effective mismatch depends on the concentration of Ge [1].

1. R.Hull, "Misfit strain and accomodation in SiGe heterostructures", in a book *Germanium Silicon: Physics and Materials* (ed. by R.Hull and J. Bean), Academic Press, San Diego, 1999.
2. F. Stillinger, T. Weber "Computer simulations of local order in condensed phases of silicon", Phys. Rev. B, **31**, pp. 5262-5271, 1985.
3. O. Trushin, E. Maras, A. Stukowski, E. Granato, S.-C. Ying, H. Jónsson and T. Ala-Nissila "Minimum energy path for the nucleation of misfit dislocations in Ge/Si(001) heteroepitaxy", Modelling Simul. Mater. Sci. Eng. **24** p.035007, 2016.

P1-29: Exploring energy landscape of magnetic nanostructures with Nudged Elastic Band Micromagnetics

O.S. Trushin[1], N. Barabanova[1], E. Granato[2], S.C. Ying[3]

1. Yaroslavl Branch of the Institute of Physics and Technology of RAS, Yaroslavl, Russia, otrushin@gmail.com.
2. LAS, National Institute for Space Research, São José dos Campos, Brazil
3. Department of Physics, Brown University, P.O. Box 1843, Providence, Rhode Island, 02912, USA

Magnetic nanostructures have attracted new interest in recent years [1] due to its potential for application in new generations of computer memory. Micromagnetic model is an important tool for theoretical studies of magnetic nanostructures. It assumes a phenomenological description of the magnetic system where the total energy of the system is a functional of a continuous magnetization function. Numerical implementation of the model assumes spatial discretization of the system using fine grid. We focus here on the numerical study of the thermal stability of the magnetic state which is an important issue concerning the reliability of nanomagnets as memory elements. This is related to magnitude of energy barriers separating different magnetic states. corresponding to local minima of the energy functional. Theoretical estimates of energy barriers can be done using Nudged Elastic Band method within micromagnetic model [2]. We have developed our own code implementing NEB within micromagnetics [3]. In this work we have studied the energy landscapes of ring shaped magnetic nanostructure. These structures are particularly interesting for magnetic memory, since the shape provides conditions for magnetic flux closure that helps prevent mutual interference of neighboring memory cells.
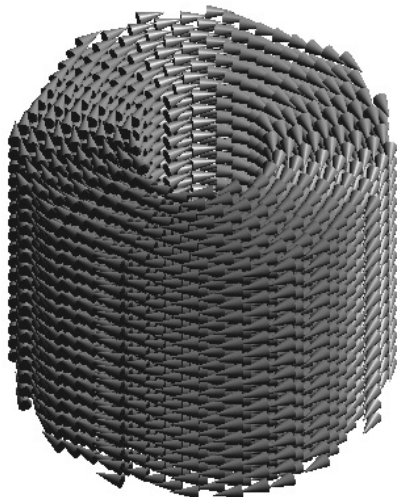
Fig.1 Side view on the model. Cones show local magnetization vectors at grid points.
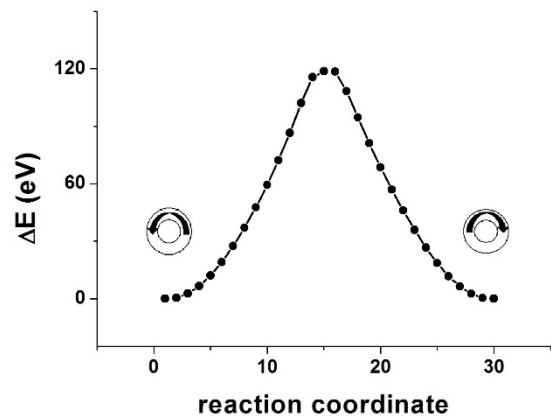
Fig.2 Energy profile along the transition path between two states of magnetization of the nanoring.

Single layer permalloy nanoring with thickness 50 nm, internal radius 10 nm and external radius 30 nm has been considered (fig.1). As the result of simulation we were able to identify several local minima corresponding to different magnetic states of the ring. The lowest energy minimum corresponds to a vortex state. Energy barriers separating local minima were determined that vary from dozens up to hundreds eV (fig.2). This is much higher than thermal energy at room temperature and implies thermal stability of the magnetic structure. Our finding shows potential reliability of the magnetic nanoring as an element of magnetic memory.

1. M. Klaui and C. Vaz "Magnetization configurations and reversal in small magnetic elements", *in Handbook of magnetism and advanced magnetic materials*, ed. by H. Kronmuller and S. Parkin, v. 2, John Willey & Sons, Ltd., 2007.
2. D. Suess, et al. "Reliability of Sharrocks equation for exchange spring bilayers", Phys. Rev. B, **75**, p.174430, 2007.
3. O. Trushin, N. Barabanova "Micromagnetic software package MICROMAG and its applications to study elements of spintronic", Russian Microelectronics, **42,** pp. 176–183, 2013.

P1-30: Depth profiling of magnetic tunneling junction using ION TOF

O.S. Trushin[1], S. Simakin[1], S. Vasiliev[1]

1. Yaroslavl Branch of the Institute of Physics and Technology of RAS, Yaroslavl, Russia, otrushin@gmail.com

Magnetic Tunneling Junction (MTJ) is an important element of modern MRAM cell. It is believed that MRAM might be the next generation of computer memory because it combines both fast access rate and nonvolatility [1]. Therefore optimization of the technology for MTJ fabrication is of very important task. Achievement of high functional characteristics of MTJ requires intensive quality control at different stages of the technological route. In this work we discuss different aspects of quality control during this process with emphasis on the depth profiling of multilayer structure using Secondary-Ion Mass Spectrometry (SIMS). Multilayer structure of the following composition (from bottom up to topmost layer): 5 Ta/30 CuN/5 Ta/3 NiFe/16 IrMn/2.0 CoFe/0.9 Ru/2.5 CoFeB/MgO /2.5 CoFeB/10 Ta/ 7 Ru has been deposited on Si wafer using magnetron sputtering at Singulus Timaris PVD cluster tool[2]. Bottom electrode contains relatively thick conductor bus (CuN) and exchange biased magnetic layer CoFeB together with artificial antiferromagnet structure for strong pinning of its magnetic state. It is separated from the upper electrode (containing free magnetic layer CoFeB) by ultra thin insulating layer of MgO with thickness less than 2 nm. Before starting the lithography process for MTJ fabrication it is very important to get complete information about quality of as-deposited multilayer film. For this purpose visual inspection of the cross section of the structure has been performed using Transmission Electron Microscopy (Fig.1). Further analysis assumes control of chemical composition of different layers in the stack. It has been done here using depth profiling with cation SIMS (ION TOF). This analysis has been done in the regime of registering both positive and negative secondary ions while using Cs ions for sputtering target and Bi ions for probing. Typical results of such analysis for particular elements are shown in Fig.2.
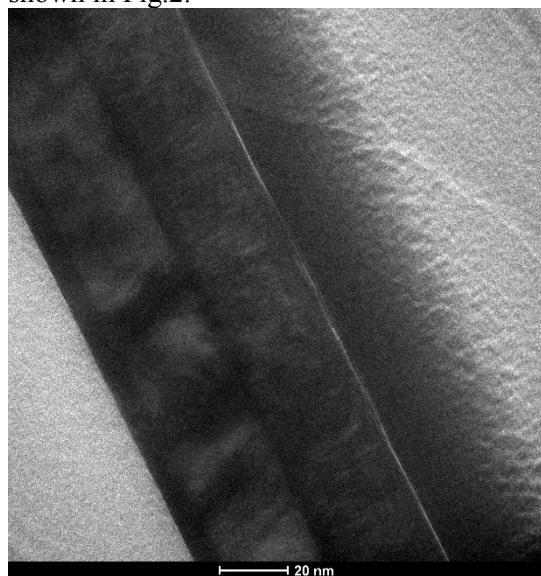
Figure 1 TEM bright field image of the cross section of the MTJ multilayer structure (Tecnai G2 F20 U-TWIN).
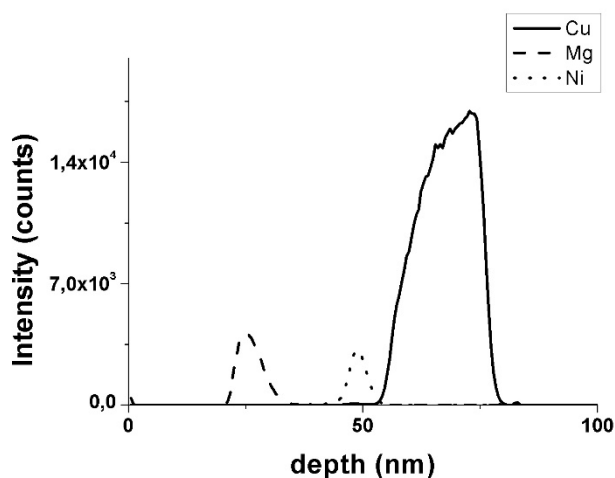
Figure 2 Results of depth profiling using cation SIMS (ION TOF) for particular elements.

Comparing these profiles with requested structure of MTJ stack listed above one can see overall good qualitative agreement. Although thicknesses of layers are not well reproduced because of limited accuracy of SIMS depth profiling but order of different layers corresponds to initial guess. Thus we conclude that depth profiling using SIMS might be useful tool in optimization of MRAM technology. The work has been done on the equipment of the Center for Collective Use of Scientific instruments "Micro and Nanodiagnostics"[3].

1. H. Yoda, MRAM Fundamentals and Devices, Handbook of Spintronics: Springer Reference, 2016.
2. http://www.singulus.com/uploads/tx_pspublications/Timaris_230616.pdf
3. http://nano.yar.ru/en/

P1-31: Correlation of conductivity switching effect and clusters size incorporated from the gas phase to silicon oxide in MIS structure

A.A.Popov, A.E.Berdnikov

Yaroslavl Branch of the Institute of Physics and Technology, Institution of Russian Academy of Sciences, str.Universitetskaya 21, Yaroslavl, 150007, Russia, E-mail: imiraslab4@yandex.ru

Previously we found conductivity switching effect in metal – insulator – semiconductor structure with SiO_2 insulator deposited by plasma of low frequency glow discharge enhanced chemical vapor deposition (LF PECVD) [1]. This structure can be used as non-volatile memory and reprogrammable logic arrays. Investigations of this effect show that current canal have several nanometers diameter, but this structure have bad ability for size decreasing. We supposed that conductivity switching effect connected with nanosize particle formed in gas phase and embedded in growing films.

We produced MIS structures with different area of metal. Insulator SiO_2 in this structure was produced by LF PECVD under technological conditions optimized for big size area of metal (10^6 um^2) MIS. Thickness of insulator was approximately 40 nm. Investigation of conductivity switching effect on this structures show that yield drastically dropped if MIS area became lower than 10^4 um^2. This means that a cluster with the size necessary for the existence of a conductivity switching effect is absent in this area. So, concentration of this clusters approximately are $1/10^4$ um^{-2} or taking into account the thickness of the film the volume concentration is $2.5 \cdot 10^{-3}$ um^{-3}.

Also we investigated the distribution of clusters size incorporated in deposited films. This investigation was produced on base of AFM data in supposing of conformal film deposition by LF PECVD. Result present in fig.1. Interpolation curve is described by exponential equation also presented in fig.1.

$$y = 30{,}23e^{-0{,}6882x}$$
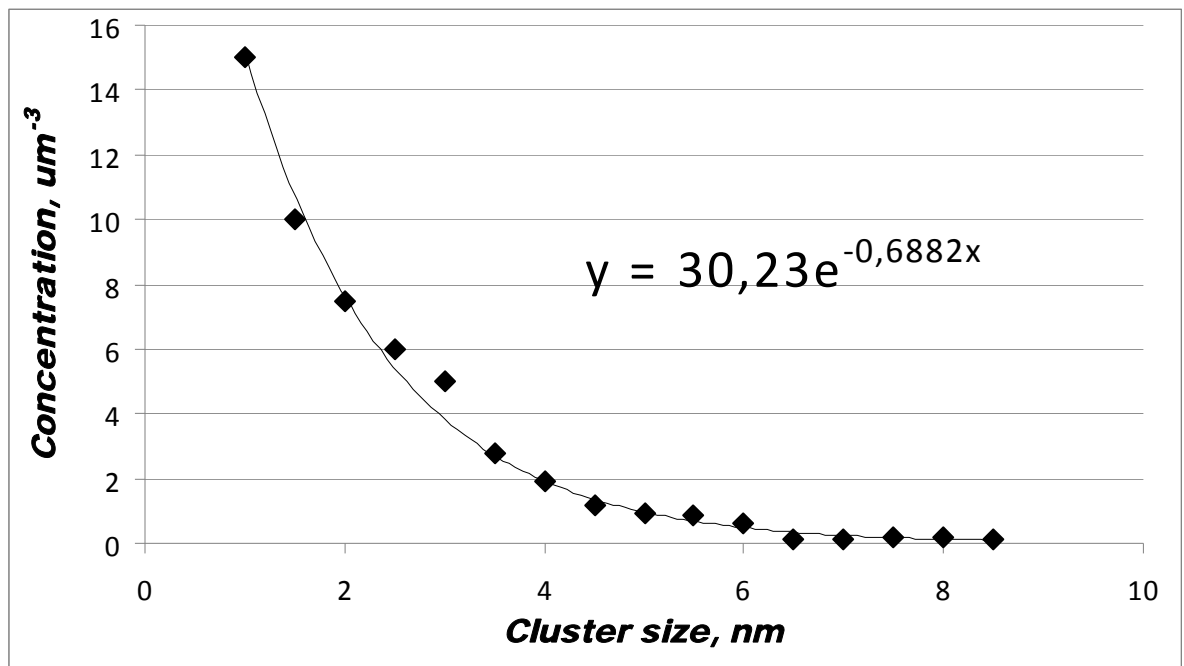
Fig.1. Cluster size distribution in LF PECVD deposited film.

Using this equation we find that in MIS structure must be cluster with size 13-14 nm for existing of conductivity switching effect.

1. A.E. Berdnikov, V.N. Gusev, A.A. Mironenko, A.A. Popov, A.V. Perminov, A.S. Rudy, V.D. Chernomordick "Conductivity Switching Effect in MIS Structures with Silicon-Based Insulators, Fabricated by Low-Frequency Plasma-Enhanced Chemical Vapor Deposition Methods" *Semiconductors*, Vol. 47, No. 5, pp. 641-646, 2013

P1-32: Method of production of dielectric layer for MIS structures with conductivity switching effect.

A.E. Berdnikov, <u>V.N. Gusev</u>, A.A. Popov

Yaroslavl Branch of the Institute of Physics and Technology, Institution of Russian Academy of Sciences, str.Universitetskaya 21, Yaroslavl, 150007, Russia, E-mail: gusev@yf-ftian.ru

The present work is considering the formation and use of the silicon oxynitride as the dielectric layer for the MIS structures with conductivity switching effect. Previously we found this effect in MIS structures with insulator produced by low frequency PECVD [1].

For the deposition of the dielectric layer the method of magnetron sputtering of silicon was used. Silicon target was bombardment by ions of chemically active plasma. The plasma formed by electric discharge in a gas mixture of argon, oxygen and nitrogen, which provide chemical reaction with sputtered silicon. A film with thickness of 55 - 60 nm from oxynitride silicon SiO_xN_y deposited on a p-type monocrystalline silicon substrate. The total pressure of gas mixture in the magnetron chamber was in the range of $1-5*10^{-4}$ Torr. Content of oxygen and nitrogen was 6-8% by volume and-3 – 5%by volume respectively.

The chemical composition of the formed films was determined by auger method. Under described conditions, the silicon content in the film was 36 - 42 at.%, nitrogen 4-6 at.% oxygen 52 - 57 at.%.

For study the properties of this film were made the aluminum contact electrodes with different area, on back surface of silicon wafers continual layer of aluminum was deposited also. When a voltage is applied between the substrate and the top metal electrode of MIS structure bipolar bistable conductivity switching effect was observed, which illustrated by current-voltage characteristics (Fig.1,2).
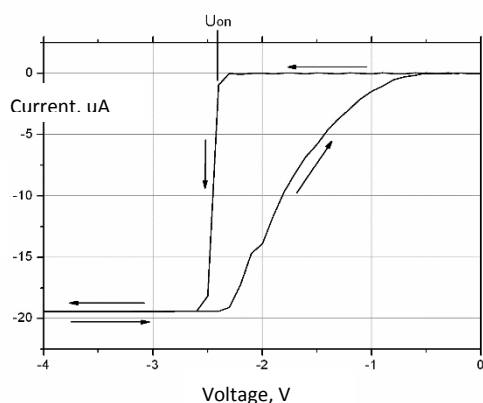
Fig. 1. The current-voltage characteristic of a test structure illustrating the transition to the conductive state when negatives bias voltage applied.
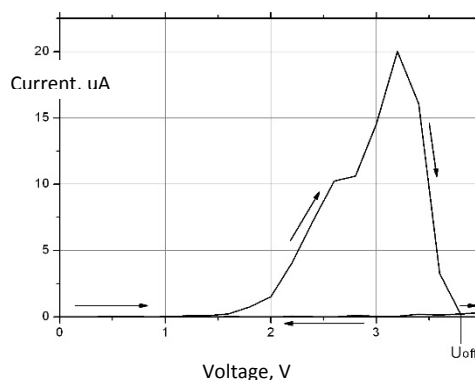
Fig. 2. The current-voltage characteristic of a test structure illustrating the transition to the nonconductive state when positives bias voltage applied.

In this work we show that silicon oxynitride deposited by magnetron sputtering are suitable for dielectric in metal – insulator – semiconductor structure with conductivity switching effect. This structure can be used as non-volatile memory and reprogrammable logic arrays.

1. A.E. Berdnikov, V.N. Gusev, A.A. Mironenko, A.A. Popov, A.V. Perminov, A.S. Rudy, V.D. Chernomordick "Conductivity Switching Effect in MIS Structures with Silicon-Based Insulators, Fabricated by Low-Frequency Plasma-Enhanced Chemical Vapor Deposition Methods" Semiconductors, Vol. 47, No. 5, pp. 641-646, 2013

P1-33: Investigations of the influence of the gas medium on the switching characteristics of memory cells based on TiN-SiO$_2$-W open sandwich structure

E.S. Gorlachev, V.M. Mordvintsev, S.E. Kudryavtsev

Yaroslavl Branch of the Institute of Physics and Technology, Russian Academy of Sciences, Yaroslavl, Russia,
Mordvintsev-Viktor@yandex.ru

In this work we report the study of the gas medium effect on the operation of non-volatile electrically reprogrammable memory cells based on conducting nanostructures (CN) produced by the electroforming phenomenon. We studied memory cells based on TiN-SiO$_2$-W open sandwich structure [1] with a SiO$_2$ layer thickness of $\sim$20 nm and a TiN lower electrode thickness of 50 nm. The cells were placed in a vacuum chamber and underwent electroforming with a 0-12 V bias in the initial vacuum of ~10^{-4} Torr obtained with a turbomolecular pump. To reach the pressure targets, the studied gas (dry air, high-purity nitrogen or argon) was supplied into the chamber using an inlet system. The studies were performed both for increase and decrease of pressure in the range of 10^{-2}-10^2 Torr with a half order of magnitude steps. The memory cells were switched on using a repeating single 5 V pulse with a duration of 30 ms. The cells were switched off by applying a 100 ns pulse with an amplitude of 6 V from an external pulse generator. The investigations for each pressure point included 30 consecutive ON/OFF cycles with the measurements of the current in the ON state for the voltage of 1 V and of the number of 5 V pulses required to switch on. The experiments showed that for the dry air the memory cells stop switching on upon reaching a certain critical threshold pressure, which varied for different samples in the range of 10-30 Torr. This corresponds well to our previous results of switching failure upon air pressure increase [2]. Another phenomenon taking place was the increase of the average current in the ON state by several times with the increase of the air pressure. At the same time, the average number of pulses required for the memory cell to switch on also showed an increase with pressure growth. The phenomenon of the memory cell failure to switch to the ON state was also observed for the inert gases. For N$_2$ the threshold pressure was in the range of 1-300 Torr, for Ar it was in the range of 10-100 Torr. The obtained results show a principal role of the gas medium pressure in the switching of memory cells, with the gas itself playing only a secondary role, which allowed us to propose a model of the deactivation of the CN formation. According to our previous studies [1], the Si CN formation takes place due to the electron impact breaking Si-O bonds in the SiO$_2$ molecules on the open surface of the SiO$_2$ layer during the switching on and thus removing oxygen to the gas medium. However, if the gas medium atom/molecule hits the activated SiO$_2$ molecule during that process, it would "withdraw" the electron impact energy and prevent the Si CN formation. On the assumption of this model, we can estimate the life time of the activated SiO$_2$ molecule on the dielectric surface using the gas pressure p and the relative molecular mass M_r. From the kinetic theory of gases, the flux density J of particles onto a surface is:

$$J = \frac{1}{4} n \bar{v} \,. \tag{1}$$

Replacing the particles concentration n and their average velocity $\bar{v}$ with the well-known expressions, we can calculate the flux density measured in m^{-2}·s^{-1} as follows:

$$J = 1.65 \cdot 10^{23} \frac{p}{\sqrt{M_r}} \,. \tag{2}$$

Assuming that the activated SiO$_2$ molecule effective size is ~1 nm^2, eq. (2) allows to calculate the period of it being hit by gas molecules, which for Ar at 10 Torr, when the memory cells begin to failure, is 30 ns. Therefore, the life time of the activated SiO$_2$ molecule can be estimated as ~10^{-8} s.

1. V.M. Mordvintsev and S.E. Kudryavtsev, "Investigation of electrical characteristics of memory cells based on self-forming conducting nanostructures in a form of the TiN-SiO$_2$-W open sandwich structure", *Russ. Microelectron.*, **42**, pp. 68-78, 2013

2. V.M. Mordvintsev, S.E. Kudryavtsev, V.L. Levin and L.A. Tsvetkova, "Influence of the pressure of the gas medium and duration of controlling pulses on the stability of characteristics of memory cells based on electroformed Si-SiO$_2$-W structures", *Russ. Microelectron.*, **39**, pp. 313-322, 2010

P1-34: Investigation of magnetic metamaterials growth with in situ resistance monitoring

A. Chernykh, L. Fomin, V. Berezin, G. Mikhailov

Institute of Microelectronics Technology and High Purity Materials RAS, b. 6, Academician Ossipyan str, Chernogolovka, Moscow Region, 142432, Russia, E-mail address: chern@iptm.ru

Magnetic metamaterials consisting of ferromagnetic nanoislands separated by thin dielectric or antiferromagnetic (NiO, FeMn) layer have been grown, and research of growing technology in nanoscale range has been performed. The work is motivated by potential developing of new sensors and devices for spintronics. For sample fabrication, pulse laser deposition of the metal from the target on the heated substrate under high vacuum was used. For the purpose of the growth process monitoring and investigation the electric resistance of the condensate deposed on the sapphire substrate was measured. Resistance measurements both in-situ and ex-situ were also supplemented by condensate investigation performed with atomic force, magnetic force and scanning electron microscopies. This allows correlating conductive properties of the grown film with its morphology, island dimensions and geometry (Fig.'s 1 and 2). The investigation was made of all stages of pre-percolated film growth, essentially Ostwald ripening stage studying. The latter occurs at small supersaturation existing at relatively high substrate temperature (400-700°C) and low deposition rate (0.1-1 nm/min) and is characterized by growth of large islands due to diffusion resorption of small islands of subcritical dimension. This leads to non-trivial termination of condensate electric resistance decrease and even to its observable increase during condensate deposition. Ostwald ripening process is stable in-time and elongated enough to grow condensate film with desirable parameters (Fig. 2). Developed nanotechnology allows growing metallic islands with 1-100 nm dimensions in different stages of percolation, fabricating of metamaterial composed of metallic and dielectric materials, as well as supplemented thermal annealing in vacuum or in oxygen to control conductive properties of metamaterials.
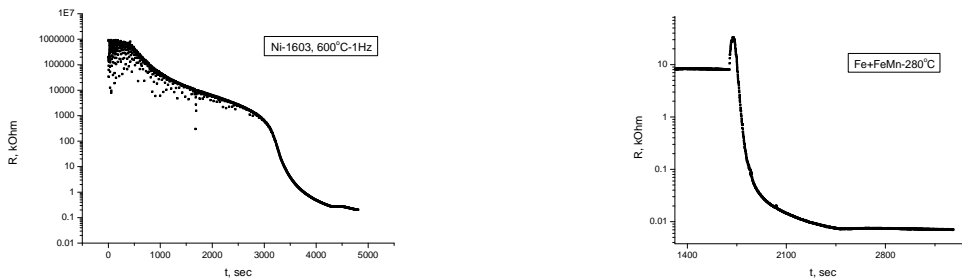
Fig. 1. Typical dependences of electrical resistance of metallic islands (left) and metamaterial fabricated by
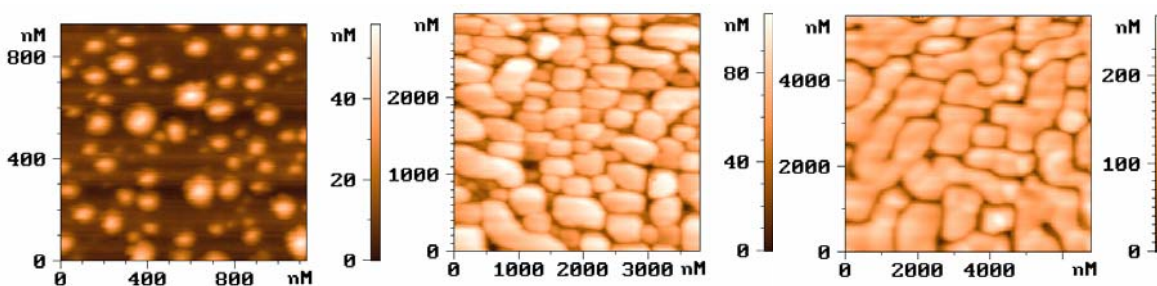
deposition of FeMn on Fe-islands (right) versus growing time.

Fig. 2. AFM images of Fe-islands at different growth stages (from left to the right): beginning of Ostwald ripening, its termination, and beginning of percolation stage. Growth condition T=600°C, v=0.5nm/min.

P2-1: Analysis of the boundary structure silicon substrate—silicon dioxide

N. Parfenov

Moscow aviation Institute (national research University), Moscow, Russia, E-mail: sedennik@mail.ru

Currently, the structure of Si / SiO2 is widely used in microelectronics and mechatronics in the creation of structures of SOI and MEMS devices.

However, it is also known that the structure of Si / SiO2 depending on the manufacturing technology of the devices can have local defects that can have a negative impact on the stability and reliability of electronic devices.

The aim of this work is the study of causes and mechanism of formation of local defects in the silicon wafer and the structure of Si / SiO2 finding ways to reduce them.

In one study it was shown that after the growing of silicon crystals by the methods of Czochralski or zone melting and selective etching on the plate surface was discovered microdefects in the form of strips. Despite detailed investigation of defects, the cause and mechanism of their formation is still not known [1,2].

When you create a sensor of the diaphragm type was used monocrystalline silicon (100) orientation, and the dielectric was applied vitreous dielectric.

This work is devoted to study of the defects that were detected on the silicon substrate and at the interface of Si / SiO2 structure . [3,4].

According to studies the SEM images of the silicon surface, phase boundary of silicon—a vitreous dielectric, obtained using scanning electron microscopes TM-3000, Quanta 200 3D confocal microscope Nikon Eclipse control software was discovered, the local micro-defects in the form of strips, defects in the form of roughness of the surface and the pores, voids, foreign particles.

Defects on the surface of the silicon wafer were significantly reduced by selection of the modes of etching, the concentration and temperature of Etchant.

1.   Rainey K. «Defects and impurities in semiconductor silicon». M.: Mir. 471 S. 1984

2.   Vavilov V. S., Kiselev V. F., Mukashev B. N. «Defects in silicon and on its surface». *GL. Physical ed.-Mat.* lit Moscow: Nauka. 216 S. 1990

3.   Sokolov L. V. , Arkhipov S. V. Shkolnikov, V. M.*,* «Investigation of the mechanism underlying the anisotropic chemical etching in the formation of bulk micromechanical structures in silicon (100)». *Microelectronics*. volume 32. No. 3. S. 194—201. 2003

4.   Parfenov N. M. Timoshenkov S. P., Timoshenkov S. A. «Study of the effect of etching on the surface morphology of silicon». *Automation. Modern technology*. No. 8, p. 36-39. 2016

P2-2: Radiation heat transfer between silicon wafer and lamp-based reactor with inclusion of quartz glass

V. Prigara, V. Ovcharov, A. Kurenya,V. Rudakov

*Yaroslavl Branch of the Institute of Physics and Technology, Institution of Russian Academy of Science,
Yaroslavl, Russia, vladovcharov@rambler.ru*

Thermal processes constitute an integral part of the technology of micro- and nanoelectronics. Among these are the perspective processes of semiconductor wafer treatment by incoherent radiation.

Emissivity of the silicon wafer increases nonlinearly as its temperature increases. The result is that the temperature bistability effect in the silicon wafer may cause when a high power incoherent energy flux passes through it. The point of the effect is that at the same values of the parameters for the wafer heat treatment, its temperature can take on different values depending on whether the wafer is being heated or cooled. However, the design of the thermal chamber, as a rule, involves the isolation of the working zone of the chamber from the heating block. In particular, for this purpose the quartz glass of a specific brand is used in setup for the temperature-gradient heat treatment [1]. As a result, the working wafer temperature dependence on the parameter controlling thermal treatment process is represented by hysteresis loop with wafer temperature jumps occurring at a monotonous increase and decrease of the parameters [1]. Either heater temperature or heat exchange coefficient is chosen as a controlling parameter for the modeling of the heat-exchange process between a silicon wafer and the elements of the lamp-based reactor.

The heater in [1] representing a block of the tungsten-halogen lamps is simulated as the tugsten plate of emissivity ε_λ in the wavelength interval 0-20 mkm. In this case, the real spectral interval of heater radiation is narrowed down towards a smaller wavelength interval of 0-5 mkm. The spectral interval changes of the heater radiation have an effect on the working wafer temperature. In addition to the spectral limitation of the heater, the quartz glass window exchanges radiant energy with other elements of the thermal reactor, being a source of its own radiation and reemitting radiation fluxes incident on the window from the working wafer and the heater.

The net radiation method [2] was used for evaluation of the effect of the quartz glass on the silicon wafer temperature. Using the method [3], the problem of the heat exchange between a semitransparent gray wafer and two gray opaque glazings between which the wafer is disposed is analytically solved. Here the heat system of four flat, two-dimensional and extending to infinity wafers is considered. Two extreme wafers of blackbody characteristics are the radiator and the absorber of heat radiation. Two intermediate ones are the wafers of the working silicon and quartz glass, whose properties are dependent on the temperature and the incident wavelengths. The analytical expressions for net radiation terms arising between the wafers are obtained.

The model can be used for the calculation of the radiation-convection-conduction interaction problems in a heat system modeling IR-lamp annealing in a thermal reactor that is controlled by the heater temperature and the heat exchange coefficient.

1.   V.Rudakov, V.Ovcharov, A.Kurenya,V.Prigara, «Bistable behavior of silicon wafer in rapid thermal processing setup», *Microelectron. Eng.*, 93, pp.67-73,2012

1.   2.J.Zeegers, H.A.L.van Dijk, «A note on the net radiation method applied to a system composed of a semitransparent film between two glazings», *Sol. Energy Mater.and Sol.Cells*,33, pp.23-30, 1994.

2.   R.Siegel and J.R.Howell. «Thermal radiation heat transfer». *Hemisphere Publ. Corporation*, Washington, 3-d ed., 1992.

P2-3: Получение многослойных структур с заданным показателем преломления

С. Алалыкин, Р. Закирова, В. Кобзиев, Н. Костенков, П. Крылов, И. Федотова

Удмуртский государственный университет, Ижевск, Россия, E-mail: ftt@udsu.ru

Для разработки различных устройств необходимо получение пленок с заданными характеристиками, в частности, с заданным значением диэлектрической проницаемости или показателем преломления. Варьировать характеристики пленок можно, задавая состав нанокомпозитов. Например, в [1] показано, что изменение концентрации наночастиц ZnS в оксидном стекле позволило модифицировать показатель преломления полученных стекол. Согласно [2], если характерные размеры составляющих компонентов нанокомпозитов меньше длины волны зондирующего излучения, то такой композит можно рассматривать как однородную оптическую среду, обладающую некоторым эффективным показателем преломления, отличным от показателей преломления веществ, образующих данный композит (модель эффективной среды). Изменение показателя преломления связано с изменением плотности материала, диэлектрической проницаемости и т. д. Возможности синтеза многослойных структур с заданным показателем преломления до конца не исследованы.

Цель настоящей работы заключалась в получении и исследовании многослойных структур ZnS/SiO_2, ZnS/Al_2O_3 и $ZnSe/SiO_2$ с заданным показателем преломления. Задачей работы являлась также проверка применимости некоторых моделей для расчета значения эффективного показателя преломления многослойных пленок в зависимости от концентрации и показателей преломления исходных компонентов.

Многослойные структуры ZnS/SiO_2, ZnS/Al_2O_3 и $ZnSe/SiO_2$ с суммарной толщиной 0.40 ± 0.03 μm и различным количеством пар слоев сульфида цинка и диэлектрика получены методом ВЧ магнетронного напыления. Для получения многослойных структур с заданными толщинами использовался программно-аппаратный комплекс, использующий микросистему управления оборудованием [3]. Толщина слоев диэлектрика была постоянной. Толщина слоев полупроводников увеличивалась, в то время как число пар слоев уменьшалось.

Рентгенофазовый анализ и электронная микроскопия показали, что многослойные структуры ZnS/SiO_2 являются аморфными, размер зерна, оцененный по микроизображениям, не зависит от толщины прослойки ZnS и составляет ~3−4 nm. Структура ZnS/Al_2O_3 и $ZnSe/SiO_2$ зависит от толщины слоев полупроводника: при малых толщинах ZnS (ZnSe) образцы рентгеноаморфные, при больших толщинах наблюдаются дифракционные максимумы, принадлежащие полупроводнику. По оптическим спектрам пропускания с использованием конвертного метода [4] были определены толщины и показатель преломления полученных структур.

Проверена применимость моделей Максвелла−Гарнета и Бруггемана, а также формулы Луйенги для расчета значения эффективного показателя преломления структур. В области слабой дисперсии расчетные значения эффективных показателей преломления достаточно хорошо коррелируют с экспериментальными данными. Для поглощающих структур отклонение теоретического значения показателя преломления от экспериментального возрастало при увеличении поглощения пленок.

1. R. Saoudi, M. Moussaoui, S. Tonchev, A. V. Tishchenko «Modified optical properties of glasses nanostructured by ZnS particles», *J. Quant. Spectr. Radiat. Transfer*, vol. 113, N 18, pp. 2499–2502. 2012.

2. Головань Л.А., Тимошенко В.Ю., Кашкаров П.К. «Оптические свойства нанокомпозитов на основе пористых систем», *УФН*, т. 177, вып. 6, сс. 619–638, 2007.

3. С.С. Алалыкин, П.Н. Крылов «Микросистема управления оборудованием», *ПТЭ*, № 5, сс. 160–161, 2009.

4. В.В. Брус, М.Н. Солован, Э.В. Майструк, И.П. Козярский, П.Д. Марьянчук, К.С. Ульяницкий, J. Rappich «Особенности оптических и электрических свойств поликристаллических пленок CdTe, изготовленных методом термического испарения», *ФТТ*, т. 56, вып. 10, сс. 1886–1890, 2014.

P2-4: Mossbauer study of the dynamic and mechanical properties of frozen water films on the clay surface

A. A. Zalutskii

Yaroslavl Technical State University, Yaroslavl, Russia, zalutskii@mail.ru

The report deals with the composite idea, consisting in the fact that silicate layers of the clay and interlayer iron complexes in conjunction with water-forms a single complex. For the analysis of the "structure" of the adsorbed mineral mesh water applied scanning probe technique based on the Mossbauer isotope ^{57}Fe in two forms (Fe^{2+} and Fe^{3+}).

For the first time from the analysis of the temperature dependence of the parameters of the
Spectra ($S_B/S_A = R = N_O/N_P$) the ratio ortho/para-spin isomers in the frozen water (Fig.) and the localization of the Mössbauer probe on the surface of natural aluminum silicates have been determined.
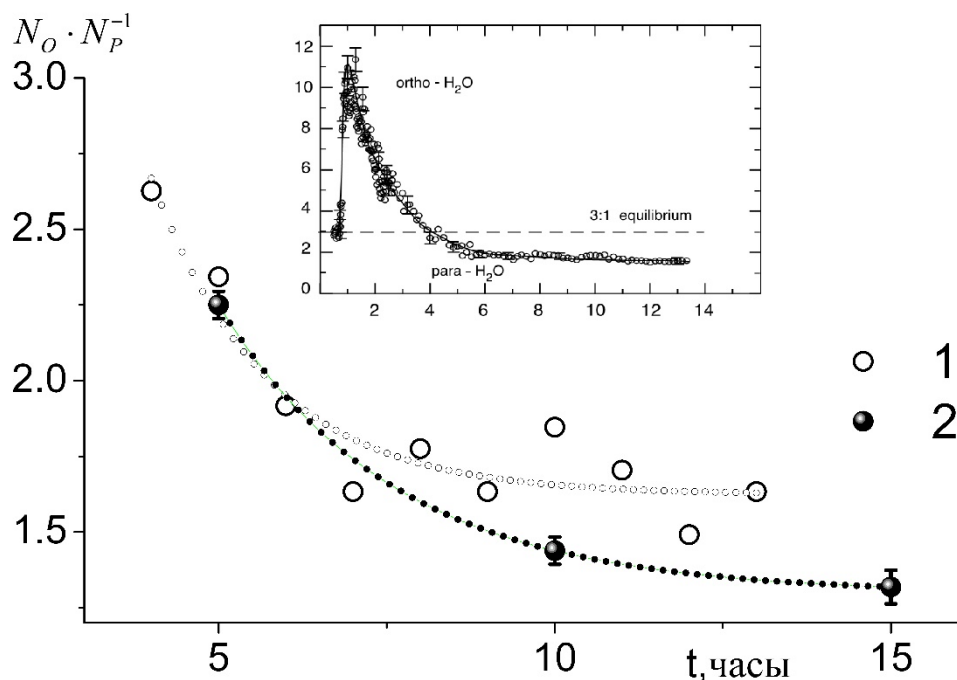
Fig. The results of the comparative analysis of the time ortho/couple relationship of the concentrations of isomers of H_2O from experimental data obtained by MS for the "frozen" water on the aluminosilicate surface (2) and with the help of terahertz spectroscopy for water vapor into the carbon filter (1).

The transformation temperature Mossbauer spectra of is-follow system is explained in the framework of traditional models that adequately describe phase transitions of two types («order-disorder» and «order-order»).

By the method of Mossbauer spectroscopy and an attempt of quantitative evaluation of elastic parameters of «supercooled» water (shear modulus, Poisson's ratio, grüneisen parameter). The ice structure is satisfactorily described in the framework of fractal geometry («Menger sponge», «Kantorova dust»).

P2-5: Наноразмерная характеризация мультислойных магнетронных нанопленок из Cr, Cu, Al, Ni

А.П. Кузьменко, Нау Динт, Мьо Мин Тан,

[1]ФГБОУ ВПО « Юго-западный государственный университет», Россия, Курск, E-mail addres: apk3527@mail.ru

Изучено наноструктурирование при магнетронном распылении (МР) металлических нанопленок на установке МВУ ТМ-Магна из металлических мишеней ООО ГИРМЕТ Cr(99.99%), Al(99.99%), Ni (99.99%), Cu (99.99649%). с размерами 100 ×6 мм на подложки из ситалла с размерами 15×15 мм. По аналогии с [1], полученные МР мультислои были охарактеризованы методами дифракционным РФА GBC EMMA и структурного анализа АСМ AistNT SmartSPM с наноиндентором типа Берковича, а также методом рентгеновской фотоэлектронной спектроскопии (РФЭС) – SPECS, PHOIBOS.

Первым всегда наносился адгезивный слой из Cr, затем проводящий слой из Cu или Al, третьей выступала защитная пленка из Ni. Толщины всех слоев варьировались в зависимости от времени или мощности распыления мишени. Скорость роста нанопленок из Ni – V_{Ni} была близкой к скорости V_{Cr} и сотавила 0.8 нм/с, тогда как для Al – V_{Al} = 1.5 нм/с, а Cu – V_{Cu} – 3 нм/с.

Анализировалась как средняя – R_a, так и среднеквадратичная величина шероховатости – R_{RMS} (R_q) и устанавливался режим МР, при котором формируемые нанопленки удовлетворяют условиям:

$$R_a = \min\{R_{ai}\}_q \to \min\{R_{qi}\},$$

где i – изменяется по числу изучаемых режимов, как показано на рис. 1.

а   *б*
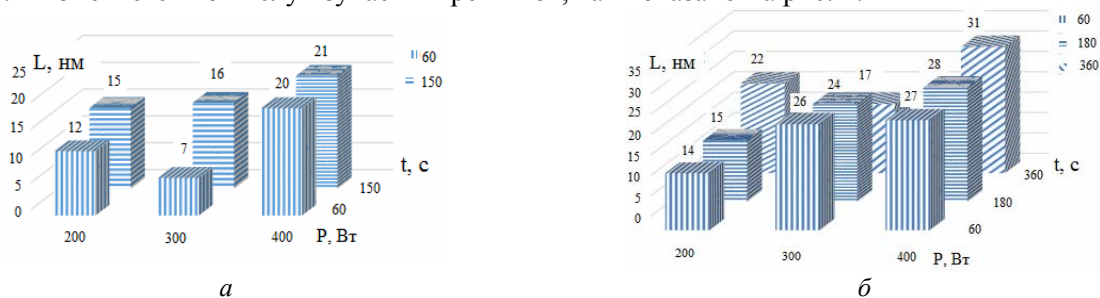
Рис. 1. Изменение расчетных размеров области когерентности для однослойных нанопленок из Ni и Cu при МР на разных режимах

Химическое структурирование МР нанопленок было изучено методом РФЭС из типовой резистивной мишени (РС 3710, Cr – 37.52, Ni – 9.97 %, остальное Si) на подложке из ситалла и Cu, а также из Al из Al мишени на ситалле с толщинами вплоть до 225 нм в поверхностном слое толщиной 3 нм с площади 5 мм. Для нанопленки из алюминия в остовном состоянии Al (2p) было обнаружены окисление (Al^{+3}) – Al$_2$O$_3$ и недоокисленные металлическое состояние – Al^{+0} с E_b – 74.1 и 71.7 , а также остовные линии O1s – 531.5 и C1s – 285.0 эВ с нестехиометричностью. В нанопленкахх из РС 3710 мишени наблюдались остовные линии 2$p_{3/2}$: для Ni^{+2} – 853.2, Cr^0 – 573.8 эВ, согласующиеся с ее составом. Проведен анализ на АСМ мульти нанослоев наноиндентором типа Берковича (типа 3-х сторонняя пирамида с углом при вершине – 70.2996°, площадь следа индентора – 3h_p^2tan^{2}θ. Изучено изменение нанотвердости (H_n) при разных мощностях 200, 300, 400 Вт на медных магнетронных пленках, нанесенных в течение 50, 180, 360 с. Обнаружен аномальный рост нанотвердости при P = 300 и 400 Вт с 2.6 до 7.5 ГПа и с 1.8 до 11.6 ГПа, соответственно, тогда как при P = 200 Вт наблюдалось понижение нанотвердости с 4.3 до 1.8 ГПа. Следует отметить также, что при кратковременном нанесении медных пленок (50 с) H_n изменялась обратно пропорционально P и составляла 4.3 ГПа для 200 Вт, 2.6 ГПа – 300 Вт и 1.8 ГПа – 400Вт, соответственно.

1.   А.П. Кузьменко, Нау Динт, Мьо Мин Тан. *Известия Юго-Западного государственного университета. Серия техника и технологии*, №3(16), С. 60 – 71, 2015.

2.   Bizhou S., Liping P., Xuemin W., Jianjun W., Weidong. W. *Journal of Wuhan University of Technology-Mater. Sci. Ed.*, V. 30, No. 2, pp. 380 – 385, 2015.

3.   J. Nishizawa and K. Suto, «Semiconductor Raman laser», *J. Appl. Phys.*, 51, pp.2429-2431, 1980

Р2-6: Электрические характеристики пленок лэнгмюра-блоджетт титаната бария

А.П. Кузьменко, И.В.Чухаева, П.В. Абакумов

¹ФГБОУ ВПО «Юго-западный государственный университет», Россия, Курск, E-mail addres: apk3527@mail.ru

Изучены диэлектрические пленки Ленгмюра-Блоджетт (ЛБ) из наночастиц стабилизированного титаната бария – $BaTiO_3$ (ST BTO) различной толщины (32, 128 и 352 нм), полученные на установке KSV NIMA 2002 методом вертикального лифта по ранее описанным методикам [1]. МДМ-структуры создавались на стеклянных подложках. Одним из металлических электродов была платиновая нанопленка (толщиной ~ 30 нм), полученная на подложке с помощью магнетрона Jeol JFC 1600. Вторым электродом был либо проводящий зонд NSC14/Ti-Pt (радиусом менее 30 нм) при изучении пьезоотклика на сканирующем зондовом микроскопе (СЗМ) SmartSPM AIST-NT, либо зонд из Pt-Ir электрода, срезанного под углом, используемый в туннельном микроскопе на этой же платформе. В последнем случае по получаемым вольт-амперным характеристикам (ВАХ) МДМ структур изучались механизмы транспорта носителей заряда. Для исследования температурной зависимости пьезомодуля в режиме микроскопии пьезоотклика (МПО) полученная пленка ST BTO размещалась на опциональном термостолике СЗМ. Нагрев и термостатирование образца (с точностью до $0.1^{\circ}C$) осуществлялось с помощью контроллера температуры PTC10 (Stanford Research Systems). Для исследования МПО между зондом из Ti-Pt и металлической пленкой из Pt подавался биполярный сигнал (± 10 В) треугольной формы с частотой следования ~ 34 кГц, совпадающей с резонансной частотой прижатого кантилевера. При изучении ВАХ на туннельном микроскопе между зондом из Pt-Ir и пленкой из Pt подавался одиночный импульс треугольной формы с полярностью от +2 до –1 В.
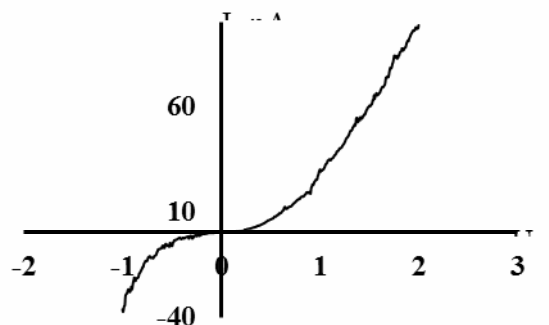
Рис.6. Вольт-амперные характеристики структуры Pt-Ir/ ST BTO/Pt

Установлено, что наиболее полное соответствие при таком анализе достигается для механизмов, в которых токи, либо ограничены пространственными зарядами (токи ограниченные пространственным зарядом – ТОПЗ), либо описываются моделью Пула – Френкеля (ПФ) [2]. Для изученных пленок титаната бария пьезомодуль и температура Кюри, которые составили 40 пм/В и 347 К; 14 пм/В и 352 К; 4.5 пм/В и 356 К соответственно. Рассчитаны показатель преломления – 1.96, диэлектрическая проницаемость – 61.5, постоянная Кюри-Вейса – $C \approx 3 \cdot 10^3$ К для пленки толщиной 32 нм. Измерены ВАХ МДМ структуры на основе пленки ST BTO толщиной 32 нм. Согласно механизму переноса заряда ТОПЗ оценена концентрация ловушек $N_t = 2.4 \cdot 10^4$ см$^{-2}$, характерная энергия распределения $E_0 = 0.05$ эВ, концентрации доноров $N_d = 9.4 \cdot 10^6$ см$^{-2}$ и глубину залегания $W_{d0} = 1.5$ эВ.

1.   A.P. Kuzmenko, I.V. Chuhaeva, P.V. Abakumov et al. *Journal of nano- and electronic physics*, Vol. **7** No 4, P. 04025-1 – 04025-4, 2015.
2.   К. А. Насыров, В. А. Гриценко, *УФН*, Т 183, № 10, С. 1099 – 1114, 2013.

P2-7: Technogenic nanoparticals for nanotechnologies in construction

A. Guryanov[1] , V.M. Lebedev[2]

1. Samara State Technical University, Samara, Russia, gurjanovam@mail.ru.
2. Petersburg Nuclear Physics Institute, Gatchina, Russia, lebedev@pnpi.spb.ru

Recycling of the industrial waste is an important environmental and economic problem. Slurries are a unique man-made product. The use of them as additives increases the strength, moisture resistance and durability of building materials with cement. The qualitative improvement of properties of building materials with cement thanks to slurry additives is due to the fact that they affect the formation of structural parameters of the final product at the micro and nanoscale [1,2]. The method of neutron small-angle scattering (SANS) was used to determine structural parameters of basic types of nanoscale slurries. This definitely makes it possible to consider slurry wastes to be nanotechnogenic raw materials.

The SANS intensity $I(q)$ depends on the scattering power of the compositional inhomogeneity of the matter and the contrast at the phase boundary. It is the function of the neutron pulse sent at scattering

$$q = \frac{4\pi}{\lambda} \sin \frac{\theta}{2}, \tag{1}$$

where θ is the angle of neutron scattering.

The SANS intensity $I(q)$ carries information about the structure of scattering particles (scattering centres) over the atom. Provided that $qR_c < 1$ (Guinier regime), the intensity of the small-angle scattering $I(q)$ is determined by the average (characteristic) size and shape of scattering particles:

$$I(q) = I(0) \exp\left(-\frac{R_g^2 q^2}{3} \right), \tag{2}$$

where R_g is the particle radius of gyration. From the experimental data on small-angle scattering in the Gunier regime it is possible to assess the particle radius of gyration R_g and their typical size R_c.

If the condition $qR_c > 1$ (Porod regime) for the intensity of the small-angle scattering $I(q)$ on fractal objects has been fulfilled, there happens to be a power characteristic from the transmitted neutron pulse:

$$I(q) \propto q^{-n}. \tag{3}$$

The deviation of the exponent n from the Porod asymptotic behavior ($n = 4$) indicates fractal properties of scattering objects and makes it possible to determine their fractal dimension. In the case of volumetric or mass fractals the exponent coincides with the fractal dimension $n = D_V$ and takes on the value from the interval $1 < D_V < 3$. In the case of scattering by objects with a fractal surface, the fractal dimension is $D_S = 6 - n$ it takes values from the interval $2 < D_S < 3$. The exponent is respectively in the interval $3 < n < 4$. Thus, by the slope of log-log linear segments of the SANS dependencies it is possible to determine the scattering objects of a particular fractal type (volume or surface) and the fractal dimension.

The SANS intensity spectra from the sludge samples were measured using the diffractometer "Membrana-2" installed at the reactor WWR-M in the Petersburg Nuclear Physics Institute. The wavelength of slow neutrons was equal to $\lambda = 0,3$ nm. The range of the recorded transmitted neutron pulses q varied from $0,03$ nm^{-1} to $0,8$ nm^{-1}. The samples of scattered neutrons were recorded in the range of angles $\theta = \pm 0,017$ rad.

According to SANS experimental data the average radii, fractal dimensions, differential scattering cross sections and distribution functions by sizes for scattering object were performed.

The obtained results show that slurries are composed of the nanodispersed component and it is quite possible to refer them to nanotechnogenic raw materials. A slight change in the structural parameters of slurries at various stages of completion (wet or dry) demonstrates their stability.

1.   A.M. Guryanov, «Nanoscale investigation by small angle neutron scattering of modified portland cement compositions», *Procedia Engineering*, 111, pp.283-289 (2015)

2.   A. Guryanov, S. Korenkova, Yu. Sidorenko, «Research on the nanolevel influence of surfactants on structure formation of the hydrated portland cement compositions» *MATEC Web of Conference*, 86**,** 04011 (2016)

P2-8: Self-organization nanostructured objects on (0001) surface of Sb$_2$Te$_3$

N.A.Abdullayev[1], N.M.Abdullayev[1], <u>K.Sh.Gahramanov</u>[1], S.Sh.Gahramanov[2], I.T.Mamedova[1]

1. Institute Physics of G.M.Abdullayev, Azerbaijan National Academy of Sciences, Baku, Azerbaijan..
kamil.qahramanov@yahoo.com.   2. Azerbaijan Technical University, Baku, Azerbaijan.

On the cleaved surfaces of layered crystals $A^V_2B^{VI}_3$ and films deposited from them, clusters with a grid hexagonal base were found that effectively affect the thermoelectric properties of the films. Due to their unique physical properties, especially thermoelectric properties, thin films of Bi_2Te_3 and Sb_2Te_3 semiconductors were the subject of intensive experimental and theoretical studies.

The purpose of this work was to identify nanoscale layers in foil based on $A^V_2B^{VI}_3$ crystals and to study their thermoelectric properties.

Thin films were obtained by thermal spraying on a foil of the same material.

Electron microscopic images were obtained on a scanning probe microscope (SPM) from Solver NEXT and AFM-BRUKER Nano N8 Neos in *2D-3D*.

In the studied island films based on the $A^V_2 B^{VI}_3$ -impurity, a periodic distribution of nanoislands on the (0001) surface with a high distribution density (on an area of 1μk) was revealed. The elements of their real structure are revealed: steps with nanoislands, intersections with dislocation lines, point vacancy defects and clusters.

The late stage of thin film growth is characterized by the fact that the interaction of new-phase islands, which originated earlier than the so-called clusters, begins. Such we consider nanoformations on the (0001) $A^V_2 B^{VI}_3$ surface. At the same time, we can accept the existing basic types of interaction of nanoscale types of clusters on the surface (0001).

The process of formation of phases on the surface (0001) of $A^V_2 B^{VI}_3$ includes such basic stages as nucleation of new phase centers, their independent growth and development of these processes in interaction with each other - Oswald ripening. This phenomenon reflects the late stage of development of the phase nuclei in time. The phase of the Oswald ripening can be the main one, determining the shape of the distribution of nanoislands in size and having grid structures in the base, which are called dislocation meshes.

The peculiarity of the nucleation of a new phase on the surface of substrates from $A^V_2B^{VI}_3$ in comparison with the homogeneous formation in the bulk is the hexagonal mesh structure, the scheme of which is shown in the inset on the left at the top of the figure. On the right and left are individual hexahedrons. The arrows in the figure show fragments of mesh structures on the *(0001) Sb$_2$Te$_3$* surface**.**
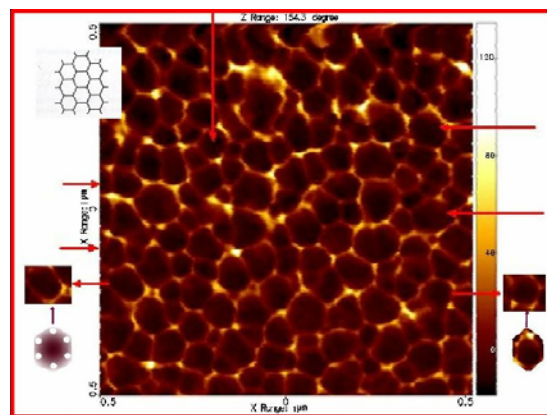
Fig. Thin film surface image

The values of the coefficient of thermoelectric power of thin films obtained by us are in the range (185-225) V/K, specific electrical conductivity (600-1300) $\cdot 10^2$ Om/ см; Power factor (45-50) W/mK, thermoelectric efficiency (2.8-3.4)$\cdot 10^{-3}$ K^{-1}, which agrees with the data of [1]. These results were obtained at T= 330K.

1. Ю.Г. Полистанский. «Разработка эффективных полупроводниковых термоэлементов на основе соединений A^{V}B^{VI}, A^{IV}B^{VI} и технологических способов их получения». Москва: МИСиС,1994.

P2-9: Аттракторы в наноструктурированных слоистых кристаллах

С. Багиров[1], А.Кахраманов[2], С.Кахраманов[3]

1.Институт Физики НАНА,Баку, Азербайджан. E-mail adress: sarhad@physics.ab.az 2. Бакинский Государственный Университет, Баку, Азербайджан E-mail adress: adilqakhramanov@gmail.com 3.Азербайджанский Технический Университет, Баку, Азербайджан.

Под влиянием интеркаляции в различных слоях $A_2^V B_3^{VI}$ накапливаются примеси, происходят количественные изменения: между ее отдельными слоями рвутся старые связи и возникают новые , разрушаются некоторые квинтеты в структуре Bi_2Te_3 <Cu>, на их местах формируются отдельные нанообъекты фрактального характера. Происходящие изменения приводят к неустойчивым состояниям – к точкам бифуркации. Возникшие флуктуации хаотичны, некоторые из них затухают, остаются только те, которые образуют новые структуры – аттракторы, притягивающие к себе множество траекторий развития системы, создающие особый конус. В качестве его наглядной модели показаны наноостровки между слоями Te(1) – Te(1) Bi2Te3 <Cu>.

Key Words and Phrases: нанообъекты, хаос, динамика, структуры, аттракторы, циклы, дифференциальные уравнения, устойчивость

Объектами изучения являются аттракторы динамических систем, в частности так называемые *странные аттракторы.*

Целью работы было наноструктрурирование примесями и выявление морфологических особенностей межслоевой поверхности (0001) Bi_2Te_3 <примесь> с притягивающимися аттракторами. Электронно-микроскопические изображения получали на сканирующем зондовом микроскопе (СЗМ) марки Солмер НЕКСТ. Рентгендифрактометрические исследования поверхности (0001) проводились на дифрактометре фирмы Philips Panalytical (XRD).

В докладе рассматриваются физико-химические процессы формирования на поверхности (0001) кристаллов $A^V_2B_3^{VI}$ с позиций далеких от термодинамического равновесия и самоорганизации фрактальных структур в среде $T_e^{(1)} – T_e^{(1)}$ (между квинтетами кристаллической структуры). Исследованы процессы самоорганизации примесей меди на межслоевой поверхности (0001) $A^V_2B_3^{VI}$ <примесь>. Показано, что формирующиеся примесные образования носят ступенчато-слоевой характер с наноостровками, высота нановыступов, образующихся в процессе вертикальной направленной кристаллизации у кромки ступеньки составляют 5-20 нм.

На поверхностях (0001) происходит перестройка при наличии между квинтетами теплового поля. Она связана со значительным отклонением и переходом меди из вакансий и межслоев в область $T_e^{(1)} – T_e^{(1)}$. Здесь формируются наноостровки (НО), ступени. Эти нанообъекты самоорганизовываются, превращаясь в различные паттерны. Самоорганизация и образование паттернов в виде наностровков в Bi_2Te_3 <In-Cu> связана с понятием диссипации, ассоциирующиеся с затуханием движения атомов Cu из накопившихся слоев и вакансий из которой процесс по притягивающей траектории неизбежно выходит на определенный цикл и сохраняет в нем свою устойчивость в виде различных нанообразований. Эти циклы можно отнести к так называемым предельным циклам [1]. По утверждению [1] любая динамическая система находит свой необычный поток, свой предельный цикл и остается в нем навсегда. В системе Bi_2Te_3 <In-Cu> наблюдается свой предельный цикл в виде закономерно распределенных нанообразований в среде $T_e^{(1)} – T_e^{(1)}$.

1.   Г.А.Мучник « Как воспользоваться упорядоченным беспорядком», *Ж. Химия и жизнь,* наука №5, 1985, стр. 30-35

P2-10: Поверхностные нанообъекты в монокристаллах CuGaS$_2$ и CuInSe$_2$

Н.А.Абдуллаев, И.Гасымоглу.

Институт физики Национальной академии наук Азербайджана имени академика Абдуллаева.,

Аз-1143 Баку, Азербайджан, abnadir@physics.ab.az

Методом Бриджмена-Стокбаргера получены монокристаллы CuGaS$_2$ и CuInSe$_2$. На примере CuInSe$_2$ и CuGaS$_2$ изучены морфология их поверхности. Приведены структуры их поверхности с множеством наноостровков высотой не более 3нм для CuGaS$_2$ и 100нм для CuInSe$_2$.

Тройные соединения A^{I}B^{III}C$_2$ ^{VI} (A^I—Cu, Ag, B^{III}—Ga, In, C^{VI}—S, Se,Te) со структурой халькопирита привлекают внимание исследователей в связи с перспективами их практического применения в качестве элементов преобразователей солнечней энергии [1-2]. При этом важное значение приобратает качество поверхности кристаллов.

Нами была исследована морфология поверхности CuInSe$_2$ и CuGaS$_2$ в 3d-масштабе.
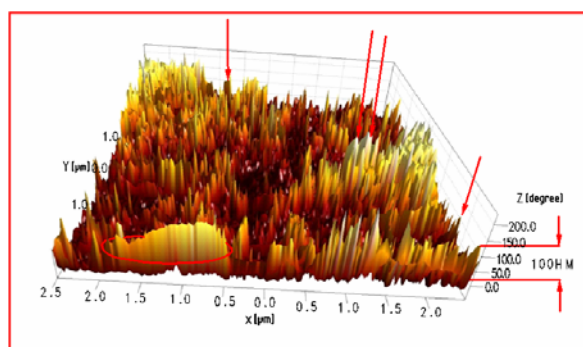
Рис-1. AFM-изображения поверхности CuInSe2 в 3d-масштабе. Стрелками отмечены наноостровки
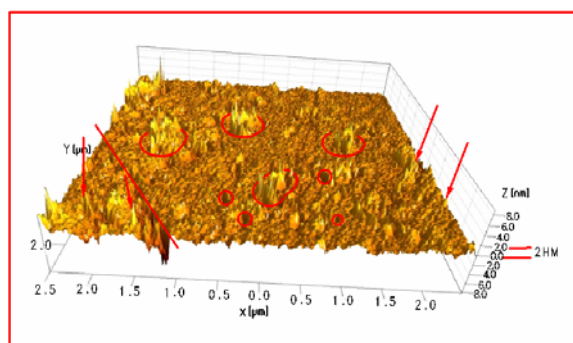
Рис-2. AFM-изображения поверхности CuGaS2 в 3d-масштабе. Стрелками отмечены наноостровки

На рис 1 и 2 даны AFM-изображения в 3d-масштабе для CuInSe$_2$ (рис.1) и для CuGaS$_2$ (рис.2).

Исследования структуры поверхности монокристаллов CuGaS$_2$ и CuInSe$_2$ проведены с целью выявления на их поверхности нанослоевых фрагментов.

Полученные образцы были исследованы на рентгеновском дифрактометре Bruker D8 Advance; AFM-снимки были сняты на микроскопе марки AFM-BRUKER Nano N8.

Из результатов исследованй дифракции рентгеновских лучей выявлены положения рефлексов характерные для исследованных систем.

Исследованные поверхности отличаются размерами наноостровков и плотностью их распределения (ПР): в CuInSe$_2$ высота ~100нм и ПР больше чем на поверхности CuGaS$_2$: здесь высота h=3нм и ПР меньше. Наноостровки разнятся и по форме, на рис. 1, слева внизу наблюдается коагулированная область. Такая область слившихся наноостровков незаметна для поверхности CuGaS$_2$ (см. рис.2). Такие морфологические особенности для CuInSe$_2$ более востребованы для солнечных преобразователей.

1.   J.I.Shay, J.H. Wernick. «Ternary Chalcopyrite Compounds», Oxford, Pergamon, 1974
2.   Б.М. Шкловский,А.Л. Эфрос «Электронные свойства легированных полупроводников» М.Наука, 1979

P2-11: SiN$_x$ films deposition on gallium arsenide in inductively coupled plasma under strongly diluted reagents

A. Okhapkin, S. Korolyov, P. Yunin, M. Drozdov, S. Kraev, E. Skorohodov, O. Khrykin, V. Shashkin

Institute for Physics of Microstructures, Russian Academy of Sciences, Afonino, Nizhny Novgorod region, Russia, poa89@ipmras.ru

In manufacture of gallium arsenide based semiconductor devices, silicon nitride dielectric coatings deposited in inductively coupled plasma (ICP) can be used. Despite the literature information for obtaining ICP silicon nitride films [1], its deposition on GaAs from strongly diluted reagents is still insufficiently studied. Thereby, the dependences of deposition rate and SiN$_x$ film properties on process parameters using 4% mixture of silane in argon were studied. The process was carried out on Oxford Plasmalab 80 Plus. As a result, amorphous silicon nitride films with thicknesses from 60 to 150 nm were obtained on GaAs using SiH$_4$/Ar+N$_2$ plasma. It turned out that the maximum deposition rate was observed with a certain excess of nitrogen (N$_2$/SiH$_4$ = 3). The preliminary activation of gallium arsenide surface in nitrogen plasma for 2 minutes also promoted faster deposition due to the nitrogen implantation into the substrate material and the formation of local growth centers. The increase of radio frequency (RF) power was accompanied by an increase of deposition rate to 47.7 nm / min (at 25 W). The further RF power growth resulted in decrease of deposition rate because of enhanced argon ions bombardment of films (see Fig. a).
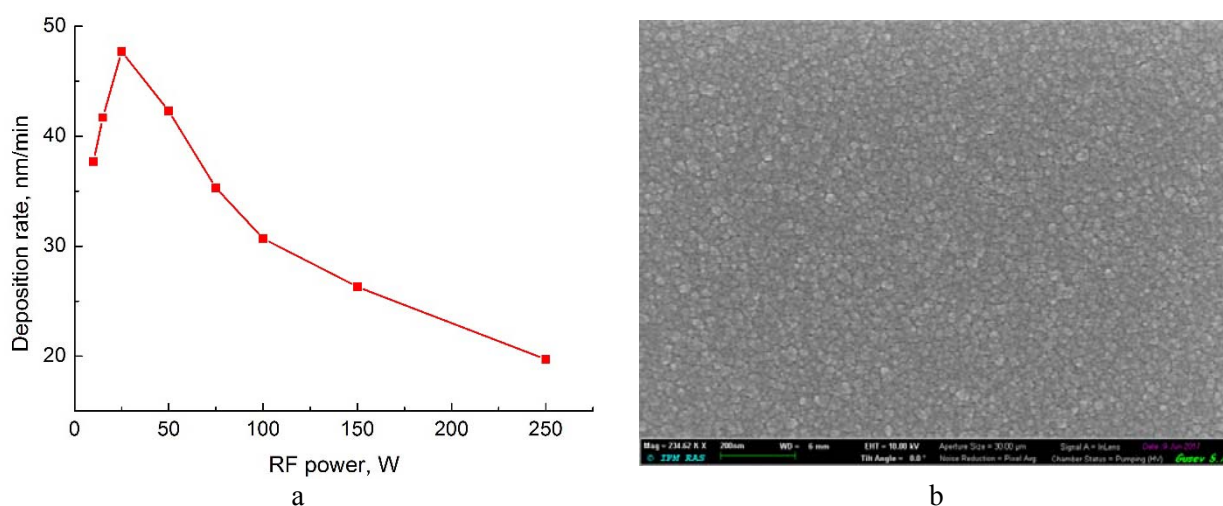
Fig. Dependence of the deposition SiNx rate on RF power (a) and electron microscope image of the grown film surface (b).

Also, with higher RF power values, the density of films increased from 2.3 to 2.6 g/cm^3 and the roughness was reduced to 0.5-0.8 nm (according to X-ray reflectometry data). In general, films surface contain grains 30 to 50 nm in diameter (Fig. b). Elemental analysis of deposited coatings (secondary ion mass spectrometry) showed that there is a significantly large content of oxygen. Supposedly oxygen was desorbed from reactor walls, where it was adsorbed during the working chamber opening to atmosphere. This, perhaps, determines the lower films density in comparison with literature data (3.1 g /cm^3).

1. A. Kshirsagar, P. Nyaupane, D. Bodas, S.P. Duttagupta, S.A. Gangal, "Deposition and characterization of low temperature silicon nitride films deposited by inductively coupled plasma CVD", *Applied Surface Science*, 257, pp.5052-5058, 2011.

P2-12: Corrugated surface structures in bismuth chalcogenides

E.M. Gojayev, S.Sh. Gahramanov, S.I. Mammadova

Azerbaijan Technical University, Baku, Azerbaijan. geldar-04@mail.ru

Materials with corrugated and stepped structures-nanowires of different size and density have been obtained. A mechanism of formation of the above nanostructures has been described due to plastic deformation effect under a pressure of thermal wave forming corrugated structures. To increase as much as possible the thermoelectric figure of merit of materials, the electron conductivity should be possible higher with the lowest thermal conductivity. One of the ways to accomplish this purpose is reducing dimensions of thermoelectric component parts for efficient phonon scattering on the edges of these nanostructures. In order to solve these problems, we employed nanostructured material technology using self-organization effects of low-dimensional nanostructures by growing crystals under different rate, annealing and thermal fluctuation conditions. Crystals were prepared by vertical directional crystallization method at a temperature gradient $\Delta T = 100$ degrees/cm and crystallization rate 1; 2 and 2.5 cm/hour. Nano-steps and corrugated structures, dislocation centres play a decisive quantum-mechanical role in the localization and transfer of charge and heat. Anharmonic vibrations of structure-forming atoms of layers are one of the factors yielding a relatively uniform linear crystal growth. With increase in elastic stress pressure created by thermal wave, the linear order of alignment is violated and quintet layers are deformed with a periodic distribution of wrinkles (Fig.). The value of thermal pulse forms an elastic deformation, and when some critical compressive stress is over the limits, quintet layers are aligned in corrugated wavy structures, which attenuates compressive stress. This occurs with increase in the rate of crystal growth by a factor of 2 and 2.5. The wavelength of wrinkles is determined by elastic characteristics and the thickness of quintet layers. The method of calculation of deformed layer thickness versus the wave period [1] can help to determine the number of quintet layers in a corrugated structure. A change in the average "wavelength" λ corresponding to the wrinkles was described by a simple power dependence $\lambda(x) \sim x^m$. The investigated materials differed in the value m. In order to describe their properties correctly, physicists introduced a concept of wrinklon, i.e. structural element whose recurrence characterizes the entire ensemble of wrinkles. A single wrinklon is responsible for a transition area where two wrinkles with the "wavelength" λ are combined to form a larger one. Each wrinklon in this case is matched by certain size L determined by material characteristics and the value of λ. In this case one can use the expression of the form, $\lambda(x)/h \sim (E \cdot h/T)^{0.25} \cdot (x/h)^{0.5}$ where h is layer thickness, E is Young's modulus, and T value characterizes the tensile force.
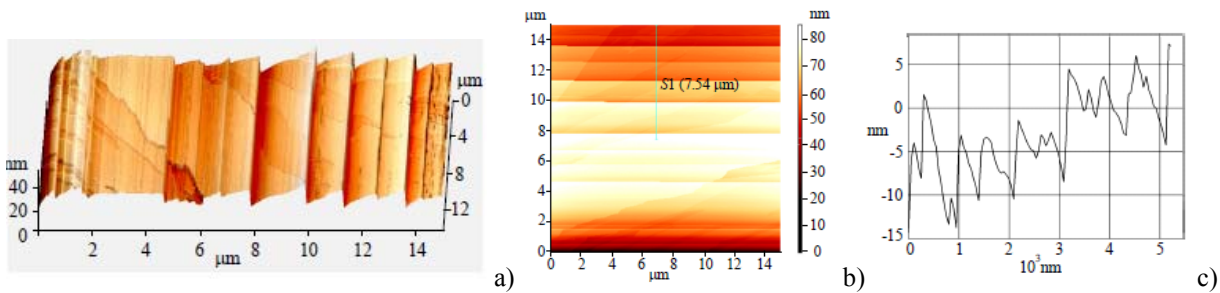
Fig. Corrugated structures $Bi_2Te_3<Ni>$: a) 3D AFM image of surface; b) 2D surface; c) cut profilogram in Fig. b).

Obtaining the right size wrinkles is directly related to crystallization front temperature. Its rise leads to increased viscosity of crystallized area and reduced ability of elastic energy accumulation, owing to which the height of the structure is reduced. Thus, the wavelength of wrinkle and its height correlate in a very small range with crystallization front temperature. It should be noted that the results obtained are in agreement with the authors' theoretical research [2].

1.   H. Vandeparre, M. Pineirua, F. Brau, B. Roman, J. Bico, C. Gay, W. Bao, C.N.Lau, P.M.Reis, P.Damman. «Wrinkling Hierarchy in Constrained Thin Sheets from Suspended Graphene to Curtains», *Phys. Rev. Lett*. 106, 224301 (2011), 22.

2.   L.P. Bulat, V.T. Bublik, I.A. Drabkin, V.L. Karatayev, V.B. Osvensky, G.I. Pivovarov, and D.A. Pshenai-Severin, «Bulk Nanostructured Thermoelectrics Based on Bismuth Telluride», *J. Thermoelectricity* 3, 67 – 72 (2009).

P2-13: Study on phase formation behavior of the nickel-modified nanostructured silicon

Yu. Shilyaeva, O. Volovlikova, A. Berezkina, A. Sysa and S. Gavrilov
Institute of Semiconductor Physics, National Research University of Electronic Technology, Moscow, Russia,
shyliaeva@gmail.com

The nickel-modified nanostructured silicon allows to implement a number of different applications. It is known as promising material for use in devices of silicon microelectronics, for gas sensing and for active layers of betavoltaic batteries[1,2]. Moreover, the nanostructured nickel silicides, which can be obtained during the solid-phase interaction between the Si and Ni, come into use in recent years[3,4]. Nevertheless, it should be taken into account that the solid-phase reactions in nanocomposites can occur at the interfaces at relatively low temperatures non-typical for similar processes in macrosystems. In this regard, the problem of estimating and predicting the thermal properties of such materials is of primer importance. The present work focuses on the influence of the interphase boundary "nanostructured Si – Ni" on phase formation behavior during heating.

In this paper, Si/Ni nanocomposites were formed by electrochemical etching of *n*- and *p*-type silicon and subsequent cathodic electrodeposition of nickel. Samples morphology and spatial distribution of elements in the nanostructured Si/Ni layer were inspected using scanning electron microscopy (SEM) and energy-dispersive X-ray spectroscopy (EDS), respectively.

In order to investigate solid phase interactions by differential scanning calorimetry (DSC) there were obtained Si/Ni nanocomposite samples on the basis of Si membrane. The investigation of the phase formation behavior of Si/Ni nanocomposites was conducted using the precalibrated differential scanning calorimeter Netzsch DSC 204 F1 Phoenix (Netzsch-Geratebau GmbH, Germany). The heating of the samples of 1–3 mg in the temperature range from 25 to 500 °C was carried out in press-fitted aluminium crucibles at a rate of 20 °C/min in an argon atmosphere. To accurately define the temperature characteristics the DSC curves were computer processed with modelling thermal effects using a normal distribution.

X-ray diffraction (XRD) characterization was carried out to perform phase identification of the samples before and after heat treatment using "RIKOR-8" X-ray measuring complex ("Institut Rentgenovskoy Optiki", Moscow, Russia).

The results of present study clearly show the differences in phase formation behavior of Si/Ni nanocomposites from the reference Si/Ni sample based on monocrystalline Si. The temperature characteristics of solid-phase interactions differ from those of Si/Ni thin film and macroscopic systems.

1.   I.M. Antropov, G.B. Demidovich, and S.N. Kozlov, «Sensitivity of porous silicon-nickel composite to methane adsorption», *Tech. Phys. Lett.*, 37(3), pp.213-215, 2011
2.   S.T. Revankar and T.E. Adams, «Advances in Betavoltaic Power Sources», *J. Energy Power Sources*, 1(6), pp.321-329, 2014
3.   L. Jen-Yi, H. Hsiu-Ming, and L. Kuo-Chang, «Growth of single-crystalline nickel silicide nanowires with excellent physical properties», *Cryst.Eng.Comm.*, 17, pp.1911-1916, 2015
4.   K. Dong-Joo, S. Jin-Kyeong, L. Mi-Ri, H. Jung-Hwan, K. Gil-Sung, O. Takeshi, and L. Sang-Kwon, «Ferromagnetic nickel silicide nanowires for isolating primary CD4+T lymphocytes», *Appl. Phys. Lett.*, 100, p.163703, 2012

P2-14: Hydrothermal synthesis of nanoparticles of iron oxide

E.V. Magazynska

A.A. Galkin Donetsk Physico-Technical Institute, Donetsk, Ukraine;E-mail: xmara23@mail.ru

Nanostructured particles of iron oxides (NIOP's) with their availability for manufacturability and low toxicity are promising materials for medicine, aerospace industry, military equipment, robotics, etc. An important and frequently used method to obtain NIOP's is the hydrothermal method (HTM). HTM controls easy the morphology and dispersity of the product and it is also attractive from the point of view of the possibility of obtaining submicron weakly aggregated monodisperse NIOP's [1]. The purpose of this work is study how the composition of the initial reagents and their concentration and reaction medium affect on the nanostructure of the NIOP's, followed by annealing in a reducing atmosphere. To characterize the materials obtained, XRD, SEM and TEM, FTIR, and EDX were used. The syntheses were carried out in an autoclave with heating to 220°C and holding for a specified temperature for 12 hours. $Fe(NO_3)_3 \cdot 9H_2O$ was precursor. Reagents $NH_4H_2PO_4 \cdot 2H_2O$, Na_2SO_4, $Mg(ClO_4)_2$, $NaClO_4$ and PVP were used as substances forming the morphology and dispersity of iron oxide particles. The thermal treatment was carried out after synthesis at 600°C for 1 h or at 300°C for 5 h in a H_2/Ar flow. Figure shows the synthesis scheme.
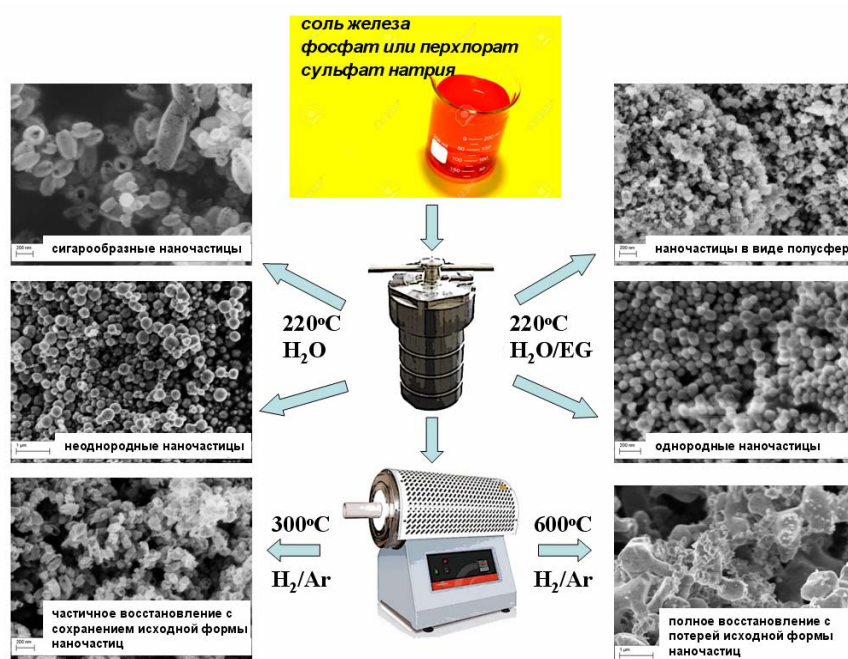
Figure. Scheme of nanoparticle preparation.

During HTM, nano-sized particles of α-Fe_2O_3 were prepared in various forms: cigar-shaped particles, hemispheres, rings, hollow spheres and particles with irregular form. Subsequent heat treatment at 600°C turns α-Fe_2O_3 into metallic iron. The initial shape of the nanoparticles is destroyed, and they are fused into large and irregular particles. The treatment temperature of 300°C permits to retain its shape, and α-Fe_2O_3 is reduced to magnetite Fe_3O_4.

Owing to the excellent physical properties of the NIOP's, it assumes that the prepared iron oxides with various morphologies will use as gas sensors, nanorobots, catalysts, biosensors, carriers of biologically active and medicinal substances and so forth.

1. W. Wu, X. Xiao, S. Zhang, J. Zhou, L. Fan, F. Ren, and C. Jiang. «Large-Scale and Controlled Synthesis of Iron Oxide Magnetic Short Nanotubes: Shape Evolution, Growth Mechanism, and Magnetic Properties». *J. Phys. Chem*. C, 114, 16092–16103, 2010

P2-15: Thermodynamic and kinetic properties of grain boundary ridges on the $[11\bar{2}0]$ tilt grain boundaries in Zn

V.G. Sursaeva, A.S. Gornakova, A.B. Straumal

Institute of Solid State Physics, Russian Academy of Sciences, Chernogolovka, Ac. Ossipyan str. 2, Moscow district, 142432 Russia sursaeva@issp.ac.ru

Grain boundary ridge is a one-dimensional grain boundary defect, and is formed when two sections of grain boundaries meet. The purpose of this work is the experimental study of the thermodynamic and kinetic properties of grain-boundary ridges on the tilt grain boundary in zinc. Under kinetic properties, we mean the experimental determination of the grain boundary mobilities with ridges, ridges and parameters of the inhibition of the grain boundary ridge motion. Under thermodynamic properties, we understand the determination of temperatures of phase transition of coarsening – disappearance of ridges on moving boundaries.

It was experimentally determined

1. the temperatures of phase transitions roughening of the grain boundary ridges

2. mobility and the activation enthalpy of motion for grain-boundary ridges

3. the parameters of the inhibition of grain-boundary ridge

Made the assumption that the degree of inhibition is determined by the structure of the ridges. The more perfect the ridge structure, the less the inhibition effect.

P2-16: Study and analysis of composition variation influence on chemical reactions sequence and thermal effects in Al-Zr multilayer thermite materials

L.I. Sorokina[1], E.A. Lebedev[1], D.G. Gromov[1], D.I. Smirnov[1], Y.P. Shaman[2], K.N. Nekludov[1]

1. National Research University of Electronic Technology, 124498, Russia, Moscow, Zelenograd, Shokin Sqr., 1, larisa.ivanovna95@gmail.com
2. Scientific Manufacturing Complex "Technological Centre", 124498, Russia, Moscow, Zelenograd, Shokin Sqr., 1, Bld. 7.

Multilayered thermite materials are extremely interesting and promising for different purposes of micro- and nanoelectronics, including self-propagating high temperature synthesis, reactive bonding, microelectromechanical systems and much more. In this work, we investigated comparatively new bimetallic multilayered foils based on aluminum and zirconium with different stoichiometry to determine the phase transformations sequence that realized in such structures during heating. The obtained theoretical and experimental results will allow to optimize the composition and to improve the performance.

Theoretical prediction of the phase transformation sequence was made based on the rule: If there is an excess of one of the original phases and the possibility of several compounds formation, the system will go on the sequence, which reduces the internal energy density as quickly as possible. Probable paths of the sequence of phase transformations in the case of excess zirconium: Al_3Zr_2 → Al_3Zr or Al_2Zr → Al_4Zr_5 or Al_2Zr_3 → $AlZr_3$. Probable paths in the case of excess aluminum: $AlZr_3$ → Al_2Zr → Al_3Zr.

Two sets of multilayered foils with compositions of 3Al:1Zr and 1Al:3Zr were deposited onto different substrates surface using two sources magnetron sputtering system. Multilayer foils consist of 16 alternating bilayers (one Al and one Zr layers) with a thickness of 250 nm.

To determine the temperatures of the basic phase transformations the differential scanning calorimetry was used. For these purposes, multilayer films were removed from the NaCl substrates in deionized water and washed in isopropyl alcohol. After that, samples of foils on a silicon substrates were heated and annealed at thermal effects temperatures and finally studied using X-ray diffractometer. The experimental results of the X-ray study at annealing temperatures in the case of excess zirconium showed the presence of phases: Al_3Zr_2 +Zr; Al_3Zr + Al_4Zr_5; Al_3Zr + Al_3Zr_5 + $AlZr_3$. The experimental results of the X-ray study at annealing temperatures in the case of excess aluminum showed the presence of phases: Al_3Zr +Zr; $AlZr_3$ + Al_2Zr + Al_3Zr; $ZrAl$ + $ZrSi_2$.

To measure the combustion rate we used the high-speed camera at 10000 fps. The front propagation rate for 4 microns thick 1Al:3Zr foil was about 0.3 m/s and 0.65 m/s for 3Al:1Zr. Multilayer structures were easily ignited after thermal and spark excitation.

We have explored reactive phase formation in magnetron sputter-deposited Al-Zr multilayer films with a 1:3 and 3:1 molar ratio**.** Thermal effects, phase formation and combustion properties of Al-Zr multilayered foils were investigated via differential scanning calorimetry (DSC), X-ray diffraction and high-speed camera. Thermodynamic calculations for this system were performed for the first time to predict the sequence of chemical reactions that occur in the composite, and achieved results were in good agreement with experimental data.

P2-17: Surface defects in radiation resistant insulators irradiated with swift heavy ions

G. Aralbaeva[1] , J. O'Connell[2] , V.Skuratov[3,4,5] , A.Akilbekov[1] , A.Dauletbekova[1] , M.Zdorovets[6,7]

1. L.N. Gumilyov Eurasian National University, Astana, Kazakhstan, aqm_555@mail.ru. 2. CHRTEM, Nelson Mandela Metropolitan University, Port Elizabeth, South Africa. 3. FLNR, Joint Institute for Nuclear Research, Dubna, Russia. 4. National Research Nuclear University MEPhI, Moscow, Russia. 5. Dubna State University, Dubna, Russia. 6. Institute of Nuclear Physics, Astana, Kazakhstan. 7. Ural Federal University, Yekaterinburg, Russia.

As it has been shown recently, large amounts of energy deposited due to severe electronic excitation in the wake of high-energy heavy ions can generate remarkable changes in the surface topography in a variety of materials. Among materials where surface effects of dense ionization are less studied are radiation-resistant ceramics and oxide crystals, like Al_2O_3 and MgO, having a relatively high threshold of electronic stopping power for structural disorder enhancement. Because these insulators are considered as candidates for inert matrix fuel hosts for fission reactors, high-energy heavy ion irradiation simulating a fission product's impact is of considerable practical interest due to the large number of fission track recoils in reactor fuel. In this report we present and discuss the results of complementary atomic force microscopy (AFM) and high resolution transmission electron microscopy (TEM) examination of hillock morphology on surface of single crystalline Al_2O_3 and TiO_2 irradiated with swift (E >1 MeV/nucleon) Kr, Xe and Bi ions. Fig. 1 and Fig. 2 demonstrate TEM and AFM images of surface defects in TiO_2. The AFM and TEM data on the morphology of surface hillocks and the near-surface track region in selected simple oxides will be presented and discussed including temperature dependent feature sizes.
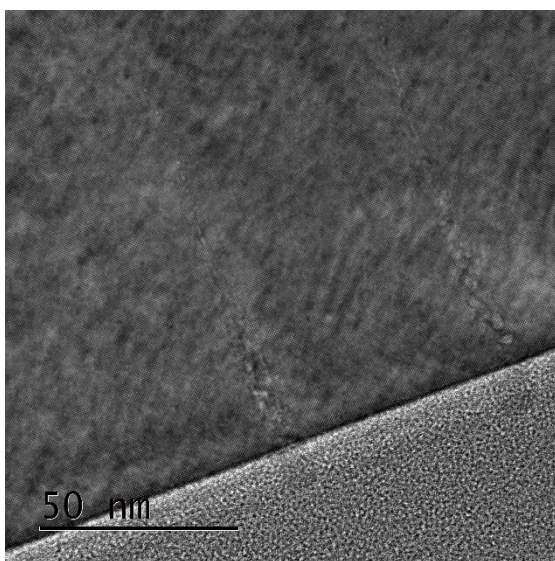

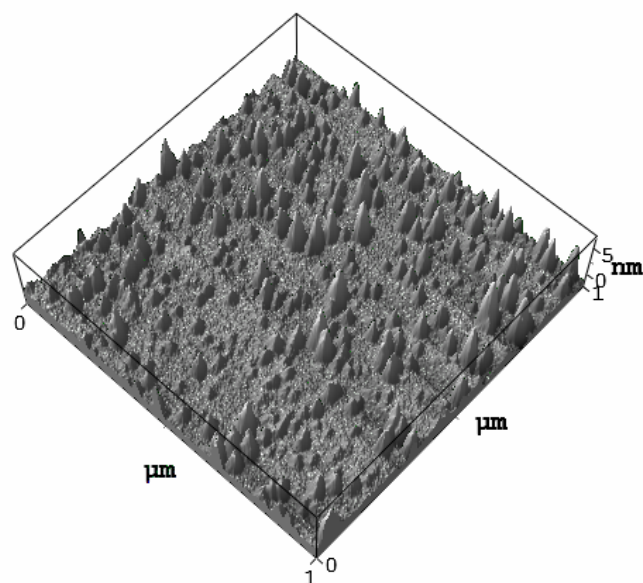Fig. 1. TEM image of TiO_2 irradiated with 700 MeV Bi ions. T= 300K

Fig. 2. 3D AFM image of TiO_2 surface after 220 MeV Xe ion irradiation at 800K.

P2-18: Use of focused ion beam for fabrication of field-emission cathodes based on SiC

A. Kolomiytsev, A. Svetlichniy, I. Jityaev

Southern Federal University, Taganrog, Russia, E-mail askolomiytsev@sfedu.ru

Silicon carbide is currently one of the most promising materials for the production of nanoelectronics devices. Particularly interesting are the structures formed on the surface of silicon carbide during its high-temperature destruction - graphene and nanocarbon films. The excellent electrical properties of graphene combined with the high stability and stability of SiC substrates open new possibilities for creating high-speed nanoelectronics devices. Graphene films are considered as most promising for the development of field-emission structures of nanoelectronics [1,2].

Field-emission cathodes based on graphene/SiC can be manufactured using Focused Ion Beam (FIB) technology. FIB nanopatternning allows precise nanofabrication of cathodes with advanced topography [3].

The presence of graphene on the SiC surface, its degree of perfection, and the film thickness were estimated by Raman scattering (RS) spectra. It was shown that annealing at a temperature of 1250°C promotes the formation of a graphene film with film-forming cluster sizes of ~10 nm.

In this study, the planar field emission cathode was fabricated by FIB local milling with a FEI Company DualBeam system Nova NanoLab 600, combining a Ga+ FIB and a field emission SEM.

The analysis of SEM image shows that the cathode with a tip radius of about 50 nm, angle 16˚ and 1 micron length was obtained after fabrication. The size of the inter-electrode distance is nearby 15 nm.

The current–voltage characteristic of the planar structure was obtained by applying a voltage up to 10 V. The analysis of the CVC measuring shows that the electron emission is observed at low voltages (1V or less). In the voltage range from 0 V to 10 V the emission current increases from 0 to 18 nA. Low threshold field emission can be explained under the assumption of the presence of graphene nanoclusters on the point cathode surface. Due to the flexibility and scalability of the technology, it is possible to create multi-point cathodes, which will allow to increase in the total emission current.

The work demonstrated that low-threshold field-emission cathodes can be formed based on graphene films on SiC. FIB method provides the formation of the cathodes with the tip radius of about 50 nm and inter-electrode distance - 15 nm.

1.   1 G.N. Fursey, M.A. Polyakov, A.A. Kantonistov, A.M. Yafyasov, B.S. Pavlov, and V.B. Bozhevol'nov, «Field and explosive emissions from graphene like structures», *J. Techn. Phys.*, 83 (6), pp.71–77, 2013.
2.   R.V. Konakova, O.B. Okhrimenko, A.M. Svetlichnyi and O.A. Ageev «Characterization of Field-Emission Cathodes Based on Graphene Films on SiC», *Semiconductors*, 49 (9), pp. 1242-1245, 2015.
3.   3 O.A. Ageev, A.M. Alekseev, A.V. Vnukova, A.L. Gromov, A.S. Kolomiytsev, B.G. Konoplev, S.A. Lisitsin «Studying the resolving power of nanosized profiling using focused ion beams», *Nanotech. in Russ.,* 9 (1–2), PP. 26-30, 2014.

P2-19: Theoretical explanation of effect of reduction of energy plasmons Si (111) at implantation of ions with the big dose

A.S. Rysbaev, I.R. Bekpulatov, J.B. Khujaniyazov

Tashkent State Technical University, Tashkent, Uzbekistan

bekpulatov85@mail.ru

In work it is resulted theoretical explain to experimentally found out effect of reduction of energy of excitation of superficial and volume plasma fluctuations valency electrons silicon Si (111) at implantation of ions B, Ba and alkaline elements with big dose D> 10^{16}sm^{-2}. Observable effect of reduction of energy plasmons Si (111) explain strong attenuation of fluctuations valency electrons owing to strong disordering crystal structure Si (111) up to full amorphicity.

The big interest nanosystems represent in connection with development to them of effects of dimensional quantization. To such effects carry formation of quantum points when the sizes of particles of the semiconductor are commensurable with de-Broglie's in the length a wave electron; change of width of the forbidden zone at the expense of localisation excitons; colouring of metal particles in view of plasmon a resonance. Dimensional effects are most brightly expressed for nanoclusters, i.e. particles with the sizes less than 5 nm.

Providence earlier us [1-2] experimental researches of spectra of characteristic losses of energy electrons with E_p=30 ÷ 300 eV, reflected from the silicon implanted by ions In^+, Ba^+ and alkaline elements with dose $D > D_a$ have shown, that the major feature of these spectra is reduction of energy superficial and volume plasmons with growth of a dose of an irradiation of a matrix extrinsic ions. In the given work we try again theoretically to explain effect of reduction of energy observed in experiment plasmons *Si* (111) at implantation of ions with the big dose.

For definition of a spectrum of energetic losses of a primary bunch in it is ion - implanted *Si*, we will start with the following elementary structure near-surface area. There is a broken layer in the thickness α, it borders with not broken pure *Si*, occupying other semi space (fig. 1). In drawing area α > z > 0 - area of the disturbance layer, z > α - area of a clear material.

$$\varepsilon_0(\omega) = 1 - \frac{\omega^2_{po}}{(\omega - iv)^2} \tag{1}$$

The clear material can be characterised volume dielectric transmittivity (1) in which ω^2_{po} -square of plasma frequency valency electrons clear *Si*, ν- attenuation in system fluctuating valency electrons, ω - current frequency on which the response of environment to external influence is investigated.

In a long-wave limit, dielectric transmittivity it is ionic - alloyed semiconductor can be written down in the form of the total.

$$\varepsilon (\omega, z) = \varepsilon_0 (\omega) + \varepsilon_s (z), \tag{2}$$

where $\varepsilon_0 (\omega)$-dielectric transmittivity of the initial clean semiconductor, and

$$\varepsilon_S(z) = \frac{4\pi e^2}{m} N_{imp}(z) \sum_{t=v} \frac{Z_{эфф,1}}{(\omega^2_{1c} - \omega^2 pe)} \tag{3}$$

represents static polarization spanning electrons impurity ions. Sum $\sum_{l>v}$ propagate on all filled covers impurity an ion, located below a valence zone, i.e. It is supposed, that $\omega^2_{lc} >> \omega^2_{pv}$; $\omega^2_{pv} = 4\pi e^2 N_v/m$- a square of plasma frequency valence electrons the semiconductor, ω^2_{lc} - a square of frequency of transition spanning electrons with l-covers impurity an ion in a zone of conductivity of the semiconductor, N_{imp} (z) - a coordinate profile of distribution of the introduced impurity on depth, $Z_{eff, 1}$ - effective number electrons, taking part in transition l→c.

1.   Rysbaev A. S., Khujaniyazov J. B., Rakhimov A. M., Bekpulatov I. R. Formation of Nanosize Silicides Films on the Si(1111) and Si(100) Surfaces by Low_Energy Ion Implantation. // *Technical Physics, 2014, Vol. 59, №. 10, pp. 1526–1530*.

2.   Rysbaev A.S., Khuzhaniyazov Zh.B., Normuradov M.T., Rakhimov A.M., and Bekpulatov I. R.. Peculiarities of the Electron Structure of Nanosized Ion_Implanted Layers in Silicon. // *Technical Physics, 2014, Vol. 59, No. 11, pp. 1705–1710.*

P2-20: Controlling of the radiation resistance of perovskite-based solar cells by optimizing of the nanofractal structure of surface

S.E.Maksimov, N.R.Ashurov, B.L.Oksengendler

Institute of Polymer Chemistry and Physics, Academy of Sciences of the Republic of Uzbekistan, Tashkent,;
maksimov_s@yahoo.com; polymer@academy.uz;

In recent years, the organic-inorganic perovskites [1] having the conversion rate of up to 22% are considered among the most promising materials for solar energy converters. These materials, however, quickly degrade under the action of both light and ionizing radiation [2]. In this paper, a new idea is proposed for controlling of the stability of perovskites by radiation by selecting of the degree of surface roughness (fractality). The idea is related to the recently discovered effect on the width of the valence bands ΔE_V^T by the Tamm surface states of a crystal with a significant degree of ionicity [2,3] (Fig. 1). It can be seen from Fig. 1 that ΔE_V^T is determined locally by the sign and by the local curvature of the surface: $\Delta E_V^T \approx \Delta E_{V(0)}^T - \gamma \Delta \varepsilon$, where $\Delta E_{V(0)}^T$ is the width of the zone of flat surface, $\gamma \sim 1/R$ is proportional to the curvature and is in slope opposition tj the radius of curvature. Then, according to the basic concept of radiation destruction of these materials (the Dexter-Varley mechanism) [2], we obtain for the probability of ionization destruction $\eta = \exp\left[-\left(E_{V(0)}^T - \gamma\varepsilon\right)\big/\hbar\omega_D\right]$, where ω_D is the Debye frequency.

Integrally, over the entire integral surface with the scale of δ, we get $\langle\eta\rangle = \int \eta(R, \delta, D_f) f(R) dR$, where R is the radius of the individual element fractally divided into n generations of the original scale δ, and D_f is the fractal dimension. Obviously, the fractal geometry with concave regions of radius {R} will correspond to the maximum radiation resistance.

$$E_V^{(1)} > E_V^{(0)} > E_V^{(2)}$$
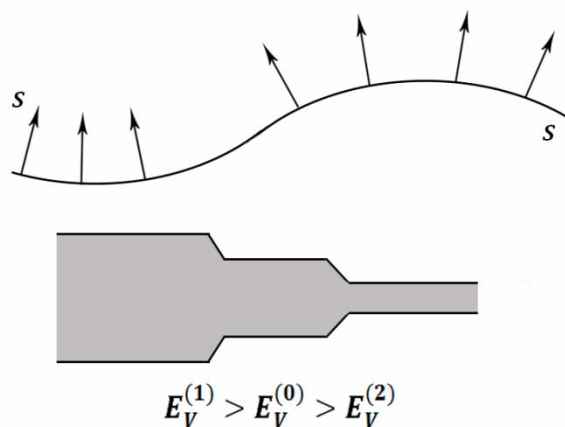
Fig.1. Dependence of the width of the surface zone of the Tamm states $(E_V^{(0)})$ on the type of curvature: (0) is the intermediate region; (1) is the concave region; (2) is the convex region.

1.   N.R.Ashurov, B.L.Oksengendler, S.E.Maksimov et al., «Current state and perspectives for organo-halide perovskite solar cells. Part 1», *Modern Electronic Materials*. 2017. (in press)
2.   B.L.Oksengendler, N.R.Ashurov, S.E.Maksimov, M.I.Akhmedov, I.N.Nurgaliev, «Mechanisms of radiation degradation of solar cells based on organic-inorganic perovskites», *Geliotechnika (Solar Engineering)*, 1. pp.48-57 (2017) (in Russian).
3.   B.L.Oksengendler, V.N.Nikiforov, S.E.Maksimov, «Tamm States of Fractal Surfaces», *Doklady Physics*, 62(6) pp.281–283 (2017).

P2-21: MANIFESTATION OF QUANTUM SIZE EFFECTS IN TWO-COMPONENT SEMICONDUCTOR NANOSTRUCTURES

D.A. Tashmukhamedova, Kh.Kh. Boltayev

Tashkent state technical university Tashkent city, Uzbekistan

e-mail: *ftmet@rambler.ru*

One of the perspective directions optoelectronics, microelectronics and nanoelectronics - creating on the surface of semiconductor materials selected nanofilms and nanocrystalline phases. By reducing the size of the nanocrystals and nanofilms to a value commensurate with the electron mean free path or the de Broglie wavelength, there is a sharp change in their physical properties and begin to manifest quantum size effects.In the case of nanophases created on the surface or in the bulk of a solid, there are additional factors associated with the formation of the interphase boundary.

This work is devoted to the evaluation of critical dimensions nanofilms and nanocrystals $BaSi_2/Si$ and $CoSi_2/Si(111)$, at which there is a noticeable change in their electronic properties.

Ion implantation, thermal and laser annealing, as well as to study the composition and structure of the samples was carried out on the same experimental device in an ultrahigh vacuum (P = 10-7 Pa). Implanted Co^+ and Ba^+ ions in the energy range $E_0 = 0.5$-5 keV at dose $D = 10^{14}$-10^{17} cm^{-2}.

In this work, based on analysis SEM pictures and Auger electron spectra, we have tried to build a model of the surface of Si, implanted barium ions with different energies and doses.

Cluster phases had a shape close to a circle with a diameter d = 10-15 nm, the distance between them is ~ 30-35 nm. Increasing the dose to $D = 2 \times 10^{15}$ cm^{-2} leads to compaction of the atoms (molecules) in the cluster phases and increasing their sizes in the surface 1.5-2. This near surface completely amorphing. With increasing doses, along with a slight increase in the size of the phase, occurs the appearance of new phases.Already at $D = 10^{16}$ cm^{-2}, there is overlap of the individual phases of cluster boundaries. At $D = 4 \times 10^{16}$ cm^{-2} occurs equally throughout the surface alloying and enriching the surface of Ba atoms. Further increase in the dose does not lead to a noticeable change in the surface composition.

Particular attention is is given to research of the electronic properties of nanostructured $CoSi_2/Si$ phases, since their lattice parameters are close to each other.

Collaborative analysis SEM and HEED images suggested that nanocrystals of metal silicide $BaSi_2$, $CoSi_2$ and their film crystallizes in a cubic lattice. These nanocrystals have a cylindrical shape (surface - a circle).

P2-22: INFLUENCE OF Ca NANOSCALE PHASES DEPENDING ON THE ENERGY INTENSITY OF THE TRANSMITTED LIGHT THROUGH THE CaF$_2$

B.E. Umirzakov[1], Y.S. Ergashov[1], B.D. Donaev[2]

[1]Tashkent state technical university Tashkent city, Uzbekistan

[2]Karshi engineering economical institute, Karshi city, Uzbekistan

e-mail: yergashev@rambler.ru

In the present study investigated the influence of the formation of nanoscale phase and films of Ca to the composition and electronic structure of the surface of monocrystals of samples of CaF$_2$ (111).

Study of the intensity of light from the transmitted light in 0,6-6 eV photon energy for the monocrystalline samples of CaF$_2$ (111) irradiated with the ions Ar$^+$ with E$_0$ = 1 keV different doses showed that in the case of "pure" and the ion irradiated CaF$_2$when increase hv from 0.6 eV to 6 eV value of intensity slowly decreases. At the same time the value of intensity-ion irradiated CaF$_2$ in the whole research area hv less than intensity of pure CaF$_2$.At a dose of D = 5 · 10^{14} cm^{-2} decreasing of intensity consist on average 20-25%, for D = 10^{15} cm^{-2} the average value of intensity decreases by 35-40%, while for D = 5 · 10^{15} cm^{-2} light intensity decreases 5-6 times. After bombardment with a dose of D = 5 · 10^{16} cm^{-2} through the CaF$_2$ film in the investigated area hv = 0,6-6 eV practically no light passes. These results can be explained as follows.

Previously we showed that at low doses of Ar$^+$ ions on the surface CaF$_2$appear separate cluster phase enriched Ca atoms. With increasing ion dose increases the size of these phases, and at D = 10^{15} cm^{-2} is ~ 30-40 nm. When D> 10^{16} cm^{-2} occurs overlapping boundaries separate phases and the entire surface is covered with atoms of Ca with thickness d ~ 10-15Å.Therefore UVES curve structure changes, a decrease in the quantum yield of photoelectrons and the intensity of the transmitted light with the increasing of dose of ions is due with increasingsize of cluster phases of Ca. Apparently, the formation of these phases is accompanied with some increase in the concentration of Ca and not irradiated sections of the surface layers CaF$_2$.This lead to an increase intensity of the peak of Caat the hv = 7-7,5 eV, displacement initial part of curves energy distribution CaF$_2$towards smaller energy of photoelectrons.These changes are associated with the formation of various defect levels near the bottom of of the conduction and the valence band top. When D≥5 · 10^{15} cm^{-2} concentration of these levels increases sharply and is formed narrow impurity band, which merge with the conduction bands and valence bands. Consequently, the band gap decreases. In particular, when D = 5 · 1015 cm-2 intensity of transmitted light was about 70-80%, and a value of Eg~7.5 eV.

Can assume that while about 80% of the surface CaF$_2$is covered with atoms Ca and of nonirradiated areas CaF$_2$ formed impurity band with a width of ~ 4-4.5 eV. Starting with D = 4 · 10^{16} cm^{-2} light practically not passes through the CaF$_2$, i.e. the surface is completely covered with atoms of calcium.

P2-23: ELECTRONIC AND CRYSTAL STRUCTURE OF NANOCRYSTALLINE PHASES Si, FORMED ON THE SURFACE CaF$_2$

S.B. Donaev, B.E. Umirzakov, D.A. Tashmukhamedova

Tashkent state technical university, Tashkent city, Uzbekistan

e-mail: sardor.donaev@gmail.com

One of the basic problems in modern nanoelectronics is to obtain the ordered nanocrystals (the same composition, the number of atoms and size, regular spacing between the nanocrystals) on the surface of various materials. A special place is the formation of self-organized nanostructures - ie the spontaneous formation of a large number of nanostructures because of the peculiarities of the behavior of the system matrix - adsorbed atom.

In researches we used epitaxial film of CaF$_2$on a substrate of Si(111), since the surface of CaF$_2$(111) has the lowest free energy and therefore it is atomically smooth. Before the study was carried out thermal annealing of the film at T $\approx$ 1100 K for 50 - 60 minutes. The film surface CaF$_2$/Si(111) consists of parallel strands, the respective surface (1x1).This suggests that the used films have sufficiently high crystal perfection and atomically smooth surface. Additional reflections characteristic for twinned growth and faceting, were not observed. Bombardment mainly carried by ions Ar$^+$ c E$_0$ = 1 keV, varying the irradiation dose in the range of 10^{12} cm^{-2} to 10^{14} cm^{-2}.At low doses of irradiation (D $\leq$ 10^{13} cm^{-2}) surface size defective areas were very small and, therefore, they are almost impossible to detect using SEM (SEM sensitivity of approximately 2 - 3 nm). Therefore, in these cases, the state of the surface was controlled by the AES (Auger electron spectroscopy) and SEM were obtained after deposition of Si atoms in the ion-implanted surface of CaF$_2$.When D $\leq$ 8 • 10^{12} cm^{-2} deposition of Si led to the formation of islands of various sizes, without strictly regular character. Apparently, at these doses of irradiation is not yet formed homogeneous defect structures. Ordered nanoclusters appear, since D = (2 - 4) · 10^{13} cm^{-2}. The most regular of the same size nanoclusters formed when Si atoms adsorbed onto CaF$_2$, irradiated by ions with a dose of D = 5 • 10^{13} cm^{-2}. At this dose, the surface CaF$_2$ is not yet loses its crystallinity, but the formation of defect centers enriched Ca atoms with surface size d = 1,5 - 2 nm. Si atoms sputtering to a thickness of approximately one monolayer and subsequent heating at T $\approx$ 800 K led to the formation of CaF$_2$ on the surface of monocrystalline phase of Si with a diameter of 10 - 15 nm.The distance between the centers of the islands was 50 - 60 nm. In the Auger spectrum occur intensity peaks at energies 92 and 95 eV. Formation silicide active metals (BaSi$_2$, NaSi$_2$) usually leads to the formation of an additional peak in the energy range 94 - 96 eV. Therefore, the peak with E $\approx$ 95 eV due to the formation of compounds type of CaSi$_2$.

Thus, the presence of similar centers in CaF$_2$ surface provides a regularly spaced nanocrystalline phase and solid nanofilms Si.

P2-24: Illumination influence on the morphology of the black silicon formed by Ni-assisted chemical etching

O. Volovlikova*, S. Gavrilov, A. Berezkina and G.Silakov

National Research University of Electronic Technology, Moscow, Russia,
*5ilova87@gmail.com

Black Silicon has been receiving a great deal of attention due to their interesting physical properties and promising potential technological applications in the field of sensing, emitting and energy. The b-Si can be produced by reactive ion etching (RIE) in fluorine, bromine and chlorine plasmas [1, 2], maskless RIE employing CF_4 [3] due to auto-masking of the surface at random spots. Ni-assisted chemical etching (MACE) method attracted great interest from the whole world on the aspect of fabricating low-reflective silicon nanostructures – black silicon [4]. Antireflective properties of the b-Si depend on the geometric parameters of the porous layer particularly porosity, pores diameter, thickness. The morphology of these layers depends on the treatment conditions: electrolyte composition, ratio of the contact areas of metal and silicon with the electrolyte [5], metal type [6], and etching duration [7], light intensity of frontside and backside illumination [8].

In this paper, black silicon layers were formed by Ni-assisted chemical etching. Wafers of p-type Si ((100), 0.01 Ω·cm) are used as substrates. Preliminary to be etched single-crystalline wafers were washed with piranha etch (mixture of sulfuric acid H_2SO_4 (98%) and hydrogen peroxide H_2O_2 (30%) (1:2 in volume)) at 130˚C during 10 min. Then they were rinsed in deionized water and dried by jet of isopropyl alcohol vapor. Si wafers were rinsed in HF-H_2O solution (1:5 in volumes) to remove native SiO_2. Subsequently, a Ni thin film (99.99 % purity) was deposited by magnetron sputtering. Ni films with thickness of 50 nm were deposited on Si surface. Etching solutions contained HF (40%)/ H_2O_2 (30%)/ H_2O in volume ratio 2/1/10. Treatment duration was 20, 40 and 60 minutes. Front side illumination was 0.06, 31 and 539 mW/cm^2. Porosity, layers thickness were calculated by gravimetric analysis by analytical balance XPE205 Mettler Toledo. Samples morphology was inspected using scanning electron microscopy (SEM).

The results of present study clearly show the increasing of the sample porosity and porous layers thickness with light intensity. Etching rate range from 20 to 79 nm/min at the light intensity from 0.06 to 539 mW/cm^2, respectively. Ni-assisted chemical etching is simultaneously processes: metal-assisted (MACE) and photoelectrochemical etching. In present work contribution of each component was established.

1. G.S. Oerlein, J.F. Rembetski and E.H. Payne, «Study of sidewall passivation and microscopic silicon roughness phenomena in chlorine - based reactive ion etching of silicon trenches», J. Vac. Sci. Technol. B 8, 1199 (1990).
2. H. Jansen, de Boer M, Legtenberg R and Ewenspock M «The black silicon method: a universal method for determining the parameter setting of a fluorine-based reactive ion etcher in deep silicon trench etching with profile control», J. Micromech. Microeng. 5, 115 (1995).
3. M. Gharghi and S. Sivaththaman «Formation of nanoscale columnar structures in silicon by a maskless reactive ion etching process», J. Vac. Sci. Technol. A 24, 723 (2006).
4. Zhihao Yue, Honglie Shen, Ye Jiang , Jiale Jin Wei Wang «Formation and mechanism of silicon nanostructures by Ni-assisted etching», J Mater Sci: Mater Electron 25, 1559 (2014).
5. C. R. Becker, S. Apperson, Ch. J. Morris, Sh. Gangopadhyay, L. J. Currano, W. A. Churaman, and C. R. Stoldt, Nano Lett. 11, 803 (2011).
6. X. Li and P. W. Bonn, Appl. Phys. Lett. 77, 2572 (2000).
7. M. Lipinskia, J. Cichoszewski, R. P. Socha, and T. Piotrowski, Acta Phys. Polon. A 116, 117 (2009).
8. Purnima Narayanan B.E. Photoelectrochemical etching of isolated, high aspect ratio mic rostructures in n-type silicon (100), University of Mumbai, 2007.

P2-25: Transport phenomena and physical properties of low-dimensional solid solutions $TlGa_{1-x}Sb_{1-x}S_2$

S.M. Asadov,[1] S.N. Mustafaeva[2], V.F. Lukichev[3]

1. Institute of Catalysis and Inorganic Chemistry, Azerbaijan National Academy of Sciences, Baku, Azerbaijan, E-mail: salim7777@gmail.com. *2. Institute of Physics, Azerbaijan National Academy of Sciences*, Baku, Azerbaijan, E-mail: solmust@gmail.com. *3. Institute of Physico-Technology, Russian Academy of Sciences, Moscow, Russia, E-mail: lukichev@ftian.ru*

The width of forbidden gap and a number of other parameters of semiconductor compounds $TlGaS_2$ and $TlSbS_2$ are determined by the nature of the bond, in particular, in the cationic sublattice of the ions. Therefore, it is of interest to study the ion substitution process in the cation sublattice of these wide-gap semiconductors with a layered structure. $TlGaS_2$ crystallizes in the monoclinic and $TlSbS_2$ in triclinic syngony; express anisotropy of physical properties, are optically active, and characterized by high photosensitivity. Study results of dielectric, photoelectric, and optical properties of solid solutions of the $TlGaS_2$–$TlSbS_2$ system are presented below. It is established that in the frequency range from $5 \cdot 10^4$ to $3.5 \cdot 10^7$ Hz, the real part of the complex dielectric permittivity (ε') of TlGaS2 varies from 22 to 23.5, i.e. characterized by weak dispersion. In $TlGaS_2 <0.5\%$ Sb>, the ε' values were lower, decreasing from 14.4 to 11.6 as the frequency increased.

In contrast to ε', the imaginary component of the complex dielectric permittivity (ε'') has undergone a more substantial frequency dispersion, decreasing by a factor of 3.5–4 with increasing frequency from $5 \cdot 10^4$ to $3.5 \cdot 10^7$ Hz for both crystals. In antimony-doped $TlGaS_2$ crystals, there were more significant dielectric losses compared with $TlGaS_2$. In both crystals the curve tgδ (f) had a decreasing character. The shape of the experimental curve tgδ (f) in the studied crystals is characteristic for the frequency variation of dielectric losses, taking into account the contribution of the electrical conductivity of the crystal. AC-conductivity of the $TlGaS_2$ crystals in the frequency range f = $5 \cdot 104$–$2 \cdot 105$ Hz varies according to the law σac ~ f 0.6, at f = $2 \cdot 10^5$–$1.8 \cdot 10^7$ Hz - according to the law σac ~ f 0.8, and for f ≥ $1.8 \cdot 10^7$ Hz the quadratic dependence of σ_{ac} on the frequency was observed. In contrast to $TlGaS_2$, in $TlGaS_2 <0.5\%$ Sb> crystals the ac-conductivity varied according to the $\sigma_{ac} \sim f^{0.8}$ law in the whole studied frequency range. The values of the ac-conductivity in both crystals differed insignificantly from each other.

Calculated values *R* of the average hop distance for $TlGaS_2$ and $TlGaS_2 <0.5\%$ Sb> crystals were 81 and 77 Å, respectively. These values are ~ 5–6 times higher than the average distance between the centers of localization of charge carriers in the studied crystals. The average time of hops in crystals is determined: $9.9 \cdot 10^{-8}$ s for $TlGaS_2$ and $5.7 \cdot 10^{-8}$ s for $TlGaS_2 <0.5\%$ Sb>. The scattering of localized states near the Fermi level of 150 and 154 meV is estimated. The concentration of deep traps responsible for the conductivity of the crystals on an alternating current is determined: Nt = $8.8 \cdot 10^{17}$ cm-3 for $TlGaS_2$ and 10^{18} cm-3 for $TlGaS_2 <0.5\%$ Sb>.

From obtained data it follows that with the introduction of antimony in $TlGaS_2$, the mean distance and time between hops decrease, and the concentration of deep traps and the energy spread of the localized states in the forbidden gap increase. In the structure of the absorption edge of $TlGaS_2$ single crystals and the solid solution $TlGa_{0.995}Sb_{0.005}S_2$ at low temperatures, it is possible to detect an absorption band associated with the formation of an exciton near the straight edge. In $TlSbS_2$ crystal and similar in composition to it, the $TlGa_{0.03}Sb_{0.97}S_2$ solid solution, this band is not observed.

From the temperature dependence of the position of the exciton peak for the $TlGa_{0.995}Sb_{0.005}S_2$ composition in the temperature range 100–200 K, it is established that the positive temperature coefficient of the maximum of the exciton band persists. If we take into account the weak dependence of the binding energy of the exciton on temperature, this indicates an increase in the width of forbidden gap (E_g) of $TlGa_{0.995}Sb_{0.005}S_2$ with temperature. The value of E_g for crystals of the $TlGaS_2$–$TlSbS_2$ system was also determined from the photoconductivity spectra. An increase in temperature from 160 to 290 K led to a noticeable decrease in E_g for both $TlSbS_2$ and $TlGa_{0.03}Sb_{0.97}S_2$. Thus, due to the partial substitution of Ga → Sb in the $TlSbS_2$ lattice, it is possible to modify the photocurrent spectra and to control the width of forbidden gap of $TlSbS_2 <Ga>$ single crystals by temperature variation.

P2-26: Features of electrophoretic deposition process of nanostructured anode material based on Si powder and CNT for Li-ion batteries

N. Melkozyorova[1], E. Lebedev[1], A. Alekseyev[1], D. Gromov[1], E. Kitsyuk[2], R. Ryazanov[2], A. Sysa[1]

1. *National Research University of Electronic Technology, 124498, Russia, Moscow, Zelenograd, Shokin sq., 1, i.see.st4r@gmail.com*
2. *Scientific Manufacturing Complex "Technological Centre", 124498, Russia, Moscow, Zelenograd, Shokin sq., 1, bld. 7.*

The development of new technologies for the creation of composite anode materials for lithium-ion batteries is an urgent task considering the increasing requirements for energy storage and conversion devices. Silicon has outstanding theoretical capacity, but its use, for example, in the form of thin films is very difficult due to the high speed of degradation, which is caused by a threefold increase in the volume of material in the cyclic process of lithium intercalation. A possible solution to this problem is to develop composite materials based on silicon powder and carbon nanotubes. In this case, it is assumed that CNTs form a sound conductive network in which silicon particles are evenly distributed. Thus, carbon nanotubes have two functions: on the one hand, they provide high electrical conductivity, and on the other hand relieve mechanical stresses from silicon particles surface.

For the formation of such composite materials in this work the method of electrophoretic deposition has been used. This technique has incredible potential due to its simplicity, compatibility with the integrated technology and the possibility of formation of multicomponent coatings.

During the experiments, the method of slurry preparation was developed, features of the deposition process were investigated and optimized. In addition, the specific discharge capacitive characteristics of the obtained materials were measured, as well as the material degradation during cyclic charge-discharge process was investigated. The total duration of the deposition process was not more than 300 seconds and the applied voltage was varied in the range 40-120 V. Interestingly, the deposition was carried out even when the electric field strength of 5 V/cm, however, the deposition rate was quite low. The thickness of the precipitate obtained at the maximum values of the electric voltage was about 25 μm. On the basis of obtained results the dependence of the thickness of sediment from the applied voltage was determined.

The possibility of local deposition of composites on the topological pattern was also demonstrated, which opens up opportunities to design and create miniature planar lithium-ion batteries

P2-27: Formation of platinum silicide on thin amorphous and polycrystalline silicon layers

A. Novikau[1], S. Prakopyeu[1], K. Chizh[2], V. Yuryev[2], O. Nalivaiko[3], P. Gaiduk[1]

[1]Belorussian State University, Minsk, Belarus / e-mail: novikaua@bsu.by
[2]General Physics Prokhorov Institute, Moscow, Russia
[3]JSC "Integral", Minsk, Belarus

Over the past two decades, there was a qualitative breakthrough in the development of thermal imaging devices based on uncooled IR focal plane arrays. At present, two types of bolometer are commonly used as sensors in uncooled IR imagers: the ones based on vanadium oxide (VOx) or amorphous silicon (a-Si:H) thermistors [1]. It should be noted that CMOS compatibility of α-Si termistors is an important advantage of the temperature sensor material: a CMOS-compatible manufacturing process considerably decreases the production cost and simplifies its massproduction. Attractive possibility consists in utilization of metal/poly-Si Schottky junctions for formation of sets of connected temperature sensors on bolometer membranes. In our recent article, platinum silicide Schottky diodes formed on phosphorus doped polycrystalline Si films were demonstrated to be a promising alternative to SOI-diodes in monolithic uncooled microbolometer [2].

It is obvious, that silicide formation on top of amorphous and polycrystalline silicon were studied insufficiently because of uncertain perspectives for microelectronics. At present, however, the investigation of silicide formation on top of amorphous silicon becomes a promising objective that associated with research and development of new generation of uncooled microbolometers, specifically membrane-type silicon microbolometers based on Schottky diodes.

Thin 200 nm thick α-Si or poly-Si layers of were grown at different 300 – 650 °C temperatures by CVD and MBE on top of SiO_2. Formed $Si(100)/SiO_2/$(α-Si or poly-Si) structures were used as substrates. Polycrystalline Si layers were doped with P^+ at a dose of $2 \cdot (10^{14} - 10^{15})$ cm^{-2}. Thin (~25 nm) films of platinum were deposited on top of poly-Si layers by magnetron sputtering. The subsequent and rapid thermal annealing in nitrogen ambient at 350-550 °C was carried out for silicide formation.

Morphological and structural properties of the samples before and after annealing were investigated by scanning electron microscopy. The structural properties were investigated by bright-field and dark-field transmission electron microscopy and electron diffraction analysis. The Raman spectroscopy was used for structural evolution comparison before the silidization process.

It was established by SEM, that annealing of $Si(100)/SiO2/poly-Si$ structures at 350 °C results in platinum silicide formation of 41,8 nm thickness. The thickness of platinum silicide monotonically increases with annealing temperature and was estimated to be 55,6 nm at 550 °C. Analysis of TEM and STEM images confirmed the formation of metal silicide films as well as a complete consumption of the whole layer of the nanocrystalline silicon during the reaction with the metals. Also the temperature dependence of sheet resistances was measured and comparison of subsequent and rapid thermal processing was carried out.

1.   C. V. Hoof and P. D. Moor, *in Handbook of Infrared Detection Technology,* edited by M. Henini and M. Razeghi, Elsevier, 2002, Chap. 12, pp. 449–480.
2.   V.A. Yuryev et.al. *J. of Appl. Phys*. 117, 204502, 2015

P2-28: GaSb(001) surface in aqueous Na_2S - solution: modifications of chemical and electronic properties

T.V. Lvova[1], M.V. Lebedev[1], I.V. Sedova[1], M.S. Dunaevskii[1], O.V. Rakhimova[2].

1. *Ioffe Institute, St. Petersburg 194021, Russia; E-mail: tatyana.lvova.12@mail.ru; 2. State Electrotechnical University, St. Petersburg 197022, Russia*

GaSb is very attractive material for fabrication of optoelectronic devices in the near-IR spectral region. It is also employed as a substrate for epitaxial growth of (Al,Ga,In)(As,Sb) compounds which are widely used for high-speed electronic and longer-wavelength optical devices. The key issue for fabrication of high quality devices is the preparation of a GaSb surface with controlled chemical composition and electronic properties. Recently different techniques have been developed for getting the oxide-free GaSb surface, including sulfur passivation in aqueous and nonaqueous sulfide solutions [1, 2], chemical etching with acidic solutions.

In this paper we study sulfide passivation n-GaSb(001) in the 1M aqueous solution of sodium sulfide (Na_2S) at room temperature. The temporal evolution of both solution pH and temperature has been controlled to get insight into physical and chemical processes occurring during passivation at the interface of GaSb/sulfide solution. Electronic structure and chemical composition of native oxide-covered and of passivated GaSb(001) surface were analyzed by x-ray photoemission spectroscopy (XPS) and photoluminescence (PL) at different stages of the sulfide passivation process. Surface morphology of the samples was studied by atomic force microscopy (AFM).
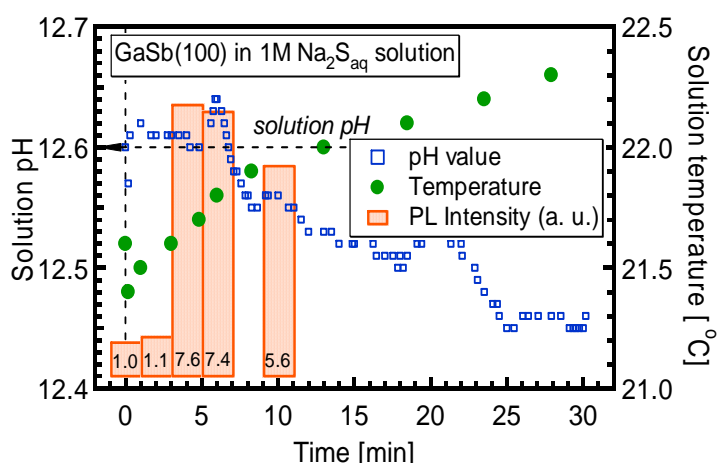

Fig. 1. Time evolution of the aqueous Na_2S solution pH and temperature at the interface with n-GaSb(100) in comparison to photoluminescence intensity of n-GaSb(100) surface passivated for different time with the same solution

It is found that GaSb(001) surface sulfidization in the aqueous Na_2S solution proceeds in two stages (Fig.1). At the first stage lasting < 4 minutes, the native oxide layer is removed and a passivating sulfide layer starts to form. The pH value (~12.6) of the solution does not change at this stage, whereas the photoluminescence intensity increases. At the second stage (> 5 minutes) composition of the passivating layer is found to is stabilized, whereas the pH value of solution decreases up to 12.45, and the photoluminescence intensity decreases as well. XPS study shows that the second stage GaSb(001) surface does not contain the native oxide layer and is covered with a sulfide protecting over layer. This layer consists of gallium and antimony sulfides with a Ga/Sb atomic ratio of 0.6. The thickness of the passivating layer is rather small. Even after 30 min treatment, it does not exceed a few monolayers.

The performed investigations of the chemical processes at the GaSb/Na_2S solution interface can be related with the evolution of the surface electronic structure. This makes possible the optimization of the GaSb(001) surface passivation treatment.

1.   M. V. Lebedev, E. Kunitsyna, W. Calvet, Th. Mayer, and W. Jaergermann, «Sulfur Passivation of GaSb(100) Surfaces: Comparison of Aqueous and Alcoholic Sulfide Solutions Using Synchrotron Radiation Photoemission Spectroscopy». *J. Phys. Chem.* C 117, pp. 15996–16004, 2013 D.

2.   E.V. Kunitsyna, T.V. L'vova, M.S. Dunaevskii, Ya.V. Terent'ev, A.N. Semenov, V.A. Solov'ev, B.Ya. Meltser, S.V. Ivanov, Yu.P. Yakovlev «Wet sulfur passivation of GaSb(100) surface for optoelectronic applications» *Appl.Surf.Scien*, 256 , pp 5644-5649, 2010

P2-29: Formation of surface states during the operation of the field effect transistors

A. Volkov[1]

1. *Zelenograd Research Institute of Physical Problems, Georgievskiy prospekt 5, Zelenograd, 124460, Russia;*
e-mail: artem.n.volkov@yandex.ru

The processes occurring at the interface between bulk silicon and its dioxide (Si/SiO_2) during the operation of the metal-oxide-semiconductor-field-effect-transistors (MOSFETs) can significantly affect on the lifetime of the MOSFETs and devices based on them. One of these processes is the formation of surface states at Si/SiO_2 interface during the operation of the MOSFETs. As a rule, this process is based on the dissociation reaction of the Si-H bonds formed after the formation of thin films of silicon dioxide during annealing in a hydrogen-containing atmosphere and located on the surface of SiO_2. This process can proceed according to several mechanisms, depending on the energy of the charge carriers initiating the dissociation reaction of the Si-H bond.

For investigation of the surface states formation rate and prediction of the lifetime of the MOSFETs, the accelerated test method is often used. For the mathematical description of the results of accelerated tests, as a rule, the power-law dependence of the lifetime (t_L) on the substrate current (I_{sub}) proposed by Mistry [1]:

$$t_L = A(I_{sub})^{-m}, \tag{1}$$

when t_L – is lifetime; A – is empirical coefficient of proportionality; I_{sub} – is substrate current; m – is empirical parameter, is used. In this paper, the experimental data [2, 3] was analyzed to determine the surface states formation rate during the operation of the MOSFETs. As a result of the analysis:

- the basic physical mechanisms that initiate the process of dissociation of Si-H bonds and the formation of surface states at Si/SiO_2 interface during the operation of the MOSFETs are determined;

- a method for determining the energy of charge carriers participating in the process of dissociation of Si-H bond, based on the analysis of the power-law dependence of the lifetime (t_L) on the substrate current (I_{sub}) was shown;

- a method for determining the mechanisms of the formation of surface states at Si/SiO_2 interface during the operation of the MOSFETs, based on the analysis of the power-law dependence of the life time (t_L) on the substrate current (I_{sub}) was shown;

- the parameters of the MOSFETs that influence the physical mechanisms that depend on the energy of the charge carriers, which initiate the process of dissociation of Si-H bond and the formation of surface states during the operation of the MOSFETs, were determined.

1.   M. Prabhakar. *Characterization and modeling of hot carrier degradation in sub-micron n-MOSFETs*. P.37. Nashville, Tennessee, 2002.

1.   2 K. Hess et. al., «Giant Isotope Effect in Hot Electron Degradation of Metal Oxide Silicon Devices», *IEEE TRANSACTIONS ON ELECTRON DEVICES*, 45 (2), pp. 406 – 416, 1998.

2.   J.M. Rafi, F. Campabadal, «Hot-carrier degradation in deep-submicrometer nMOSFET's: lightly doped drain vs. large angle tilt implanted drain», *Solid-State Electronics*, 45, pp. 1391-1401, 2001.

P2-30: Determination of ion induced mechanical stresses and modification depth in thin films

A. Babushkin, I. Uvarov, I. Amirov

Yaroslavl Branch of the Institute of Physics and Technology RAS, Yaroslavl, Russia, artem.yf-ftian@mail.ru

A new technique allowing to determine the mechanical stress and the depth of stress modification in films caused by ion bombardment is developed. It is based on two types of test micromechanical structures made of the same film: a cantilever and a bridge. The stress in the film can be represented as the sum of the average stress (σ_0) and the stress gradient (σ_1):

$$\sigma(z) = \sum_{k=0}^{\infty} \sigma_k \left(\frac{z}{h/2}\right)^k \approx \sigma_0 + \sigma_1\left(\frac{z}{h/2}\right). \tag{1}$$

Bending of the bridge depends on the average stress, while the cantilever bending is determined by the stress gradient:

$$\sigma_0 = \frac{\pi^2 E}{12 L^2}\left(3A^2 + 4h^2\right), \tag{2}$$

$$\sigma_1 = \frac{Eh}{R}, \tag{3}$$

where E is the Young's modulus of the film material, h is the film thickness, L is the bridge length, A is the bending amplitude of the bridge, and R is the curvature radius of the cantilever.
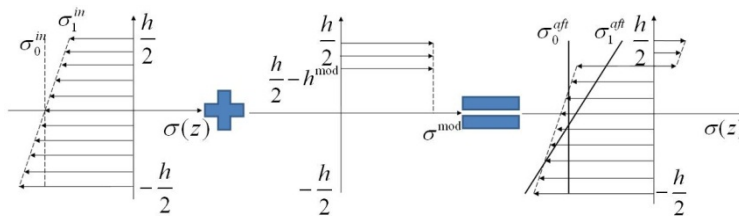

Fig.1. Schematic illustration of the change in the stress field caused by ion bombardment.

Relation of the ion-induced stress (σ^{mod}) and the stress modification depth (h^{mod}) with the mean stress and the stress gradients before and after the bombardment is described as follows (Fig.1):

$$\begin{cases} h^{mod} = h\left(1 - \frac{1}{3}\frac{\Delta\sigma_1}{\Delta\sigma_0}\right) \\[2mm] \sigma^{mod} = \Delta\sigma_0 \dfrac{1}{1 - \dfrac{1}{3}\dfrac{\Delta\sigma_1}{\Delta\sigma_0}} \end{cases} \tag{4}$$

The technique is used to determine the influence of argon bombardment with an average energy of 30 eV on a chromium film with a thickness of 200 nm (Fig.2 and Fig.3). The depth of stress modification is several orders of magnitude greater than the ion penetration depth, and it is close to the thickness of the film.
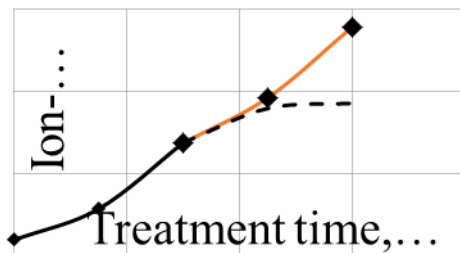

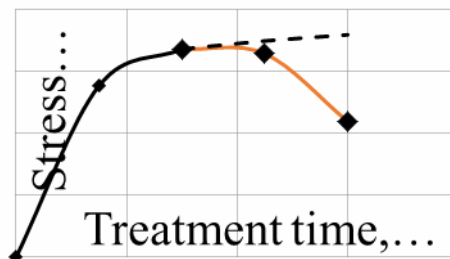Fig. 2. Dependence of the ion-induced stress on the treatment time.

Fig. 3. Dependence of stress modification depth on the treatment time.

P2-31: MODELING AND CALCULATION OF ELECTROMECHANICAL CHARACTERISTICS OF LOW-VOLTAGE LATERAL MEMS SWITCH WITH SPRING-TYPE ELEMENT OF THE TYPE "MEANDER"

Lebedev K. V.[1]

1) *Physico-technological Institute, Russian Academy of Sciences, E–mail: kiriklebov@gmail.com*

Micro and nanoelectromechanical systems (MEMS and NEMS) is a device that combines micro - and nano-electronic and micro-and nanomechanical components. A wide class of systems of MEMS and NEMS are switches. They find application in RF and microwave systems, such as adaptive antenna switching matrix and the transmitter / receiver units for wireless communication devices [1]. One of the drawbacks of Electromechanical keys – high voltage actuation. Therefore, the development of MEMS/NEMS switches with low voltage operation is an urgent task.

In this benchmark report presents the results of modeling electrostatic MEMS switch of the lateral type with a spring element of the type "meander" by method of finite elements. Thanks to the use of the spring element, the cantilever has a small coefficient of elasticity, allowing to reach relatively low values of the actuation voltage of the MEMS switch based on it (4 Volts). In figure 1. shows the actuation of MEMS switch. The distance between the cantilever and the control electrode (gap) was 60 nm.
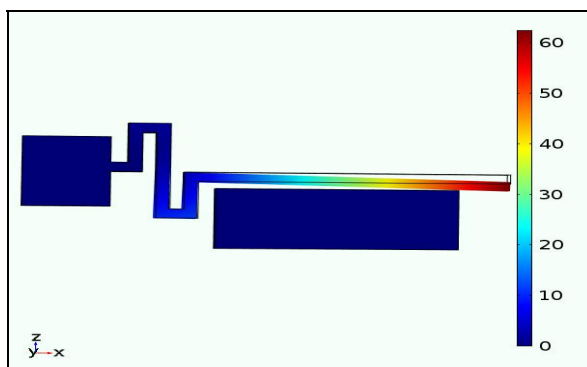

Figure 1. Actuation MEMS switch (4 V).

To verify the simulation results, we calculated the actuation voltage of the MEMS switch using the following formula [2]:

$$V_{Pull-in} = \sqrt{\frac{8kg_0^3}{27\varepsilon_0 A}} \qquad (1)$$

It was also the simulation of natural frequencies and resonant frequencies, q factor of oscillation of cantilevers made of different materials. A study of the influence of changes in geometric dimensions on-actuation voltage, carried out theoretical calculations of various electromechanical characteristics of the MEMS switch and the actuation time.

The data presented in the author's opinion are of interest to improve the performance of MEMS switches, reducing operation voltage, improving their reliability and reducing their energy consumption.

1.   Varadan V. K., Vinoy K. J., Jose K. A**.** «RF MEMS and their applications». *Chichester. West Sussex: John Wiley & Sons Ltd.* 2003. 394 p.
2.   Rebeiz G. M. «RF MEMS: Theory, Design, and Technology». *Hoboken, New Jersey: John Wiley & Sons, Inc.,* 2003. 483 p

P2-32: Control of the clusters formation in the gas phase with incorporation in LF PECVD deposition film

A.E.Berdnikov, A.A.Popov

Yaroslavl Branch of the Institute of Physics and Technology, Institution of Russian Academy of Sciences, str.Universitetskaya 21, Yaroslavl, 150007, Russia, E-mail: imiraslab4@yandex.ru

Previously we found that during plasma of low frequency glow discharge enhanced chemical vapor deposition (LF PECVD) of different silicon based films nanosize clusters appear in gas phase and incorporated in formed on substrate material. Growth conditions in gas phase and on substrate surface are differing. Because it chemical mixture of clusters and film are different. Presents of clusters in film provide unique physical properties of materials deposited by LF PECVD.

In particulars, we found bipolar bistable conductivity switching effect in metal – insulator – semiconductor structure with SiO_2 insulator deposited by LF PECVD [1]. This structure can be used as non-volatile memory and reprogrammable logic arrays. Investigations of this effect show that current canal have nanometers diameter, but this structure have bad ability for size decreasing. We supposed that conductivity switching effect connected with nanosize particle formed in gas phase and embedded in growing films.

Increasing number of particles embedded in growing films is important problem. We hoped change technological parameters for solving this problem. In glow discharge chemically active particles (CAP) appears. They diffused to growth surface or interact with each other with consequently formation particles. For increasing particles formation concentration of CAP mast be increased or diffusion time from region of CAP generation and substrate mast be increased. This claimed can be achieved by increasing low frequency power and increasing pressure of gas mixture in deposited reactor.

Investigation of stability and uniformity of low frequency glow discharge was produced previously. Pressure increasing is lead to instability of glow discharge. Light spot appears on electrode. It's means that current between electrodes is flow only in same region of interelectrode space.

Pressure increasing is stabilized discharge. So, we were increasing pressure and power simultaneously. For testing this technological change the technological regime with very low yield of MIS with conductivity switching effect was elected as initial. Pressure of gas mixture ($NO/SiH_4 = 7.5$) in this regime is 210 Pa and average LF power is 50 W. Films deposited under this regime have good dielectric property and practically stoichiometric chemical composition. If changing of technological parameters are effective MIS structure with conductivity switching effect mast be appears.

For testing structure productions we used monocrystalline silicon wafers with p-type of conductivity. On back side of wafers previously 600 nm aluminum layer was deposited and annealing. Metal electrode after SiO_2 deposition also was formed from aluminum.

MIS structure with conductivity switching effect appears then pressure was increased in 4 times and power was increasing in 8 times. This increasing was limited by appearance of spot of powder on substrate surface then pressure increasing more than 4 times.

Power and pressure increasing during LF PECVD increase number of clusters which appears and growth in gas phase after that they incorporated in growing film on substrate surface. But this method has technology problems such as instability and bad uniformity.

1.	A.E. Berdnikov, V.N. Gusev, A.A. Mironenko, A.A. Popov, A.V. Perminov, A.S. Rudy, V.D. Chernomordick «Conductivity Switching Effect in MIS Structures with Silicon-Based Insulators, Fabricated by Low-Frequency Plasma-Enhanced Chemical Vapor Deposition Methods» *Semiconductors*, Vol. 47, No. 5, pp. 641-646, 2013

P2-33: Ion Assistance Influence on the Conductivity of Carbon Films

M.A. Grushin[1], A. M. Nikonov [1], A. A. Airapetov[2], E.A. Kralkina[1], V. A. Sologub[2], K.V.Vavilin[1]

[1]*Physical faculty of MSU, Vorobjevy gory, Moscow119991, GSP-1, Russia, ekralkina@mail.ru*
[2]*PJSC "Research institute of precision machine manufacturing", Russia. 124469, Moscow, Zelenograd, Panfilovsky avenue 10 solo@niitm.ru*

Introduction. Improvement of the existing, and dev elopment of new electronic devices require the production of thin films with a variety of pre-defined electrophysical properties. A special place among the film structures is occupied by carbon films. On the basis of various carbon modifications, it is possible to obtain nearly whole range of electronic devices. This makes carbon one of the most promising materials for the electronic industry. The present paper deals with the study of the ion assistance influence on the electrophysical properties of the carbon films deposited by magnetron sputtering of graphite targets.

Experimental procedure. Deposition of the carbon films was carried out using plasma hybrid system [1]. It is based on the combined magnetron and high-frequency inductive discharge located in the external magnetic field. Magnetron provides the generation of atoms and ions of the target materials while the flow of accelerated ions used for the ion assistance is provided by the RF inductive discharge. An external magnetic field is used to optimize the power input to the discharge, to increase the ion current density in the realm of substrate and to enhance the area of uniform plasma. The value of the ion flow is controlled by the power of RF generator while the energy of ions can be controlled by the RF bias of the substrate. Carbon films were deposited by magnetron sputtering of the graphite targets. Ne, Ar and Kr were used as working gases. The energy of the assisting ions varied within 0 - 85eV, ion current density was close to 1 mA/cm^2. Films resistivity was measured with the help of two probes method.

Results. It is shown that the resistivity of the films nonmonotonically depends on the energy of the assisting ions (see Fig.1). The maximal films resistfnce is achieved at an ion energy of 45 eV. The position of the maximum does not depend on the ion mass and the current density of the assisting ions. The value of the films resistance increases with the increase of mass and the decrease of the ionization potential of the assisting ions. The reason for the increase in the resistance at the energy of assisting ions equal to 45 eV is the formation of single-crystal carbon inclusions in the volume of the carbon film. At the energy of assisting ions close to the region of the maximum resistivity, it is possible to obtain carbon films with a region of negative differential resistance.
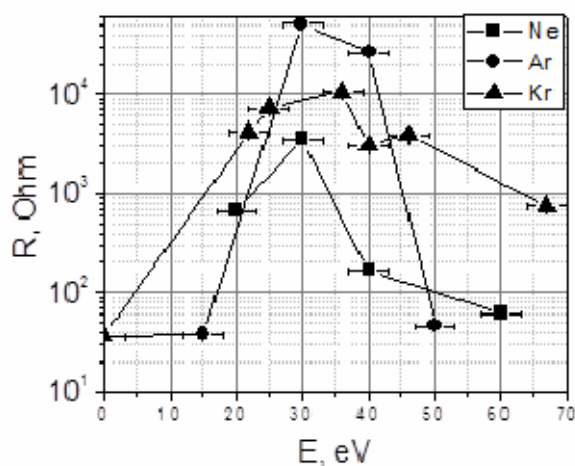

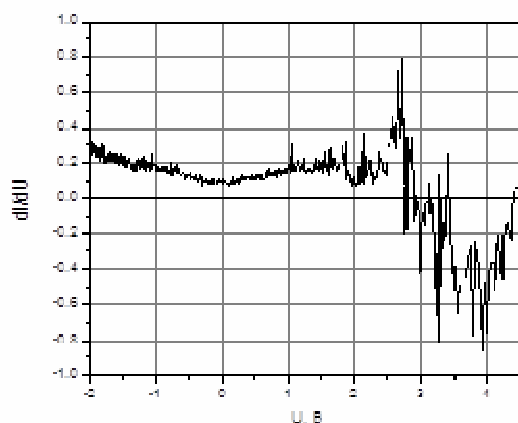Fig.1. Dependence of the film resistance on the energy of assisting ions.

Fig.2. Differential resistanct of the carbon film.

1. Вавилин К.В. и др. «Геликонный источник как элемент гибридной плазменной системы в установках для нанесения тонкопленочных покрытий с управляемой наноструктурой», *Наноиндустрия,* 2016, №2(64), с.74–86.

P2-34: Optical spectroscopy of diamond-like carbon films

J.S. Tortseva[1], A.A. Mironenko[1], M.E. Lebedev[1], A.B. Churilov[1], A.M. Nikonova[2], M.A. Grushina[2], K.V. Vavilina[2], E.A. Kralkina[2], M.G. Biryukov[3], V.V. Odinokov[3], V. A. Sologub[3]

[1]*Yaroslavl Branch of the Institute of Physics and Technology, 21 Universitetskaya, 150007 Yaroslavl, Russia, tortseva.julia@mail.ru*
[2]*Physical faculty of MSU, Vorobjevy gory, Moscow119991, GSP-1, Russia, ekralkina@mail.ru*
[3]*PJSC "Research institute of precision machine manufacturing", Russia. 124469, Moscow, Zelenograd, Panfilovsky avenue 10, solo@niitm.ru*

Interest in artificial diamonds and diamond-like carbon films as promising basic materials for microelectronics, optics and precision mechanics is due to their characteristics: high hardness (up to 100 GPa), thermal conductivity, high resistivity, optical transparency in the UV and visible spectral ranges, chemical and abrasion resistance. The ability to control the physicochemical characteristics of films and coatings during growth significantly increases the perspective for usage of such materials in various applications of science and technology.

In this work, diamond-like carbon films produced by magnetron sputtering in helicon discharge plasma are investigated by Raman scattering spectroscopy. Plasma-stimulated deposition processes with a controlled density and energy of plasma exposure provide a predicted nanostructuring of materials and allow one to implement the method of physical and chemical deposition of materials.

Acquisitions of the Raman spectra were carried out at room temperature using an EnSpectr R532 spectrometer, within the range 200-4000 cm^{-1} and a resolution of 6 cm^{-1}. The device uses a non-polarized radiation of a semiconductor laser diode with a wavelength of 532 nm and a power of 20 mW in the geometry of the normal reflection conditions.

The region 1000-1800 cm^{-1} contains well resolved, so-called D and G bands, with approximately the same intensity peaks at ~1350 cm^{-1} and ~1590 cm^{-1}, respectively. The appearance of the G-peak, which is usually called the main graphite peak, is associated with oscillations of hexahedral rings in the graphite structure. D-peak defines the disorder in the graphite structure. It was found that the change of the technological regimes of sputtering leads to a high frequency shift of the peak G-band almost 20 cm^{-1}, indicating the appearance of the hexagonal rings in the structure of the film and the formation of the "graphite" sp^2 bonds. [1].

1.   Ramamurti R. «Raman spectroscopy study of the influence of processing conditions on the structure of polycrystalline diamond films» / R. Ramamurti, V. Shanov, R.N.Singh, S. Mamedov, P. Boolchand // *J. Vac. Sci. & Tech. A: Vacuum, Surfaces, and Films.* – 2006. Vol. 24 Issue 2. – P. 179 – 189.

Р2-35: ТЕХНОЛОГИЯ ИЗГОТОВЛЕНИЯ ОТРИЦАТЕЛЬНЫХ ЭЛЕКТРОДОВ ЛИТИЙ-ИОННЫХ АККУМУЛЯТОРОВ НА ОСНОВЕ ПЛЕНОК КРЕМНИЕВЫХ НАНОКОМПОЗИТОВ

Т. Е. Шалаева[1], А. А. Мироненко[2], Д. Э. Пухов[2], И. С. Федоров[2]

1.Ярославский государственный университет им. П.Г. Демидова, Ярославль, Россия, E-mail: 2501tania@mail.ru, 2. Ярославский Филиал Федерального государственного бюджетного учреждения науки Физико-технологического института Российской академии наук E-mail: amironenko55@mail.ru

Наиболее эффективным путем улучшения эксплуатационных характеристик у литий–ионного аккумулятора (ЛИА) является переход на новые активные материалы, обладающие гораздо большей удельной ёмкостью, чем углеродные. Известно, что тонкие плёнки аморфного кремния способны обратимо циклироваться без значительных потерь ёмкости при толщине пленок от 50 до 300 нм. Дальнейшее увеличение толщины приводит к ускорению деградации при циклировании, вызванному разрушением и частичным отслаиванием плёнок .

Целью данной работы является исследование многослойных композитных пленок Si–O–Al толщиной 2 мкм, полученных методом магнетронного распыления кремниевой и алюминиевой мишеней при контролируемом напуске кислорода в рабочую камеру.

Было изготовлено 12 многослойных электродов с кремниевым композитом, условно разделенных на три группы, несколько отличающиеся толщинами активных слоев и составом. Обогащение и обеднение алюминием слоев пленок производилось путем изменения мощности магнетрона алюминиевой мишени.

На основе приготовленных пленок были собраны электрохимические ячейки, которые содержали рабочий электрод, два вспомогательных литиевых электрода и литиевый электрод сравнения. В качестве электролита использовали 1М $LiPF_6$ в смеси этиленкарбонат–диэтилкарбонат–диметилкарбонат (1:1:1). Циклирование электрохимических ячеек проводили с помощью компьютеризированного стенда для циклирования компании "Бустер" в пределах 0,01–2,0 В относительно литиевого электрода сравнения, которые соответствуют глубокому заряду и разряду аккумуляторной ячейки (рис. 1).
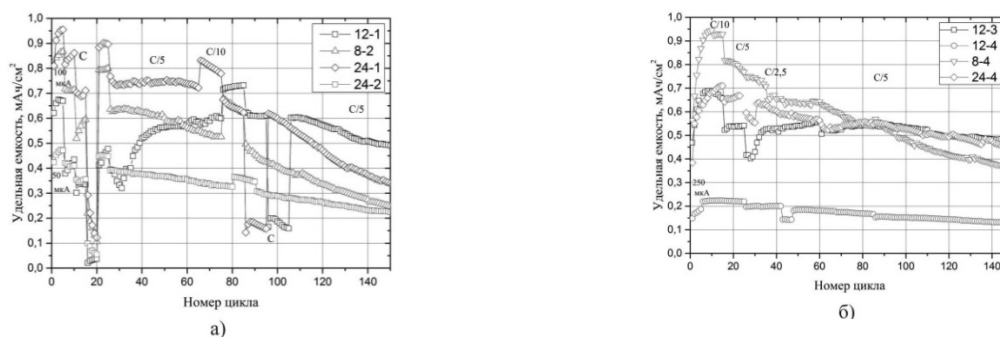

Рисунок 1 - Изменение удельной разрядной емкости анодных кремнийсодержащих структур на единицу площади. Номера образцов указаны на графиках. Толщина пленок 2 мкм. Уровни токов циклирования показаны на графиках в единицах С. (а, б)

Лучший компромисс между величиной и стабильностью удельной емкости электродов за 150 циклов заряд-разряд получен на 12 и 24-х слойных структурах. Более стабильны по емкости образцы, изготовленные при расходе кислорода 0,7 sccm по сравнению с образцами, изготовленными при расходе кислорода 1,0 sccm. Результаты электрохимических испытаний показали, что при толщинах пленок 2 мкм удельная емкость слоистых структур может составлять 0,5 мАч/см^2 после 150 циклов заряд-разряд при токе С/5.

P2-36: ИССЛЕДОВАНИЕ ПРОВОДИМОСТИ ТВЕРДОГО ЭЛЕКТРОЛИТА LiPON В ОБЛАСТИ НИЗКИХ ТЕМПЕРАТУР

А.В. Новожилова[1,2], М.Е. Лебедев[1,2], А.А. Мироненко[1], В.В. Наумов[1], А.С. Рудый[1,2], И.С. Федоров[2], А.Б. Чурилов[1,2]

[1]Ярославский филиал Физико-технологического института Российской АН
[2]Ярославский государственный университет им. П.Г. Демидова
E-mail: alena.novozhilova.2014@mail.ru

Современные литий-ионные аккумуляторы (ЛИА) находят широкое применение в самых разнообразных устройствах: от портативной электроники до электромобилей и энергетических систем. При этом основная масса ЛИА изготавливается по так называемой толстопленочной (намазной) технологии. Там, где использование толстопленочных ЛИА невозможно из-за их габаритов, альтернативой им служат твердотельные ЛИА (в англоязычной литературе all solid-state lithium-ion battery), которые изготавливаются по тонкопленочной или интегральной технологии.

В качестве электролита в таких аккумуляторах могут использоваться аморфные, кристаллические или полимерные электролиты. Наибольшее распространение, благодаря своим уникальным свойствам, таким как малое число переноса по электронам $t_e \quad 10^{-8}$, большое потенциальное окно $\Delta V \sim 5V$ и относительно большая проводимость $\sigma \sim 10^{-4}$ S/cm, получил LiPON, открытый более 20 лет назад [1-3] в Oak Ridge National Laboratory. Последний наносится в виде тонкой пленки толщиной ~ 1 мкм методом магнетронного распыления ортофосфата лития при контролируемом давлении азота. Цель настоящей работы состояла в исследовании температурной зависимости проводимости образцов LiPON в интервале температур от – 50 до 26 $^{\circ}$ C.

Экспериментальные образцы были изготовлены на установке магнетронного распыления SCR-651 «Tetra» (Alcatel, Франция) в виде многослойной структуры SiO_2/Pt 100нм/LiPON 1000нм/Pt 100нм/Ti 10нм/(SiO_2/Si). Здесь в скобках указана подложка, а последовательность слоев в строке соответствует направлению «сверху-вниз». Далее для простоты эта структура будет обозначаться как Pt/LiPON/Pt.

Морфология, элементный и фазовый состав пленок LiPON контролировались методами электронной сканирующей микроскопии, энергодисперсионного анализа и рентгеновской дифрактометрии. По данным рентгеноструктурного анализа пленки LiPON являются рентгеноаморфными. Измерение сопротивления пленок LiPON, нанесенных на «свидетели», выполненное стандартным четырехзондовым методом показало, что у образцов практически отсутствует электронная проводимость.

Для измерения ионной проводимости использовался испытательный стенд, эквивалентная схема которого показана на рисунке 1, где слева представлена эквивалентная схема структуры Pt/LiPON/Pt. Согласно схеме исследуемый образец представляет собой два индукционно связанных электрических слоя, соединенных сопротивлением $R_{вн}$. Строение слоя потенциалопределяющих ионов (лития у одного из платиновых электродов и кислорода у противоположного) во многом схоже со строением двойного электрических слоя. Поэтому для обозначения слоя потенциалопределяющих ионов и индуцированных ими электронов в настоящей работе используется термин «двойной электрический слой».

Измерения проводились в два этапа. Сначала исследовались разрядные кривые структуры Pt/LiPON/Pt через внешнюю нагрузку с номиналами от 10 кОм до 10 Ом. Цель измерений состояла в определении порогового значения сопротивления нагрузки, при котором кривая разряда не изменяется, поскольку ниже этого значения ток ограничен внутренним сопротивлением $R_{вн}$. Разрядные кривые для различных значений нагрузки приведены на рис. 2. Как показали результаты измерений пороговое значение сопротивления нагрузки составляет ~ 5 Ом, т.е. имеет место соотношение $R_{вн} \gg 5$ Ом. В соответствии с общепринятыми оценками это означает, что $R_{вн} \geq 50$ Ом или $\rho \geq 3.2 \cdot 10^5$ Ом $\cdot$ см, а удельная ионная проводимость - $\sigma \leq 3.1 \cdot 10^{-6}$ См $\cdot$ см$^{-1}$.
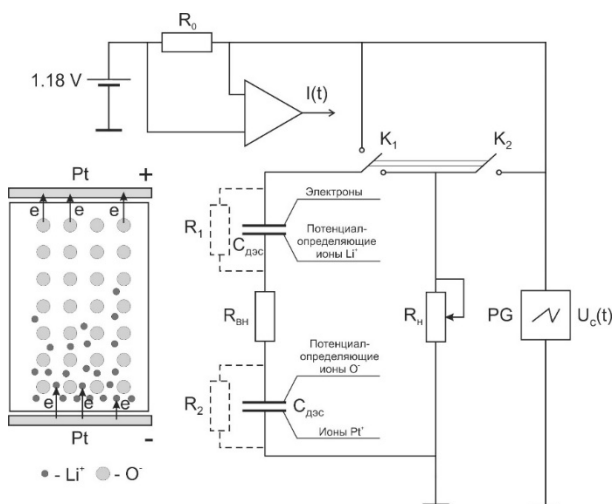
Рисунок 1 – Эквивалентная схема измерения заряда-разряда структуры Pt/LiPON/Pt: $R_0 = 100$ kΩ, $R_{вн}$ - сопротивление слоя LiPON, $R_н = 0$, 1 МΩ - сопротивление нагрузки, K_1, K_2 – транзисторные ключи, PG – осциллограф OWON PDS8202T (1 МΩ), $C_{дэс}$ - емкость двойного электрического слоя.
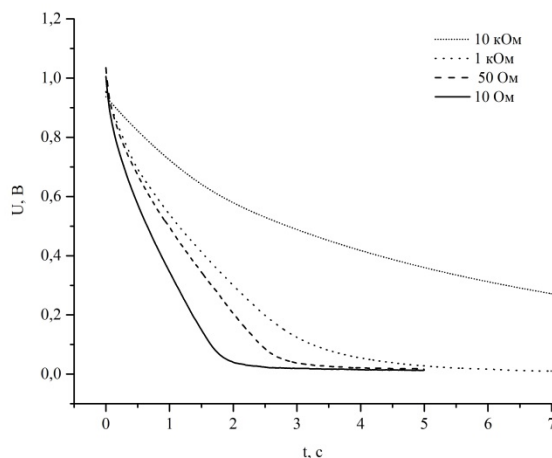

Рисунок 2 – Кривые разряда структуры Pt/LiPON/Pt через образцовые сопротивления номиналами 10 кОм, 1 кОм, 50 Ом и 10 Ом при
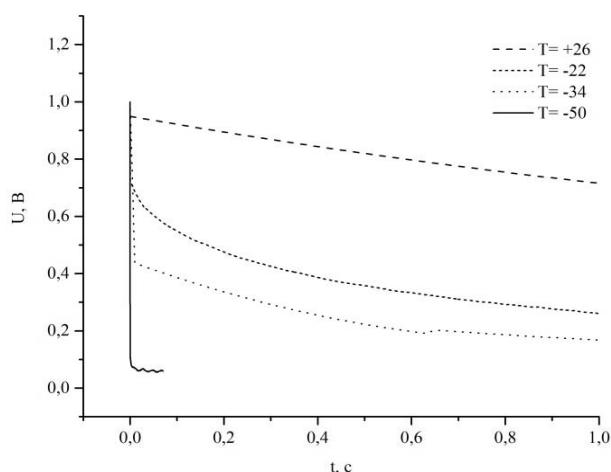
температуре 26°C

Рисунок 3 – Кривые разряда структуры Pt/LiPON/Pt через образцовое сопротивление 10 кОМ в интервале

температур от от – 50°C до 26°C.

На втором этапе исследовалась температурная зависимость кривой разряда через внешнее сопротивление 10 кОм (рис. 3). Согласно кривым на рис. 3 с понижением температуры подвижность ионов лития значительно снижается и увеличивается вклад в поляризацию деформационной составляющей. Если ток разряда при комнатной температуре определяется целиком процессами переноса заряда, то с понижением температуры становится заметен вклад в ток процессов релаксации деформационной поляризации. Об этом свидетельствует ступенчатое уменьшение тока на начальном участке кривой разряда. Тем не менее дрейфовая и диффузионная составляющие тока переноса наблюдаются вплоть до температур – 50°C.

Резюмируя сказанное, можно утверждать, что разработанная технология нанесения пленок LiPON методом высокочастотного магнетронного распыления на установке SCR-651 «Tetra» позволяет воспроизводимо получать пленки LiPON с требуемой ионной проводимостью, которая уверенно наблюдается вплоть до температуры – 40°C. Работа выполнена на оборудовании Центра коллективного пользования научным оборудованием «Диагностика микро- и наноструктур».

1. Bates J.B., Dudney N.J., Gruzalski G.R., Zuhr R.A., Choudhury A., Luck C.F., Robertson J.D., «Electrical properties of amorphous lithium electrolyte thin films», *Solid State Ionics*, 1992. V. 53-56. P. 647.
2. Bates J.B., Dudney N.J., Gruzalski G.R., Zuhr R.A., Choudhury A., Luck C.F., Robertson J.D., «Fabrication and characterization of amorphous lithium electrolyte thin films and rechargeable thin-film batteries», *Power Sources*, 1993. V. 43-44. P. 103.
3. Xiaohua Yu, Bates J.B., Jellison G.E., «Characterization of lithium phosphorous oxynitride thin films», *Proceedings of the Symposium on Thin Film Solid Ionic Devices and Materials*, 1995. V. 95-22. P. 23.